

Continuous production of two archetypal metal- organic frameworks using conventional and microwave heating

Abstract

Metal-organic frameworks have emerged as one of the key materials of interest over the last decade, with the number of publications and MOF structures registered with the Cambridge Crystallography database increasing year on year. One of the key reasons for this interest is the potential for very large internal surface areas of MOFs and the ability to tune pore sizes in order to target materials for the intended applications. The general range of surface areas of MOFs vary greatly, although a majority of MOFs exhibit surface areas of over $1000 \text{ m}^2\text{g}^{-1}$, with an expected potential of possibly greater than $10000 \text{ m}^2\text{g}^{-1}$ and large internal volumes, which in turn results in a number of useful properties for applications such as gas storage and separation, heterogeneous catalysis and even for use as medical devices. MOFs can also mimic some of the useful properties of zeolites such as molecular sieving², with the potential for tuneable pore sizes allowing a more optimal pore size for the selected application. However, MOFs are rarely produced at a large scale and are yet to become a viable alternative to current technologies.

Here we have selected two archetypal MOFs to investigate, with the aim of producing continuous synthesis routes for these MOFs. We selected two MOFs with well documented syntheses in the literature in order to allow us to quickly ascertain the relative performance of our materials and optimise these. We also explore the possibilities of using unconventional heating methods such as microwave heating in order to exploit the potential benefits of this heating technique.

MOF-5, with structure $\text{Zn}_4\text{O}(\text{BDC})_3$ (BDC = benzene dicarboxylate) is one of the most commonly synthesized MOFs with potential applications such as hydrogen storage and catalysis. Here we showed that the formation mechanism of MOF-5 from solution is actually very complex and features multiple metastable crystalline phases. Importantly, we show that for MOF-5 formed through a common synthetic technique will always transition through at least one metastable crystalline phase before formation of MOF-5. Parameters affecting the synthesis of MOF-5 were then analysed and optimised in order to gain a deeper understanding of the process chemistry, how process intensification affects the final product and create a continuous MOF-5 synthetic procedure. We have

Abstract

demonstrated that MOF-5 can be formed continuously with high Langmuir Surface Areas ($>2000 \text{ m}^2 \text{ g}^{-1}$) while also producing yields of greater than 80%, giving space-time yield (STY) of $50 \text{ kg m}^3 \text{ day}^{-1}$ suggesting that MOF-5 should be scalable to a high degree.

HKUST-1, Cu-BTC (BTC = benzene tricarboxylate), has the potential to be used in gas applications such as short chain hydrocarbon separation³, hydrogen storage⁴ or purification⁵ and H_2S sequestration⁶. Here we demonstrate a scalable continuous synthesis of HKUST-1 with a space time yield of $80 \text{ kg m}^3 \text{ day}^{-1}$ while maintain a Langmuir surface area of $>2000 \text{ m}^2 \text{ g}^{-1}$. Further optimisation of this system by varying the solid concentrations and the residence time was investigated.

We then show that microwave heating can be used to produce HKUST-1 in several orders of magnitude faster than by conventional heating. The use of microwave technology for continuous production system of HKUST-1 enabled STY of $80000 \text{ kg m}^3 \text{ day}^{-1}$ and surface area of $>1900 \text{ m}^2 \text{ g}^{-1}$, thus strongly suggesting the significant benefits of combining continuous manufacture with microwave heating.

We have shown that continuous production of two archetypal MOFs is possible, and optimised these systems while also comparing a number of key parameters in order to provide an overview of the potential benefits of process intensification and scale up. Further, we have highlighted clearly the potential benefits of using techniques such as microwave heating in order to exploit the beneficial changes to process chemistry of this heating method.

List of Publications

The following publications have been made as a result of work from this thesis:

1) Colin McKinstry, Edmund J. Cussen, Ashleigh J. Fletcher, Siddharth V. Patwardhan, Jan Sefcik. (2013). "Effect of Synthesis Conditions on Formation Pathways of Metal Organic Framework (MOF-5) Crystals." Crystal Growth & Design **13**, (12), 5481-5486.

2) Colin McKinstry, Edmund J. Cussen, Ashleigh J. Fletcher, Siddharth V. Patwardhan, Jan Sefcik. (2015). "Scalable Continuous Solvothermal Synthesis of Metal Organic Framework (MOF-5) Crystals" (Awaiting publication, submitted May 2015)

3) Colin McKinstry, Edmund J. Cussen, Ashleigh J. Fletcher, Siddharth V. Patwardhan, Jan Sefcik. (2015). "Continuous Production of high quality metal organic framework HKUST-1 via conventional and microwave heating" (Manuscript in preparation)

Acknowledgements

Acknowledgements

I'd like to extend a great many thanks to Dr. Siddharth Patwardhan, Dr. Edmund Cussen, Dr. Ashleigh Fletcher and Professor Jan Sefcik for affording me the opportunity to return to Strathclyde University for PhD study and the great amount of knowledge they brought to the table and an almost never-ending amount of patience.

I'd also like to extend my thanks to Dr Thomas Yip who has given countless hours of advice on many, many subject matters over the 3.5 years of this project. Craig McAnally, as one of the few others working on MOFs in the Chemical Engineering Department, for many discussions about MOFs, assistance with troubleshooting issues and the many, many hours of entertainment during the long hours of synthesis in the lab. Further, members of the Patwardhan research group past and present including Scott Davidson, Joe Manning, Yashodan Ghokale and Cassie Dove for putting up with me talking about MOFs rather than silica in group meetings. Dr. Fiona Coomer, Irene Cascallana Matías and Oonagh Collins for putting up with me in the lab and giving me someone to talk to during the many hours spend within the lab. They also provided countless hours of discussion, trouble shooting and generally brought excellent chat to the lab. Russell J Cathcart, whose work on DMF synthesised MOF-5 and company in the lab was greatly appreciated. Further, I'd like to thank all the members of my supervisors' research groups.

Dr. Fiona Sillars for putting up with my badgering about access to the PXRD at AMRL. Dr. Alexey Ganin and Glasgow University for facilitating access to their PXRD.

Special thanks to my parents, Dr Jim McKinstry, who earned his PhD at the University of Strathclyde in 1981, and Anna McKinstry who have supported me in all endeavours. To my eldest brother, Martin and his wife, Teresa, and children, Conor and Oran, and to my older brother, Gordon and my grandmother, Vera MacDonald.

Finally, I'd like to thank all the lab technicians. Ian Airdrie, Stuart Adams, John Wilkie and lab manager, Jim Murphy.

Table of Contents

Abstract.....	i
List of Publications	iii
Acknowledgements	iv
Chapter 1 - Introduction	1
1.1 Porous Materials.....	1
1.2 Metal Organic Frameworks.....	4
1.3 MOF Synthesis Methods.....	8
1.4 Applications of MOFs.....	10
1.4.1 Heterogeneous Catalysis.....	10
1.4.2 Gas Storage and Separation.....	11
1.5 Issues with MOFs.....	17
1.5.1 Interpenetration.....	17
1.5.2 Chemical and Thermal Stability.....	19
1.6 Scale Up	20
1.6.1 Importance and Difficulties of scale up.....	20
1.6.2 Steps in Scale-Up.....	23
1.6.3 Issues at large scale.....	25
1.6.4 Key parameters to consider when scaling up	28
1.7 Aims and Scope.....	30
Chapter 2 – Background and Literature Reviews	32
2.1 MOF-5 background.....	32
2.2 MOF-5 Synthetic Routes.....	32
2.3 Role of solvent in MOF-5 synthesis.....	35
2.4 Zinc Precursors.....	37
2.5 Solvothermal synthesis Conditions for MOF-5	42
2.6 MOF-5 and related crystalline phases.....	53
2.7 Moisture driven breakdown of MOF-5 to MOF-69c	60

Table of Contents

2.8 Selection of starting parameters for MOF-5 synthesis.....	62
2.9 Literature Review of HKUST-1 Synthesis.....	63
2.10 HKUST-1 solvothermal synthesis parameters	65
2.11 Solvent Choices for HKUST-1 Synthesis	70
2.12 Selection of starting parameters for HKUST-1 synthesis	72
2.13 Potential Applications of unconventional heating methods.....	73
Chapter 3 - Experimental.....	80
3.1 MOF-5 Synthesis, Process Intensification and Optimisation.....	80
3.2 Scale Up and Continuous Synthesis of MOF-5	82
3.3 Understanding and Optimisation of HKUST-1 Batch Syntheses	84
3.4 Solvothermal Continuous Synthesis of HKUST-1.....	86
3.5 Use of microwave heating for MOF-5 synthesis	87
3.5 Use of microwave heating for HKUST-1 synthesis.....	89
3.6 Continuous Microwave Enhanced Synthesis of HKUST-1	90
Chapter 4 – Analytical and characterisation techniques	92
4.1 Sample Collection and Storage	92
4.2 Crystal Structures	92
4.2 X-ray Diffraction.....	95
4.3 Infrared Spectroscopy	100
4.4 Nitrogen Sorption and Porosity.....	105
4.4.1 Adsorption Types	105
4.4.2 Physisorption	105
4.4.3 Chemisorption	106
4.4.4 Adsorption Isotherms	107
4.4.5 Volumetric Analysis of Porosity	109
4.4.6 Activation of MOFs.....	110
4.4.7 Langmuir Model.....	110
4.4.8 Branauer, Emmett and Teller (BET) Model	113
4.4.9 Barrett, Joyner and Halenda (BJH) Theory	115
4.5 TGA-DSC.....	118
4.6 Scanning electron microscopy (SEM).....	118

Table of Contents

Chapter 5 – Results and Analysis for MOF-5	120
5.1 Understanding the formation mechanism of MOF-5 and key parameters affecting batch synthesis	120
5.2 Understanding the effects of salt hydration on MOF-5 formation.....	126
5.3 Understanding the effect of metal:ligand ratio on MOF-5 formation.....	128
5.4 Process Intensification of Batch MOF-5 Formation	129
5.5 Continuous Synthesis of MOF-5.....	132
5.6 Process Intensification of Continuous MOF-5 Synthesis	138
5.7 Optimisation of Continuous Flow Process Chemistry	140
5.8 Use of DMF as alternative solvent for MOF-5 production.....	141
5.9 Comparison of Continuous MOF-5 Output of DMF and DEF solvent systems.....	142
Chapter 6 – Results and Analysis for HKUST-1.....	145
6.1 HKUST-1 Formation and Mechanistic Study.....	145
6.2 Comparison of batch syntheses	146
6.3 Process Intensification of HKUST-1 Batch Syntheses	150
6.4 Solvothermal Continuous Synthesis of HKUST-1.....	153
6.5 Post Processing of HKUST-1.....	158
Chapter 7 – Use of Microwave Heating for MOF Synthesis.....	161
7.1 Testing of Microwave for Potential Use for MOF Synthesis.....	161
7.2 MOF-5 Continuous Synthesis using Microwaves.....	163
7.3 Microwave-assisted Batch Synthesis of HKUST-1	167
7.4 Continuous Microwave Enhanced Synthesis of HKUST-1	171
Chapter 8 – Economical Potential of Scale Up of MOF synthesis.....	174
8.1 Initial Study into Feasibility of MOF-5 Manufacturing.....	174
8.2 Initial Study into Feasibility of HKUST-1	176
Chapter 9 – Conclusions.....	182
9.1 Conclusions concerning MOF-5 formation with conventional heating.....	182
9.2 Conclusions concerning MOF-5 Formation with Microwave Heating.....	184
9.3 HKUST-1 Conclusions	184
9.4 Comparison of MOF-5 and HKUST-1.....	187

Table of Contents

9.5 Future Work	187
References	190

Chapter 1 - Introduction

1.1 Porous Materials

Porous materials refer to materials with internal passage ways. The degree these passages go through the materials can vary, but the pores act as passageways from the external surfaces present to internal surfaces present within the material. Internal surface area is used to describe the area that surrounds any closed pores or voids, and pores that extend from the surface of the material into the material that are deeper than they are wide. This final distinction is important as external surface is hereby classified as the surface on the outside of the material including any pores that are wider than they are deep. Within porous materials, this allows for a clear distinction between external and internal surfaces, a useful distinction with some of the materials contained within this thesis. Addition of pores, either during or post-synthesis allows the overall surface area to be greatly increased. This technique is the only useful method for increasing surface area that also maintains practicality. A great deal of chemistry occurs at the boundary between phases, and so increasing the surface area in this way and allowing transport of gas or liquids into pores, thus porous materials are of great use to catalysis, gas storage and gas separation processes.

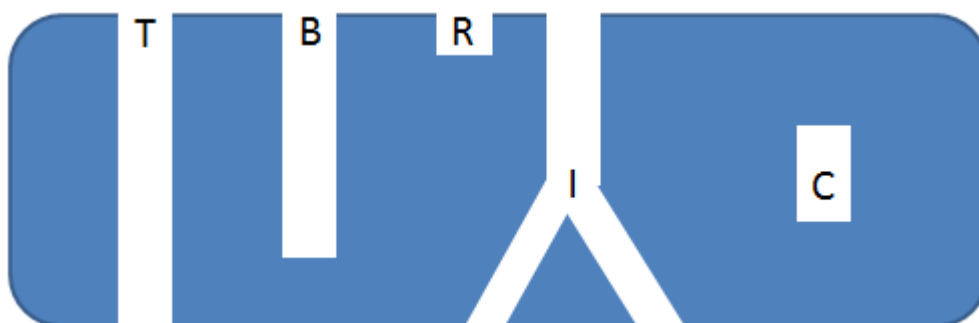


Figure 1 - Examples of porous solid featuring 5 different pore types. T represents transport pores, B – Blind pore, R – Surface roughness, I – Interconnected pore, C – Closed pores

Chapter 1 - Introduction

Figure 1 shows the 5 different pore types that exist within porous solids. Through pores, marked as “T” above, allow travel completely through the adsorbent allowing for gas adsorption to occur and also allowing transport to other regions of the material, and are important when considering applications in membrane technology. Blind pores are only open at one end, but gas adsorption may still occur if the internal surface area is suitable. R represents surface roughness, as the “pore” does not meet the IUPAC (the International Union of Pure and Applied Chemistry), requirement that it should be deeper than it is wide⁷. Interconnected pores can be formed where multiple pores meet, and can be made up of through and/or blind pores. Closed pores are voids within the adsorbent that have no connective pathway to the surface of the material and so are not accessible for the purpose of gas adsorption, though smaller gas molecules than used for analysis may be able to enter the pore.

Within this, the pores are also classified by entrance types⁸. Cylindrical pores are the same width at the opening as the main pore width. Funnel pores are considerably wider at the opening before closing toward the small pore width, while ink bottle pores feature a narrower opening relative to the main pore width.

IUPAC defines the standard classifications for both pores sizes and the isotherms of adsorption types⁸. Micropores are pores of 2nm or less. Mesopores fall within 2-50nm and macropores are greater than 50nm wide. Within this, it is not uncommon to split the micropore grouping into 3 sub-groups. Supermicropores have widths 1.4-2nm, micropores have width between 0.5-1.4nm and ultramicropores have a maximum width of 0.5nm. These descriptions allow a clear indication of pore size to be quickly inferred. The high porosity of MOFs makes them a material of key interest and the concept of using specific lengths of organic molecules to tune this pore size may allow MOFs to be tailored for their application allowing a more efficient material.

Chapter 1 - Introduction

Porous materials have been employed for years in applications involving gas storage and separation, as well as catalysis and have recently come into use as medical devices. Porous materials allow for substantially higher surface areas per unit mass and have landscapes more suitable to gas adsorption. The specific surface area ($\text{m}^2 \text{g}^{-1}$) of porous materials has increased vastly over recent years. For a long period of time Zeolite Y, discovered 1842, had the highest recorded surface area⁹, $904 \text{ m}^2 \text{ g}^{-1}$. In 1992, Mobil patented a number of mesoporous silica materials including MCM-41¹⁰ (Mobil Composition of Matter) with surface area usually around $1000 \text{ m}^2 \text{ g}^{-1}$. As carbon based materials were further examined, new disordered carbon structures with surface areas of up to $2030 \text{ m}^2 \text{ g}^{-1}$ were reported in 2001¹¹. However, the advent of metal organic frameworks has vastly increased the surface area beyond this. With early metal organic frameworks reaching $3000 \text{ m}^2 \text{ g}^{-1}$ (MOF-5) and more complex MOF materials allowing this to increase to $4500 \text{ m}^2 \text{ g}^{-1}$ for MOF-177⁹. Better understanding and alterations to synthesis techniques has since allowed the Langmuir surface area of MOF-177 to be increased to $6000 \text{ m}^2 \text{ g}^{-1}$ highlighting the benefits of a deeper understanding of process chemistry. Further work using computer modelling has suggested that the upper limit of surface areas of MOFs is likely to be $>14600 \text{ m}^2 \text{ g}^{-1}$, or greater¹.

Two main categories within porous materials can be formed: amorphous solids which do not show long range order and crystalline porous solids which do exhibit long range crystal order. Amorphous porous materials, such as carbon aerogels, lack this long range order and so the pore size distribution of the sample can be more varied. While this results in a reduced ability to tailor a material to a specific need, amorphous materials are often cheaper to produce than crystalline materials thus offsetting this requirement. Crystalline porous materials, such as zeolites and metal-organic frameworks, have a set of repeating structure and repeat syntheses will show very similar pore size distributions. The types of pores seen within these materials vary, including different sizes of pores, allowing it to have micropores, mesopores or macropores, with the possibility to form bi- or tri-modal materials

Chapter 1 - Introduction

with pores in more than one category. Zeolite materials are generally naturally occurring aluminosilicate materials and have been used greatly for applications for gas separation and catalysis. The pore size range of zeolites is limited by the nature of the bonding within the material, and often results in very small pore sizes resulting in specific molecules being physically too large to enter pores. For this reason, zeolite structures are often called “molecular sieves”. However, the total number of zeolite materials is limited to 206 by the underlying chemistry, limiting the usefulness of this material type compared to the number of MOFs which is almost limitless.

Porous Materials and nanotechnology are two of the fastest growing fields within chemistry, with the current market for nanotechnology being a multibillion dollar industry, with growth estimates putting it as a trillion dollar industry by 2015¹². Within this field, metal organic frameworks are one of the most promising compounds for future use.

1.2 Metal Organic Frameworks

Metal Organic Frameworks (MOFs), also known as coordination polymers have been known in the literature for many years with materials that could be described as MOFs published as early as the 1950s¹³ and 60s¹⁴, though this type of material has gone from a rarely researched material type to being a class of material of great interest within the scientific research community in the time since 1990. Metal organic frameworks (MOFs) are a crystalline compound consisting of a metal cation centre coordinating with organic ligands with two or more functional groups. The linear repetition of the metal centre bonding to ligand bonding to metal centre allows a variety of shapes of framework to be formed, with a cubic topology being very common, though more complex shapes are formed when introducing ligands with several functional groups.

Chapter 1 - Introduction

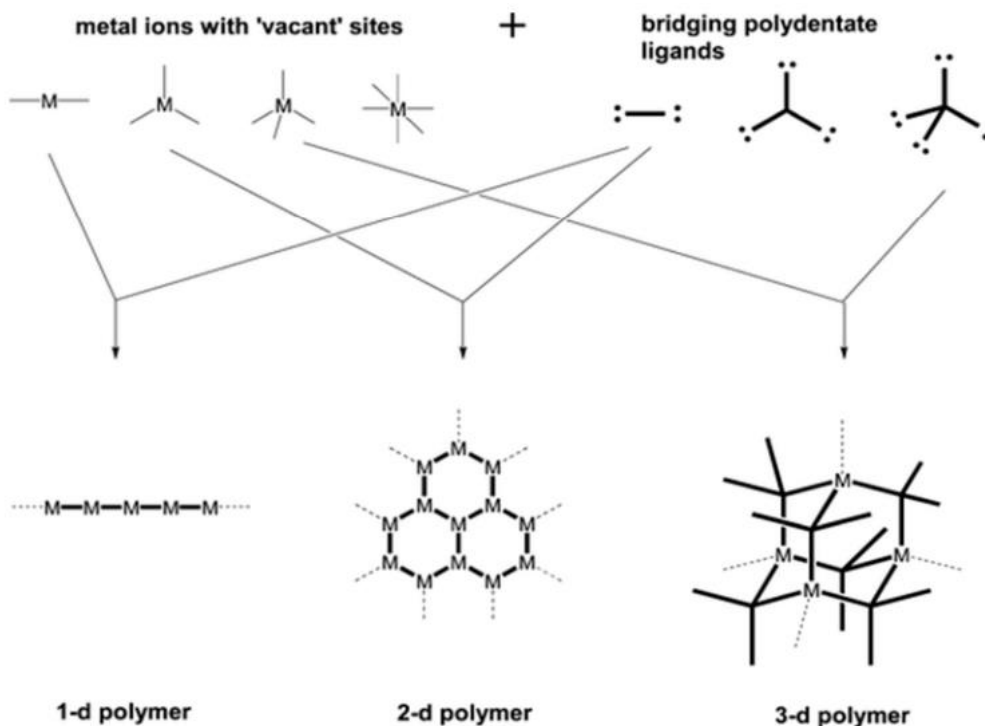


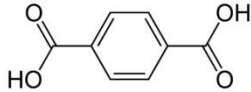
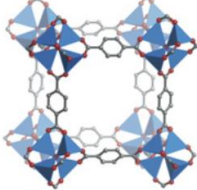
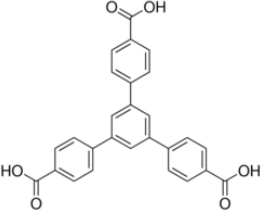
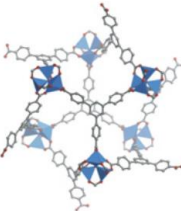
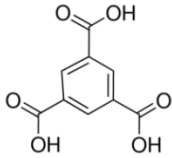
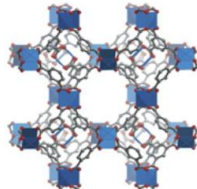
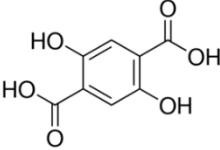
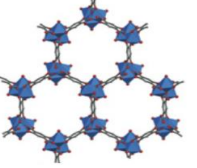
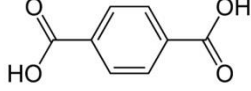
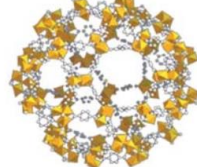
Figure 2 - Basic representation of MOF formation¹⁵. MOFs can be “built” from a wide variety of metal centres, and with polydentate ligands in order to form complex structures.

MOFs are of great interest due to several key features: firstly, supramolecular design of MOFs allows a number of organic ligands, with two or more functional groups, to be linked to metal ion coordination centres giving myriad variations, and tuneable properties in synthesized structures¹⁶. In Figure 2 this is shown, if the metal ion or complex metal cation is capable of coordinating three or more ligands then a 2D or 3D framework can be formed. Some real world examples of the metal centres and ligand groups used to form well characterised MOFs are shown in Table 1.

The scaffold-like nature of frameworks means almost no inaccessible ‘dead’ space within the structure, allowing gas storage applications to be taken further than would be possible by zeolites or activated carbon compounds¹⁷, and effectively introduced almost unlimited pore connectivity. Furthermore, potential for functionalizing MOF compounds, either during

Chapter 1 - Introduction

Table 1 - Selection of Unit Cells, Metal Centres and Ligand groups for 5 of the most commonly studied MOFs. Metal centres are shown via coloured polygons, with the ligand groups in grey.

Name	Metal Centre	Ligand Group	Unit Cell
MOF-5	Zn ₄ O		 18
MOF-177	Zn ₄ O		 18
HKUST-1	Cu-Cu Dimer		 18
MOF-74	Zn-Zn Dimer		 18
MIL-101	Cr-Cr Dimer		 19

synthesis or post-synthesis^{20,21} gives rise to a variety of potential uses for MOFs in a number of fields, including gas storage²², gas separation²³, catalysis²⁴ and medical devices²⁵. The generally high surface area, low density, uniform cavities, simple synthesis procedure, crystalline properties which allow identification unambiguously by x-ray diffraction make MOFs a very popular field¹⁶, with considerable growth in the research field as shown in Figure 3.

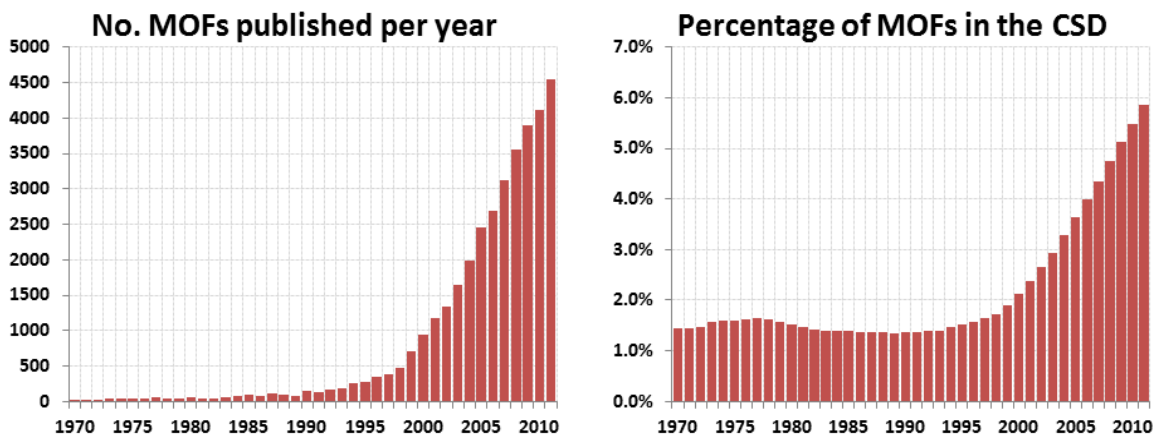


Figure 3 - Number of new MOF structures published per year, Percentage of all crystal structures in the Cambridge Crystal Database that are classified as MOFs²⁶, showing the increase in known MOF structures year on year.

Therefore MOFs exhibit a large degree of variability in metal ions or the complex metal centres and the ligand groups used. In theory, this should allow for a MOF to be designed for an application in order to produce a more efficient material. The ability of MOFs to tailor frameworks to the point of changing both pore structure and the surface chemistry is vital to the application of MOFs for gas adsorption. Selective gas adsorption, whereby one species is preferentially adsorbed in significantly higher quantity than other species present, can occur within these frameworks due to a number of effects. Steric reactions can result in the selective exclusion of molecules that are too large to enter pores. The surface chemistry can allow selective adsorbate-surface interactions, creating a landscape that will preferentially adsorb certain species. The rate of diffusion of different molecules can be dramatically different based on these parameters, potentially allowing for selective adsorption of specific species.

1.3 MOF Synthesis Methods

There are multiple different methodologies for producing metal-organic frameworks. Different synthesis routes can result in significantly different final properties of the material, and synthesis times for reactions can vary by orders of magnitude by changing the method of formation.

Table 2 - Comparison of key parameters of different synthesis techniques for formation of MOFs

Synthesis Method	Reaction Temperature (°C)	Reaction Duration	Energy Mechanism	Delivery
Solvothermal	80-300	10-48 h	Convection	
Microwave (Solvothermal)	50-300	30 seconds – 1h	Absorption of electromagnetic radiation	
Sonochemical	Ambient (bulk)	0.25 – 2 h	Cavitation	
Mechanochemical	Ambient	2h	Mechanical	
Slow Diffusion	Ambient	days	No external energy required	
Electrochemical	Ambient	<1 h	Electrical	

The synthesis of MOFs is most commonly completed using solvothermal methods. Solvothermal synthesis usually involves sealing the metal salt, the organic ligand and the solvent within a pressure vessel inside an autoclave and heating for extended periods of time, often 10-48 hours. In order to be classified as solvothermal synthesis, the reaction temperature must be greater than the boiling point of the solution, resulting in significantly elevated pressure within the reaction vessel. Hydrothermal synthesis is a subset of solvothermal synthesis wherein water is used as the solvent.

While microwave and sonochemical syntheses are generally technically solvothermal syntheses, the heating method is switched from traditional convective heating to either electromagnetic radiation (microwave) or the use of ultrasonic sound waves to heat the process. As microwaves and ultrasonic waves both interact in interesting ways with the solution, the time frame for these experiments can often be greatly reduced compared to equivalent processes using convective heating. Table 2 further highlights the potential

Chapter 1 - Introduction

benefits of microwave heating with the reaction times reduced by an order of magnitude or more in many cases.

However, these microwave methods require the solvent to be polar in order for the microwaves to couple with the solvent and so are not necessarily suitable for all syntheses.

Mechanochemical synthesis uses mechanical energy to provide the energy required to produce the MOF structure. Mechanochemical synthesis is often quoted as being solvent free synthesis, but often a small amount of solvent (compared to equivalent solvothermal synthetic routes) is added. This technique allows rapid production of MOFs with minimal solvent use, however this technique faces significant difficulties with scalability due to heat transfer issues at larger scale.

Slow Diffusion generally implies that the reaction mixture of solvent, metal salt and organic ligand has been sealed in a container with a reservoir of an amine based species that acts to catalyse the reaction. The bulk liquids are kept separate but are within the same atmosphere and so, over time, the volatile amines will evaporate and then diffuse into the reaction solvent allowing the MOF to form. This method is very slow compared to other methods, but also does not require outside energy to be input, often operating at ambient temperature.

Within all methodologies for MOF formation, the underlying mechanisms that drive the assembly of the framework is generally never elucidated upon, due to a stronger focus upon the final product and the application testing. In order to fully scale up a system the mechanism would need to be further probed in order to gain a more complete understanding of what is occurring within solution.

1.4 Applications of MOFs

1.4.1 Heterogeneous Catalysis

As MOFs have well defined pores with specific widths, they can be shape and/or size selective allowing for selective behaviour similar to those exhibited by zeolites to be used.

MOFs as materials for catalysis can be split into two approaches. The first approach is to use the MOF as a support material, with a catalytically active material immobilised within the pores of the MOF, usually by synthesizing the MOF then releasing the metal from a complex in a solution with the MOF already present. MOF-5 has been used for multiple catalytic reactions using multiple different metals supported, a selection of which are shown below in Table 3.

Table 3 - Selection of metals with catalytic activity supported on MOF-5 and the reactions that can be carried out using this technique

Metal Supported	Type of Reaction	Reference
Palladium	Hydrogenation (Cyclooctene + H ₂)	27
	Hydrogenation (Styrene + H ₂)	27
	Hydrogenation (Ethyl Cinnamate + H ₂)	28
	Sonogashira coupling (Cyclooctene + H ₂)	29
Copper	Methanol Synthesis from Syngas	30
Ruthenium	Oxidation of Benzyl Alcohol	30

In the second approach, the MOF itself can also contain catalytically active metal centres or have ligands with functional groups, or featuring aromatics allowing for functional activity and therefore require no further modification before usage. HKUST-1, for example, has shown catalytic activity for a number of reactions without addition of any other catalytically active material to the pores, or any post-synthetic modification.

Chapter 1 - Introduction

Table 4 - Selection of reactions catalysed using unaltered HKUST-1 as a catalyst

Reaction	Reference
Cyanosilylation (Benzaldehyde + Cyanotrimethylsilane)	31
Isomerisation of α -Pinene	32
Cyclisation or Citronellal	
Rearrangement of α -Pinene	

However, MOFs for use of catalysis requires very careful selection of the MOF to be used due to the thermal and chemical stability of MOFs and the reaction conditions, such as temperature, pressure and pH required for catalysis.

Further, as many catalytic reactions require very fine control of input composition, water is often removed from inputs prior to reaction, mitigating any extra costs incurred from having a non-water stable MOF material used.

1.4.2 Gas Storage and Separation

1.4.2.1 Hydrogen Storage

Due to the limited supply of fossil fuels remaining, and the effect that combustion of fossil fuels for energy consumption has on the environment, hydrogen is suggested to be one of the possible fuel sources of the future. Hydrogen is abundant, has an energy density greater than petrol (142 and 47 MJ kg⁻¹ respectively³³) and importantly does not produce CO₂ or other greenhouse gases when combusted. However, for applications where portability is an issue it is easier to store petrol due to being a liquid at room temperature. Hydrogen could be stored in high pressure tanks, or via cryogenic liquefaction but both methods would require heavy equipment and, in the case of cryogenic liquefaction, significant energy input. Further, this represents a potential hazard especially when considered for the automobile industry due to relatively high energy crashes being a prominent risk. Physisorption of hydrogen onto porous materials, such as MOFs may allow these conditions to be moved towards ambient conditions with the United States Department of Energy (US DOE) setting a target of storage

Chapter 1 - Introduction

of 6wt% and 45 g L^{-1} at temperatures within the range -30 to 50°C , operating at pressures under 100bar. This allows for the material to operate within safer conditions, sets the mass of hydrogen relative to the storage material and also sets the minimum energy density required.

Storage of H_2 using MOFs has been of particular interest after MOF-5 was synthesized in 1999. MOF-5 has very high surface area and significant hydrogen uptake³⁴, suggesting that MOFs as a material may have applications within this area.

However, as of 2014, no materials have been produced that are capable of meeting the US DOE targets for H_2 storage. As with surface areas of reported MOFs, the hydrogen uptake varies amongst reports due to the correlation between surface area and uptake³⁵. Selected reported uptakes of hydrogen storage using MOF-5 are reported below in Table 5.

Table 5 - Selection of reported Hydrogen storage capacity at different temperature and pressures for MOF-5

wt% H_2	Temperature (K)	Pressure (bar)	Reference
4.5	78	0.8	34b
1	298	20	34b
1.32	77	1.01	34a
1.51	77	1.31	34c
5.09	77	100	34d

Part of the reason MOFs are touted as one of the potential hydrogen storage methods that could meet the US DOE targets is due to the nature of adsorption of hydrogen onto the internal surfaces of the MOF with the ligands and any exposed metal centres within the cations bonding with the hydrogen.

Larger linkers have higher binding energies and allow binding of hydrogen on both sides of the organic linker. By adding in additional functionality to the ligand, the binding energy can be manipulated³⁶. For example, terephthalic acid as ligand having binding energy of 4.16 kJ mol^{-1} , by adding an $-\text{NH}_2$ group to molecule will increase this binding energy to 4.72 kJ mol^{-1} .

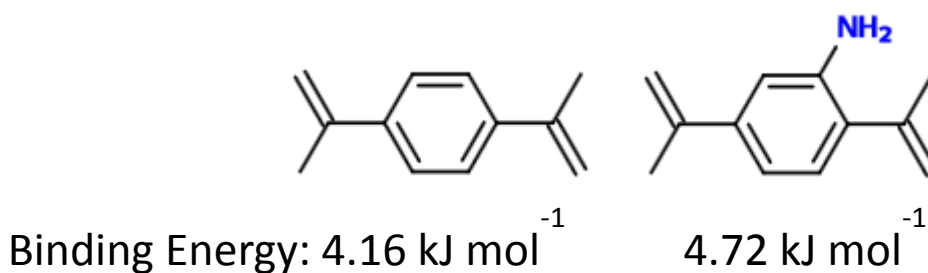


Figure 4 – Comparison of H₂ binding energies of two ligands with similar structures

Metal centres, such as the Zn₄O metal centre of the MOF-5, and the IRMOF series, has been calculated to have higher binding energies than the ligand groups³⁶ and altering the metal centre, even without alteration of ligand will alter the binding energy to the metal site considerably as d-orbitals interact with the antibonding orbital of hydrogen, resulting in a stabilisation of the bonding between the hydrogen and the metal. Surface area of the MOF material is also shown to scale linearly with the hydrogen uptake, and so further reinforces the importance of maximising the surface area of the MOF material^{34d}.

1.4.2.2 Carbon Capture and Storage

Due to the major environmental concern about climate change caused by the increasing concentrations of greenhouse gases present atmospherically, carbon capture and storage has increasingly been a key field with strong links to chemistry and chemical engineering. The concentrations of these gases have been increasing year on year since the industrial revolution began. For instance CO₂ concentration has risen from <300 ppm in the pre-industrial era to approximately 400ppm in 2015. CO₂ represents the largest cause of the increase in temperature and so increasingly the concept of carbon capture and storage (CCS) is being applied. Current technologies, known as “amine scrubbing”, often use liquid sorbents such as amines which react with CO₂ to form carbamates and can be used to selectively remove CO₂ from a vapour stream in a process. However, as the amines require

Chapter 1 - Introduction

regeneration and are usually dissolved in large quantities of water which must also be heated, this involves a significant energy cost, often around 30% of a power stations output may be used to capture this CO₂ and regenerate the sorbents³⁷, and this technology is not yet widespread. Traditional solid sorbents include calcium oxide (CaO) which will bond selectively with the CO₂ in order to produce CaCO₃. As this method does not require heating solvents as well as providing the energy required to regenerate the material, the associated energy cost is considerably lower than with amine scrubbing technology. As both these CCS methods require chemisorption to store CO₂, switching to a material where CO₂ would selectively be undergoing physisorption onto a material would result in reducing this energy penalty more significantly.

One of the core reasons MOFs are suggested for CCS over activated carbons and zeolites is the considerably larger surface areas present within many MOFs. As such, a number of key criteria have been suggested in order for a MOF material to be suitable for CCS³⁸.

Firstly, stability of the MOF is required. The vapour stream output of a coal gas plant, for instance, will generally feature N₂, O₂, CO₂ and H₂O in significant quantities at elevated temperatures. The system is also likely to require elevated pressure. Therefore it is essential that the MOF material is stable when exposed to these compounds, can survive the thermal effects and has mechanical strength sufficient to not undergo collapse. Long term stability must be considered. Any material being used for CCS on an industrial scale will be exposed to many cycles of pressure, thermal treatment and adsorption-desorption.

Secondly, selectivity of CO₂ is required. Without sufficient selectivity, the other components of the stream will be adsorbed in sufficient quantities to render the process overly inefficient. CO₂/N₂ selectivity is vitally important as N₂ is likely to be the component with the highest partial pressure in the vapour stream, with approximately 10-15% CO₂, though as high as 30% for some processes³⁹.

Chapter 1 - Introduction

Cost of materials is a final consideration. In order for the process to be economically viable, the cost of generating MOFs for CCS would need to be sufficiently low. As most MOFs are currently produced at small scale in batch processes this is an issue for the potential application of MOFs for CCS. Developing scaled up process, continuous processes and increasing the overall efficiency of MOF production would be required before MOFs could be widely used for CCS.

Many MOFs have been screened for their ability for use in CCS. As described above, high surface area alone is insufficient for a MOF to be applicable. MOF-5 and MOF-177 have high surface areas (generally > 3000 and $4500 \text{ m}^2 \text{ g}^{-1}$ respectively) and have excelled at a number of potential applications but show very little CO_2 uptake compared to other MOFs and also are known to breakdown in the presence of water^{34c, 40}, which would constitute part of the flue gas stream. The CO_2 uptake of a selection of commonly synthesised MOFs is shown below in Figure 5⁴¹.

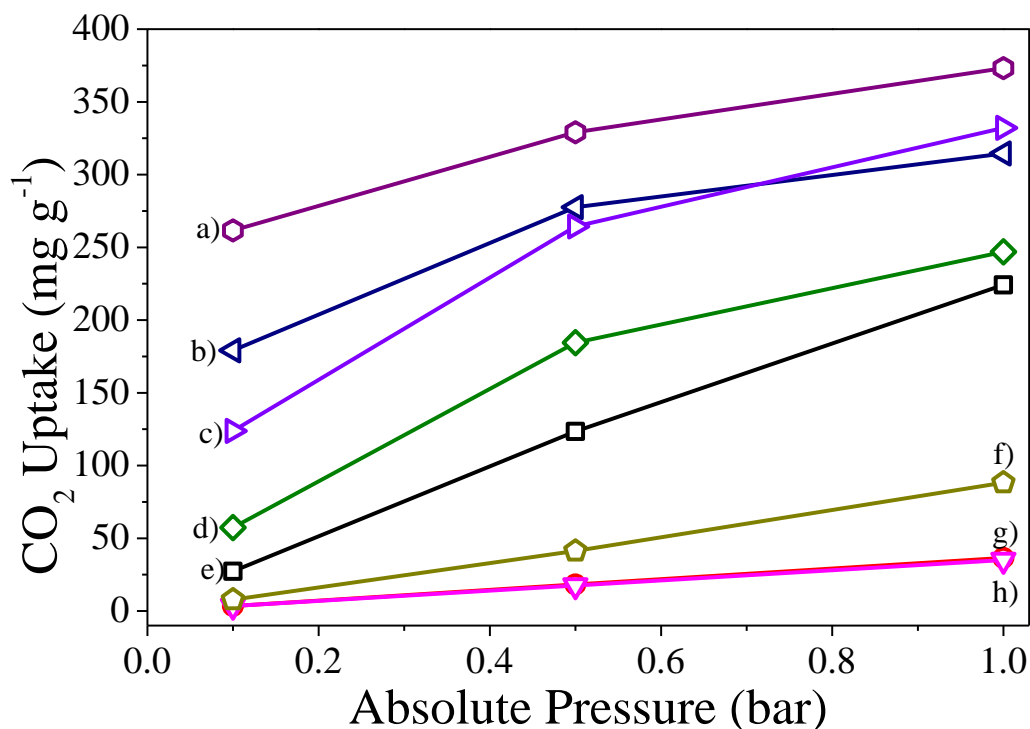


Figure 5 - CO₂ uptake of various MOFs at 293-298K⁴¹. a) Mg-MOF-74, b) Ni-MOF-74, c) Co-MOF-74, d) Zn-MOF-74, e) HKUST-1, f) MIL-47, g) MOF-5 (Circles), h) MOF-177 (Triangles).

This highlights the importance of MOF chemistry and tailoring materials to a purpose. MOF-74 was screened in a number of homologues showing considerably different CO₂ uptake with Zn-MOF-74 having adsorbed only 22% of the CO₂ per gram that Mg-MOF-74 would under the same conditions.

1.4.4.3 Alternative to Cryodistillation

Current methods of separating short chain hydrocarbons generally used for fuel require use of cryodistillation to separate different species in order to obtain a reasonably high purity of a single species. However, cryodistillation requires cooling to temperatures as low as 110K, while operating at high pressures. This results in high capital, operating and maintenance costs for the unit operation. As this is a potential market for MOF applications at an

Chapter 1 - Introduction

industrial scale, it is important to confirm that adsorption onto a MOF, in order to separate different gaseous species, is commercially viable. The cost for this process must be lower than the cryodistillation process by a large enough margin that a business would be likely to pay the capital costs in order to alter the plant and use MOFs rather than cryodistillation.

Based upon the figures given by Solgado *et al.* based on an input stream of 75% propylene and 25% propane, to achieve a purity of 99.5% propylene would require energy input of 7.665 GJ/tonne of product. Due to the temperatures and pressures involved, this operation would also have significant capital and maintenance costs, however, we will simply be comparing the energy costs as a qualitative measure. However, it may be difficult to reach the same levels of purity with MOF based separation with 80-90% being a more reasonable outcome, though multiple stages could be used to increase this separation value without greatly increasing the cost. This reduces the energy cost per tonne of propylene drastically when switching from cryodistillation to MOF based separation. For an average sized plant, producing 200,000 tonnes of propylene per year this would alter the energy cost from £51 million to around £70,000. The main reason for the drastic reduction in cost is the much closer to ambient conditions used for the MOF separation process, resulting in a reduced energy cost but also will have a knock on effect upon the maintenance costs. As such, MOFs do represent a significant area of interest in replacing the cryodistillation techniques that have been employed for the last 70 years⁴².

1.5 Issues with MOFs

1.5.1 Interpenetration

The synthesis of porous metal organic frameworks often relies upon the occupation of pores by solvent molecules while the MOF structure is formed. However, as the organic linkers increase in length or the concentration of the MOF precursor increases it becomes

Chapter 1 - Introduction

increasingly likely that lattices will form within other lattices. For example, the interpenetrated and non-interpenetrated MOF-5 structures are shown below.

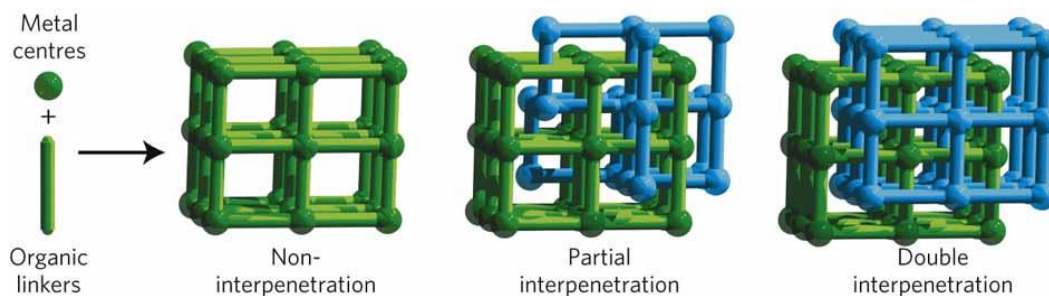


Figure 6 - Simplified version of an interpenetrated cubic MOF structure. From Yang *et al.*⁴³

The first framework will form with a metal cation or ligand present within its voids. This unreacted species will then begin to form the MOF network resulting in a second crystal structure forming interwoven through the first. Importantly, these two structures are independent and do not interact beyond this. The occupation of the pores with other sections of framework is due to the inability to remove the interpenetrating framework without destroying the entire MOF material. As such, in the above diagram to remove the blue framework one would also need to destroy the green framework. The total pore volume of the material is greatly reduced due to the partial filling of voids within the MOF structure. However, this reduction in channel diameter could allow for desirable gas adsorption features⁴⁴. While this could potentially be exploited⁴⁵, interpenetration is generally not a sought after occurrence and generally occurs when solutions are overly concentrated or the nucleation of crystals is too fast compared to growth. This presents a potential issue with scale up. Interpenetration generally reduces the available surface area of the MOF, resulting in a less desirable product. However, due to the expense of solvent purchase and heating costs, running at a high concentration is also desirable.

Chapter 1 - Introduction

Along with interpenetration, which affects MOFs of specific topologies alone, surface area reduction in MOFs is also considered to be due to the presence of a number of unreacted partially formed sections of the framework, including metal ions and unreacted ligand. This is likely to affect a wider variety of MOFs and is likely to become more severe with higher concentrations⁴⁶.

1.5.2 Chemical and Thermal Stability

A large number of MOFs exhibit thermal stability up to around 400 °C⁴⁷, though some have been shown to remain intact up to temperatures of around 500 °C⁴⁸. Thermal stability of MOFs is an important factor when considering the potential applications. Some catalytic reactions, where MOFs may act as either a support for catalytic material or act as the catalyst themselves as detailed in Chapter 1.4.1 may require sufficiently high temperatures as to exclude MOFs from being a possible selection.

Chemical stability is also an issue as many applications of MOFs would require exposure to chemicals which can result in the breakdown of the framework. Water is prevalent in a multitude of applications and represents one common chemical that has stability issues within MOFs. For many MOFs, water represents an issue to the stability long term due to the lability of the ligand groups. The bonding energy between the metal centre and ligands plays a further role, with the bonding energy often being sufficiently low that water, or other nucleophilic species can undergo a substitution at this location, effectively destroying the framework. Many MOFs, including MOF-5, MOF-177 and the IRMOF series are built upon the Zn_4O^{6+} complex cation bonded to carboxylate function linkers^{18, 49}. Due to the d^{10} electron configuration, this bonding does not feature and ligand field stabilisation⁵⁰, therefore the bulk of substitution reactions that can disrupt the framework bonding are only prevented by any steric factor. However, many other metal centres, such as the Cu^{2+} dimer formation that makes up many cupric MOFs, features a d^9 electron configuration. In turn, these materials will show ligand field stabilisation and therefore nucleophilic substitution is less

Chapter 1 - Introduction

favourable⁵⁰. HKUST-1 has the Cu-Cu dimer metal centre described and, while highly adsorbent of water from the air does not undergo any structural changes, and is often said to be stable in humid air. However, sufficiently high concentrations of water, such as submersing the powder in water⁵¹ or exposing the sample to water vapour at elevated temperatures will result in irreversible breakdown of the material⁵². Other MOFs, including the MIL (named Matériel Institut Lavoisier for the institution that first synthesized them) series based around Cr²⁺, show no breakdown even when exposed to water in the ways described above⁵¹. Stability of MOFs is a serious issue for any material and due to the wide variety in operating conditions for potential MOF applications, the MOF would need to be chosen with all components and conditions in mind ahead of time on a case by case basis.

1.6 Scale Up

1.6.1 Importance and Difficulties of scale up

As outlined earlier in Chapter 1, MOFs offer a wide range of desirable properties and show promise in a number of applications. However, MOFs are not used on an industrial scale yet because they are not available at larger scale required for industrial testing because they are not used leading to a circular problem.

The importance of scale up can be highlighted in two main ways. Firstly, for any material to be used at large scale it must be produced at large scale. While laboratory syntheses can produce materials, the overall output is likely to be insufficient relative to requirements for industrial processes. Another important aspect of scale up is the cost of the final product, which is impacted directly by the capital costs of the plant. The capital costs rarely are shown to be linearly related to capacity, with the general relationship between capacity and capital costs being given by Equation 1.

Chapter 1 - Introduction

Equation 1 - Estimation of capital cost variance with capacity⁵³.

$$C_2 = C_1 \left(\frac{S_2}{S_1} \right)^n$$

When C represents the capital cost for given S, the operating capacity. The value of n is often given as 0.6, however, this serves only as an approximation and should only be used when insufficient data is available to adequately calculate the true costs with scale. Further, it does not appear as if any values for specific MOFs or MOFs in general have been published due to the lack of research in producing MOFs at large scale, however for any value of $n < 1$, capital costs will be proportionately reduced when scaling up.

Further, the bulk of the processes described in the literature for MOFs are small scale batch reactions, usually of scale < 50 ml of solution. While MOFs have properties and applications discussed above that are likely to be of significant use for many industrial processes, the lack of scalability within these processes is an issue. Developing current MOF technologies to show scalability, increased efficiency and, where possible, the switch to continuous flow are all likely to add value to MOFs. In order to scale up efficiently, it may be imperative to switch from use of batch synthesis to continuous synthesis. The choice between continuous and batch production is not necessarily definitive, however the following guides are suggested⁵³:

Continuous Production	Batch Production
High production rate	Low production rate
Single reaction	A range of reactions
Fouling issues a major issue	Fouling considerably less of an issue
Good catalyst life (where applicable)	Shorter catalysts lifespan
Proven process design	Uncertain design
Established market	Less requirement for an established market

Chapter 1 - Introduction

More expensive process	Cheaper process
Fine quality control at steady state	Batch production may lead to variations between batches

However, while in theory a batch system can be scaled up to any size, batch processing has a number of potential drawbacks such as the required downtime per cycle and the potential for large variations between batches. The limitations of batch systems can be avoided by making the switch to continuous processing. Continuous processing represents a number of advantages such as theoretically no downtime and improved quality control at steady state conditions. However, continuous processes also require a more complex, specialised design reducing versatility of the equipment while increasing capital costs, whereas a batch system is more easily adapted to altering the process suitability⁵³. For specialised plants, it is expected that both scale up and the switch from batch to continuous processing would allow for the most cost-efficient production at the long term. Therefore it is important to consider scale up and continuous processing together.

However, scale up of a chemical process must consider not only the safe scale up but also a number of issues related to the underlying process chemistry that may not scale linearly and must be considered for a cost-effective, efficient scale up.

Table 6 - Some difficulties in scale up reproduced from Industrial Process Scale-up⁵⁴.

Critical Scale-Up Factor	Potential Risks
Residence Time Distribution (RTD)	In scale-up often the RTD is affected by fast large scale eddies which may cause shortcut flow and more back-mixing. In reactors it may cause less conversion and more by-product formation. In separations it may cause poorer selectivity.
Mixing	Mixing velocity reduces with scale-up and for some reaction types it may reduce selectivity.
Mass transfer	Mass transfer across interfaces can be slower with scale-up, due to areas of low turbulent intensity causing bubble or droplet coalescence.
Heat transfer	Heat transfer rates at scale-up can be lower due to lower specific surface area.

1.6.2 Steps in Scale-Up

Therefore to scale up a reaction process in a manner that is both safe and efficient the following parameters are important to consider.

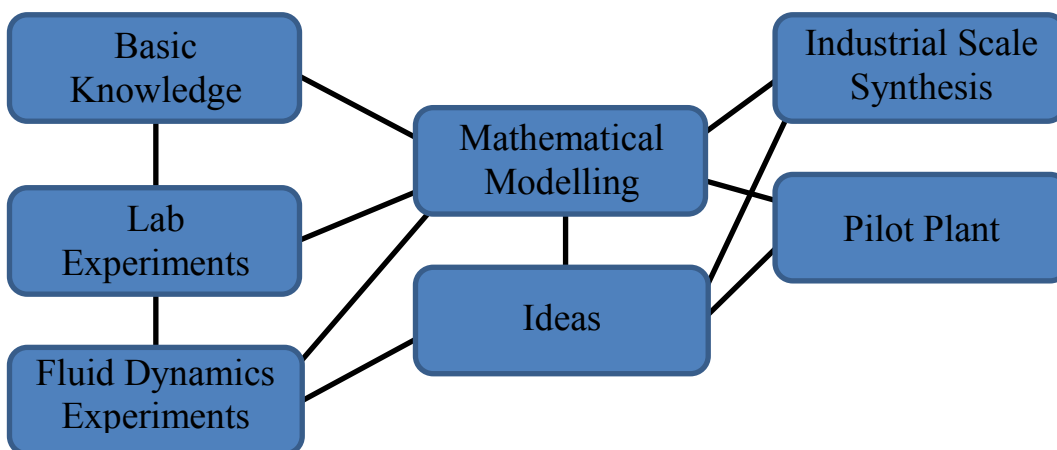


Figure 7 - Key elements in developing a large scale process, recreated from Donati and Paludetto⁵⁵

Figure 7 highlights the key steps in scale up and how these steps interact with each other. For this project, we mainly focus upon the “Basic Knowledge” and “Lab Experiments” steps. Initially it is important to have a basic understanding of the chemical process. Laboratory experiments and review of published syntheses for the target phase may allow insight into the effect of certain reaction parameters and ideal operating conditions (Chapter 5). For complex crystallisations, this may also allow insight into the subtleties of the formation mechanisms (Chapters 5 & 7). Scale up must be predictable in order to anticipate potential problems, requiring a deeper understanding of the synthesis process before large scale synthesis should be considered. Understanding the key reaction parameters is vital to efficient scale up. Exploration of the best reaction parameters including, but not limited to, reaction duration, temperature and reactant compositions should be determined at small scale, although it is possible for reaction conditions to be significantly altered with scale.

Chapter 1 - Introduction

Understanding the effects of deviating from the perceived optimum reaction parameters will allow for operating closer to the ideal conditions for production of the intended material.

After determination of the reaction parameters, a mini-plant is often considered the next step⁵⁶ with a typical scale usually less than 0.1 kg h^{-1} of production. At this point, the knowledge gained via the initial lab experiments can be used to attempt to develop a continuous process. The scale considered here is likely of similar scale to any experiments carried out in previous steps. This allows for trouble shooting of reaction conditions when considering the implications of flow chemistry. Further, this serves as a proof of concept for further continuous processing to be considered. Again, of importance here is understanding the underlying process chemistry; residence time distributions and the quality of the product output are of vital importance and the steady state conditions of the reaction system. When considering a continuous process it is also important to understand the effects of flow upon the system. Flow can alter the formation of many crystalline materials, although very little has been published concerning the effect of flow upon metal organic frameworks. However, this is beyond the scope of the current project. This may have significant impact upon the ability to form high quality MOFs under flow conditions. Optimisation and understanding at this scale allows for a more cost effective scale up, limiting waste and raw material cost while providing useful information for the scale up process. Although it is unlikely that the process parameters and costs will scale linearly to larger scales, at this point economic analyses should be carried out in order to determine if the process is viable for scale up.

The next step in the scale up of a process is likely to be modelling of the chemical parameters as well as the physical properties of the equipment used in order to fully understand the larger scale process. This allows a more complex and deeper understanding of a number of important parameters, including physical rates, mixing issues and the underlying thermodynamics. Understanding the effects of flow and mixing more completely

Chapter 1 - Introduction

will allow for minimal waste and preventing equipment issues, such as non-optimal design or issues with reactor construction at large scale.

After iterations of the previous steps in order to gain deeper understanding, if the process is considered economically viable and analyses have shown no other major issues with scale up of the syntheses, the next step is likely to be development of a pilot plant⁵⁷. A pilot plant can be skipped, however generally it is considered too great a risk to do so unless all unit operations are already known, applied and understood at industrial scale, no novel techniques have been used, compositions of all feed stocks are known and accounted for and a complex recycle flow is not required⁵⁷. If any of these criteria are required, a pilot plant is likely to be used as an intermediary between lab-scale and industrial scale. As MOF formation at large scale is a novel process, this step would be required. Pilot plant is large scale relative to lab scale but is unlikely to be at the scale intended for full scale industrial production. As the full feasibility of the system is not yet known, this serves to reduce the capital costs at this stage therefore reducing the financial risk undertaken⁵⁶. This allows testing of the materials and construction of any custom made vessels. Further optimisation may be considered here also allowing for more useful information to be gained about the effect of the process at large scale and any mathematical models applied to be tested for accuracy with scale. When optimisation and modelling of this scale are completed and the economics considered, the final step is the design and construction of a full scale plant⁵⁶.

1.6.3 Issues at large scale

A number of potential issues arise when considering the transition from small scale laboratory reactions to large scale processing of a material. Failure to properly account for various reaction parameters may lead to the failure to create the targeted product, or in a worst case scenario may lead to runaway reactions or over pressurisation of the system

Chapter 1 - Introduction

resulting in catastrophic results such as fatalities, property and environmental damage and severe business ramifications⁵⁸.

Feed stocks also represent an issue when considering scale. Reactions at a small, laboratory scale often use high purity chemicals, with purity of chemicals quoted in many scientific publications, whereas this high degree of purity adds considerable cost when scaled up as large scale bulk chemicals are often significantly cheaper but lack the very high degree of purity. The lower concentration of unwanted components in the feed at small scale results in any issues with synthesis due to impurities being masked and is unlikely to be seen until chemicals of lower purity are studied. The presence of greater concentrations of species unwanted for the reaction process at large scale may inhibit formation of the target phase, cause side reactions or cause other alternative side effects.

Heat transfer issues must also be accounted for when scaling up. Heat transfer issues can not only affect the operating conditions of the reactor, but may also be a significant safety issue. When dealing with a large bulk volume, large temperature variations may occur without appropriate mixing. The effect of small temperature changes can shift the equilibrium point of reactions and may result in significant alterations to the final product, deviating from conditions considered optimal. Reactive heat issues also present a potential concern. At small scale, energy output from reactions can be harder to observe, due to the relatively small amount of energy output due to the scale⁵⁹. Further, the surface area available to output the heat relative to the reactive volume is considerably greater at small scale via the Square-Cube law. These effects, for most reactions, are unlikely to be seen at small scale and are likely to require scale up to pilot plant scale before they become evident.

Mass transfer issues can also result in significant changes to the final product and are often related to heat transfer issues due to the role of mixing in both. Without well mixed solutions, concentration gradients within solution can often occur, which can result in

Chapter 1 - Introduction

alteration to the equilibrium of the solution altering the phases produced from the targeted phase to alternative phases, or lead to damaging build-up of certain reaction components.

When considering MOF chemistry, concentration gradients may have significant effect upon process quality with high concentration of reactants likely to result in interpenetration, as detailed in Chapter 1.5.1.

Flammability issues must also be considered at large scale. For instance, many metal-organic framework materials have syntheses involving the presence of metal salts, including nitrates, which can present a possible issue due to their explosive potential if not handled correctly.

Further storage of bulk chemicals at such large scales can represent a significant issue. Due to the requirement to have sufficient supply to counter fluctuations and interruptions to supply, these chemicals often have to be stored in very large quantities often representing days-weeks' worth of supply⁵³. As such, due care must be taken to safely store chemicals.

When considering reactions involving these species, care must be taken to prevent the flammability of these chemicals presenting a greater safety issue. Toxicity and handling issues present a risk at all stages of process development; though scale up increases these risks. It is important to have accounted for any toxic by-products and any environmental or health implications of contact or release of species involved in synthesis.

Design issues with materials and shapes may become more evident at larger scales⁵⁴. The complex understanding and modelling of systems should allow for reactor shape issues to be accounted for before synthesis as outlined previously. Corrosion is of particular issue also, especially in MOF chemistry which can include chloride salts which represents a common corrosive. Fouling may not be apparent in small scale syntheses due to the time it can take to become an issue. At large scale this may embody a significant risk to the process.

The waste products of process may also signify a significant issue when scaling up processes. At small scale, most waste products can be disposed of relatively easily. At larger

Chapter 1 - Introduction

scales, disposal or storage of these unwanted waste products may represent a significant safety issue, or otherwise be an issue that prevents scale up.

1.6.4 Key parameters to consider when scaling up

When considering scale up a number of factors are important to the final product being suitable for scale up.

The raw material costs are of vital importance and will represent one of the largest costs in most processes. At this point, it is also important to know if the process itself requires breakdown of the solvent and also the potential recycling costs for any unreacted raw materials or solvent must be considered⁵³.

The space-time yield (STY) allows direct comparison of synthesis methods giving the dry yield of the material in terms of time and volume of reactor used, usually quoted in units of $\text{kg m}^{-3} \text{ day}^{-1}$. However, as the materials produced here are porous materials and the surface area of the final product will often vary by synthesis method therefore we introduce a number of metrics involving the total surface area production per m^3 of reactor space based upon the average surface area of samples produced and the dry yield. This allows for a more accurate description of the material being produced. Running at a very high solid concentration may allow for a very high STY but will usually cause issues with interpenetration of the metal-organic framework formed. We have also considered the overall surface area produced by a system as a comparison, derived from the average Langmuir SSA and the STY of the product. While this allows comparison of the useful surface area of the material, this metric is used in conjunction with others to provide an overview of the system. Further, though this quantitatively represents the total production of a system, it is important to consider that the exceptionally high surface areas of MOF materials tend to be one of the key targets of production. When considering convention

Chapter 1 - Introduction

process intensification, it seems likely that the reduction in production cost per gram of MOF would also result in a reduction in surface area. A significant drop in surface area is likely to bring the available surface area of the material in line with more commonly used, cheaper materials. Also of vital importance is the comparison of surface area per unit cost. Though this value can only be approximated, this also provides useful information on the viability of the process. As such, several metrics of measuring the costs and economic analysis are based upon estimates but are vital when considering the potential viability of scale up.

Operating conditions of reactor must also be considered as operating at high temperatures or pressures can add significant cost to a project. Along with this, understanding the underlying process chemistry may allow for optimisation and improvement of the system, resulting in a more efficient system⁵³.

When considering scale-up, the importance of continuous processing is also highlighted. By operating a continuous reaction system over a traditional batch system, it is likely that the system will produce higher output per unit time and, in theory, could have zero downtime. However, the most interesting application of continuous manufacture applied to MOFs is that when the reactor reaches steady state the output of the system should be more consistent than equivalent batch process and therefore a product would likely be formed without the inconsistent properties that may be associated with the batch process. The capital cost and design complexity of continuous processing is increased compared to batch systems but the benefits in output can outweigh this issue, allowing greater economic viability.⁶⁰

The solvent required is also of vital importance. Environmental concerns, the ability to easily, and efficiently recycle solvent and the costs and environmental impact of disposing of any broken down solvent will result in changes to the process.

Washing, drying and activation processes for the MOF must also be considered. Washing allows removal of unreacted ligand and will generally increase the porosity per unit mass.

Chapter 1 - Introduction

The material must then be separated from the solvent and dried and activated. Activation generally requires heating at elevated temperature and pressure close to vacuum and so the requirements for energy and capital costs for these projects will vary with the exact conditions required.

1.7 Aims and Scope

The aims of the project can be considered as follows.

Firstly, we aim to select established metal-organic frameworks from the literature as a basis for our project. As we aim to produce continuous processing systems, selection of the “best” MOF or the MOF with the best performance in a given application is less important than serving as a model system. For this reason, we selected MOF-5 and HKUST-1 due to representing relatively simple cubic crystal structures, two of the most common metal ions (Zn and Cu respectively) used in MOF synthesis and the large number of publications surrounding batch syntheses of both materials. This serves to allow us to survey literature in order to attempt to determine the optimal reaction parameters ahead of synthesis and also allows a wide range of reported syntheses to contrast and compare results again.

For selected metal-organic frameworks we wish to establish and develop a reliable synthesis method that can serve as the basis to scale up a reaction. Due to the complexity of the field, the scope does not allow for synthesis of a new MOF or a MOF with limited characterisation within the literature as comparison of our materials to reported syntheses is a key metric for consideration. This includes optimisation of parameters as well as building a deeper understanding of the underlying reaction chemistry occurring. As such, we also have interest in determining the formation mechanisms of the MOFs analysed as well as gaining any insights into kinetics. However, due to the underlying mechanisms of formation and the likelihood of metastable compounds being produced, it is beyond the scope of this project to attempt to completely characterise these compounds.

Chapter 1 - Introduction

We then aim to scale these systems up to a larger scale, though still “bench scale” while creating a continuous synthesis system for these MOFs. These systems must then be optimised and the procedure of process intensification must be considered in order to fully determine the potential benefits of this. Further, due to the core aim considering the production of materials at scale, we must consider more parameters than simply the surface area of the material and the phase purity. Continuation of the scale up process beyond this point is also out with the scope of the project.

As microwave heating techniques have shown promise within this field of chemistry, we also aim to develop continuous production systems for these MOFs to exploit any benefits this heating technique can bring us.

Based on the data collected during synthesis, we also aim to complete brief, provisional analyses as to the feasibility of producing these MOFs at scale.

In order to meet these aims, we also require to completely characterise the materials produced in a number of ways and carry out a variety of other analyses upon each system to provide metrics for comparison.

Chapter 2 – Background and Literature Reviews

2.1 MOF-5 background

Within the family of MOFs, we have selected two MOF materials to focus on – one of which is MOF-5, a zinc based MOF with structure $Zn_4O(BDC)_3$ where BDC represents the organic ligand benzene dicarboxylate. MOF-5, first synthesized in 1999 by Yaghi *et al.*⁴⁹, is probably the most studied MOF with numerous publications concerning its properties and applications. MOF-5 is chosen here due to its wide range of properties allowing it to be used in a huge variety of processes. The synthesis process however, has never been analysed in depth hence large inconsistency in its processing appears in the literature, e.g., significant variations in several key parameters, including reaction time and temperature. MOF-5 has a surface area generally ranging from 800 – 3200 m²/g⁶¹. Interestingly, some MOFs are known to show negative thermal expansion, due to the way the organic ligand groups bend and twist when heated⁶². The overall chemical reaction for formation of MOF-5 using zinc nitrate is as follows: $Zn(NO_3)_2 \cdot xH_2O + 3 H_2BDC \rightarrow Zn_4O(BDC)_3 + 8 HNO_3 + 15H_2O$.

2.2 MOF-5 Synthetic Routes

MOF-5 has been synthesized using a number of methodologies including single step solvothermal^{34c}, two-step solvothermal⁶³, microwave assisted solvothermal⁶⁴, ultrasonic solvothermal synthesis⁶⁵ and diffusion methodology⁴⁹. Analysis of the benefits of each synthesis technique is required to provide the basis for our experiment, as well as consideration for scale up and continuous operation of each method.

The synthesis routes shown below represent the highest surface area produced by each of the synthesis routes. Solvothermal without addition of base or surfactant has the highest recorded BET and Langmuir SSA values. The yield values are included, where they were given.

Table 7 - Comparison of key reaction parameters for each synthesis method for MOF-5 formation.

Year	Method	Yield (%)	BET Surface Area ($\text{m}^2 \text{g}^{-1}$)	Duration (h)	Temperature ($^{\circ}\text{C}$)	Solvent	Zinc Salt
2011 ⁶⁶	(Addition of TEA) Solvothermal	-	2777	2.5	25	DMF	Acetate
2010 ⁶⁷	Fast Addition	87	3235	1	100	DEF	Basic Acetate
2006 ⁶⁴	Microwave	27	2869	0.15	95	DEF	Nitrate
2007 ^{34c}	Solvothermal	-	3800	10	80	DEF	Nitrate

Solvothermal synthesis is the most commonly applied synthesis route used within the literature, as described in Chapter 1, with multiple subsections including single step, two steps, microwave assisted and ultrasonic assisted. Solvent choices are severely limited however, due to the chemistry occurring within the system. The solvent must be aprotic, not containing a dissociable hydrogen atom, as well as being polar, in order to provide suitable ionic solubility for the reaction to occur. As a result, only diethyl formamide and dimethyl formamide are known to be suitable for this synthesis technique.

Single step solvothermal synthesis involves the addition of the metal salts and ligand precursor and heating for a pre-set time at a specific temperature, normally in an autoclave in order to increase the pressure slightly. The temperature range used for this reaction is usually in excess of 100 $^{\circ}\text{C}$ for time periods generally greater than 10 h, though shorter duration syntheses have been published. Despite the substantial inconsistencies in reaction parameters, this has shown to be, by far, the most commonly applied of any synthesis techniques and is detailed below in Chapter 2.5.

Chapter 2 – Background and Literature Review

Two step solvothermal synthesis involved addition of the metal salt and organic precursor to the solvent as with single step solvothermal syntheses. Instead of heating directly to the final temperature, the solution was heated to around 60 °C in order to completely dissociate the ions present within the solution⁶³. The system was left at this lower temperature for a longer time (24-72h) to “age” the solution, before the initiation phase at a higher temperature, in the region of 105 °C for a short period of time, usually 3 h.

Microwave and ultrasonic synthesis require the use of specialist equipment to reduce the experiment time. Microwave enhanced synthesis involves the use of microwaves to create areas of increased heat. This heat increase causes the rapid nucleation of crystals. The microwaves are then turned off and the system was continued as a more typical solvothermal synthesis, requiring reduced time due to the presence of seed crystals⁶⁸. Ultrasonic synthesis operates under a similar system⁶⁵ however the hot spots are caused by using ultrasonic waves to create small bubbles which then collapse. This cavitation increases the temperature in the local area, causing the initial nucleation which is then continued by the solvothermal techniques.

The diffusion route for MOF-5 synthesis involved the use of surfactants to create a metal salt rich phase and an organic ligand rich phase. This interface allows the rapid growth of MOF materials at low temperature. While the energy requirement for the synthesis is low, the final product produced is of very low quality, with poor crystallinity and greatly reduced surface area ($\sim 1000 \text{ m}^2\text{g}^{-1}$) when compared to the solvothermal methods⁶⁹.

Solvothermal method is the most commonly applied, requiring very little specialist equipment, giving the highest surface areas and pore volumes as well as being generally safer for the larger scale experiments that are planned later in this project. As a result, solvothermal synthesis using a single step synthesis route was selected as the basis for experimental work. This route is also likely to provide the simplest, safest continuous reaction system with continuous stirred tank reactor (CSTR) and plug flow reactor (PFR) both available within the system and may allow for the switch to microwave heating allowing direct comparison. Synthesis conditions published in 58 papers were

Chapter 2 – Background and Literature Review

analysed both to find the reaction time and temperatures most commonly used but also, importantly, the ratios of metal: ligand as well as water concentration. Water concentration is likely to result in the formation of an alternative phase, similar to MOF-5 but instead based around zinc hydroxide rather than zinc oxide.

2.3 Role of solvent in MOF-5 synthesis

The solvents used in formation of MOF-5 play an active role in synthesis as the solvent must partially breakdown in order to catalyse the reaction. As such, understanding this mechanism and the impacts this will have during continuous synthesis and potential large scale synthesis is vital to the efficient synthesis of high quality MOF-5. Importantly, the hydrolysis reaction of the DEF solvent will not occur below 80 °C^{34c}, therefore any solvothermal syntheses need to occur above this temperature.

By monitoring the concentrations of species, Hausdorf *et al.*⁷⁰ generated the following schematic showing the complex pathways that DEF will go through when exposed to water and sufficiently high temperature. Though no pathways for the breakdown of DMF have been published, it can be assumed that the behaviours of both species will be very similar and the breakdown of DMF will follow the equivalent pathways due to the similarity of the compounds structures.

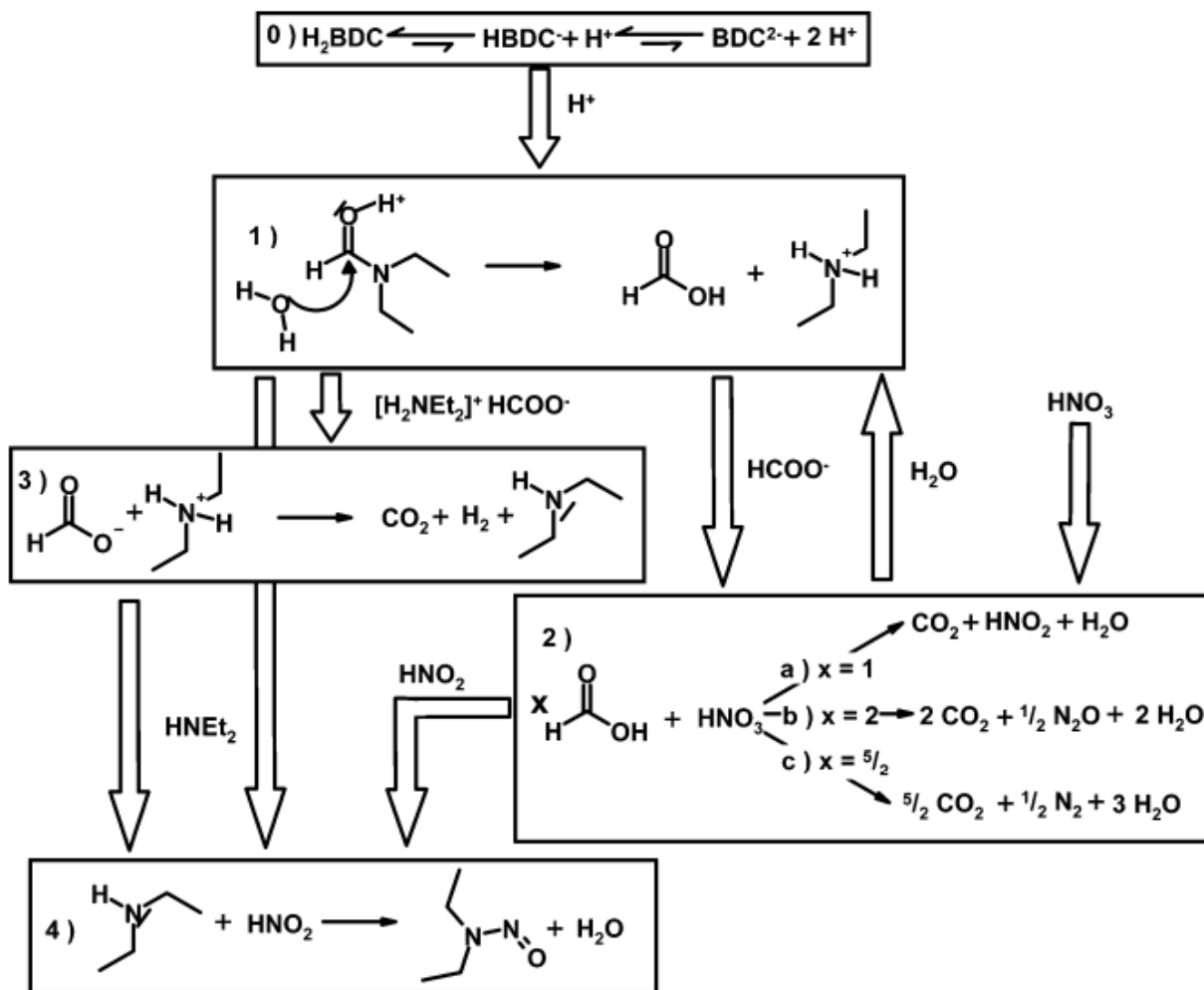


Figure 8 - Reaction Scheme for some of the reactions present within the MOF solution⁷⁰.

Step 0: Deprotonation of H₂BDC in solution. Weak acid, will occur slowly (as DEF is (di)aprotic, it will take in protons)

Step 1: Water + DEF → Formic Acid + DEF hydrolysis monomer

Step 2: Formic Acid + Nitric Acid → CO₂, N₂O, H₂O

Step 3: Deprotonated formic acid + DEF hydrolysis monomer → CO₂ + H₂ + diethylamine

Step 4: Diethylamine + Nitrous Acid → nitrosamine + water

This reaction is noted to occur at temperatures of 80°C and above^{34c}. It is important to note that the presence of water is required for this reaction to occur and that this water will cause the breakdown of

the solvent. Due to the high cost of solvent and the associated environmental concerns of disposal of this solvent and its breakdown products, recycling of this solvent would be required in order for the process to be economically viable. However, also of importance is the overall amine species concentration within the solution. While amine presence is vital to formation of MOF-5, it is also important to limit this concentration as sufficiently high concentrations will promote formation of a framework with the amine acting as ligand rather than the BDC groups⁷¹.

2.4 Zinc Precursors

While the organic ligand precursor is set, the metal ions can be provided by a number of sources, most commonly in a salt complex. 5 common zinc salts have been used for the synthesis of MOF-5. The metal salt selection may result in different quality or product or yield, significant alteration to the economic outlook of the material or have disposal issues due to the anionic species of the salts. Firstly, we consider the relative costs of different zinc salts, based upon the price for small scale purchases from a supplier.

Table 8- Approximate pricing data for 5 zinc salts for potential MOF-5 synthesis based on current price from Sigma Aldrich (as of April 2014).

Zinc Salt	Chemical Formula	Price £/kg
Zinc Nitrate (Hydrate/Tetrahydrate/Hexahydrate)	$Zn(NO_3)_2 \cdot x H_2O$	49.80
Zinc Sulphate Hydrate	$Zn(SO_4) \cdot H_2O$	44.40
Zinc Acetate	ZnOAc	45.20
“Basic” zinc Acetate	$Zn_4O(Ac)_6$	71900.00
Zinc Oxide	ZnO	60.00

Chapter 2 – Background and Literature Review

“Basic” zinc acetate is approximately 1000 times more expensive than the other zinc salts and so is immediately discounted as a viable option for our synthetic procedure as any benefits of using this salt are unlikely to balance the excess costs.

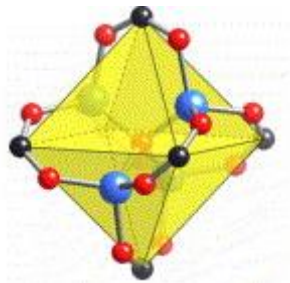


Figure 9 - Structure of "basic" zinc acetate, with the Zn_4O cation present in the starting material. This cation is the metal centre for MOF-5.

It is important to note however, that basic zinc acetate already has the Zn_4O cation intact, as show in Figure 9, within the precursor material. The existence of this cation may allow high quality MOF-5 to be formed in times far shorter than seen in a number of the above syntheses.

When considering the zinc salts used in published synthesis procedures, zinc nitrate is by far the most commonly used precursor with 50 reported uses. Zinc acetate was only reported as being used 3 times, with basic acetate, chloride, oxide and sulphate zinc salts having only 2 reports of each.

As hydration of the salt is the key factor in determining water concentration, which as highlighted above may be a key issue in MOF-5 production, the hydration of zinc nitrate within the literature was considering in greater depth in Figure 10. Furthermore, of these papers the hydration of zinc nitrate salt used can be split as follows. A single paper used dehydrated zinc nitrate and 4 papers do not mention specifically the water content of the salt used.

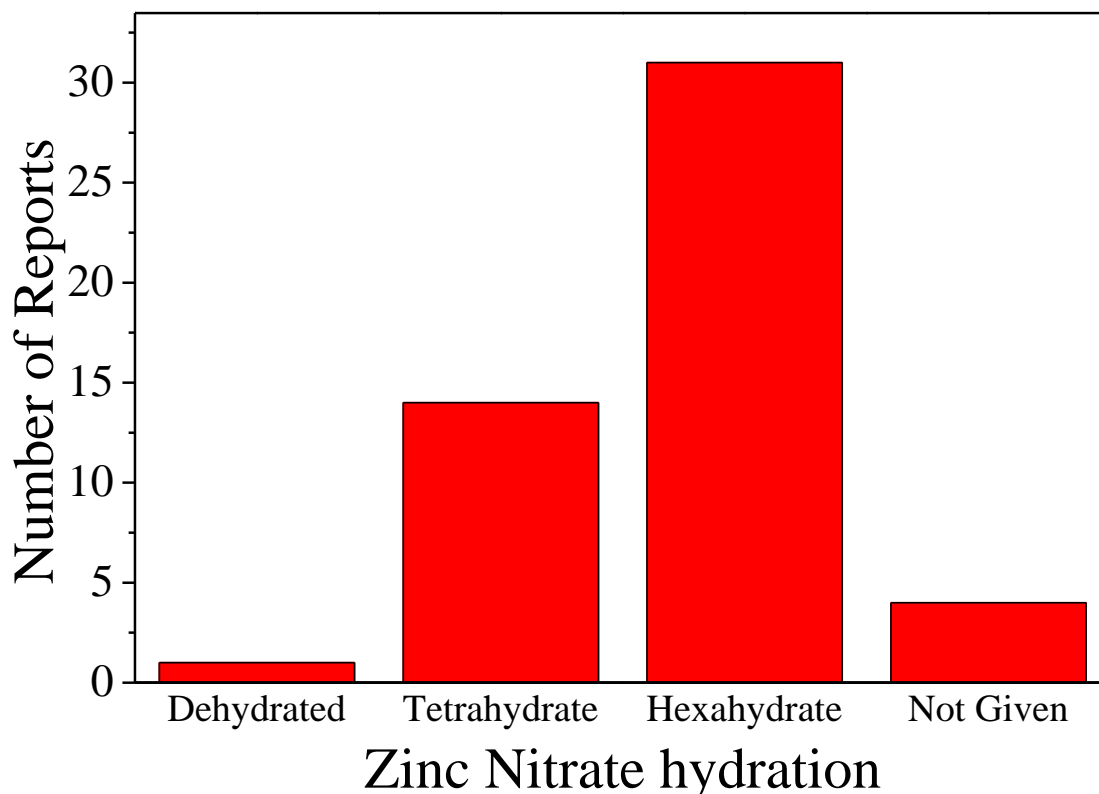


Figure 10 - Comparison of number of reports showing each hydration level of zinc nitrate salt, showing the majority of published syntheses using hexahydrate salt.

Biemmi *et al*⁷². used high throughput synthesis to characterise MOF-5 produced using different salts, this appears to be the only direct comparison of the effect of altering zinc salts. The initial concentrations of Zn and BDC are kept identical through each run. The salts use are $\text{Zn}(\text{NO}_3)_2 \cdot 6\text{H}_2\text{O}$, ZnO, $\text{Zn}(\text{OAc})_2 \cdot 2\text{H}_2\text{O}$, ZnCl_2 and $\text{ZnSO}_4 \cdot 7\text{H}_2\text{O}$. Samples were prepared using the standard solvothermal route in DEF solvent, heated at 110°C for 48 hours and so is anticipated to have formation mechanisms similar to the region of the time-temperature (t-T) space we plan to use for future syntheses.

The following PXRD results were given:

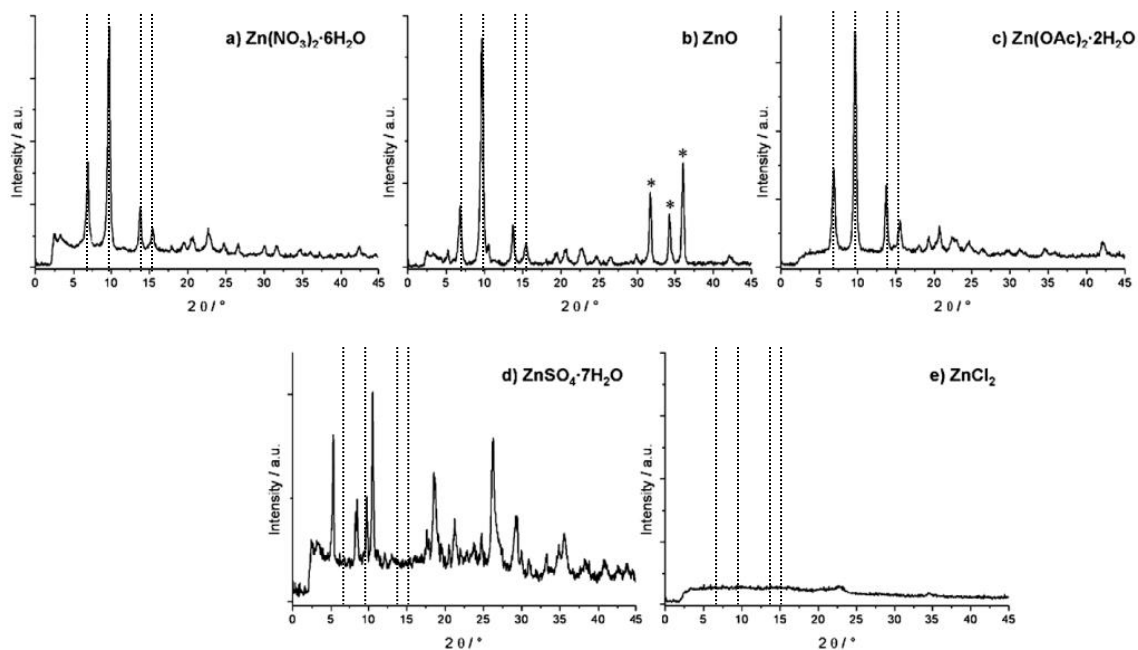


Figure 11 - PXRD Results for various zinc salts used for attempted MOF-5 production using solvothermal heating in DEF (110C, 48 hours). Taken from Biemmi *et al*⁷². b) * indicates Bragg peaks for ZnO remaining in the final product. Dashed lines indicate the location for MOF-5 Bragg peaks.

The results here show that zinc nitrate and zinc acetate produce MOF-5 with no major impurities. Zinc oxide produces MOF-5 with remnants of crystalline zinc oxide present. The phase generated when using sulphate salts is unidentified but importantly does not contain MOF-5. Zinc chloride produces only amorphous material over the given timeframe analysed. This would suggest that zinc nitrate and zinc acetate are the only two viable salts for analysis.

Scanning Electron Microscopy (SEM) was used to analyse the MOF-5 produced by nitrate, oxide and acetate zinc salts. The SEM given is as follows:

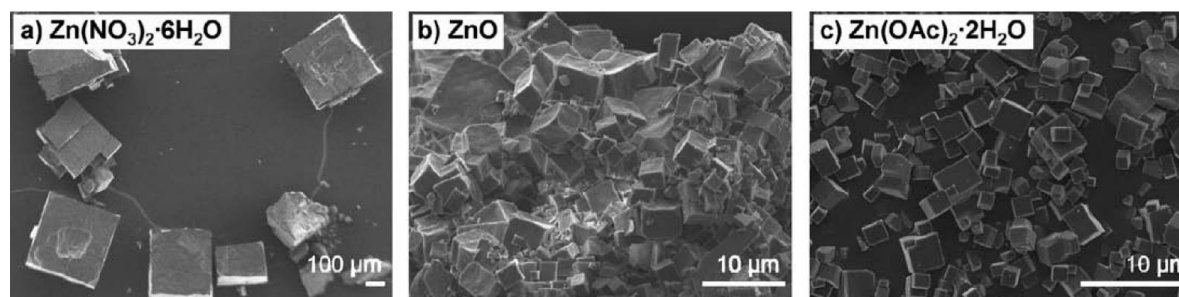


Figure 12 - SEM images of MOF-5 produced by 3 different zinc salts from Biemmi *et al*⁷². Nitrate and Acetate salts show the small cubic crystals associated with MOF-5. Zinc oxide synthesis results in cubic crystals in an agglomerate.

Chapter 2 – Background and Literature Review

MOF-5 produced from nitrate salt has considerably larger size than MOF-5 from ZnO or acetate salt. The crystals produced from zinc acetate are well shaped and distinctly cubic. This is hypothesized as being due to the higher nucleation rate of crystals within the acetate solution compared to the nitrate solution due to the increase in basicity of the acetate solution. This effect can be seen in other synthetic routes. Zinc acetate can be used to produce MOF-5 at room temperature in times as short as X hours, whereas using nitrate salts the time for crystallisation is in the order of weeks.

It is important to note also yield data and surface area analysis are not given and so it is difficult to directly compare the effect upon synthesis of using zinc nitrate or zinc acetate. However, the kinetics of zinc acetate in the early steps for MOF-5 production and the comparable price to zinc nitrate suggest zinc acetate may be a better option for MOF-5 production.

2.5 Solvothermal synthesis Conditions for MOF-5

A time-temperature map of MOF-5 synthesis conditions collected from the literature^{23-24, 29, 34c, 49, 61, 64-69, 72-73} shown below in Figure 13, this will be used to determine the operating window which we shall use as a basis for our MOF-5 syntheses. It is important to note that while we compare two parameters in an attempt to gather any data on trends that may exist, in almost all cases we are comparing data with multiple variations in parameters. As such, this only serves as a guide for potential trends rather than being quantifiable information.

We first compared the overall t-T space in which MOF-5 reactions were reported in the literature, though the number of distinct conditions used was limited as a number of papers follow the exact synthetic conditions of previous work. For reactions occurring at ambient conditions, where temperature was not explicitly stated, we have assumed 25°C as the reaction temperature.

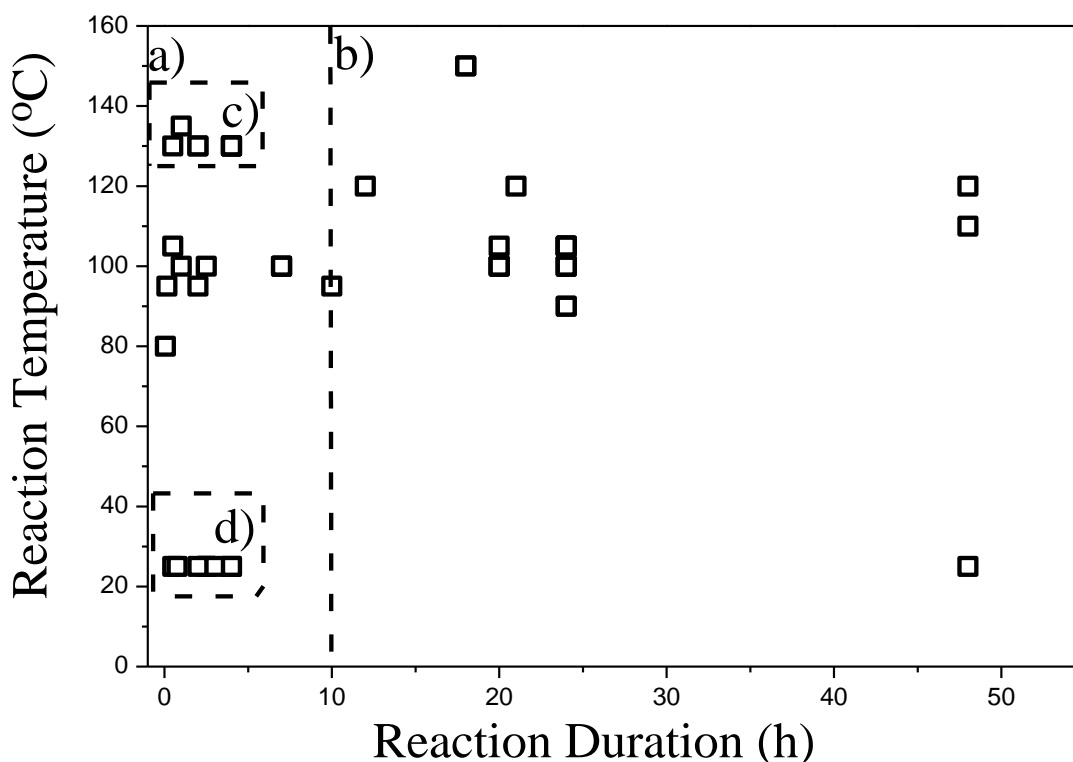


Figure 13 - time-Temperature space for MOF-5 reaction reported in the literature. a) represents the reactions under 10 h b) represents syntheses taking over 10 h. Within zone a), c) is the subset of conventional solvothermal syntheses, d) is the subset of reactions requiring amine addition to proceed.

Chapter 2 – Background and Literature Review

This space can be divided into 2 distinct regions, marked a) and b). As we wish to produce MOF-5 with a high space-time yield, we discounted b) as these syntheses generally take too long to be effective and are out with the scope of this project. The region marked a) has sufficiently short synthesis durations to be possible. While this seems like an ideal operating point for the continuous reaction to occur within, this region requires the use of either basic zinc acetate salt or the addition of an amine species. The basic zinc acetate salt is orders of magnitude more expensive (as shown above in Table 8) than the other zinc salts that have been used for MOF-5 synthesis and so the benefits are greatly outweighed by the economic downsides of using this salt. The addition of amines also adds expense and has considerable environmental impact. Therefore this region can be excluded. However, two sub regions exist within this area. Within the region marked as Figure 13c), MOF-5 is often synthesised solvothermally, using zinc salts other than basic zinc acetate within that meets our major criteria for going on. As a result, we chose to investigate further the t-T space of 110-140°C and 0-6h. Figure 13d) groups syntheses using unconventional heating techniques such as microwave and ultrasonic enhanced heating methods. These are of considerable interest and the scope of this project included microwave heating as a method for production of MOFs. However, for the early stages of this project we plan on focussing on more widely used synthetic techniques and so must exclude this region for the initial part of this project.

A large number of papers do not include the yield data for their reactions. Further, in many cases the BET Surface Area or the Langmuir Specific Surface Area is commonly quoted without any key information about the quality of the processing such as the fit range, c-values etc. This may lead to inaccuracies in the data due to the limitations of the models described in Chapter 4. However, surface area is one of the key measures of product quality due to being one of the key selling points of MOFs and allowing a direct quantitative comparison between syntheses. Beyond this, MOF-5 synthesis occurs over a multitude of time and temperature conditions and even within solvothermal synthesis can be produced via conventional heating, microwave heating or sonication. As such, the data here is used to attempt to identify general trends in a qualitative fashion we might expect to see rather than any quantitative comparisons.

Around 60 papers detailing MOF-5 synthesis were reviewed in order to determine which parameters were most likely to alter the yield and quality of the material produced.

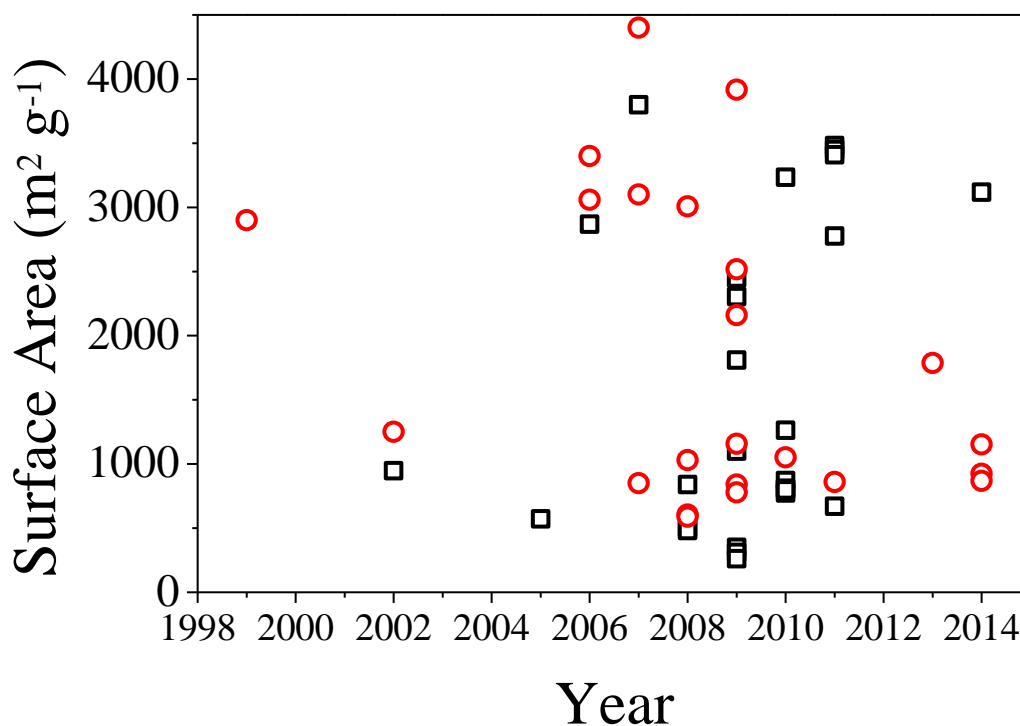


Figure 14 - Comparison of reported BET surface areas (Squares) and Langmuir SSAs (circles) for selected papers published in any given year. Maximum reported value with Langmuir SSA of 4400 m²g⁻¹.

We first compared the reported surface areas as a function of year of publication as shown in Figure 14 in order to see if syntheses had clearly improved with time, potentially rendering earlier syntheses obsolete. Here we can see that MOF-5 publications were limited until 2006 at which point a great deal more publications began to emerge as interest in the field increased. From the 2900 m² g⁻¹ SSA reported by Yaghi *et al*⁴⁹. in 1999 the maximum reported surface area has not increased by a great factor to 4400 m² g⁻¹ reported by Kaye *et al*^{34c}. in 2007. The reports of MOF-5 in the period of 2006-2012 show massive variations in reported surface areas showing how syntheses can result in large variations in the surface area of the final product. These generally can be split into two clusters with large numbers in the 200-1400 m² g⁻¹ region and a secondary cluster above this with higher surface areas generally > 2000 m² g⁻¹. The reason for this clustering is not obvious, and may not be a true effect.

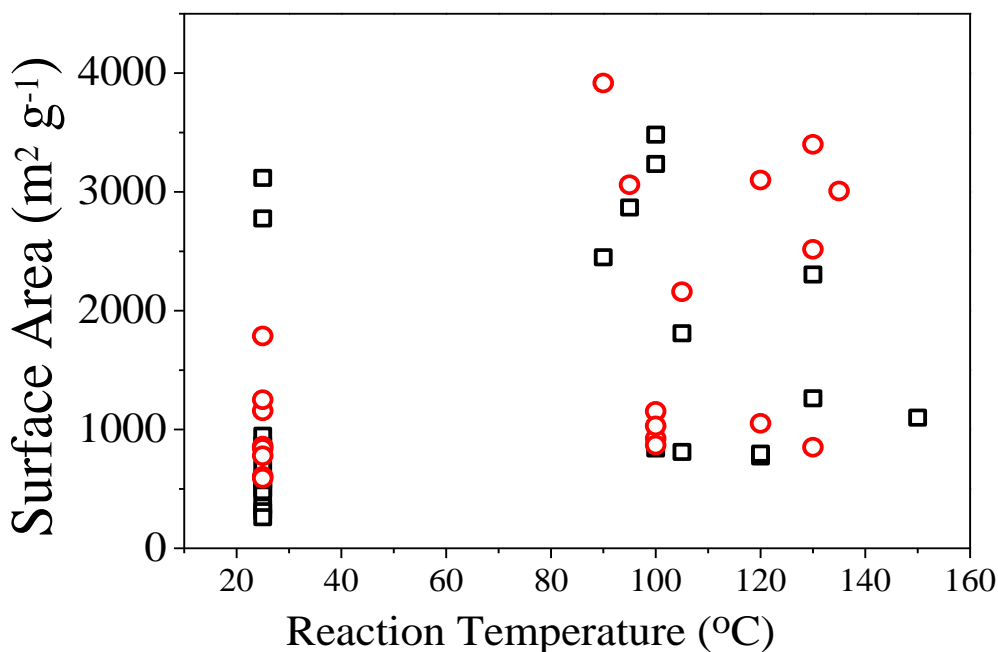


Figure 15 - Comparison of reported BET surface areas (squares) and Langmuir SSA (circles) against the temperature the reaction was carried out at (°C). Solvothermal syntheses occur at $T > 80$ °C, while syntheses using amine addition are grouped together at much lower temperature.

Figure 15 compares the surface area reported against the temperature of the reaction. It is important, once again, to note that here we are not comparing the total energy input nor accounting for duration. The grouping here has a large number of reactions occurring at 25°C, which we have used as approximate room temperature when temperature was not explicitly stated by was noted as “ambient”. Beyond this, we do not see any particularly obvious trends. The general working range appears to be in the region of 100-140°C, although the reported surface areas vary wildly within this region as we do not account for any conditions other than temperature. This is important given our anticipation of working within that approximate region of temperature space. Again, we are using this data to suggest operating windows that may suit the facilitation of a continuous MOF-5 reactor system, rather than using this as the basis of any quantitative data. The boiling points of DEF and DMF are approximately 175 and 155°C respectively. As we intend on running our continuous system under reflux rather than under pressure, it is important to consider this range as an absolute maximum, though the addition of reaction components appears to reduce the boiling point of these systems by approximately 10-20 °C.

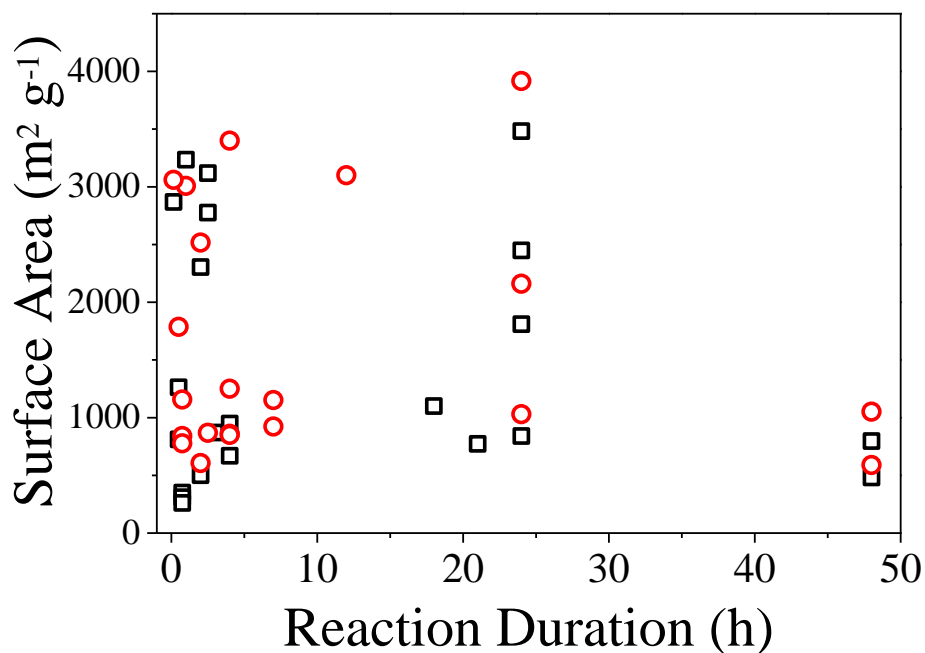


Figure 16 - Reported BET surface areas (squares) and Langmuir SSA (circles) shown against the duration of the reaction in hours. The maximum reported SSA occurs with 24 h reaction, though SSA > 3000 m² g⁻¹ are shown to have been reported with reaction duration of under 5h .

Figure 16 shows no clear trends of correlation between surface area and reaction duration. The highest surface area reported by Kaye *et al*^{34c}. occurs with reaction duration of 24 h giving a Langmuir SSA of 4400 m²g⁻¹. However, the second highest reported Langmuir SSA (3400 m²g⁻¹) occurs with a reaction duration of only 4 h⁷³ⁿ, which is likely to provide a significant gain in maximum space time yield, and therefore be overall beneficial when simply considering total surface area output of a system as a function of time.

In terms of atom efficiency and the overall goal of producing an efficient cost effective synthesis process, it is important to consider the reaction stoichiometry. We compared the general ranges analysed within reported MOF-5 syntheses.

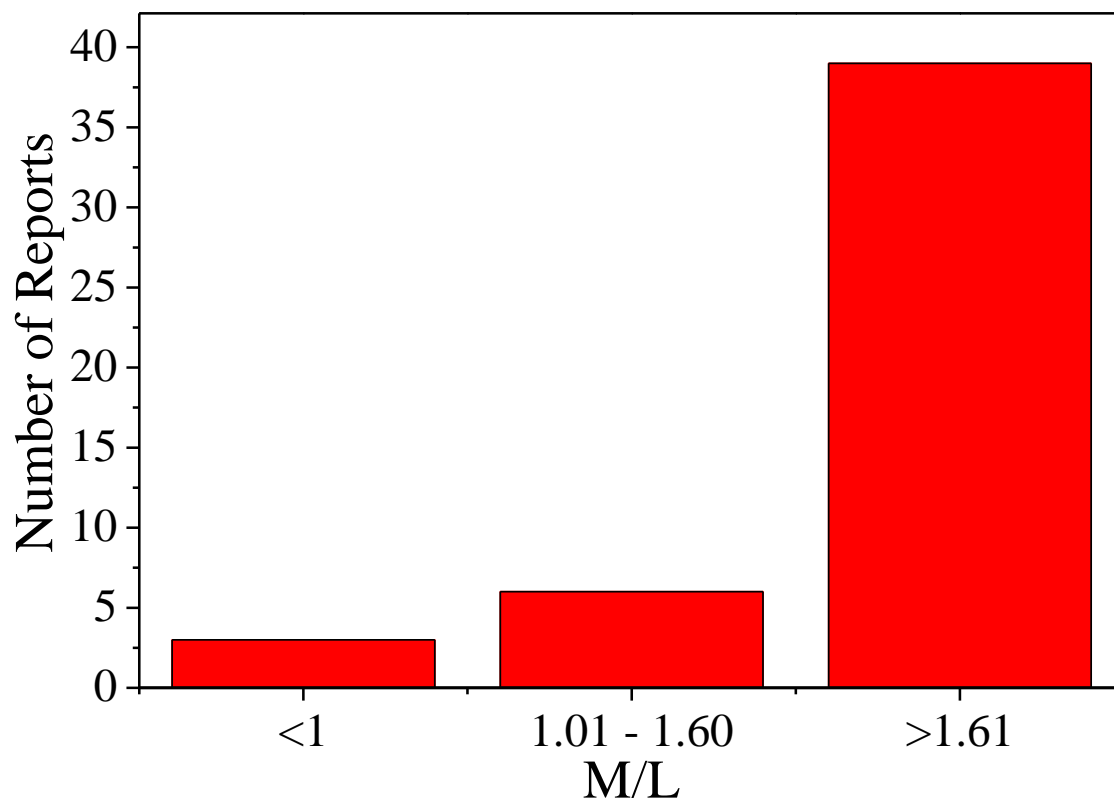


Figure 17 - Comparison of number of reports with varying M/L ratios, grouped to encompass approximately stoichiometric value of 1.33. The groups < 1 and > 1.61 represent a significant deviation from stoichiometric ratio.

In Figure 17 we see a compared the number of papers reporting MOF-5 synthesis at varying M:L conditions. As stoichiometrically MOF-5 requires 4 moles of Zinc and 3 moles of ligand (giving M/L of 1.33 as stoichiometric) we split our analysis here into 3 regions. 1.01-1.6 represents synthesis occurring at approximately stoichiometric ratio with a margin for operating slightly off stoichiometric quantities. We also compared those syntheses reporting M/L < 1, which is ligand in excess and M/L > 1.61 representing metal in excess. It is clearly shown that operating with the metal in excess is considerably more common, appearing about 4 times as often as stoichiometric and excess ligand combined. Breaking down these groupings further, we see the range of M/L values used for MOF-5 synthesis in more detail. Syntheses appear to be banded in 4 regions. 0.21-0.6 representing the small number of papers reporting the ligand used in excess for synthesis. A small group banded approximately at 1.33 representing the stoichiometric values. We then see a large number of reported syntheses at approximately 50% excess on the metal, giving M/L of approximately 2. Then the most

Chapter 2 – Background and Literature Review

common group is tightly banded around M/L of 3, with the metal concentration roughly 2.25 times the stoichiometric value. For our studies, we have chosen to compare running at stoichiometric quantities and running at a metal: ligand ratio of 3:1. This allows for the most common synthesis condition to be carried forward but as no clear link between M:L ratio and product quality or yield exists, stoichiometric ratio must also be considered in an attempt to reduce waste.

Within the below graph, the dashed line indicated the point of Zn/BDC = 1.33, the stoichiometric value for MOF-5.

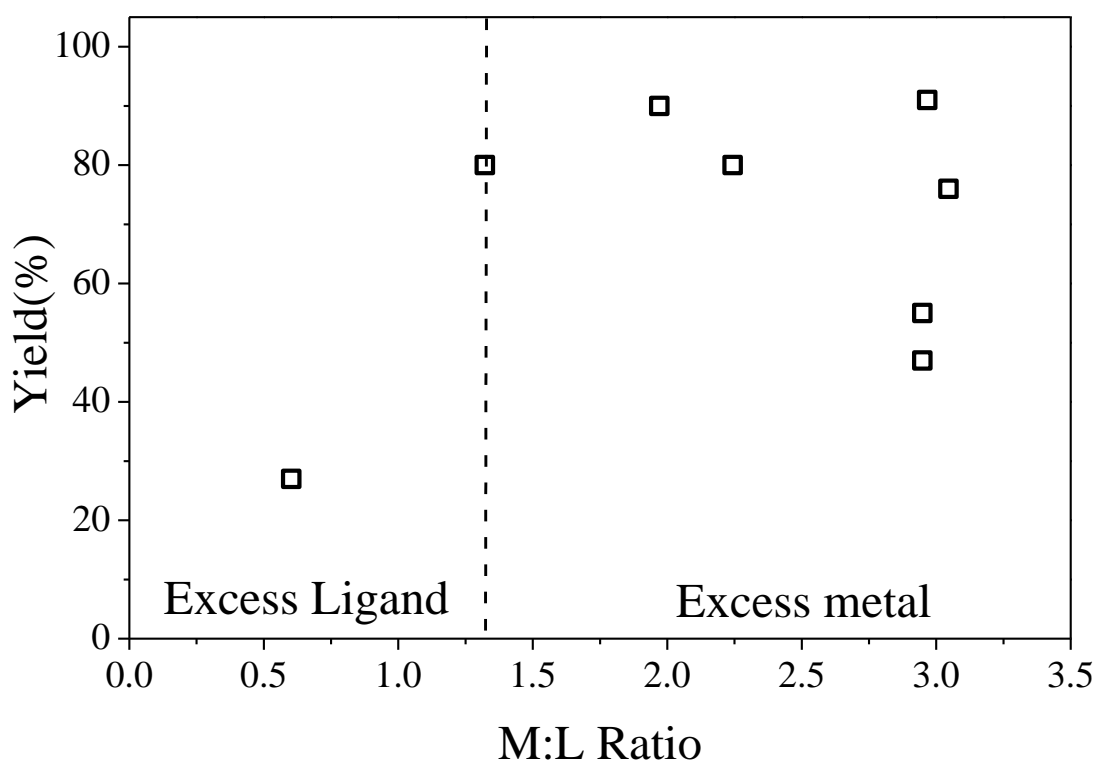


Figure 18 - Comparison of reported yields at various M:L ratios, dashed line indicates when reactants are in stoichiometric quantities. Due to the lack of published yield data, the number of data points is low on this graph.

As a large number of papers detailing synthesis are focused on producing high quality MOF-5 rather than high yields, there are only a very limited number of data points on this graph. For samples with excess quantities of zinc we generally see >75% yield. For stoichiometric concentrations of zinc or excess ligand we only have single data points which may not provide an accurate overview of this parameter. Further, MOF-5 has been reported to form with the composition $\text{MOF-5} \cdot 8\text{DEF}^{74}$ due to

the solvent presence in the pores from synthesis. With this composition, the molar mass is close to double the molar mass of MOF-5 without solvent ($1548.2 \text{ g mol}^{-1}$ compared to 749 g mol^{-1} for desolvated MOF-5). In many cases it is not made clear if the MOF-5 produced has had the solvent extracted from the pores and so values may be off by a significant margin if this is not accounted for.

Comparing the reported surface areas of to the M/L ratio is shown below in Figure 19.

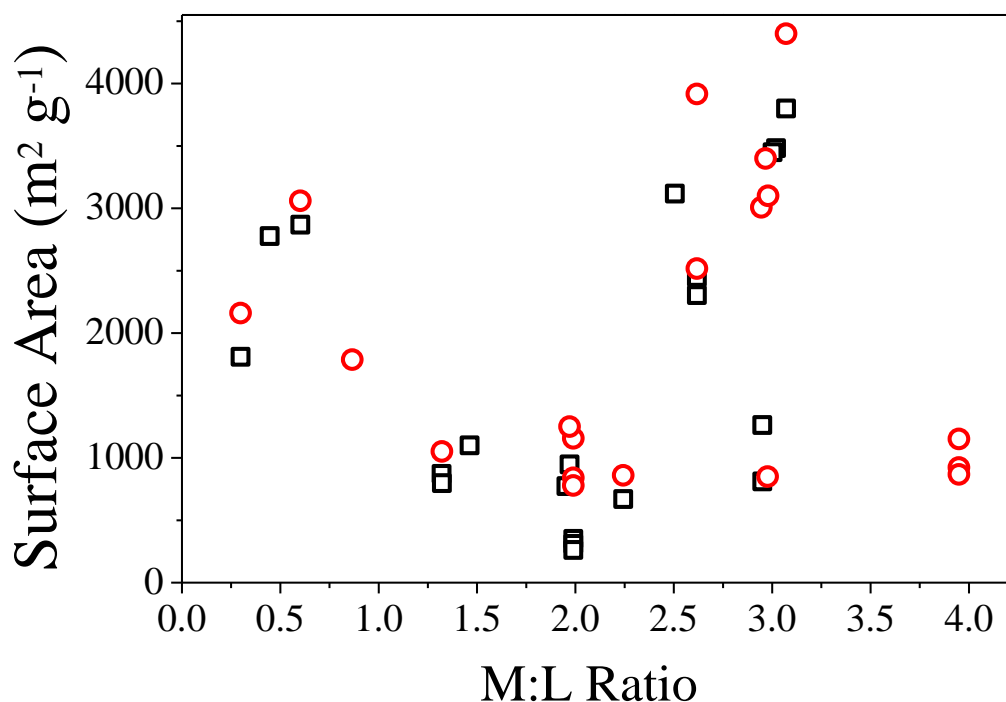


Figure 19 - Comparison of reported BET surface areas (squares) and Langmuir SSA (Circles) for various M:L ratios. The 3 highest SSAs occur with metal in excess, but ligand in excess also has shown high SSA product.

It is unclear if there is a minimum present when operating at approximately stoichiometric quantities, due to the lack of data points around this region. However, it does appear that at the most common operating point, M/L approximately 3, that a wide range of surface areas can be formed based on other conditions, while operating at $M/L = 1.33$ will produce a material at lower surface area. As this is not clear, we elect to continue with the plan to run at M/L of both 1.33 and 3, in order to determine if M/L affects the system in any significant way.

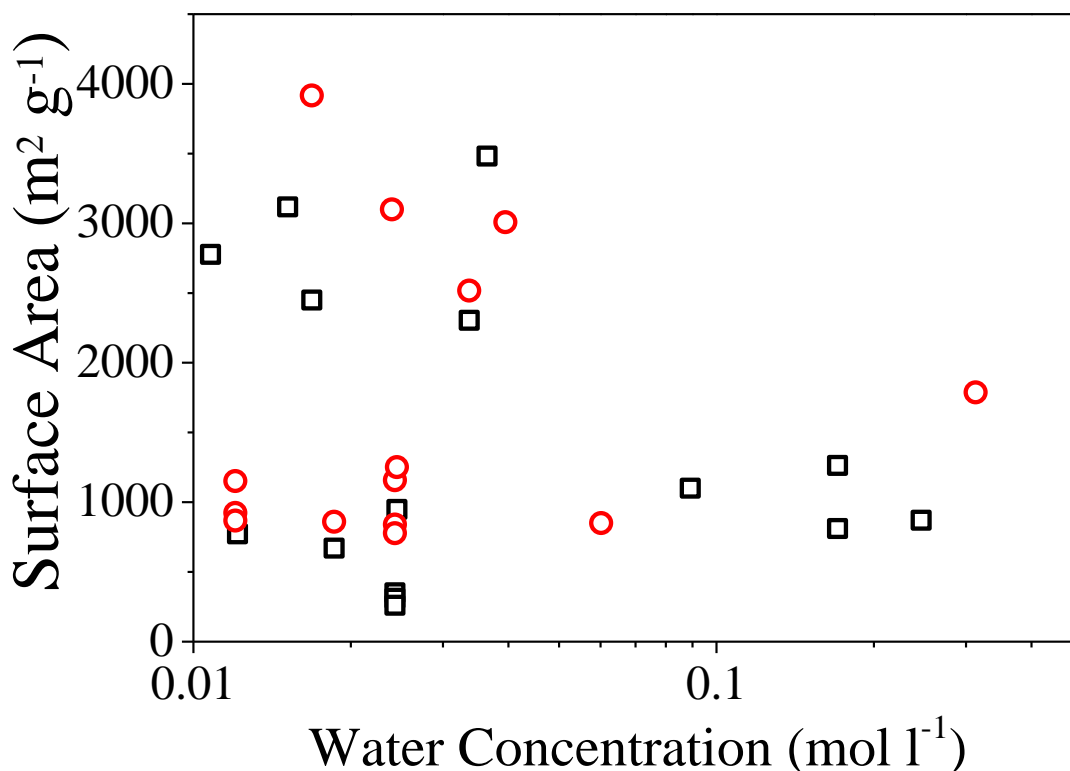


Figure 20 – Reported BET surface areas (Squares) and Langmuir SSAs (circles) of MOF-5 reported compared to the water concentration in (M). Water concentration varies by over an order of magnitude, generally due to the water present in the zinc salts.

As MOF-5 is known to breakdown when exposed to the water present in the air, and the breakdown product, MOF-69c, has been directly synthesised by modifying a MOF-5 reaction by adding water to the MOF-5 reaction mixture⁷⁰, we here compare the reported surface areas as a function of the concentration of water present, given in M here. There appears to be a slight trend for the surface area to reduce as the water concentration increases though 0.2 M of water in the reaction mixture appears to still be able to produce MOF-5 with large surface area, though significantly reduced from the maximum.. Above this point, surface area appears to be further reduced, though it is again unclear if this is a definitive effect or if the data is simply lacking at this point.

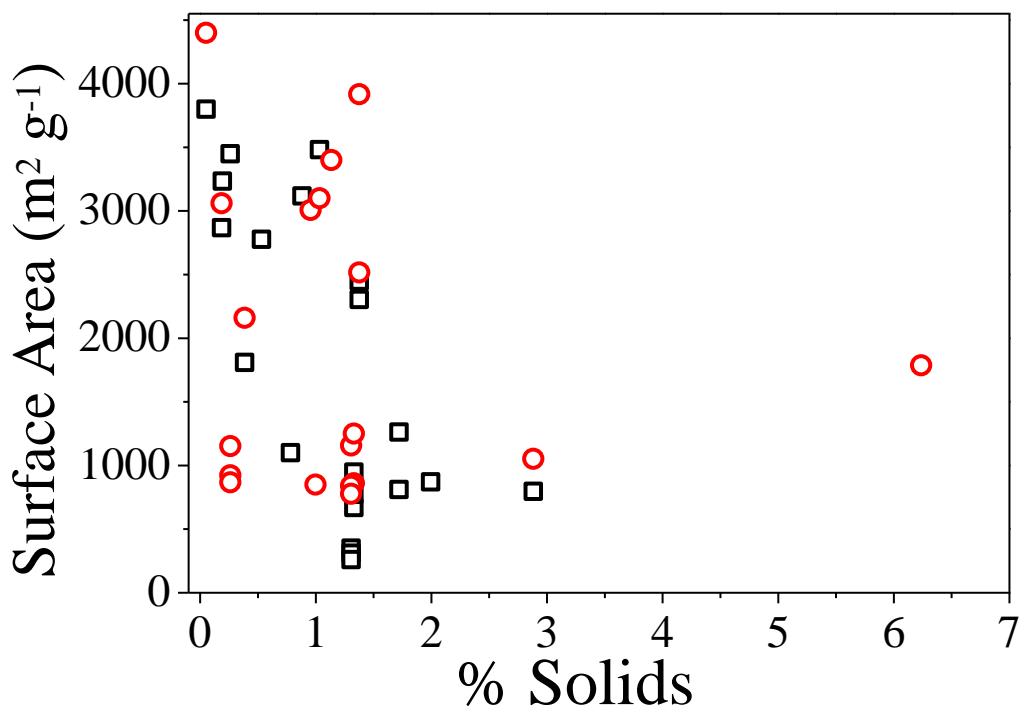


Figure 21 - Reported BET surface areas (Squares) and Langmuir SSAs (circles) of MOF-5, relative to the solid concentration of the synthesis.

The literature does not cover in great depth a range of solids with the bulk of work being carried out between 0.5-3% solids as seen in Figure 21. The potential for increasing the solids content of the MOF is vital to an economically efficient scale up. Further, we can see that the lowest concentration given is the system that produced the overall highest recorded surface area for MOF-5, running at 0.05% solids. Given a 100% conversion this would only yield 0.5g per L of solvent, and so would result in a very high cost product due to the high cost of solvent relative to energy or precursor costs. Further due to the necessary partial breakdown of the solvent the opportunities for recycling are limited without removal of the amine species formed. At 1.36% solids, surface areas as high as 3917 m^2g^{-1} have been recorded. The concentration of the reactants has been increased by a factor of 27.2 times, while only reducing the surface area from 4400 m^2g^{-1} to 3917 m^2g^{-1} , a change of only 11%. At 3% solids, the maximum SSA reported is reduced to a little over 1000 m^2g^{-1} .

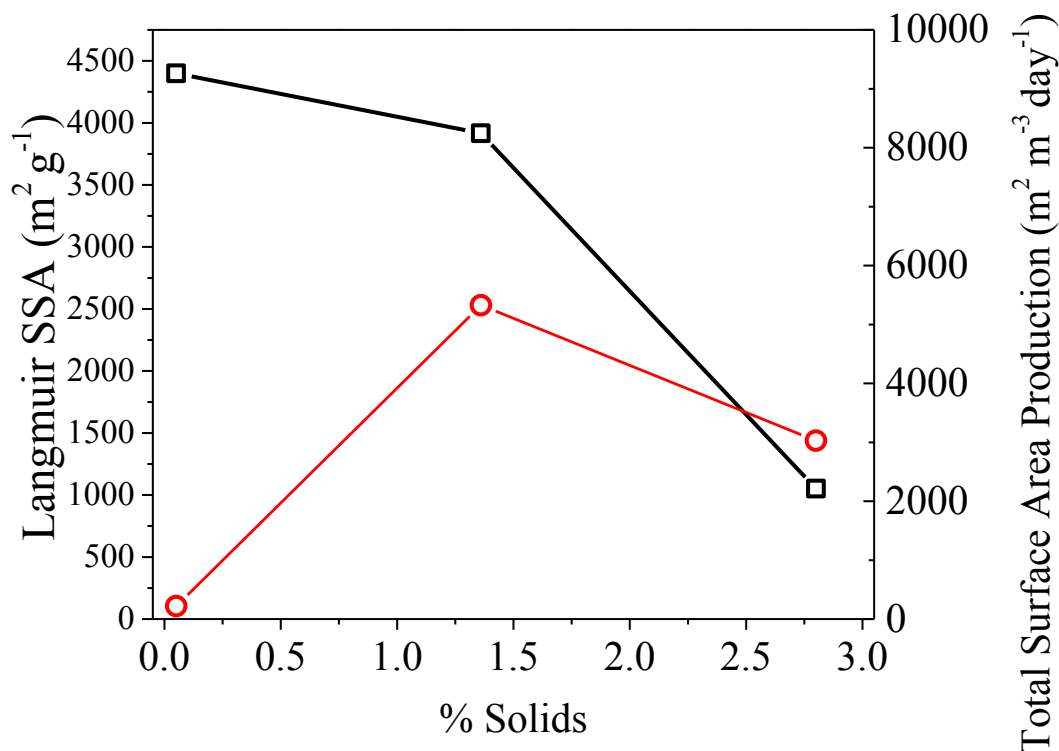


Figure 22 - Comparison of Langmuir SSA (squares) and total surface area produced (circle) (assuming 100% yield and reaction scaled to 100ml of solvent)

Again, it is important to note that while some applications would require the maximum possible surface area per unit mass, it is expected that many more applications will be more interested in the price per unit area recoverable. Assuming 100% conversion, of a 100ml scale reaction, the highest surface area MOF-5 set up would yield on 220 m^2 total surface area, compared to 5327 m^2 that would be applicable to the system when run at 1.36% solids. Due to the increased output at 3%, with only a small decrease in surface area, this value decreases to 3029 m^2 at 3% solids. Given solvent appears not to be reusable without some relatively money intensive separation of the original solvent and its breakdown products, single pass yield is an important consideration for this system, especially as if the amine species reach above a critical concentration, the system will cease to produce MOF-5 and will instead produce a different amine based structure. For systems that do not involve the breakdown of the solvent, this would be less of an issue.

2.6 MOF-5 and related crystalline phases

Importantly, a number of other phases are intrinsically linked to the MOF-5 phase. The main related phase is the MOF-69c phase with chemical formula $(\text{Zn}_3(\text{OH})_2(\text{BDC})_2)$, which also features a number of other related phases. The MOF compounds, MOF-5 ($\text{Zn}_4\text{O}(\text{BDC})_3$) and MOF-69c ($\text{Zn}_3(\text{OH})_2(\text{BDC})_2$) are linked as the zinc oxide and zinc hydroxide based MOF compounds with benzene dicarboxylate groups used as organic linkers. The scope of this review is to determine from the literature available on these two compounds the reaction mechanisms shown, and to resolve the issue of a direct link between the two phases. As a relatively complex structure, the crystal evolution within MOF-5 synthesis was noted by Park *et al* as still being unknown^{73c}. Though it has been shown that MOF-5 can be reacted in such a way as to produce MOF-69c^{70,34c}, including a reversible process back to MOF-5, no direct link shows that MOF-69c is formed as an intermediate compound during the solvothermal synthesis of the MOF-5 material. As the structure of MOF-5 relies upon the formation of the Zn_4O^{6+} cation, this zinc oxide building block can be subverted to a zinc hydroxide basic block, $\text{Zn}_3(\text{OH})_2^{4+}$. MOF-69c is a framework based upon a zinc hydroxide building block. As would appear to be a likely solution, water concentration may well be one of the triggers between the two phases.

Identification of multiple MOF-5 related phases is covered in the literature. MOF-5 is produced using one of the methodologies described above and generally allowed to decompose under a variety of conditions. Knowledge of these phases forms an important background to the identification of crystalline phases present within the MOF-5 synthesis process.

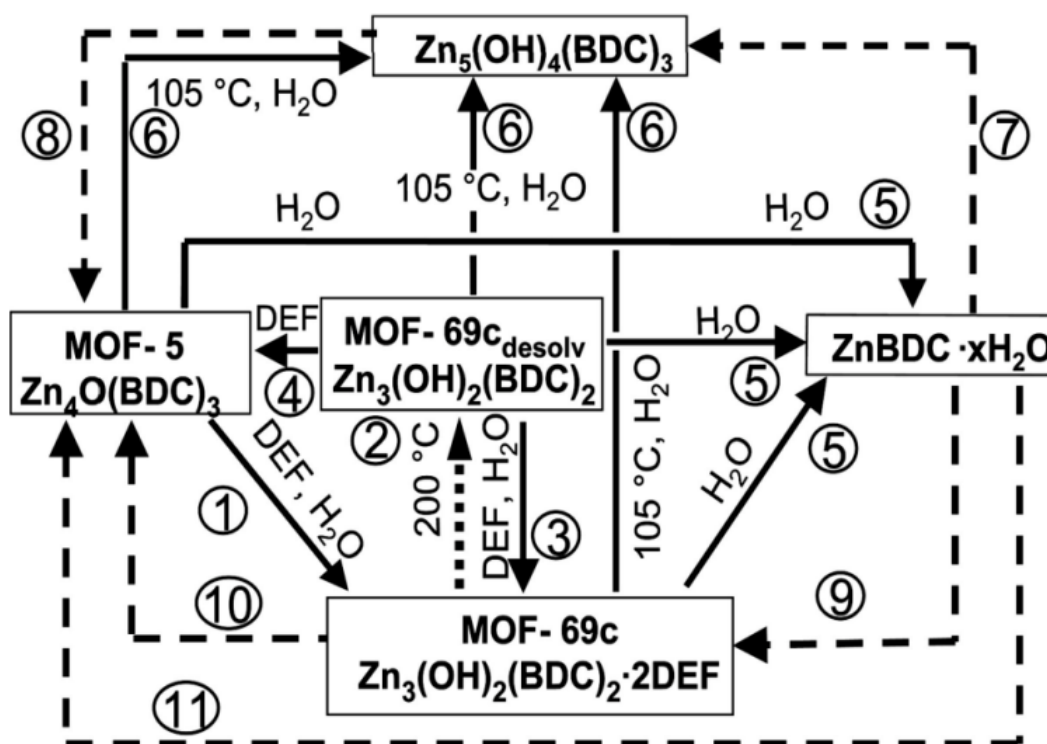


Figure 23 - Diagram showing how phases associated with MOF-5 decomposition transform between each other. Solid lines indicate reaction required DEF and/or water. Dashed lines represent reactions requiring additional reagents, usually a zinc salt or ligand.

It is important to note that the “MOF-5 made from MOF-69c” phase represents an impure MOF-5 phase, although the secondary phase present appears to be the $Zn_5(OH)_4(BDC)_3$ phase rather than the MOF-69c phase, as seen by the movement of the peak from 8.5° to 8.8° . Figure 23 also includes the variety of reaction pathways between the different phases. The solid lines show where only DEF (the solvent used in synthesis) and water were used to cause the phase change. Dotted lines indicate that other components were used in conjunction with water and DEF in order to cause that specific phase change. While these phases are noted after synthesis of MOF-5 via decomposition or further reaction, we hypothesize some of these phases may be present within the synthesis process itself, with temperatures used being within the regular range for MOF-5 synthesis, and variations in water:DEF concentration being entirely possible when operating at temperature in excess of $110^\circ C$. It is also possible other phases are formed in the synthesis process of lower stability that does not reform even under decomposition. Importantly, while this shows the ability of non-MOF-5 phases to be transformed under specific conditions to MOF-5, these represent post-synthesis changes and it is

unclear if MOF-5 forms directly from solution or would transfer through multiple metastable crystalline phases.

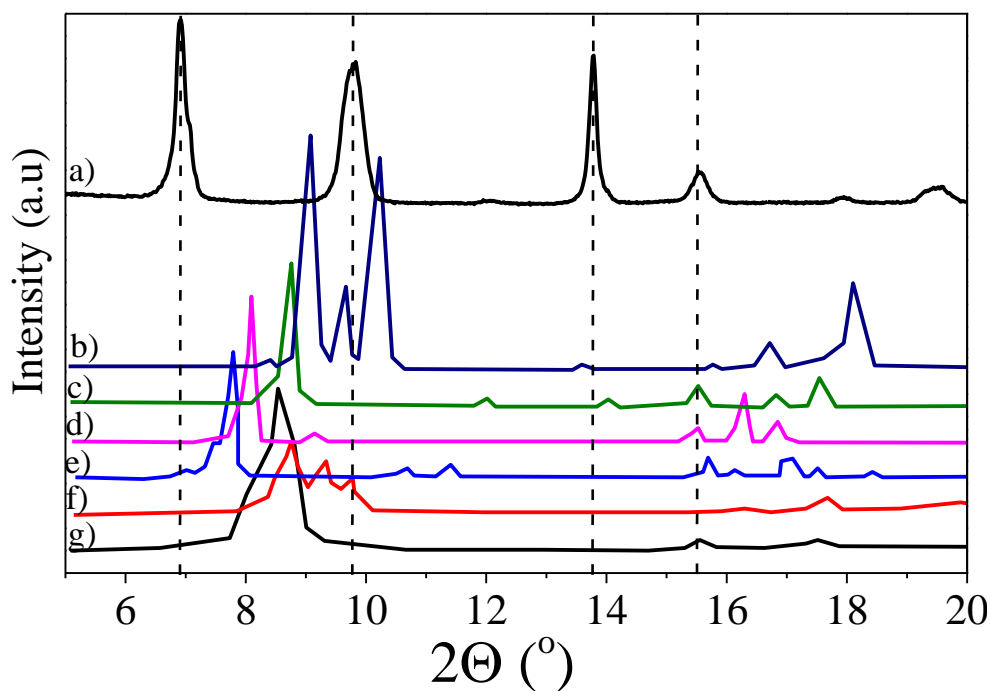


Figure 24 - PXRD showing MOF-5 and related phases. a) MOF-5, b) MOF-69c(desolv), c) $\text{ZnBDC} \cdot x\text{H}_2\text{O}$, d) $\text{Zn}_5(\text{OH})_4(\text{BDC})_3$, e) MOF-69c, f) $\text{Zn}_3(\text{OH})_2(\text{BDC})_2 \cdot \text{DEF}$, g) $\text{Zn}_3(\text{OH})_2(\text{BDC})_2$. Dashed lines indicate the position of MOF-5 Bragg peaks^{73g}.

MOF-69c is a non-porous phase of metal-organic framework, based around the zinc hydroxide cluster. The composition of a unit cell of MOF-69c is not entirely definite within the literature, though the discrepancies present can be explained when analyzing the nature of the solid state chemistry involved. The basic repeating unit and the organization of the zinc hydroxide clusters within are shown below:

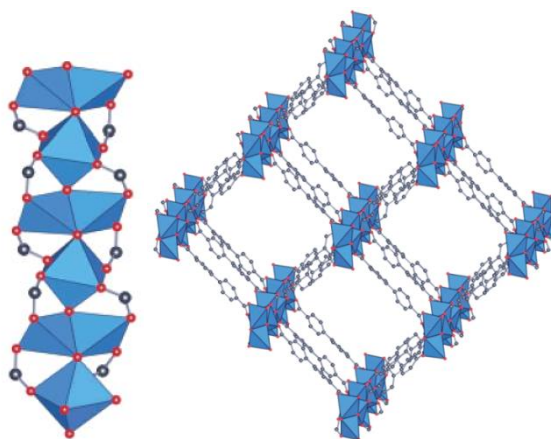


Figure 25 - Structures of the MOF-69c phase. Blue Triangles represent Zinc polyhedra. The arrangement of the zinc polyhedra is on the left, with the benzene dicarboxylic groups linking the Zn polyhedra to the next group are shown in the second image. Images taken from Rosi *et al*⁷⁵. This omits the 2 DEF molecules and such show the MOF-69c(desolv) phase.

The basic structure is $Zn_3(OH)_2(BDC)_2 \cdot 2DEF$ however the main dispute within the literature involves the issue of DEF solvent molecules bonded within the structure, altering the shape and parameters of the unit cell which then alter the powder x-ray diffraction (PXRD) results. Papers mentioning the MOF-69c phase seem to give one of 3 diffraction patterns. While the intricacies of each of these are important, the plots can be summed up by referring to the location of the largest intensity peak within the structure. The locations of the Bragg peaks within three different diffractograms are 7.8, 8.1 and 8.9 degrees 2 theta. It is important to note, that all samples were analysed using Cu $K\alpha$ radiation of 1.54Å wavelength, and while the intensities are not comparable from sample to sample, the Bragg peak locations (in terms of two theta) are.

The earliest paper discussing the MOF-69c phase is by Rosi *et al.*⁷⁶ in 2002. Rosi *et al*⁷⁵. subsequently published again concerning MOF-69c including full crystallographic data and predates the work of Loiseau *et al*⁷⁷, giving alternative crystallographic data by a matter of only 2 months. The data given by Rosi *et al.* generates a diffraction pattern with the main Bragg peak occurring at 8.1 degrees 2 theta. Diffractogram for this phase is shown below:

Chapter 2 – Background and Literature Review

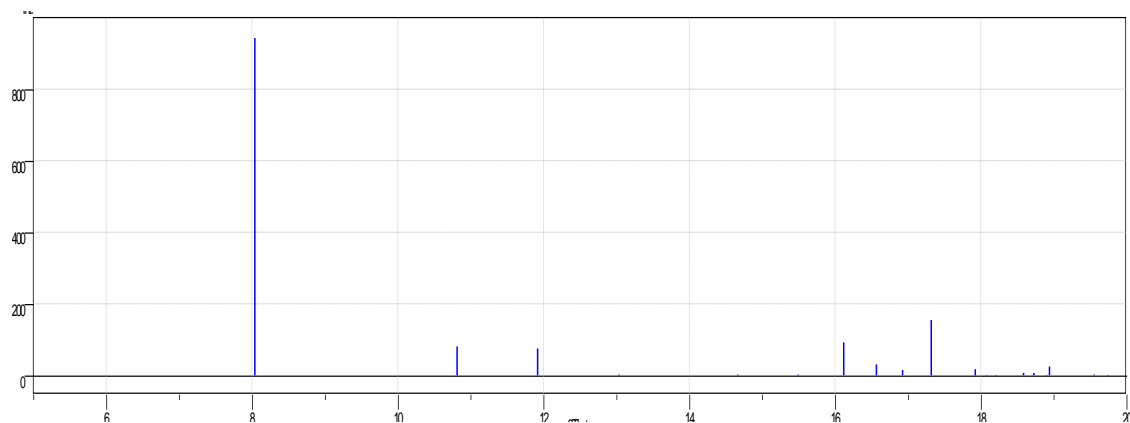


Figure 26 - The diffraction pattern of the MOF-69c phase. The highest intensity peak occurs at 8.1° 2θ. Generated from single crystal data.

Data provided by Loiseau *et al.* gives a similar, but alternative result for a compound they claim to have an identical structure to that of MOF-5, shown below:

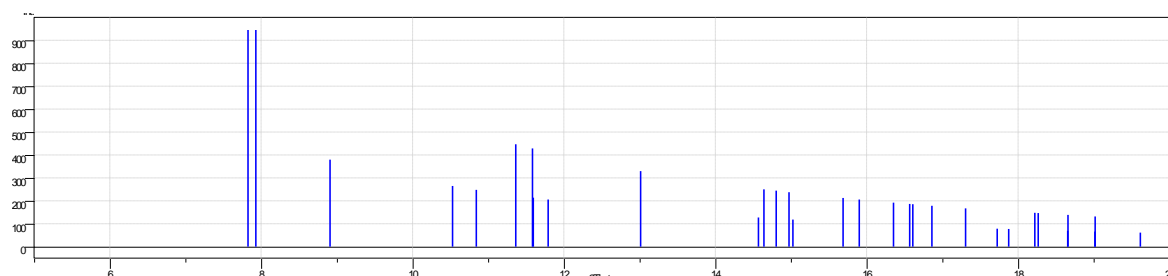


Figure 27 - XRD data from Loiseau *et al.* Bragg Peaks should occur at 7.8 and 7.9° 2θ from single crystal data showing a similar but distinct PXRD pattern to Figure 26.

It is important to note however, this is not claimed to be MOF-69c, but instead is a similar material. Further analysis would suggest that this is representative of the material with a structure of $\text{Zn}_3(\text{OH})_2(\text{BDC})_2 \cdot 2 \text{DEF}$.

Further analysis in the literature has been completed by Kaye *et al.*^{34c}, Hausdorf *et al.*⁷⁰, and Ravon *et al.*⁷⁸. includes XRD results which do not clearly define the issue of where the diffraction pattern should occur for a compound with a structure of that given for MOF-69c.

Hausdorf *et al.*⁷⁰ details various reaction schemes stemming from the central MOF-5 product and going through various zinc hydroxide based compounds and the reactions occurring between them. It was suggested here that MOF-69c has a main diffraction peak at 7.8° 2θ, and that if the solvent

molecules are removed from this compound, the shifting of the zinc hydroxide tetrahedral will shift the Bragg peak to $8.9^\circ 2\theta$.

This theory is backed up by the work carried out by Ravon *et al*⁷⁸. The synthesis of MOF-69c yielded similar results to those of the Hausdorf group, with XRD results showing a main diffraction peak at $7.8^\circ 2\theta$. Furthermore, they heated a sample of the MOF-69c compound, driving off the DEF molecules from the unit cell. This caused a notable shift in the Bragg peak location, to $8.9^\circ 2\theta$, identical to data given by Hausdorf *et al.* for the desolvated MOF-69c phase – MOF-69c(desolv).

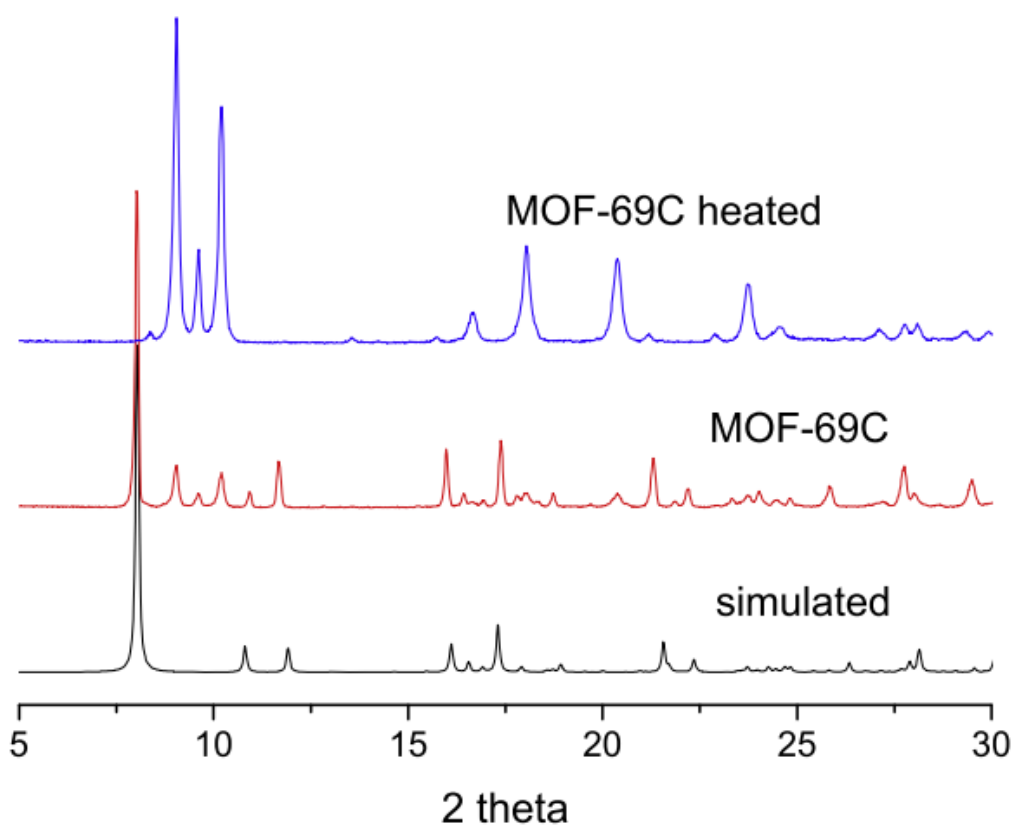
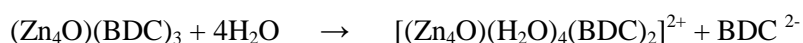


Figure 28 – Comparison of powder pattern of MOF-69c to simulated result. Heating of this material shows peak shifting due to removal of solvent molecules from pores⁷⁸ showing that MOF-69c will show a different powder pattern with occupied pores compared to empty pores.

MOF-69c is shown to be formed by breakdown of the MOF-5 unit cell when exposed to humid air by Kaye *et al.* The breakdown of MOF-5 via attack by water was originally hypothesized to be similar to the following reaction scheme by Greathouse *et al*⁷⁹:

Chapter 2 – Background and Literature Review

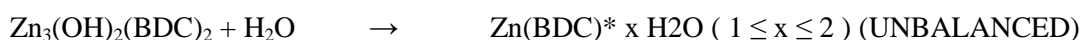


However, it was later found that the layered structure formed was created by a reaction pathway such as:



It is important to note that Kaye *et al.* give the Bragg peak location for the MOF-69c material at 8.9° 2θ . However, as their MOF-5 starting material was completely desolvated before exposure, it would stand to reason that the MOF-69c phase formed would also be present within the desolvated state, as no DEF had been added to the reaction while it proceeded.

It is important to note also, MOF-69c can be broken down further when exposed to high water concentrations with the framework completely collapsing to produce $\text{Zn}(\text{BDC}) \cdot x\text{H}_2\text{O}$ in high water concentrations⁸⁰.



As such, the MOF-69c phase and its relation to the PXRD results (simulated or experimentally gained) can be summarized as follows:

Table 9 - Comparison of chemical formula, Bragg peak locations of published MOF-69c and MOF-69c(desolvated phases) from literature

	Peak at 8.9	Peak at 7.8	Peak at 8.1
Hausdorf <i>et al.</i> (2008)	$\text{Zn}_3(\text{OH})_2(\text{BDC})_2$ MOF-69c(desolv)	$\text{Zn}_3(\text{OH})_2(\text{BDC})_2 \cdot 2\text{DEF}$ (MOF-69c)	-
Kaye <i>et al.</i> (2007)	$\text{Zn}_3(\text{OH})_2(\text{BDC})_2 \cdot 2\text{DEF}$ (MOF-69c)	-	-
Rosi <i>et al.</i> (2005)	-	-	$\text{Zn}_3(\text{OH})_2(\text{BDC})_2 \cdot 2\text{DEF}$ (MOF-69c)
Loiseau <i>et al.</i> (2005)	-	$\text{Zn}_3(\text{OH})_2(\text{BDC})_2 \cdot 2\text{DEF}$ (MOF-69c)	-

Ravon et. Al. (2010)		$Zn_3(OH)_2(BDC)_2 \cdot 2DEF$ (MOF-69c)	
----------------------	--	---	--

However, as we suspect that Kaye *et al.* is actually producing the MOF-69c(desolv) phase, it's discrepancy from the others can be ignored. Given the nature of layered solids such as the MOF-69c (Figure 25), and the shifts present when desolvating the samples, it is highly possible that the discrepancy shown by Rosi *et al.* is due to incomplete solvation of the sample. If the number of DEF molecules per unit cell was not exactly 2, this would result in a peak shifting. Therefore, it appears prudent to refer to the phases present in the same way as Hausdorf has, with MOF-69c having a peak at $7.8^\circ 2\theta$, and the desolvated compound, hereby referred to as MOF-69c(desolv) having Bragg peak at location $8.9^\circ 2\theta$.

2.7 Moisture driven breakdown of MOF-5 to MOF-69c

MOF-5 is known to be unstable in humid air due to the weak coordination bonds between Zn and the BDC group being disrupted by water. The evidence of this reaction can be clearly seen in the following XRD, taken from Kaye *et al.*^{34c}:

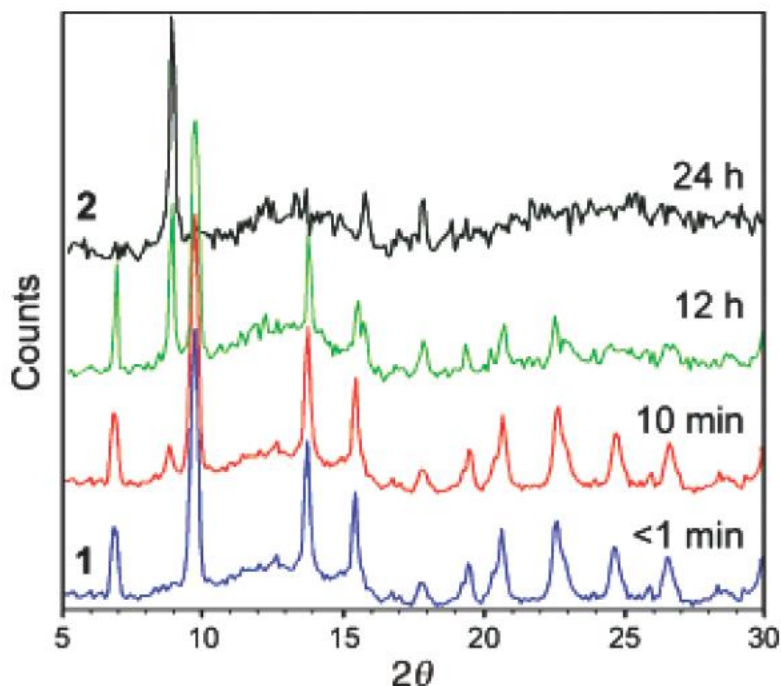


Figure 29 - Breakdown of the MOF-5 unit cell in humid air as a function of time. Image taken from Kaye *et al*^{34c}. Bragg peaks showing the partial breakdown of MOF-5 are shown after as little as 10 minutes, though complete breakdown takes over 12 h.

This breakdown process forms what is claimed to be MOF-69c herein referred to as MOF-69c(8.9), though as the MOF-5 compound was desolvated before being exposed to air, this may well be a sample of MOF-69c in a desolvated state. While this mechanism is of interest to the applications of MOF-5, this process is documented in this case only as a post-synthetic occurrence, and happens to a number of other Zn based MOF materials⁸¹. This process can be prevented from occurring by addition of methyl groups⁸² or other organic groups⁸³ to the framework to increase water stability by a large amount allowing the MOF-5 compound to still be intact after over a week of exposure to humid air. This is due to the energy of the zinc-carboxylate bonding often seen in these MOFs being weaker than the potential for a zinc-hydroxy bond. Interestingly, it has been shown that this process can be reversible, allowing MOF-5 to be regenerated from the MOF-69c compound shown here. Hausdorf *et al*⁷⁰ showed that after the synthesis of MOF-5, the MOF-69c(8.9) and MOF-69c(7.8) phases could both be reached and furthermore, that these reactions were reversible.

Chapter 2 – Background and Literature Review

It is important to note that at no point in the literature concerning MOF-5 and MOF-69c is the notion of MOF-69c forming during MOF-5 synthesis postulated, though multiple groups have published data showing the breakdown of MOF-5 after completion of synthesis to form the MOF-69c phase.

Within the literature showing the MOF-5 synthesis, through any means, the complete reaction mechanisms are not shown. Surfactant added synthesis is the most clear in terms of the synthesis of the crystalline compounds formed. Within this, the addition of specific species to the reaction solution, manipulating the overall charge of the solution to form the Zn_4O^{6+} cation, and then the BDC^{2-} anion required for the framework structure. Within solvothermal synthesis, the reaction mechanisms with respect to solid phases formed, are not shown or even hinted at. The literature can be summed up as suggesting that MOF-5 simply forms from solution given sufficient heat and time.

Importantly, for any experiments involving the synthesis of MOF-5, this breakdown must be considered. MOF-5 must be handled carefully to prevent the breakdown of the material to MOF-69c, which has been shown to noticeably occur within times as short as 10 minutes (Figure 27).

2.8 Selection of starting parameters for MOF-5 synthesis

While the data analysed above suggests some of the potential trends that may exist between experimental parameters and final product, we elected to begin with a pre-published MOF-5 synthesis route in order to begin from a point that was likely to work. This would allow for direct comparison also.

MOF-5 was first synthesized in 1999 by Yaghi *et al*⁴⁹. using the technique described as slow diffusion in Chapter 2.2. This experimental process requires the diffusion of an amine species from an amine rich phase into the reaction solvent, and requires a significant time input in order to yield crystals. For the purpose of scaling up a process viably, this process has substantial issues with scale. However, this methodology also produces crystals with a Langmuir SSA of $2900 \text{ m}^2\text{g}^{-1}$. Due to the strong interest generated about MOF-5 after first publication, refinement to the synthetic process yielded new routes, including a multitude of solvothermal reactions for MOF-5 formation.

Chapter 2 – Background and Literature Review

Solvothermal synthesis, excluding syntheses with unconventional heating mechanisms were generally the most commonly published synthetic route by the mid-2000s. While many syntheses have been published requiring the high temperatures and long durations described above, within the solvothermal synthesis field two particular methods met requirements for production of MOF-5 in a reasonably short time with high surface area. Kaye *et al*^{34c}. published in 2004 with the highest Langmuir SSA reported in the literature for MOF-5, 4400 m²g⁻¹. The synthesis is solvothermal, requiring the solution to be heated at 80 °C for 10 h, at which MOF-5 is produced in up to 86% yield. However, this process requires the addition of reactants at such low concentrations relative to the bulk of MOF-5 literature that to produce 1g of MOF-5 this way would require 1937 ml of solvent, rendering this process economically unviable due to the high cost of DEF. At 10 h duration, this would also have been on the upper boundary for feasibility within the scope of this project.

However, in 2006 a synthetic procedure to produce MOF-5 solvothermally in relatively short durations without significant penalty to the quality of the crystal was published. Mueller *et al*⁷³ⁿ. published results showing a Langmuir SSA of 3400 m² g⁻¹ at a reaction temperature of 130 °C and reaction duration of 4h. While this represents a significant drop in SSA to the results published by Kaye *et al*. this process operates in a considerably shorter time and operates with reactant concentrations 26 times greater, allowing a great deal more MOF-5 to be formed per 100 ml of solvent. This paper does not include yield data, however it is anticipated that the yield would not be sufficiently low in order to reduce the viability of this process beyond that of the synthesis described by Kaye *et al*. As such, we elected to use the conditions described by Mueller *et al*. as the starting point for our syntheses.

2.9 Literature Review of HKUST-1 Synthesis

HKUST-1 was first synthesized in 1999 by Chui *et al*⁸⁴. at the Hong Kong University of Science and Technology for which it was named. HKUST-1 is composed of a Cu-Cu dimer that forms the cation for the MOF. The ligand used is a benzene tricarboxylate group usually from trimesic acid. The

Chapter 2 – Background and Literature Review

oxygen atoms from the carboxylate groups coordinate to the Cu-Cu dimer forming a 3 dimensional structure.

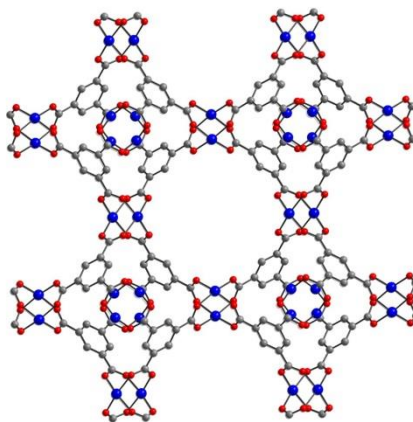


Figure 30 - HKUST-1 Unit Cell generated from crystallographic data⁸⁴. The Cu-Cu metal centre dimers are linked together via the tridentate benzene tricarboxylate ligand.

The paddle wheel type ligands bonding to the metal dimers allows for the formation of a cubic structure with a pore size of 0.9nm and unit cell length of 2.63nm.

The effect of removing solvent molecules from the crystal results in open sites for an adsorbate to interact with the MOF. This is combined with the fact that the Copper dimers form dipoles which can further increase the bonding energy of adsorbate. This is of particular interest when considering hydrogen storage⁸⁵, and the MOF also features a metal cation that is not fully coordinated when the MOF is formed.

The stability of HKUST-1 is generally considered to be relatively good. The crystal structure will absorb water from the air, reducing its overall effectiveness and adsorbance capacity for many gases, though can be advantageous in some cases, such as H₂S adsorption showing an increase in adsorption when the unsaturated metal sites are filled by water molecules⁸⁶. However, unlike MOF-5 and several others zinc based MOFs, this reaction is easily reversible and water can be driven off the structure by heating alone. HKUST-1 has stability issues with ammonia and similar compounds and this should be acknowledged as a market area HKUST-1 would not be suitable to perform in. Thermal stability studies of HKUST-1 generally stability to approximately 200°C, which may limit the potential uses as this is lower than some of the other MOFs considered here.

2.10 HKUST-1 solvothermal synthesis parameters

As with the MOF-5 literature review, we initially began by plotting a series of parameters from a number of publications. As HKUST-1 is stable and commercially available, a large number of publications appear to opt for purchasing a product rather than direct synthesis from solution.

A time-temperature (t-T) plot was used to gain an initial overview into HKUST-1 solvothermal synthesis.

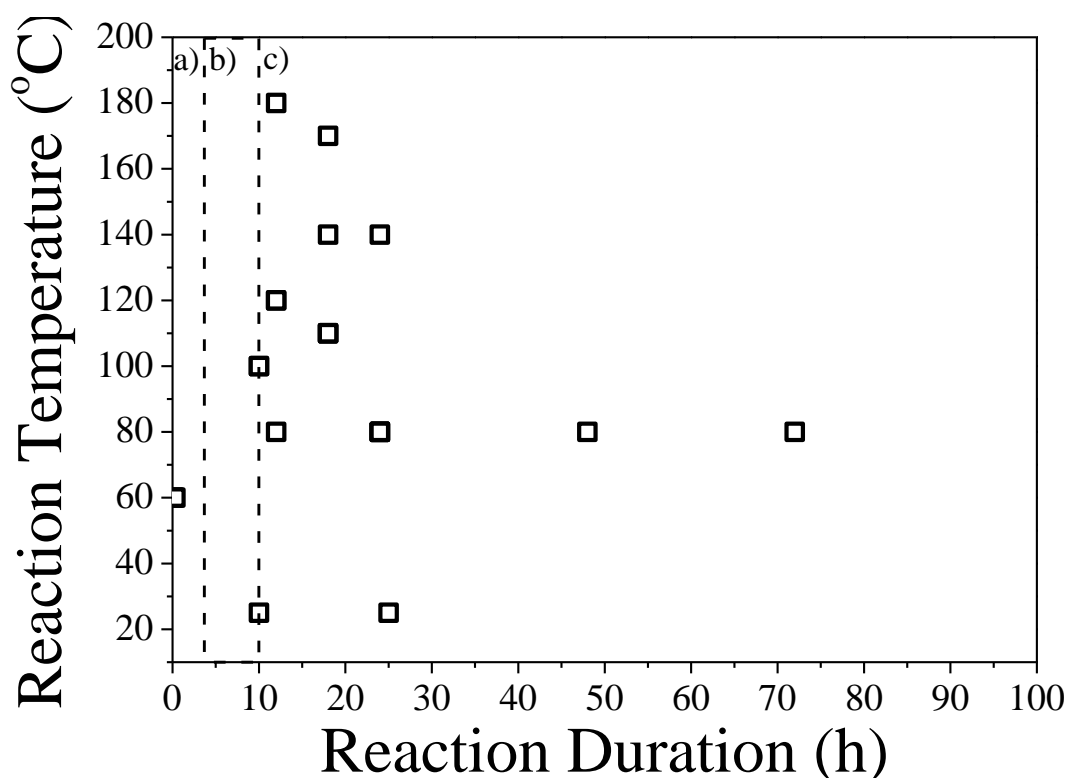


Figure 31 - Time-temperature (t-T) plot for reported HKUST-1 syntheses. Three regions were marked based upon the synthesis time required and their suitability for experimental work.

It is of immediate note that many syntheses require reactions in the order of 10s of hours. A small number of microwave and sonochemical enhanced solvothermal synthesis exist within the purple marked region. The red region describes the approximate temperature range within which we would prefer to operate, keeping residence times below 10h, with a preference for <5h. Beyond this time, the required reaction times would be overly long to be efficient for this project. Again, this suggests a

significant benefit of using unconventional heating methods with microwave synthesized HKUST-1 forming in considerably shorter time periods than via conventional heating methods. Though some syntheses have been performed at temperatures above the range shown here, at 120°C the HKUST-1 produced will begin to show crystalline Cu₂O present, with the intensity of Bragg peaks associated with Cu₂O increasing with increased temperature above this point⁷².

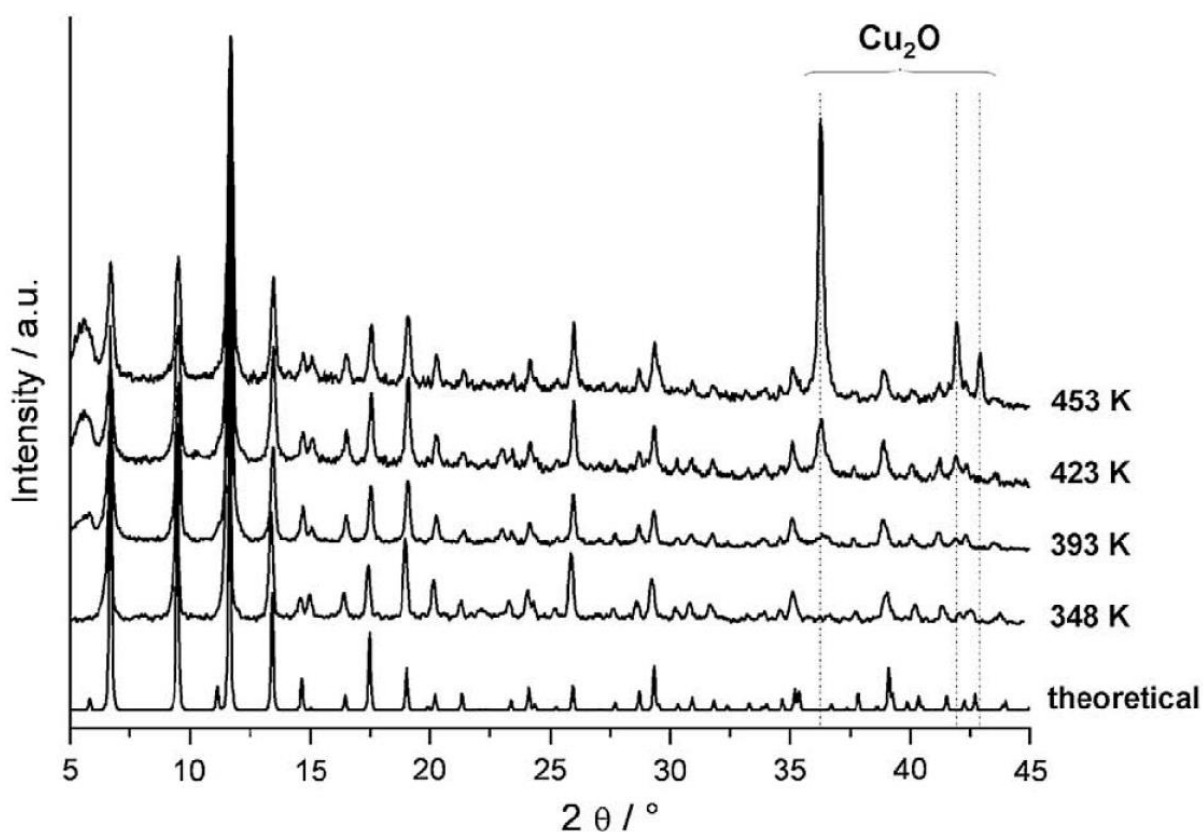


Figure 32 - PXRD of HKUST-1 showing the increased intensity of Cu₂O Bragg peaks beginning at 423 K from Biemmi *et al*⁷², showing the formation of Cu₂O is higher proportions as synthesis temperature is increased.

Further, as Figure 32 only varies temperature it is unclear if this is an effect that would occur if solvent choice, precursor concentrations and other parameters were also altered or is dependent on parameter other than temperatures alone.

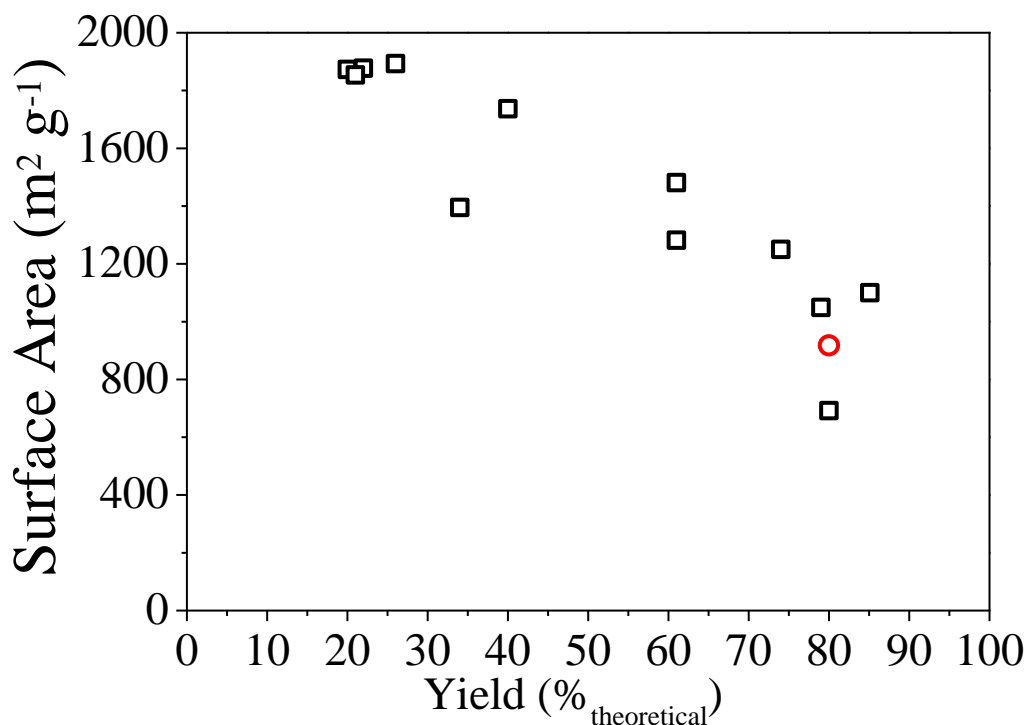


Figure 33 - BET surface areas (Squares) and Langmuir SSAs (circles) of HKUST-1 produced compared to theoretical yield, appearing to show a trend of yield decreasing as surface area increases.

While yield data is not often published, we see that there does appear to be a trend whereby surface area decreases from a maximum value of approximately $1850 \text{ m}^2 \text{ g}^{-1}$ with yields of as low as 20-30% to $1200 \text{ m}^2 \text{ g}^{-1}$ with yields greater than 80%. However, it is unclear why this trend would occur though it is possible that materials may not have been sufficiently washed or dried, resulting in ligand or solvent presence within pores increasing weight and giving the illusion of increased yield, while surface area would be reduced. It is also possible that an unknown aspect of process chemistry forces this result. Further, when considering the total surface area that a single reaction would output when scaled to produce 1g of solids at 100% theoretical yield would be 555 m^2 for the high surface area, low yield sample increasing to 960 m^2 for the lower surface area, high yield sample. This further highlights the need to consider multiple metrics for analysis rather than basing on yield or surface area alone.

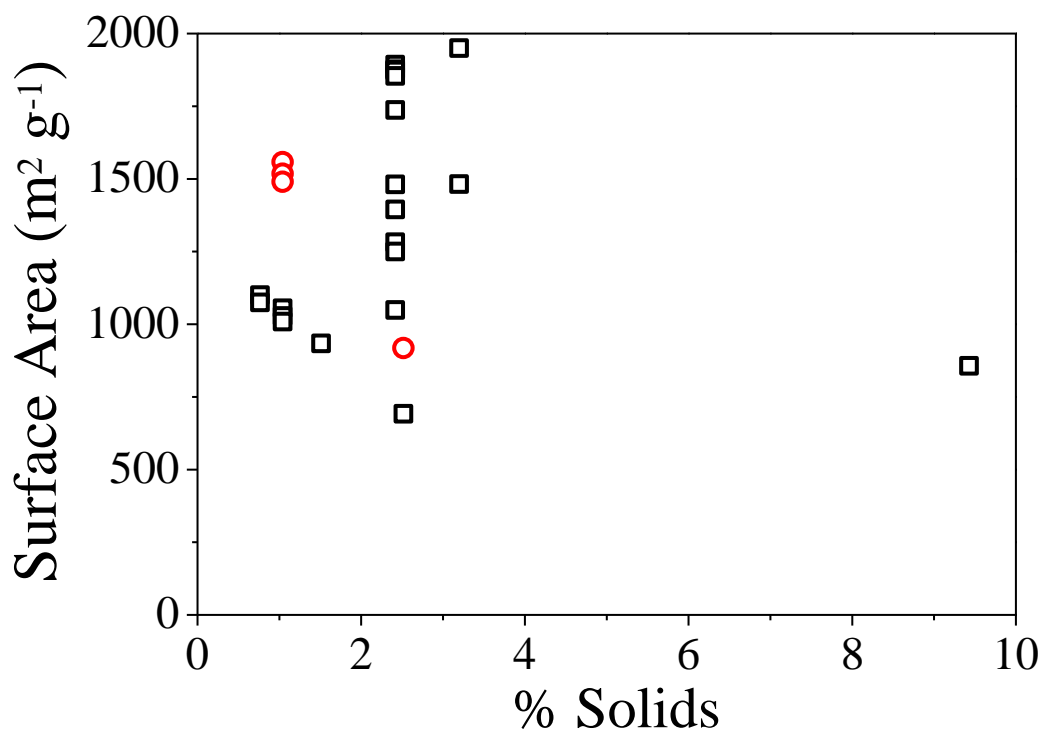


Figure 34 - Reported BET surface areas (Squares) and Langmuir SSAs (circles) for HKUST-1 synthesis relative to % solids at 100% theoretical yield. As with MOF-5, the bulk of reactions appear to have taken place at relatively low concentration with a tight banding between 0.5 – 3% solids.

Understanding the point at which surface area reduction appears to begin to reduce the surface area of the MOF formed is vital to efficient scale up as this should serve to keep the operating conditions efficient for the production of the best quality product. In Figure 34 we see a large clustering of syntheses operating at 2.4% solids with the general region being 0.75-3.2. Only a single synthesis is reported out with these conditions⁸⁷. As the reported surface areas at 3.2% are still amongst the highest reported surface areas, this suggests that it may be possible to operate at 3.2% solids without significant loss to surface area of the final product.

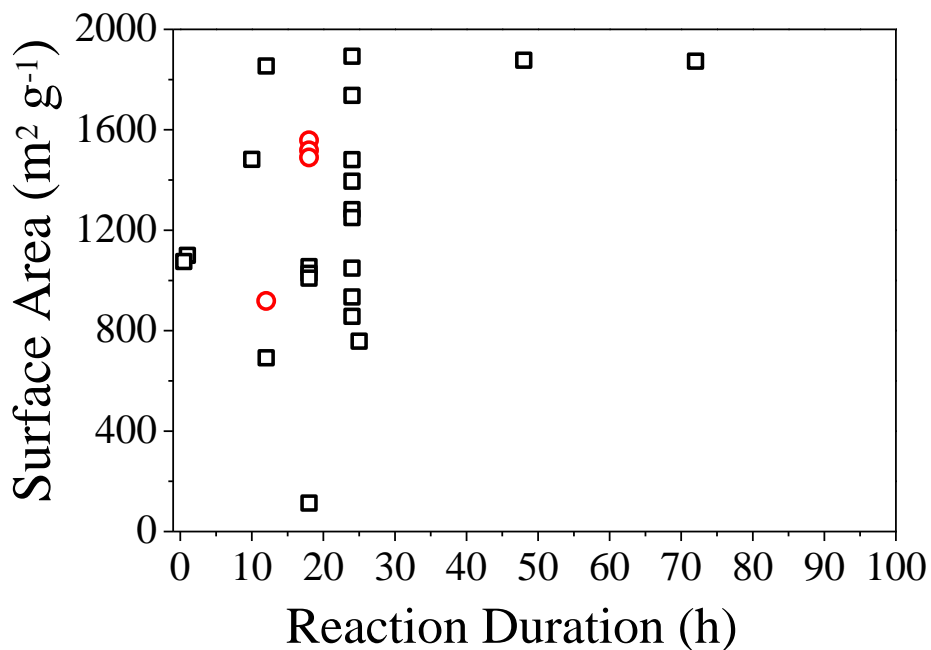


Figure 35 - Comparison of published BET surface areas (Squares) and Langmuir SSAs (circles) for differing reaction durations. Maximum reported surface area does not appear to vary much between 12-72 h.

Figure 35 shows significant variability in reported surface area even with identical durations. Further, this suggests that high surface area syntheses are viable at times 15-80 h. However, the data is lacking for shorter synthesis times, which is the region we would aim to work within if it was viable. As such, further investigation into the characteristics of HKUST-1 produced in shorter times than have been previously published is likely to be useful.

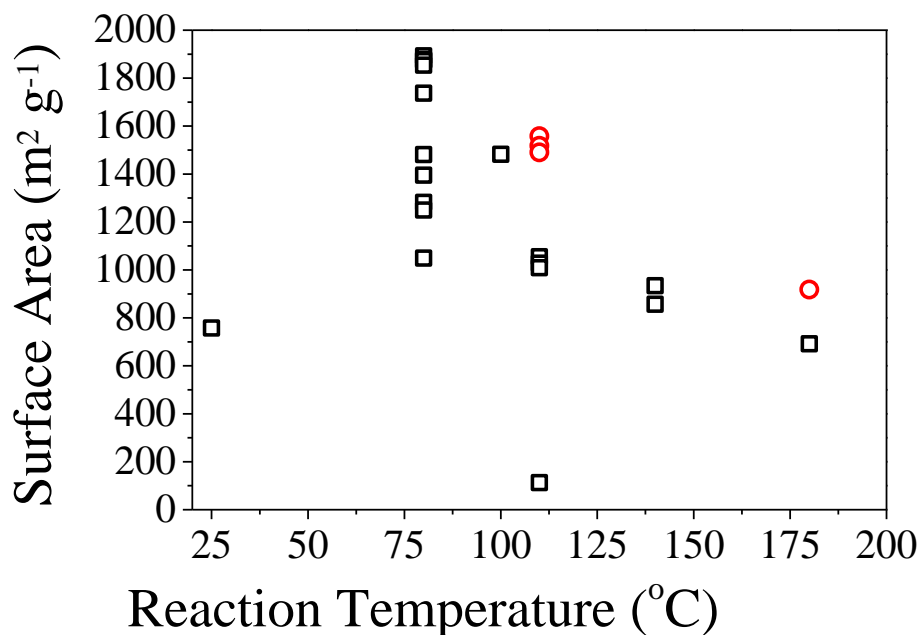


Figure 36 - Reported BET surface areas (Squares) and Langmuir SSAs (circles) compared to reaction temperature. As with MOF-5, increased reaction temperature appears to reduce the reported SSA of the HKUST-1 formed.

Figure 36 shows the effect of temperature upon synthesis. The surface area of materials appears to be reduced when operating at temperatures above 120°C, which can be rationalised as explained in Figure 32, whereby Cu₂O will be formed with HKUST-1 at temperatures of 120 °C and above, with higher temperatures favouring greater Cu₂O formation.

Water concentration of the HKUST-1 system varies more dramatically than was seen for MOF-5 formation, with syntheses varying from <0.01 mol l⁻¹ to synthesis where water is used as the main solvent. As such, it is thought that water concentration is generally less of an issue than for some other MOF syntheses.

2.11 Solvent Choices for HKUST-1 Synthesis

Within the reviewed literature for HKUST-1 solvothermal synthesis occurred primarily using a selection of 5 solvents. DEF, DMF, ethanol, NMP and water appear to be the most commonly used solvents, though unlike MOF-5 where generally a single solvent was used, in this case we generally

Chapter 2 – Background and Literature Review

see a combination of solvents. Further, each of these solvents can be used individually with successfully reported synthesis. As a result, it is important to note the roles each of these solvents play within the reaction system. Much as was the case with MOF-5 synthesis, DEF, DMF and NMP will undergo a hydrolysis reaction which will form amine species which appear to drive the MOF formation reaction process forward. Ethanol acts as a cheaper solvent that also appears to have slower kinetics when used as no amine species are formed as ethanol does not undergo any degradation. Water is generally used as a cheap method of diluting the overall system as the concentration of reactants is important to the final surface area of the material. Further, as hydrolysis of DEF/DMF/NMP solvents will produce species that appear to drive the formation of certain MOFs at faster rates, combining both solvent types may yield benefits. However, while aprotic solvents such as these are required for materials such as MOF-5 and MOF-177, HKUST-1 will form from ethanol solutions without DMF/DEF/NMP addition. Water can seemingly be added to the system without resulting in significant ill effects to the quality of the material produced. The most common solution compositions are DMF/ethanol/water in equal quantities and ethanol as a single solvent.

The important factors are all linked together, but essentially the most important metrics are the reaction time, the yield and the average surface area. However, when scaling this process up the changes in the process chemistry will have more important effects on the quality of the final product. Ethanol does not break down in the process and so can theoretically be almost infinitely recycled with only minimal losses. DMF is known to breakdown when exposed to water and heat and hence cannot be easily recycled. The amines produced from this breakdown also present an environmental risk. Furthermore the heat capacity of each solvent must be considered as this potentially would be a significant cost alteration as energy consumption is expected to be a considerable proportion of total production cost. Ethanol has an approximate heat capacity of 2.3 kJ/kg K compared to 4.2 and 2.0 kJ/kg K for water and DMF respectively. While DMF actually has a lower heat capacity, the addition of water also increases the heat capacity of a DMF/water/ethanol solution to approximately 2.8 kJ/kg K. When the energy usage is compared to the pure ethanol synthesis, and is scaled up this will be a significant amount of energy.

However, without sufficient data on the key factors detailed above, we must consider the effects of both solution compositions via experimental methods in order to determine the likely optimal solution for this system.

2.12 Selection of starting parameters for HKUST-1 synthesis

As with MOF-5, as described in Chapter 2.8, we elected to begin with a previously published synthesis route and vary single parameters from there rather than developing our own synthetic procedure from scratch.

Like MOF-5, HKUST-1 was first synthesised and published in 1999 by Chui *et al*⁸⁴. However, unlike MOF-5 the initial process described is solvothermal, occurring in an ethanol solution heated to 180 °C for 12 h to provide a yield of 60%. Further, the crystals produced showed a BET surface area of 692 m² g⁻¹, which would be considerably improved upon in later publications.

Chowdhury *et al*⁸⁷. in 2009 published a synthesis procedure using 3 solvents – DMF, water and ethanol. By operating at 100 °C for 10 h, this provided crystals of 1482 m² g⁻¹ BET surface area, a significant increase from the work published by Chui *et al*. The yield for this reaction is not given, however the lower operating time and temperature combined with the high surface area reported suggest that the use of 3 solvents as the reaction solution may be of merit.

In 2010, Kim *et al*⁸⁸. published a synthetic route requiring heating at 80 °C for 24 h. Operation at this temperature allows for the process to run at significantly lower pressure than previously described reactions. While this is a minor issue at this stage, this may have a significant effect upon the capital cost of a potential system at industrial scale. Using ethanol alone as a solvent, this produced crystals at up to 76% yield with BET surface area of 1700 m² g⁻¹. While the reaction time for this synthesis is longer than would be ideal, reducing the reaction time while maintain the other experimental parameters was considered.

Chapter 2 – Background and Literature Review

As such, we elected to begin experiments with solvothermal HKUST-1 synthesis using the process described by Chowdhury *et al.*, with the alteration to a reduced temperature and duration. In order to fully understand the effect of changing the solvent from pure ethanol to a combination of ethanol, DMF and water we elected to alter the procedure from Chowdhury *et al.* to a pure ethanol system also, in order to directly compare the effect of the reaction solution.

Within the published reports of HKUST-1 synthesis, a route for producing the MOF using solely water as the solvent is of particular interest. The potential scale up of a system using only water as a solvent would likely result in significant financial benefits. Further to this, the synthesis also occurs at room temperature and so energy costs for the reactor section of a scaled up equivalent to this process would be greatly reduced. Huo *et al.*⁸⁹ report formation of HKUST-1 in short times (1-24h) with high surface areas, while also demonstrating the system can produce significant yields. Further, the reactor system is scaled from 100ml to 2000 ml scales. This synthesis essentially combines the ability to produce HKUST-1 while keeping solvent costs low, producing high yield, high surface area and high space-time yield and scalable. As such, this must be investigated further and may represent a suitable basis for the continuous reactor.

2.13 Potential Applications of unconventional heating methods

Microwave assisted synthesis has been around in organic chemistry since 1986⁹⁰ and inorganic chemistry from the late 1980s⁹¹ onwards. The increased uptake of this technique for synthesis has been due to the rapid synthesis of products which can often take in the region of hours using more conventional synthetic techniques. The heating from microwaves requires a molecule within the reaction to have a dipole moment as this moment is affected by the radiation causing heat within the reaction. A dipole molecule, such as water, will rapidly try to align with the field. The field will oscillate at a given frequency, causing rapid movement of the molecules, causing heating.

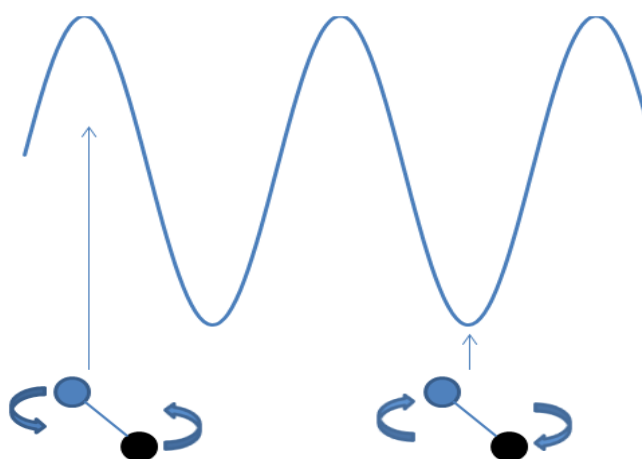


Figure 37 - Molecules attempting to align to radiation field. This oscillation caused rapid heating of molecules with a dipole moment.

The bulk of microwaves used in domestic situations, and small scale chemistry operate at 2.45GHz. This rapid oscillation caused rapid heating rates allowing a high temperature to be reached very quickly. While the dipole moment is essential to the use of microwave radiation, the absorbance of radiation can be increased by the presence of ionic species within the solution, due to the Conduction Effect. The conduction effect means that a solution with ions present will have the ions move within the solution under the effect of the electric field. This movement increases the number of collisions causing greater expenditure of energy, further adding to the heating effect of the microwave system. The nature of chemistry means that increasing rates for experiments is always sought after, though this is often balanced by increased energy input (higher temperatures) or alternative reaction pathways (use of catalysts). Microwave synthesis does not appear to have an increase in energy consumption but does result in a large number of reactions showing a large reduction in synthesis time compared to conventional heating techniques. The exact reason why this occurs is purely speculative with, as yet, no definitive answer⁹⁰. The possible reasons can be seen when looking at the Arrhenius equation, which relates rate of reaction to kinetic and thermal effects.

$$k = k_0 e^{\frac{-E_a}{RT}}$$

Equation 2 - Arrhenius Equation

Chapter 2 – Background and Literature Review

Here we relate the rate of reaction, k , to the two factors determining the rate. The pre-exponential factor, k_0 determines the number of collisions occurring in a given space over a given time. The second factor shows the thermal effects on the system. Logically, one of these two factors would appear to be manipulated by the presence of microwave radiation allowing an overall increase in the rate of reaction.

It has been theorised that microwave energy directly affects the number of collisions occurring at the interface. When heating the molecules using microwave radiation we do see molecular vibrations and this would be a possible reason for this occurrence. The presence of the conduction effect would also likely result in more movement at the interface and potentially explain why this variable can be manipulated.

The alternative theory is that the Gibbs Free energy is being manipulated by the presence of the microwaves. This means microwave radiation would have the effect of both increasing the temperature within the reaction solution and manipulating the Activation Energy in a way similar to catalysing the reaction. As yet, it is unknown which of these effects, or if it is a combination of both, that results in the greatly increased reaction rate often seen within microwave synthetic techniques.

It is thought that the bulk of the changes between the microwave and conventional heating systems are down to rate at which the reactants are heated. Microwave systems generally give a heating profile far greater than conventional heating, which can result in different outcomes even when the final temperature would be the same in microwave and conventionally heated systems. Another aspect to consider as an effect is the presence of localised hotspots. Sonochemical based synthetic routes use the cavitation of bubbles to form very localised regions of high pressure and temperature and can be used to speed up reactions in this way⁹². This effect may be similar in the sense of localised heating on a small volume causing rapid reaction rate due to an increased temperature while the bulk temperature of the reaction solution is considerably lower.

Chapter 2 – Background and Literature Review

The heating rate is not purely down to the dielectric effect, and as such two highly polar solvents may heat at different rates. The ability to absorb microwave energy and then convert to heat can be expressed as a function of the loss angle, δ , usually expressed in the form of its tangent.

$$\tan \delta = \epsilon''/\epsilon'$$

Equation 3 - Definition of loss tangent

The dielectric constant ϵ' varies between solvents and is a measure of the ability of a molecule with dielectric properties to store electrical potential energy when exposed to an electric field, such as microwave radiation. In a neutral solution with a static electric field, this is equal to the ϵ_s , the dielectric constant for the material at STP. However, not all of this potential energy will be transformed to heat and so we must consider ϵ'' , which represents the efficiency of a molecule to convert this potential energy to heat. A higher loss tangent means a greater efficiency in conversion of absorbed energy and so a high ratio of ϵ''/ϵ' (a high loss tangent) allows solvents with similar dielectric properties to have very different heating rates when exposed to identical electric fields. However, ϵ' varies with temperature reducing as temperature increases.

Power dissemination through the bulk material is also vitally important. It can be given either as a function of ϵ'' or as a function of the loss tangent described above.

$$P = c|E|^2 f \epsilon'' = c|E|^2 f \epsilon' \tan \delta$$

Equation 4 - Maximum Power dissemination through bulk medium

P = power absorbed per unit volume. c is universal constant. E is the electric field present in the material and f is the frequency of the electric field. This again shows that ϵ'' is the most significant factor in determining how well a microwave will be able to heat a system.

As such, the rate of heating can be shown as the following equation:

$$\frac{\delta T}{\delta t} = \frac{c|E|^2 f \epsilon''}{\rho C_p}$$

Equation 5 - Rate of change of Temperature due to applied microwave field

Chapter 2 – Background and Literature Review

Where ρ is the material density and C_p is the specific heat capacity of the material. It is important to note that as energy is delivered via electromagnetic radiation into the full cavity, the applied power will be delivered regardless of volume.

The penetration of microwaves into a bulk solid is an important consideration, a large bulk may well only experience heating around the boundary, and so this heating depth should also be considered here.

$$D_p = \lambda_0 \sqrt{(\epsilon' / \epsilon'')}$$

Equation 6 - Maximum Penetration Depth of Microwaves into a bulk material

Where D_p is the penetration depth and λ_0 is the wavelength of radiation used. For conventional domestic microwave ovens this wavelength is 12.5 cm. The maximum penetration of microwaves, including through any boundaries such as tubing, is a potential factor when scaling up microwave systems.

Within microwave systems, it is important to note that both thermal and non-thermal effects can occur as described above. The thermal effects are obvious when comparing heat profiles of a microwave system and a system heated by oil bath.

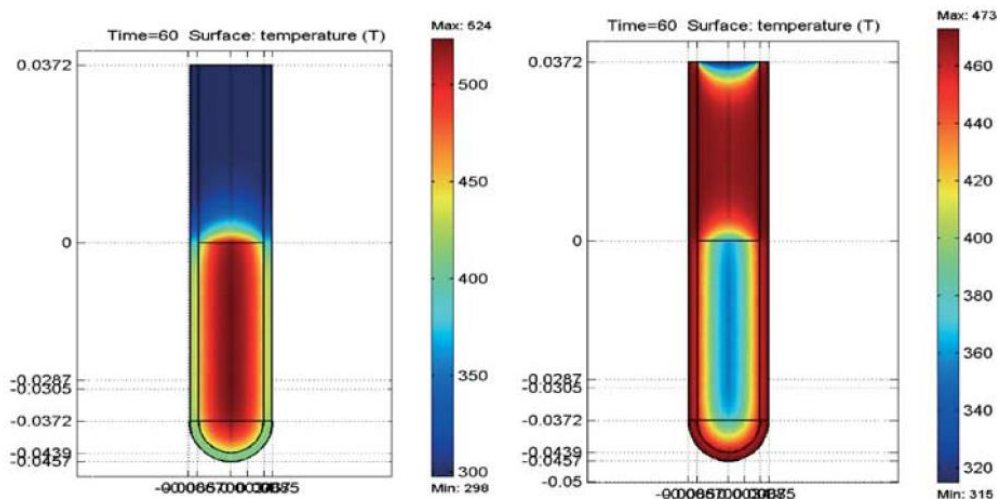


Figure 38 - Comparison of microwave heating (left) and conventional oil bath heating (right) taken from Schanche (2003). The y-axis at 0 represents the meniscus of the fluid. Temperatures are shown as coloured. This highlights the more efficient, uniform heating that microwaves can offer.

Chapter 2 – Background and Literature Review

This shows the uniform heating effect within the fluid, and also highlights the lack of heating in the vapour and gas phases of the system.

While many conventional heating systems use thermocouples for monitoring temperature within the reaction vessel, it has been noted that use of a thermocouple in a microwave solution caused a number of unwanted side effects. The metals used in the design of the thermocouple can cause local distortion in the electromagnetic field used to heat the sample and cause significant conduction away from the sample. Furthermore this can cause thermal instabilities and breakdowns to occur within the synthesis. As such, it is recommended for microwave systems that wish to monitor temperature in situ, non-contact techniques, such as optical methods of determining temperature should be used⁹³.

Furthermore, only liquid phase components can be heated by the microwave system. Vapour phase is unaffected by the presence of the electric field, and solid phase cannot move to expend energy in this way. As a result, the microwaves only heat the liquid phase, causing the vapour phase to condense back to liquid quite quickly. This results in a reduced vapour pressure relative to conventional heating even when at the same temperature. It is therefore possible to heat to higher temperatures without increasing the pressure as much as would be seen in a conventional system at this pressure.

As such, the following comparative table can be drawn up:

Table 10 - Comparison of Microwave and Conventional heating properties, recreated from de la Hoz *et al*⁹⁴.

	Microwave Heating	Conventional heating
Heat transfer mechanism	Energetic coupling	Conduction/ Convection
Heat delivery	Coupling at molecular level	Superficial heating
Rate of heating	Rapid	Slow
Mode	Volumetric	Superficial
Suitability	Selective, Material Property dependant	Non-selective, Less dependant

Chapter 2 – Background and Literature Review

Microwave systems do present some hazards however. Lack of agitation means that any inhomogeneity can result in over heating of that area creating a hotspot of significant temperature difference to the bulk. The distinct difference in heating mechanisms has a clear effect upon solution bulk temperature as shown by Schanche⁹⁵. Alteration of domestic microwaves has microwave leakage issues that represent a significant health hazard. Domestic microwave systems have no built in safety functions for vessel failure representing a potential hazard and also can provide significant power control and temperature control issues. Microwaves at reduced power often operate by reducing the time power is applied for rather than providing a constant power at a reduced rate. As such, for running chemical reactions this could be a significant issue.

Chapter 3 - Experimental

3.1 MOF-5 Synthesis, Process Intensification and Optimisation

To gain an insight into the mechanisms of formation for MOF-5 from solution, during MOF-5 synthesis, we took samples from a mother liquor at various reaction times and running at different temperatures. As discussed in Chapter 2, we selected to operate at temperatures between 110-140°C, as this is the temperature range expected to yield the best combinations of surface area and yield. Further, we also compared the formation of MOF-5 under both mixed and unmixed conditions.

Importantly, as MOF-5 is known to undergo a reaction with the moisture present in air, it required special handling. MOF-5 was dried using vacuum filtration for a time less than 90 seconds. This step is required to provide useful powder but also requires exposure to a significant volume of air, however PXRD analyses after this drying stage have shown pure-phase MOF-5 still. Samples were then stored in sealed vials within a desiccant chamber. For all analyses, MOF-5 was removed from storage then analysed immediately after opening the vials with any special preparation required for analysis being completed as quickly as possible. Though non-destructive analysis techniques were commonly used, analysed samples were never added back to the original vial to avoid contamination and also due to that sample having significantly more exposure to air already.

0.157 g (0.6 mmol) zinc nitrate tetrahydrate (Emsure $\geq 98.5\%$) and 0.0333 g (0.2 mmol) terephthalic acid (Alfa Aesar 98+%) were dissolved in 5 ml (45mmol) N-N-diethylformamide (DEF) (Alfa Aesar, 99%) in 23 mm diameter flat bottomed glass vials. As the most common synthesis methods involve the use of an excess quantity of zinc, a Zn:BDC:H₂O molar ratio of 3:1:12 was used initially. The overall concentration was set in order to give a 100% theoretical yield producing 1% solids by weight. This ratio is maintained through all MOF-5 experiments unless stated otherwise. Multiple parallel samples were placed into a pre-heated oil-bath and stirred with 5mm PTFE magnetic stirrer bars. Vials were heated for designated experimental durations varying from 30 min to 6 h in increments of 0.5-1 h. After reaching the experimental duration, vials were removed from the oil bath and the contents were vacuum dried and sealed. Due to the expense of solvent, and the volumes required to

Chapter 3 - Experimental

wash samples we elected not to wash samples formed in this way. The temperatures used were 140, 130, 120 and 110 °C. The effect of stirring upon synthesis was analyzed by repeating the above synthesis without stirring the solutions.

Due to the relatively rapid breakdown of MOF-5 when exposed to water post-synthesis, one of the key parameters that could potentially affect the synthesis of MOF-5 is the water concentration of the solution. High water concentration may result in the formation of MOF-69c. However, water is also required in order for the formation to progress as discussed in Chapter 2. As such, we studied the effect of increased hydration of the zinc salt on the reaction and products, a hexahydrate salt (0.178 g (0.6 mmol) zinc nitrate hexahydrate (Alfa Aesar, 99%)) was used for synthesis instead of the tetrahydrate salt while all other reagents concentrations were maintained. Due to altering the hydration of the zinc salt, a Zn:BDC:H₂O molar ratio of 3:1:18 was achieved instead of the 3:1:12 ratio used previously, hence, maximum theoretical yield of MOF-5 was unchanged (1 g/100 ml solution = 1% solids). Solutions were stirred and heated as described previously.

The effect of metal:ligand ratio was also investigated, using ratios of 3:1, 1.33:1 (stoichiometric), 1:1 and 0.67:1 with the metal salt being zinc nitrate tetrahydrate. The maximum theoretical MOF-5 yield was maintained at 1 g/100 ml.

Additionally, the effect of increasing solid content was investigated; a Zn:BDC:water ratio of 3:1:12 was maintained. The following maximum theoretical MOF-5 yields were examined: 3, 5, 10, 20 and 30 g/100 ml (3-30% solids). All reaction parameters were maintained as described initially with the temperature set at 140°C, except for the starting concentrations of zinc nitrate and terephthalic acid..

As DMF offers a cheaper, more widely used alternative solvent; we investigated the quality and yield of MOF-5 formed at 130 °C in a time of 4 hours, allowing a comparison of the characteristics of MOF-5 produced using DMF and using DEF. For this experiment, all conditions were kept identical at 0.157 g zinc nitrate tetrahydrate and 0.0333 g terephthalic acid in 5 ml DEF. A Zn:BDC:H₂O molar ratio of 3:1:12 and overall concentration of 1% solids was maintained by keeping all process

parameters identical, with the exception of solvent which was replaced by n-n-dimethylformamide (DMF) (Sigma Aldrich, 99.8%, anhydrous).

3.2 Scale Up and Continuous Synthesis of MOF-5

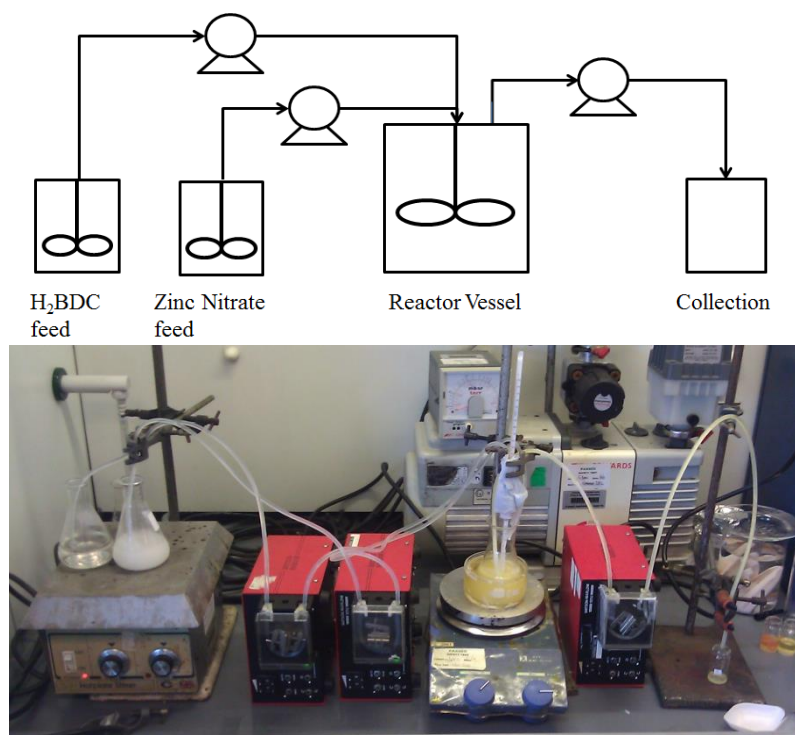


Figure 39 – Experimental Layout of the Continuous MOF-5 system and image of the reactor system in place.

The reactor set up was split into 3 sections: feed, reactor and collection (Fig. 1). Due to solubility considerations during the dissolution of terephthalic acid at the higher end of concentrations analysed here, the H₂BDC feed was heated within a reflux condenser and required heating to approx. 100°C before total dissolution of the ligand would occur. The zinc salt completely dissolved at ambient conditions, even at the higher end of concentrations analysed. Both feeds were stirred for a minimum of 30 minutes before the start of reaction to ensure mixing was complete. Calibrated peristaltic pumps (Watson Marlow 101-U) fitted with a combination of silicone and PTFE tubing were used for reactor input and output. The reactor operates at 140°C, therefore requires to be run under reflux conditions in order to mitigate the loss of solvent caused by the high temperature relative to the boiling point of the solvent and the boiling point depression caused by the reactants. The temperature of the system was monitored in-situ via thermocouple or thermometer positioned in the reaction solution. The feed tubes

Chapter 3 - Experimental

dripped into the reactor from above, while the removal of products from the reactor occurred via a tube placed at the bottom of the reactor. In order to avoid any contamination during collection, the products were collected for a period of 20-30 minutes in new, disposable glass vial before being vacuum dried before further analysis. After optimisation, the optimised experiments were then performed using DEF and DMF individually in order to compare the effect of altering the solvent upon the continuous reactor system.

The feed supply consisted of 0.314 g zinc nitrate tetrahydrate (Emsure $\geq 98.5\%$) dissolved in 100 ml solvent and 0.0666 g terephthalic acid (Alfa Aesar 98+%), dissolved in a reflux condenser, of 100 ml solvent. The initial reactor mixture consisted of 100ml solvent. This solution was heated to the reaction temperature (140°C) before 0.157 g zinc nitrate tetrahydrate and 0.0333 g terephthalic acid (H_2BDC) were added as the pumps were switched on resulting in a Zn:BDC: H_2O ratio of 3:1:12. As the solvent was heated to reaction temperature before the pumps were started or precursors were added to the reactor vessel, the time at which the pumps were turned on was therefore a true time of 0 for this experiment, and this was continued for all continuous MOF-5 reactions. Further, by adding terephthalic acid to solvent at this temperature, dissolution occurs almost instantly.

The reactor volume was set as 100ml, with total input and output set at 50 ml h^{-1} to give an average residence time of 2h. This reaction was then repeated with increased residence time, with the system set to have total input of 25 ml h^{-1} , resulting in an average residence time of 4h.

Due to the potential benefits of process intensification with respect to solid content, the feed and initial concentrations were then proportionally increased in order to reach theoretical yields of 5 and 10% for DEF, and 3 and 5% for DMF, due to formation issues with DMF at high concentrations within batch synthesis, while the temperature was maintained at 140 °C throughout. We further compared the effect of Zn:BDC ratio by using the stoichiometric ratio of zinc and BDC (4:3) in addition to the 3:1 ratio described previously. This was achieved by changing feed concentrations, while keeping the flow rates unchanged. The reactor volume was set as 100ml, with total input and output set at 25 ml h^{-1} , resulting in an average residence time of 4h.

Chapter 3 - Experimental

As the system was observed to have a start-up phase of 4-5h, it was thought that the residence time of the system could be reduced after the completion of this start-up phase in order to increase the space-time yield of the product. In order to investigate the effect of residence time after a steady state has been reached, the system was run as described above (4h residence time, 3:1 M:L ratio, 140°C, 1% solids) for a period of 5h, in order to reach steady state for this reactor system. After this 5h period, the total throughput of the reactor was doubled, giving a residence time of 2h.

3.3 Understanding and Optimisation of HKUST-1 Batch Syntheses

We reviewed literature in order to find the most consistent and reliable synthetic procedures for producing HKUST-1. Due to scalability issues and continuous processing difficulties with electrochemical and mechanochemical methods, we focused on solvothermal synthesis. We used a modified version of the synthesis route from Chowdhury *et al.*⁸⁷ as the basis for our experiments, modifying this procedure to produce material under similar conditions to Kim *et al.* for comparison.

In order to determine if HKUST-1 passes through any metastable crystalline phases and to determine the approximate kinetics of the formation of HKUST-1 we used a time resolved study of HKUST-1 formation, similar to that described for MOF-5 in section 3.1. In order to eliminate large variations in temperature when mixing solutions, we premixed and heated 75ml of ethanol containing 6.9909g $\text{Cu}(\text{NO}_3)_2 \cdot 2.5\text{H}_2\text{O}$ to 60°C while being stirred. We also heated 75ml of ethanol containing 3.333g H_3BTC with vigorous stirring to 60°C. At time = 0, we mixed these two solutions and began to draw 2ml samples at certain intervals while maintaining the temperature of the reaction vessel. Due to the small volume of solution removed, these samples were centrifuged. Owing to the increased resolution of sampling due to the faster formation of HKUST-1, it was deemed practical to use mother liquor with removal of aliquots rather than multiple parallel samples as was used for MOF-5 as described in Chapter 3.1 above. The supernatant was collected and the remaining solids mass was analysed by PXRD and FT-IR.

All batch tests were carried out with 6 ml of total solvent and the metal:ligand concentration ratio at 1.8:1, resulting in the metal being in excess (3:2 is stoichiometric). All experiments were stirred and

Chapter 3 - Experimental

heated using an oil bath and hot plate to reach the desired temperature, monitored by a thermocouple inserted into the reaction solution.

The solution was made up of equal parts n,n-dimethyl formamide (DMF) (Sigma Aldrich, 99.8%, anhydrous), deionised water and ethanol (Sigma Aldrich, 99%). 0.231g copper nitrate hemipentahydrate (Sigma Aldrich, 98%) and 0.111g trimesic acid (Sigma Aldrich, 95%) were added to the solution. The sample vials were then capped and placed into an oil bath which was preheated to the reaction temperature of 60 °C. Multiple samples were removed after differing time periods and analysed to show how yield, purity and porosity vary as a function of synthesis time. The experiment was then repeated using ethanol as the only solvent, keeping all other reaction parameters identical.

These experiments were then repeated without DMF, using only a volumetric mixture of ethanol and deionised water. The volume of water present was increased from 1ml to 3ml while the difference in the 6ml solvent was made up by ethanol.

The ethanol only experiment was then repeated with the system running at 79°C. This experiment was completed in a reflux condenser with aliquots of identical volume taken rather than multiple distinct samples as before.

As described in Chapter 2.11, a synthesis procedure for formation of HKUST-1 using only water as a solvent at ambient temperatures⁸⁹ has been published. Due to the economic benefits of this synthesis we attempted to replicate this. The solution was made up using 6ml deionised water. 0.231g copper nitrate hemipentahydrate (Sigma Aldrich, 98%) and 0.111g trimesic acid (Sigma Aldrich, 95%) were added to the solvent. A number of parallel conditions were analysed for this reaction set up.

Samples were stirred and left for periods of 24 h, the longer, higher yield producing conditions described by Huo *et al*⁸⁹. Further we heated a different set of solutions to 80 °C in order to determine what effect temperature would have upon this synthesis. Due to the post-treatment of HKUST-1 described by Huo *et al*⁸⁹. we carried out a synthesis at ambient conditions, under stirring for 24 h,

dried the sample as described above then redistributed the solids collected in ethanol and subjected to sonication.

To investigate the effect of process intensification upon the ethanol only system the experiment was repeated with the reactant concentrations increased to give approximately 6, 9 and 15% solids theoretically.

3.4 Solvothermal Continuous Synthesis of HKUST-1

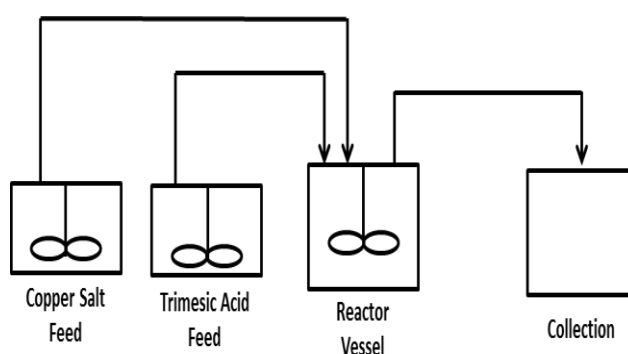


Figure 40 - Basic Layout of the Continuous HKUST-1 Synthesis System, with similar layout to the set up used for MOF-5, as shown in Figure 39.

For the continuous flow system, the basic layout of the apparatus was as shown in Figure 40. The reactor vessel itself was a reflux condenser situated in an oil bath. A thermocouple was used to monitor the temperature of the solution within this vessel. The reactor was initially loaded with 100ml ethanol and heated to the reaction temperature. At the time when the feed pumps were turned on, 4.62 g copper nitrate hemipentahydrate and 2.22 g trimesic acid were added, equivalent to 3% solids. This allowed the time the pumps go on to be a true time of zero for the reaction and should allow observation of any start-up phases before reaching steady state. The copper salt feed consists of 13.86 g of copper nitrate hemipentahydrate dissolved in 150ml ethanol. The trimesic acid feed consists of 6.66 g of trimesic acid dissolved in 150ml ethanol. Initially, the flow rate of the Watson Marlow 101-U calibrated pumps was set to deliver 33 ml hr^{-1} of each of the feeds while the collection pump was set to remove 66 ml hr^{-1} , giving an overall average residence time within the reactor of 1.5 hr. Samples were collected over a 15 minute period of time each before filtration and washing with ethanol. The

Chapter 3 - Experimental

solid output was then analysed as described below. The experiment was then repeated at 9 and 15% solids by increasing the solid precursor concentrations proportionally.

Pelletisation of the output from the continuous HKUST-1 production system was used to test if HKUST-1 could be altered from a bulk powder to a form more useful for the many potential applications. Here we compare the material in 4 states of compression; bulk powder, compressed by hand with very low compression, compressed at one tonne and compressed at two tonnes. To process the pellets, HKUST-1 was added to a pellet press and compressed at the desired strengths in order to yield pellets of 13mm diameter and approximately 2-3 mm thickness.

3.5 Use of microwave heating for MOF-5 synthesis

A tank reactor was used initially due to the considerable similarity to a previously successful system using conventional heating techniques. As the temperature is greatly influential on the MOF-5 production system we aimed to determine what power level would allow a steady state temperature that was suitable for us. Previous work completed on the MOF-5 reaction showed that a temperature of 130-140°C would produce MOF-5 of high quality in short times. The boiling point of the DEF solvent used is approx. 175 °C. Heating above this temperature is likely to cause boiling or superheating of the solvent. The MOF-5 reaction will not occur below 75 °C. As a result, we have set a temperature region of 110-140 °C that would be our preferred zone, and 100-150 °C represent our limits on what temperature would be suitable.

A domestic microwave was used for these syntheses and so temperature control was only possible through manipulation of the power level on the microwave. Using DEF solvent with no salt or ligand added was used to attempt to calibrate the system and determine appropriate power levels. Due to the risks of super-heating and the rapid heating that occurs when using microwave heating methods rather than convective heating methods, the lowest power setting, 10%, was used initially before increasing to 20%. Due to issues at 20% power causing superheating of the solvent, higher power levels were not studied. Samples were placed in the centre of the microwave cavity, and then heated. The temperature

Chapter 3 - Experimental

of samples was then measured and heating was continued until the temperature appeared to be steady.

This experiment was repeated 3 times at both power levels.

In order to bridge the gap between batch and continuous reaction systems using microwave heating for MOF-5 production, PTFE tubing was fed through the side vents on the microwave in order to facilitate pumping of solution into the microwave cavity without any modification to the external or internal casings. Within the cavity, a large bore tube or glass reaction vessel was connected via silicone tubing secured in place with cable ties and Teflon tape. This system was tested for leaks by looping several litres of solvent through the system for several hours. The large scale system is connected using PTFE tubing with silicone tubing around the outside through a PTFE ferrule. These joins are all secured by Teflon tape and cable ties. As one side of the reactor coil is not sealed in any way, this should reduce the risk of over pressurising the system, which represents a hazard with this system. Further, the connection between the small bore tubing and large bore tubing is within the microwave cavity and is designed as a weak point, allowing this to burst if the open end is insufficient to release any pressure build up. This was done as a safety consideration. This allowed for the system to be operated with the exposure to microwaves being limited in time to prevent over-heating, and if overheating occurs the burst point is within the microwave cavity.

A reactor volume of 100ml was set, with a residence time of 30 minutes. The system previously used with conventional heating operated with identical volume but had a residence time of 4 hours.

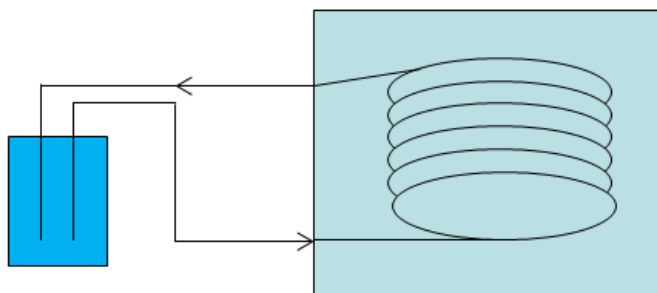


Figure 41 - Experimental layout of multiple pass MOF-5 system using microwave heating. The solution is fed in, heated then recycled. This allows for operation without heating the solution

The feed supply consisted of 0.72 g zinc nitrate tetrahydrate and 0.0666 g terephthalic acid dissolved in 200ml of DEF solvent. The solution was stirred for 1 h before the reaction was begun in order to ensure a well-mixed solution. The solution kept outside the microwave is constantly agitated but was not heated in any way.

The pumps were set to deliver 200ml h^{-1} to an internal volume of 100 ml giving a residence time of 30 minutes. The total length of time the solution was looped for was 8 h. The system was operated at 10% of maximum power. The experiment was then repeated at 20% power.

3.5 Use of microwave heating for HKUST-1 synthesis

Using a modified domestic microwave, we investigated the main parameters affecting the production of HKUST-1 using microwave heating rather than conventional convective heating.

The solutions used were made up of 0.466g copper nitrate hemipentahydrate, 0.222g trimesic acid in 10ml of ethanol. As samples could not be stirred during the heating period, samples were stirred for 30 minutes at ambient conditions before removal of the magnetic stirrer bar and immediately placed in the centre of the microwave for reaction. As domestic microwaves do not produce a completely uniform field the hotspots within the chamber vary⁹⁶, as such, we always placed the vials within the centre of the microwave to attempt to mitigate this factor as much as possible.

Chapter 3 - Experimental

The samples were then heated at 10% of the maximum power level of the microwave for 180 seconds, and was repeated twice more. To investigate the effect of increasing this reaction time, 300s and 600s reaction times were also investigated.

In order to see how heating rates affected the output of the system, the initial experiment was repeated with 20% power on the microwave.

This experiment was then repeated using theoretical % solids of 15% in order to investigate how intensification affects the formation of HKUST-1 under microwave heating.

3.6 Continuous Microwave Enhanced Synthesis of HKUST-1

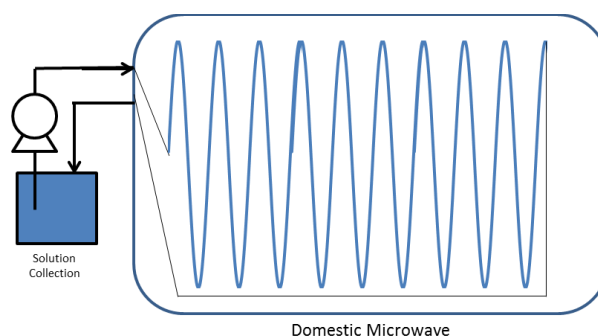


Figure 42 - Basic Layout of the modified domestic microwave continuous HKUST-1 synthesis system with looped feed

For the microwave enhanced HKUST-1 reaction system, the basic layout of the system is as described above in Figure 42. A domestic microwave was modified by feeding small bore tubing through the side vents, in order to avoid any alterations to the cavity casing and avoiding any safety issues. Due to severe issues with hotspots forming in a bulk solution, a tubular reactor system was used for this reactor.

The feed vessel consisted of 13.86g of copper nitrate hemipentahydrate and 6.66g trimesic acid dissolved in 300 ml of ethanol. This solution was kept at ambient temperature and stirred for 30 minutes to ensure complete dissolution of the reactants before the reaction was initiated by powering on microwave. This solution was then pumped through the microwave cavity at rate of 300 ml h⁻¹.

Chapter 3 - Experimental

The solution was then fed back into the original feed vessel which was stirred constantly. Samples were removed periodically.

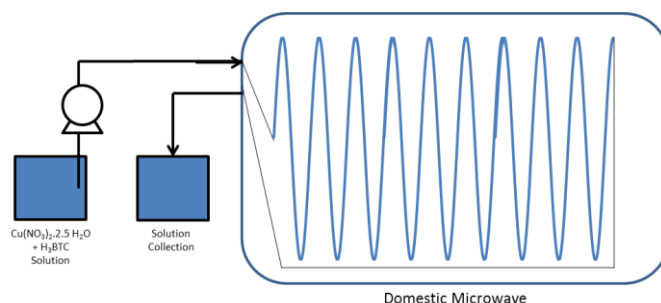


Figure 43 - Basic Layout of the modified domestic microwave continuous HKUST-1 synthesis system using a single pass

In order to investigate a single pass yield and find the highest space-time yield of materials we then switched to a single pass reactor system. The feed vessel consisted of 13.86g of copper nitrate hemipentahydrate and 6.66g trimesic acid dissolved in 300 ml of ethanol. This solution was kept at ambient temperature and stirred for 30 minutes to ensure complete dissolution of the reactants. This solution is then pumped via peristaltic pump set to deliver 300 ml h⁻¹ flow rate into a PTFE tube within the reactor system with 25ml total volume giving a residence time of 0.1 h. The microwave was operated on the lowest power setting, with the output temperature maintained at approximately 45 ± 5 °C, measured by thermocouple placed within the tubing immediately upon leaving the reactor vessel. The output temperature was monitored by thermocouple within the solution leaving the microwave cavity. This system was then repeated using a 2ml reaction tube, with flow rate of 550 ml h⁻¹ in order to probe the minimum time required to produce HKUST-1 using continuous microwave enhanced processing.

Chapter 4 – Analytical and characterisation techniques

4.1 Sample Collection and Storage

Samples were collected in individual disposable glass vials from solution to allow cooling before vacuum filtration to dry samples.

For MOF-5, samples were not washed thoroughly due to the cost of DEF solvent and the volume required. Although the samples synthesized in DMF could be washed without significant penalty, these samples were treated identically to the DEF synthesised samples in order to maintain parity. For HKUST-1 samples, samples were washed with ethanol after vacuum filtration in order to remove any excess ligand present within the sample.

MOF-5 samples were stored in a desiccation chamber due to the potential irreversible breakdown of the product upon reaction with water from air. This also limited the preparation time of samples for analysis as this reaction will occur with significant effects within 10 minutes. As HKUST-1 does not undergo an irreversible reaction through exposure to humid air, these samples did not require this extra step.

Dry mass for MOF-5 was based upon the mass loss of the material when activated for gas adsorption studies or via Thermogravimetric analysis where applicable. For HKUST-1 samples, the samples were heated to 170°C under atmospheric pressure generally, with selected samples heated to the sample temperature under vacuum showing near identical proportional mass loss.

4.2 Crystal Structures

Metal Organic Frameworks consist of a regular, repeating array of ions and organic molecules arranged in a consistent pattern in the solid state. Unlike inorganic solid materials, the organic portions of MOFs are made up of discrete molecules rather than single ions and MOF materials are made up of both discrete molecules and ions. When considering these patterns as a whole, it is

important to consider the unit cell of the crystal, the smallest repeating unit of the entire structure. The unit cell represents all the molecules and atoms present allowing the bulk crystal material to be seen as multiple units cells joined together. A MOF-5 unit cell is shown below, along with how this unit cell fits into the bulk material⁷³.

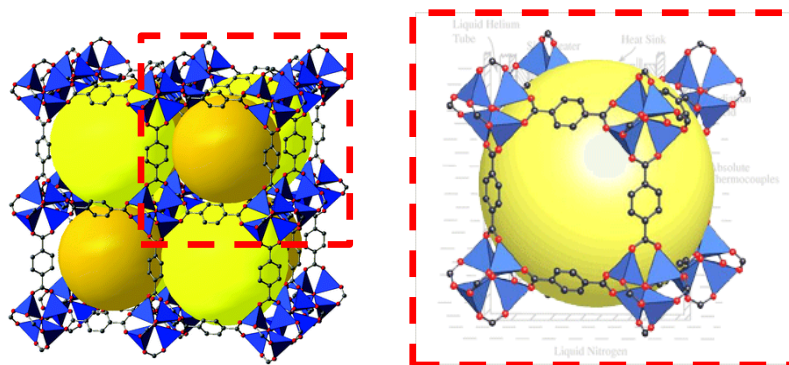


Figure 44 - MOF-5 Bulk Material on left, with unit cell highlighted and expanded to the right.

The unit cell is defined by the 3 side lengths, named a, b and c. The angles between the 3 sides are also of importance, and noted by α , β and γ where α is the angle between sides b and c, β is the angle between sides a and c, and γ is the angle between sides a and b.

7 distinct Unit cell shapes are determined by the side lengths and the internal angles⁹⁷.

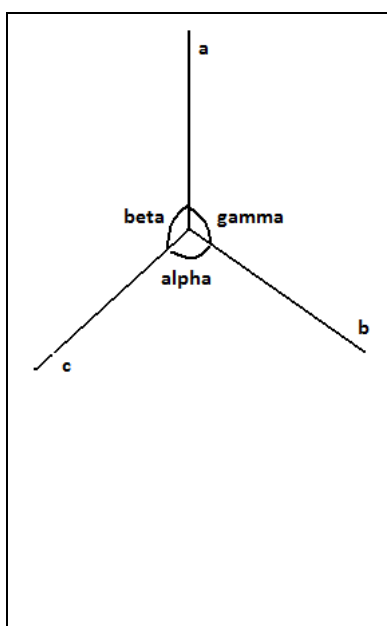
	Crystal System	Unit Cell Shape
		Cubic
	Tetragonal	$a=b \neq c, \alpha=\beta=\gamma=90^\circ$
	Orthorhombic	$a \neq b \neq c, \alpha=\beta=\gamma=90^\circ$
	Hexagonal	$a=b \neq c, \alpha=\beta=90^\circ \gamma=120^\circ$
	Trigonal (a)	$a=b \neq c, \alpha=\beta=90^\circ \gamma=120^\circ$
	Trigonal (b)	$a=b=c, \alpha=\beta=\gamma \neq 90^\circ$
	Monoclinic	$a \neq b \neq c, \alpha=\gamma=90^\circ \beta \neq 90^\circ$
	Triclinic	$a \neq b \neq c, \alpha \neq \beta \neq \gamma \neq 90^\circ$

Figure 45 - Overview of crystal systems and shape and diagram of the internal angles

Chapter 4 – Analytical and characterisation techniques

The basic lattice types must be considered in order to gain complete information about the crystal structure. The arrangement of the unit cell, for cubic systems falls into one of three categories⁹⁷:

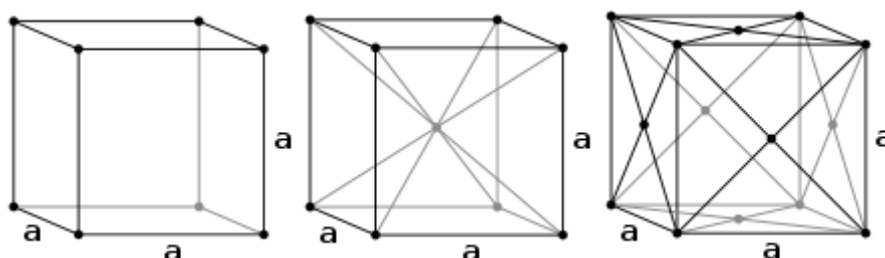


Figure 46 - Cubic Lattice Types - Primitive (P) on the left, Body centred (I) in the centre and Face Centred (F) on the right.

The MOF-5 unit cell shown above in Figure 44, and the HKUST-1 unit cell shown as Figure 30 are both cubic and conform to the primitive lattice type. These combinations of Lattice types and crystal systems give rise to the 14 Bravais lattice types. A maximum of 14 Bravais lattice types are available as not all crystal systems are compatible with all lattice types. For instance, the triclinic unit cell shape has a very low symmetry to the point that only a primitive lattice type is possible within that crystal system. It is important to emphasize, all crystal systems can be described by one of the basic 14 Bravais types.

Table 11 - Allowed Bravais Lattice types for each crystal system

Crystal System	Unit Cell Shape	Allowed Lattices
Cubic	$a=b=c, \alpha=\beta=\gamma=90^\circ$	P, F, I
Tetragonal	$a=b \neq c, \alpha=\beta=\gamma=90^\circ$	P, I
Orthorhombic	$a \neq b \neq c, \alpha=\beta=\gamma=90^\circ$	P, F, I, A and either B or C
Hexagonal	$a=b \neq c, \alpha=\beta=90^\circ \gamma=120^\circ$	P
Trigonal (a)	$a=b \neq c, \alpha=\beta=90^\circ \gamma=120^\circ$	P
Trigonal (b)	$a=b=c, \alpha=\beta=\gamma \neq 90^\circ$	R
Monoclinic	$a \neq b \neq c, \alpha=\gamma=90^\circ \beta \neq 90^\circ$	P, C
Triclinic	$a \neq b \neq c, \alpha \neq \beta \neq \gamma \neq 90^\circ$	P

4.2 X-ray Diffraction

Exploring the structure of crystalline materials can be carried out using any radiation with a wavelength comparable to interplanar spacing. As most interplanar spacings are in the region of 1-10Å, the wavelength required falls in the high energy region of the electromagnetic spectrum falling in the deep UV- γ rays, although it is also possible to use electrons or neutrons to reach the required wavelengths. Due to the increased complexity of interactions and the practical reason behind generating high energy particles, X-rays are most commonly used to probe crystal structures.

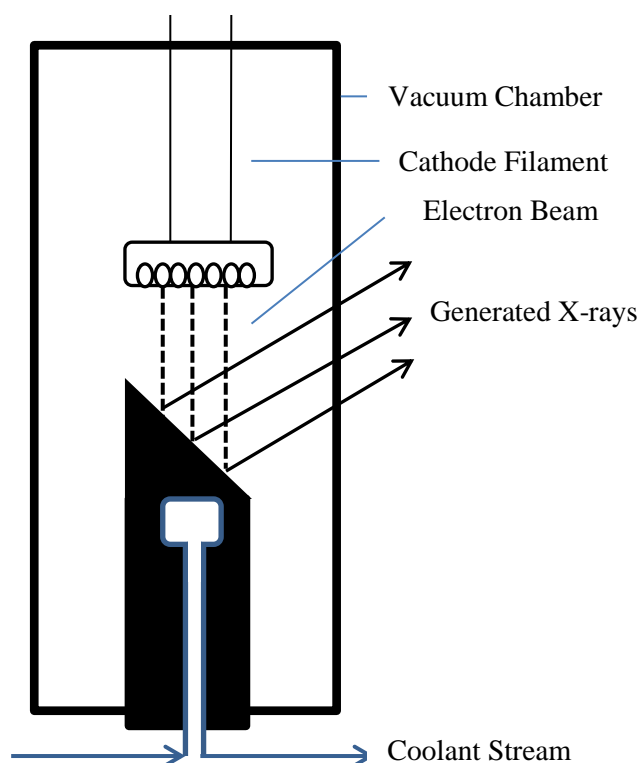


Figure 47 - The layout of an X-ray generation chamber.

When short wavelength radiation, such as X-rays, come in contact with a crystalline material two effects can occur. Firstly, the radiation can be absorbed by the material usually resulting in an electron being excited and ejected at a lower wavelength, often resulting in fluorescing which forms the basis of X-ray fluorescence analysis. Alternatively the radiation will be scattered when coming into contact with the electrons. Depending on the scattering this wavelength is changed (albeit considerably less than would occur if the radiation is absorbed as an X-ray and emitted as visible light) giving rise to incoherent scattering, or the wavelength remains constant, known as coherent scattering. Coherent

scattering will further give rise to interference between the waves of radiation, which can be measured as a core part of XRD⁹⁷.

X-rays are generated when a high energy electron beam is made to strike a positively charged metal “target” anode allowing these electrons to penetrate deep into the target.

The high energy electrons colliding with the electrons present in the copper source result in the energy level of the electrons increasing to a higher energy shell. When these electrons revert back to their previous states, radiation of a set wavelength is emitted according to Equation 7.

$$\lambda = \frac{ch}{\Delta E}$$

Equation 7 - Relationship between wavelength of emitted radiation and the change in energy level of the electrons within the atom.

Where λ is the wavelength of the emitted radiation, c is the speed of light in a vacuum, h is Plank’s Constant and ΔE is the difference between the energies of the electron shells. As electrons can be excited to three possible energy levels this results in 3 wavelengths of radiation peaking in the spectra generated this way as seen in Figure 48.

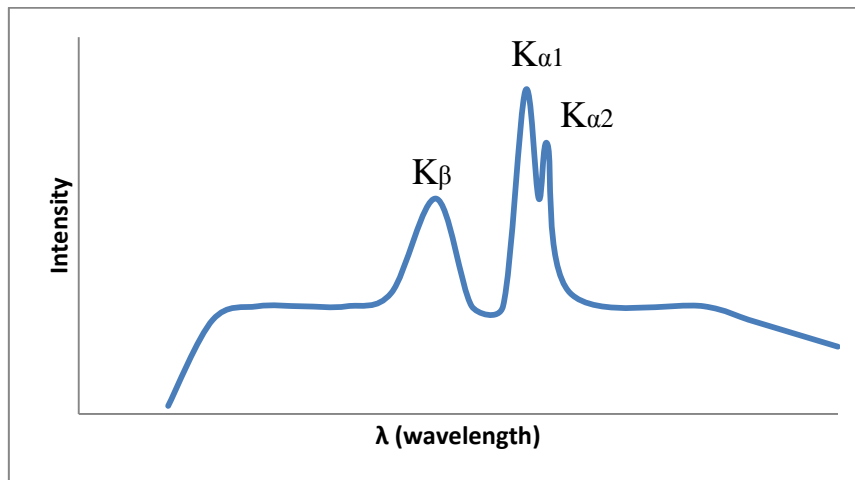


Figure 48 - Approximation of the spectra and intensities of radiation peaks generated by excitation of a Copper source⁹⁷.

K_{β} radiation is absorbed by a filter, leaving $K_{\alpha 1}$ and $K_{\alpha 2}$ peaks to be considered together where the wavelength is given by Equation 8.

$$K_{\alpha} = \frac{(2K_{\alpha 1} + K_{\alpha 2})}{3}$$

Equation 8 - Relationship between Intensity of K_{α} to $K_{\alpha 1}$ and $K_{\alpha 2}$ radiation.

PXRD relies upon the fact that when x-rays contact with a crystalline material the waves are elastically scattered in all directions by the electrons of the atoms or molecules that make up the bulk crystal materials.

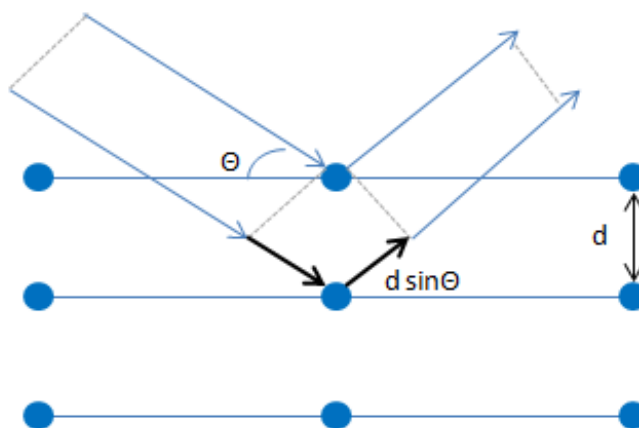


Figure 49 - X-ray scattering in crystalline material. $d \sin \theta$, marked by black arrows shows part of the extra distance the wave has to travel. θ is the incidence angle and d represents the spacing between the two molecules.

Destructive interference will occur unless the extra distance travelled by the photon is equal to an integer number of wavelengths of the radiation. Therefore for only certain incident angles of radiation, will constructive interference occur, meaning a crystal structure should have a series of spikes in the radiation being detected whenever the incident angle is in a location that allows constructive interference. William Lawrence Bragg and his father (W H Bragg) developed the relationship between wavelength of radiation, d spacing and incidence angle in 1912, earning them the Nobel Prize for Physics in 1915.

$$n\lambda = 2d \sin \theta$$

Equation 9 - Braggs Law

Where: n = layer of atoms being penetrated, λ = wavelength of X-ray being used, d = inter-molecular spacing or d -spacing of atoms within molecule, θ = Angle of Incidence beam to the parallel.

Chapter 4 – Analytical and characterisation techniques

For this, n and λ are considered constant, therefore d spacing will vary with the diffracted angle, θ . Therefore in a crystalline species with a large number of identically spaced scattering centres, the constructive interference will cause a large peak in the intensity of readings at that point. Knowing this angle, it is possible to therefore work out the d -spacing of the scattering centres causing the maxima. X-ray diffraction can be done using powdered crystalline material or using a large single crystal.

The sample is placed into the diffractometer and the beam generator and detector rotate around the sample moving from parallel to the sample holder to an angle of θ , as shown on the above diagram. If Bragg's law is re-arranged for θ , this can be used to determine the d -spacing of the molecules. Within a crystalline structure, the strict order means certain d -spacing will be present all throughout the structure. By Bragg's Law this can be used to show that at certain angles, a set crystalline structure will show spikes in the intensity of the diffracted beam. The actual value of intensity is not important and is not comparable between samples, and as such is usually defined as arbitrary units (A.U). The relative intensity of peaks is more commonly used to check the proportion of each peak within a compound. Though a single peak location may not be definitive in terms of identification of a compound, nearly all crystalline compounds have a distinct fingerprint of multiple peaks allowing it to be confirmed to within a very small degree of doubt as the target species. It is from this basis that comparisons of experimentally collected diffractograms are compared to those given within literature and generated by software are used to confirm the presence of the target phase. However, the limitation to this technique is that amorphous materials present in a mixture with crystalline materials will likely result in a low intensity, broad peak. Therefore, while the presence of narrow, high intensity Bragg peaks will confirm the material has crystalline properties, it is often important to consider other analytic techniques in conjunction with PXRD.

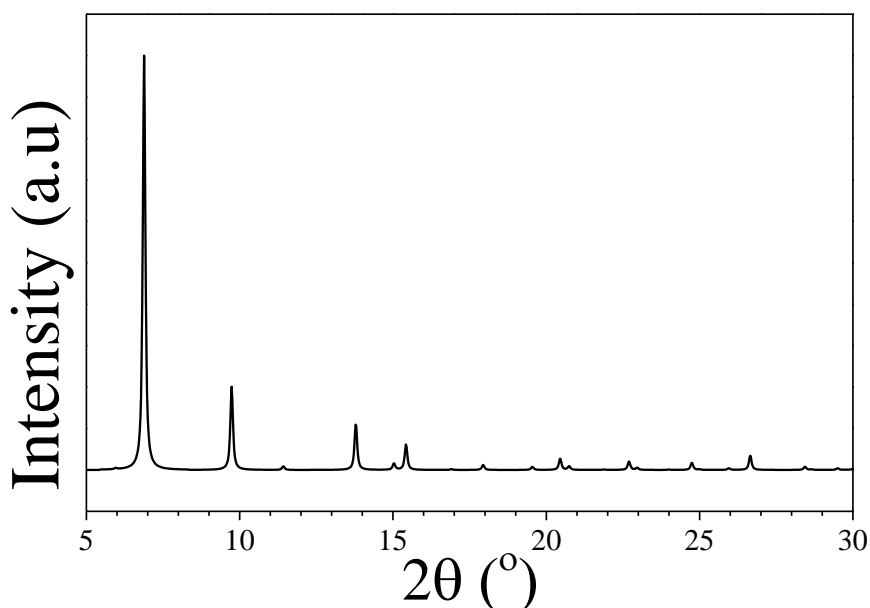


Figure 50 – PXRD pattern for MOF-5 generated from single crystal data

XRD uses an aluminium plate to hold the sample. This must be considered when analysing peaks, as the peaks at these locations are not due to the sample being analysed. As such, the locations of peaks due to Aluminium were obtained by running a blank slide. Aluminium also served as an internal standard. As it has distinct d-spacing within its structure, it has a strong peak at 38.5° which can be used to correct diffractometer errors if required. If a mixture of crystalline compounds is analysed, both sets of peaks will appear, and as such knowing the peaks of one of the compounds allows the distinction of the peaks from the alternative structure. If the crystalline structure is mixed with an amorphous (unordered) species, this will not show peaks other than those associated with the crystalline phase. As such it is important to use XRD in conjunction with other analytical methods.

All PXRD, unless otherwise stated was analysed using Cu $K\alpha$ radiation ($\lambda = 1.54 \text{ \AA}$) scanning between $5\text{-}40^\circ$ 2θ , in order to cover the main Bragg peaks of MOF-5 and HKUST-1 while also allowing the Bragg peak due to the aluminium holder to be included in the data as a secondary check that the data is correct and scan lengths were generally 0.25 h. The MOF tends to form a fine powder when dried, however any large agglomerates were ground before analysis. For MOF-5, the sample

was never ground and was analysed as is, in order to avoid any significant reaction with the moisture present in air ahead of the analysis.

4.3 Infrared Spectroscopy

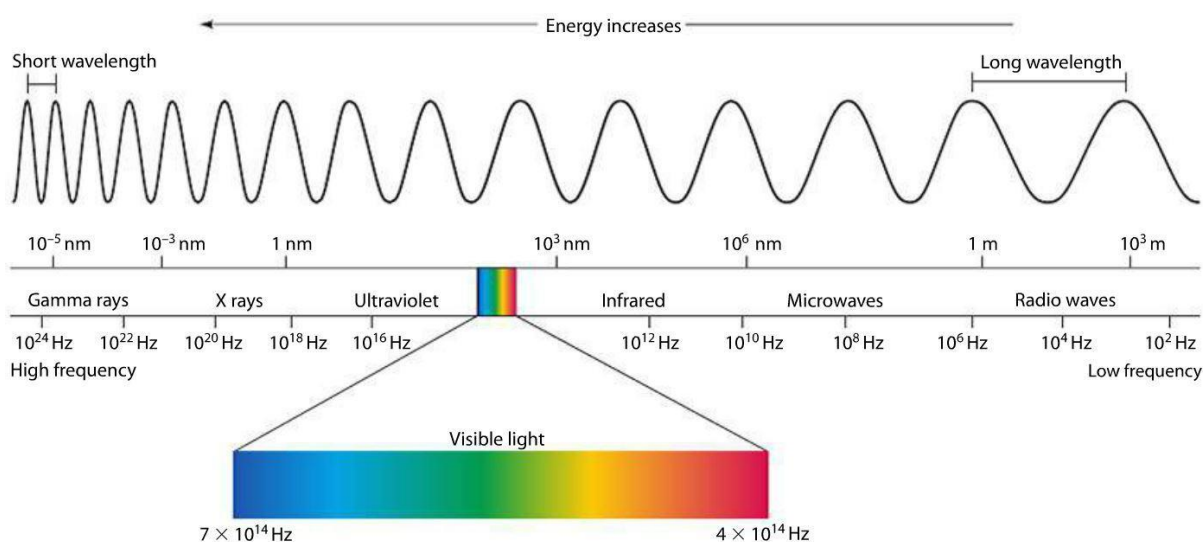


Figure 51 - Diagram showing various details of electromagnetic spectrum⁹⁸.

The bonding energy of most molecular vibrations will occur in the infrared region of the electromagnetic spectrum, as the bonding energies for most organic bonds will occur in the 2.5-16 μ m which occurs within the IR region⁹⁹. While it may be useful to consider absorption of light as a function of wavelength, it is more common to use the reciprocal of the wavelength – usually in cm, in order to have a wavenumber expressible in more acceptable units. While the 2.5-16 μ m covers most organic bonds, the lower energy of metal-organic bonding occurring results in absorption of light at lower wavenumbers, which may not be within the 4000-600 cm^{-1} approximate range that many IR spectrometers operate within.

Typical IR spectrometry occurs by passing light through a substance and detecting the amount transmitted/the amount absorbed by the substance before altering the wavelength and repeating this process. Fourier Transform Infrared Spectroscopy operates differently in that rather than transmitting at a specific wavelength, light from the entire range of the spectrometer is transmitted at once. The light is split into two paths of differing lengths. One or two of these beams pass through the substance

for analysis. Due to the differing lengths of paths, the beams can then be recombined and the interference pattern known as an interferogram. By carrying out a Fourier transform on this data, it is possible to determine absorbance as a function of wavenumber, giving a traditional IR spectrum⁹⁹.

FT-IR has a number of key benefits over conventional IR spectroscopy. Firstly, as the light transmitted covers the full range of analysis at once the technique is far quicker than having to go through the range one wavelength at a time, therefore traditional IR spectroscopy requires increasing greatly scant time to increase resolution. As traditional IR spectroscopy relies upon slits and prisms high resolution data is harder to generate, which is not an issue for FT-IR. FT-IR also allows for multiple scans to be quickly taken and added or averaged together in order to increase the accuracy of data output⁹⁹.

Attenuated total reflectance is a technique within IR spectroscopy that allows for the samples to be analysed without further preparation, such as formation of a KBr pellet which is commonly required. The light is reflected multiple times from the sample with a penetration depth generally in the 0.2-2 micrometers range. The key benefits of this technique is that it allows the sample to be recovered completely and the sample can be analysed without the further preparation steps that would be involved with formation of a KBr pellet, which can be time consuming and requires specialised tools. As this technique does not use a KBr pellet, it also prevents the chance of interference if the ground sample within the KBr pellet is too large causing interference with the radiation⁹⁹. Further, this method prevents the chance of any chemical interactions between the KBr salt and the sample.

The frequency that absorption occurs at gives data on the bonds present and the intensity of absorption can be used to give qualitative information on the number of bonds present, giving an idea of the overall structure. As with XRD, this technique's value is increased by the virtue of being a non-destructive process allowing the sample to be removed and stored for later analysis or use. While X-rays and ultraviolet radiation can be used to give knowledge on the structures present within a compound, FT-IR will give data on how the bonds within a compound vibrate when subjected to energy, with bonds of specific energies only vibrating when exposed to specific wavelengths of light.

Chapter 4 – Analytical and characterisation techniques

FT-IR relies upon the vibration of bonds present within a compound. A sample is exposed to infrared radiation and the absorbance is recorded as the wavenumber is varied. Absorbing Infrared radiation can cause a number of possible reactions from the bond such as stretching, scissoring and bending.

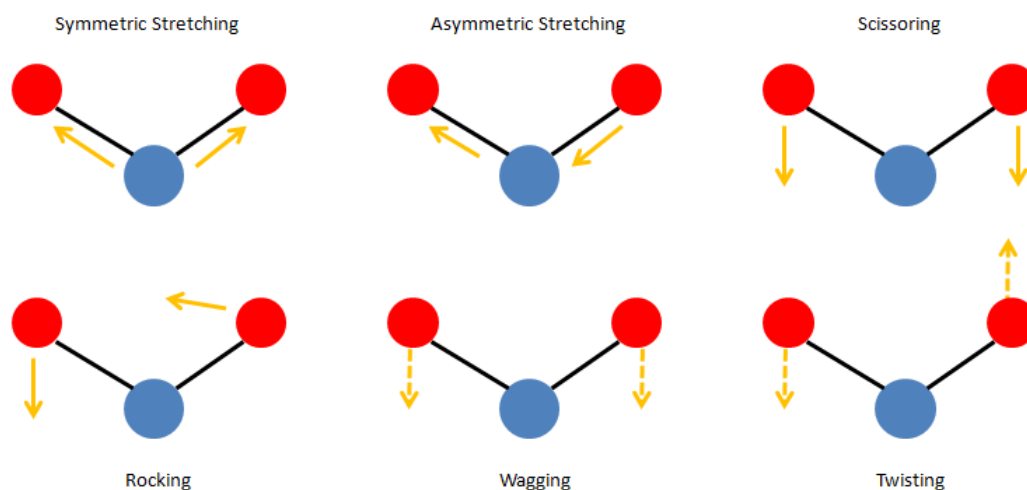


Figure 52 - Vibrational modes of a simple molecule, dotted arrows indicate the movement is in the z-plane. Regular arrows indicate the x or y plane.

As the sample is not analysed under vacuum conditions, it is necessary to take a background reading before analysing the compound in order to obtain accurate results. The absorbance of radiation is usually plotted against the wavenumber of the radiation. Wavenumber is defined by the following equation:

$$\tilde{\nu} = \frac{\nu}{c}$$

Equation 10- The relationship between wavenumber and frequency

Where, $\tilde{\nu}$ is the wavenumber (units of length^{-1}), ν is the frequency (units of s^{-1}) and c is the speed of light in a vacuum (ms^{-1}).

The wavenumbers at which a large number of bond types vibrate can be found in literature and such can be used to identify the types of bond present within the compound being analysed. Though FT-IR does not intrinsically give any data on the actual structure of the compound, the ability to show what

Chapter 4 – Analytical and characterisation techniques

bonds are present within a compound makes this an invaluable tool. Some standard vibrations are shown below in Table 12.

Table 12- Selected IR Vibrational wavenumbers¹⁰⁰

Wavenumber (cm ⁻¹)	Vibration Type
3000-3600	Water, Free OH groups
2800-3000	Aldehyde groups
1650	Zn:O-C-O coordinated groups
1600	Un-coordinated O-C-O groups
1500	Stretching of carboxylate group
1435	Zn:O-C-O coordinated groups – indicates presence of framework (MOF-5)
1380	Symmetric Stretching of carboxylate group
1300	Carbohydrate compounds – C,H,O
1280	Carbohydrate compounds – C,H,O
1220	Carbohydrate compounds – C,H,O
1100	C-C stretching
1000	C-H or para-coordinated aromatic
820	Out of plane deformation vibrations of R1–Benzene-R2 group
750	Out of plane deformation vibrations of R1–Benzene-R2 group
640	Aromatics – Benzene ring

As with PXRD, the materials here were generally ground if the particle size varied considerably. An even layer was spread onto the lens of the FT-IR and was clamped into place, tightened to the same degree as this has shown to affect the data generated. A reference is taken ahead of use but after cleaning, in order to remove the background due to the air and any remaining cleaning materials.

Chapter 4 – Analytical and characterisation techniques

Samples were generally generated at high resolution (4 wavenumbers) and with a high number of composite scans to increase accuracy (32-64 scans). Prior to use, data manipulation is required. Peak smoothing is used to reduce the noise of the data, while baseline correction is sometimes needed due to the presence of inorganics or a rough surface causing more scattering at higher wavenumbers. This results in an overall effect at high wavenumbers that can make the sample appear to have significantly higher absorbance at these wavenumbers. The main limitations of FT-IR involve the requirement for user-based data manipulation after the fact, which can result in some subjective changes to the data. Secondly, FT-IR also often relies upon the subtle shifts in the wavenumber of transmitted light due to bonding, which may not always be visible without very high accuracy scans. Finally, while FT-IR will show the bonding within a material, bonds can have energies out with the range that can be probed with this technique. This may lead to an incomplete picture of the material present.

4.4 Nitrogen Sorption and Porosity

4.4.1 Adsorption Types

Adsorption occurs when a surface comes into contact with atoms or molecules in gaseous, liquid or dissolved solid form and bonding occurs. Adsorption can be split into two distinct types – chemisorption (chemical adsorption) or physisorption (physical adsorption).

4.4.2 Physisorption

Physisorption is said to occur when the adsorbate adheres to the surface of the adsorbent material only through intermolecular interactions – van der Waals, dipole-dipole or dipole-induced dipole (such as London forces) interactions or hydrogen bonding¹⁰¹. The weak nature of these interactions allows the adsorbate to be desorbed from the surface without change to its composition and is favourable for applications that require the adsorbate to be released without requiring a large input of energy. The bonding energy of these processes usually falls into the region of 4-50 kJ mol⁻¹¹⁰².

As physisorption occurs spontaneously, the process must be exothermic in order to fulfil thermodynamic law as spontaneous process must have a negative ΔG value to satisfy the second law of thermodynamics¹⁰⁰:

$$\Delta G = \Delta H - T\Delta S \text{ (} T \text{ constant)}$$

Equation 11 - Second Law of Thermodynamics concerning "useful work"

For most common spontaneous adsorption, the entropy of the system will be negative as the degree of order of the vapour phase will increase due to the number of interactions when the degrees of freedom are restricted due to adsorption. Therefore, the process must be exothermic, $\Delta H = -ve$, in order to occur, unless the temperature of adsorption is sufficiently high.

Physisorption occurs due to two types of forces acting upon the adsorbate. Long range attractive interactions, such as van der Waals interactions represent an attractive force between the adsorbate species and the surface of the adsorbent. Dipole-dipole interactions will result in an attractive force between the surface and adsorbate. This can occur in species without a permanent dipole, will occur

due to the fluctuations in electron charge distribution. The second force that impacts upon physisorption occurs when the distance between adsorbate and surface is sufficiently small, whereby the overlap of electron clouds will result in a significant electrostatic repulsive force, which increases significantly when distance is further reduced, giving the standard Lennard-Jones potential graph.

The total potential energy for this system can then be expressed as follows:

$$\varepsilon(r) = -C_1r^{-6} - C_2r^{-8} - C_3r^{-10} + Br^{-m}$$

Equation 12 - Total Potential Energy between adsorbate and surface of adsorbent material

Where C_1 , C_2 and C_3 are dispersion constants associated with dipole-dipole, dipole-quadrupole and quadrupole-quadrupole interactions respectively. R is the distance between the centres of the adsorbate molecule and surface adsorbent site. The final term governs the repulsive forces, with B being an empirically found constant and m being an exponent for fit.

However, due to the weaker interaction of dipole-quadrupole and quadrupole-quadrupole interactions due to being factors of r^{-8} and r^{-10} , this equation is often simplified to:

$$\varepsilon(r) = -C_1r^{-6} + Br^{-m}$$

Equation 13 - Simplified expression for Total Potential Energy between adsorbate and surface of adsorbent material

Therefore, from **Error! Reference source not found.** and Equation 12, adsorbate molecules sufficiently far away from the surface will not feel an attractive force to draw the adsorbate to the surface. At low distances, repulsive forces will become dominant. Equilibrium can occur at the surface, giving a minimum potential energy state, resulting in physisorption of the adsorbate onto the surface.

4.4.3 Chemisorption

Chemisorption occurs when the adsorbate adheres to a surface through chemical bonding (covalent or ionic bonding) resulting in stronger bonding and the adsorbate being held closer to the surface of the material¹⁰¹. The nature of chemisorption also limits the adsorption to a monolayer, though physisorption between adsorbate molecules could occur beyond this. As this kind of adsorption

requires the formation of chemical bonding, the energy involved is similar to a chemical reaction and so the bonding energies will be higher than those associated with physisorption and the adsorbate itself will be chemically altered as part of this process. Further, this process is not necessarily spontaneous in low energy systems as the high activation energy of this type of bonding may require outside driving force if the system does not already have the required energy to overcome this barrier.¹⁰³

4.4.4 Adsorption Isotherms

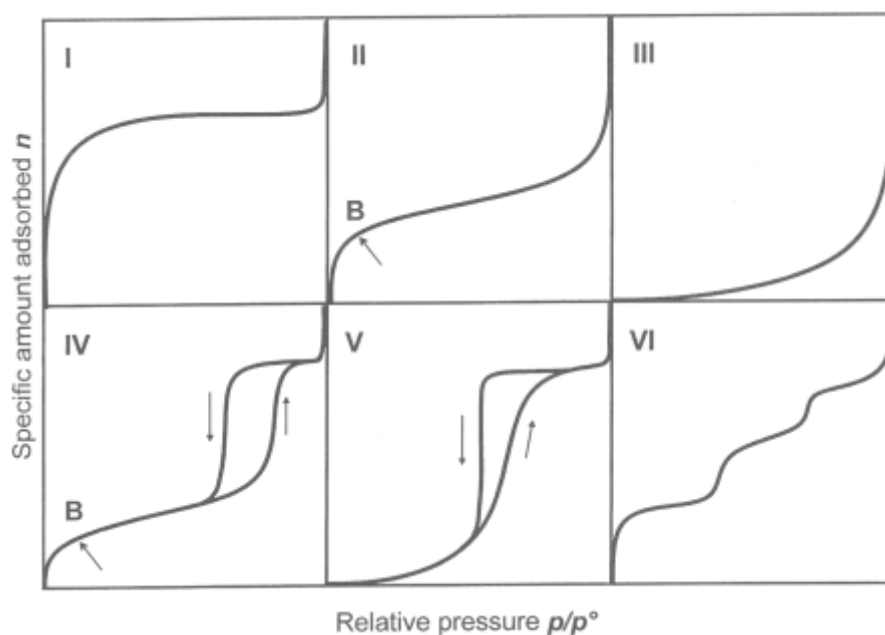


Figure 53 - The 6 Standard adsorption isotherms as defined by IUPAC⁸, used to subgroup many adsorption processes.

The characteristic adsorption isotherms can be used to determine the nature of the porosity of a material in a qualitative fashion. Type I isotherm indicates the presence of microporosity. The high energy sites in the micropores result in a high uptake of gas at low pressure range until the micropores are filled. Beyond this point, very little subsequent adsorption occurs resulting in the levelling off of the uptake, even at significantly higher pressures. Type II isotherms suggest non-porous or macroporous materials with strong interactions between the adsorbate and the surface of the material. From low pressure, until point “B” in Figure 53, monolayer formation will occur. Beyond this point, multilayer adsorption will occur, resulting in uptake at low pressure followed by uptake at high pressure due to two different mechanisms. Type III isotherms indicate a macroporous or non-porous

Chapter 4 – Analytical and characterisation techniques

material, however unlike type II this indicates a low energy of adsorption due to weak interactions between adsorbate and surface. As such, at higher pressure the behaviour exhibited is the same as Type II isotherms. However, at low pressure, the weaker interactions between the adsorbate and adsorbant result in little uptake, giving the distinctive shape at low pressure and the lack of an equivalent to point “B”. Type IV isotherms indicate the presence of mesoporosity and hysteresis occurs due to the energy of adsorption being considerably greater than the energy of condensation of the adsorbate, but otherwise have similar mechanisms of adsorption to Type II. Type V isotherms indicate mesoporosity as with Type IV, however as seen in the difference between type II and type III, the lower energy interactions of Type V give rise to a distinctly different isotherm characteristics to Type IV. Type VI isotherms represent materials with homogenous surfaces where the adsorbate forms multiple layers via epitaxial growth.

With many metal-organic frameworks the maximum pore width will generally be of the order of 1 nm, within the microporous range clearly identifiable Type I isotherms are often expected. With HKUST-1, the pore size is approximately 1nm, and the isotherm produced shows the Type I isotherm expected of this kind of porosity.

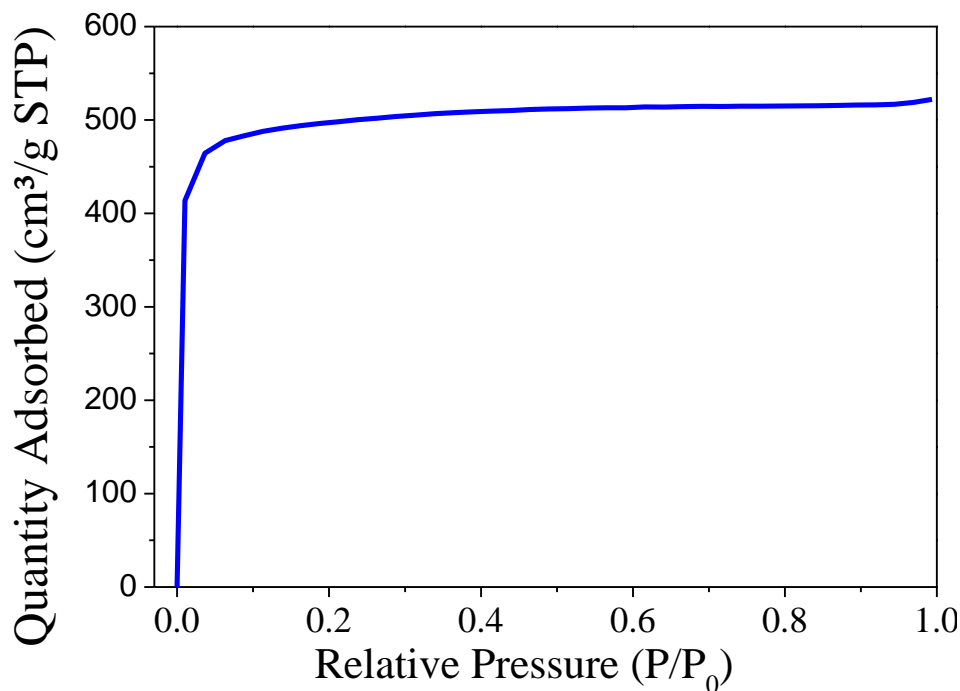


Figure 54 - Adsorption Isotherm of HKUST-1 at 77 K showing strong Type I indicating micropores. HKUST-1 from continuous reactor, discussed in Chapter 6.2.

4.4.5 Volumetric Analysis of Porosity

Volumetric analysis is carried out by applying a known volume of a gas, usually nitrogen, though IUPAC recommendations are likely to suggest argon for use in the future, within a known, confined volume in which the sample being analysed is also present. Nitrogen is dosed into this closed volume to reach a set pressure which is then allowed to equilibrate with the porous material. This is repeated until no further adsorption occurs at the desired pressure, at which point the pressure is increased until the maximum pressure, usually 1 atm. In order to do this, the nitrogen has to be at boiling point, -196°C; therefore liquid nitrogen is used to cool the entire system to the required temperature.

Volumetric analysis has associated errors due to the requirement of low temperatures and, in order to gain high quality data, pressure must be controlled to within a very fine margin. The Micromeritics ASAP 2420 used for these experiments also requires a minimum surface area of 25m² in order to gain data with reasonable accuracy.

The volumetric uptake of nitrogen can then be used with various isotherms in order to determine the available surface area. The two most commonly applied techniques, Langmuir and BET isotherms are

discussed below. However, it is important to note that a porous system may not appear porous to these analyses for a number of reasons. Firstly, closed pores may not be closed to smaller molecules than are used for analyses. For this reason, it is expected that IUPAC will recommend argon rather than nitrogen for gas adsorption studies in future due to being inert but having smaller molecular

4.4.6 Activation of MOFs

MOFs when formed will usually feature solvent molecules within pores; though can also have metal centres or unreacted ligand within the pores. In order to maximise the surface area present, MOFs require the removal of these components, known as activation. Activation generally involves heating the material to an elevated temperature at reduced pressure in order to remove volatile solvents. For solvents with a high surface tension, it can be prudent for the material to be solvent exchanged. By soaking the material in a more volatile solvent for an extended period of time, the solvents in the pores are replaced by a more volatile solvent which can then be removed without causing “damage” such as collapsing pores, to the MOF structure.

4.4.7 Langmuir Model

Langmuir Adsorption isotherm is the simplest isotherm and relies upon 3 key assumptions¹⁰²:

- 1) Adsorption occurs only in a monolayer on the surfaces
- 2) The surface is completely uniform, including all active sites being completely equivalent
- 3) Occupation of neighbouring sites does not affect the adsorption of a molecule onto adjacent sites

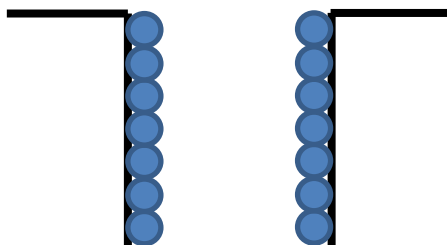
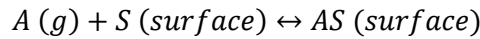


Figure 55 - Example on monolayer formation within a pore

As such, Langmuir Isotherms are used to determine the monolayer capacity of a material.

Chapter 4 – Analytical and characterisation techniques

The system is assumed to reach a dynamic equilibrium, given by the following equation:



Equation 14 - Dynamic Equilibrium for surface adsorption

The rate of adsorption and desorption (k_a and k_d respectively) affect the equilibrium position and the rate of surface coverage.

$$\frac{d\theta}{dt} = k_a p N (1 - \theta)$$

Equation 15 - Rate of change of fraction of free sites due to adsorption

$$\frac{d\theta}{dt} = -k_d p N \theta$$

Equation 16 - Rate of change of fraction of free sites due to desorption

Where p is the pressure of the adsorbate phase, N is the total number of adsorption sites and θ represents the fraction of total sites that are currently occupied. Therefore the total number of adsorption sites is N , the number of vacant sites is given by $N(1-\theta)$ and the total number of occupied sites given by $N\theta$. As the Langmuir isotherm assumes equilibrium is reached, these rates are equal and so the fraction of occupied total sites can be given as

$$\theta = \frac{Kp}{1+Kp} \quad K = \frac{k_a}{k_d}$$

Equation 17 - Fraction of total occupied sites at equilibrium

The fraction of free sites can also be expressed as the adsorbed volume, V , as fraction of the total monolayer volume if all sites were filled as shown in

$$\theta = \frac{V}{V_{mono}}$$

Equation 18 - Fraction of free sites related to volume of adsorbate and total monolayer adsorption volume

This can therefore be rearranged to give the following (Equation 19):

$$\frac{p}{V} = \frac{p}{V_{mono}} + \frac{1}{KV_{mono}}$$

Equation 19 - Rearranged form of Langmuir Isotherm

In this form, we can equate this to the equation of a straight line with form of $y = mx + c$, allowing that if $\frac{p}{V}$ is plotted on the y-axis, with p on the x-axis, the gradient of the line is equal to $\frac{1}{KV_{mono}}$, and the y-intercept is equal to $\frac{1}{KV_{mono}}$. Therefore this plot allows the volume of the adsorbate in the monolayer, V_{mono} , and the Langmuir Constant, K , to be determined. The volume of adsorbate in the monolayer can then be used to find the number of moles of adsorbate in the monolayer, assuming empirical data for the molar volume of the adsorbate is known, as shown in Equation 20.

$$n_{mono} = \frac{V_{mono}}{\text{molar volume of adsorbate}}$$

Equation 20 - Relationship between the number of moles of adsorbate in the monolayer and the monolayer volume

By calculating the number of moles of adsorbate, Avogadro's constant ($N_A = 6.022 \times 10^{23} \text{ mol}^{-1}$) and the cross sectional area of the adsorbate, A_m , we can calculate the total surface area occupied by the monolayer as shown in Equation 21.

$$S = n_{mono} N_A A_m$$

Equation 21 - Total monolayer surface area

The cross sectional area of adsorbate must be found empirically, however for N_2 sorption at -196°C , this value is 0.162nm^2 . This allows the total monolayer surface area of the material to be calculated, although most commonly this value is given per unit mass, usually in the units of $\text{m}^2 \text{ g}^{-1}$. The Langmuir model is limited by the assumptions required for the model. It can be applied to Type I isotherms as microporosity can be said to approximately equal a monolayer. As this does not hold true in actuality, due to the pore filling rather than forming only a monolayer, this model may give rise to inaccuracies. Further, assuming that the surface is uniform and the equivalence of all sites can introduce further error into any given results.

4.4.8 Brunauer, Emmett and Teller (BET) Model

The BET model, developed by Brunauer, Emmett and Teller, builds upon the Langmuir isotherm but attempts to also account for pore filling and multilayer adsorption¹⁰⁴.

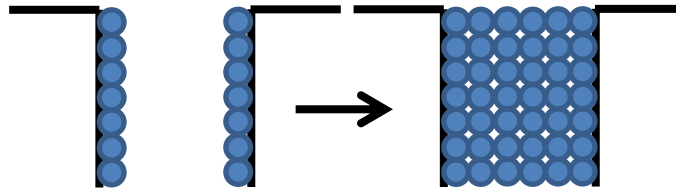


Figure 56 - Example of monolayer formation then pore filling by the adsorbate

As with the Langmuir Isotherm, this is based on a number of assumptions¹⁰¹:

- 1) As pressure increases, the interactions between adsorbate and surface sites become stronger
- 2) The number of layers present above the monolayer has no upper limit
- 3) Within any single layer, all sites are considered to have equal energy
- 4) Other than the monolayer, interaction energy is equal to the heat of condensation
- 5) Adsorption and Desorption only occur at sites exposed to the bulk volume
- 6) Exposed sites are in dynamic equilibrium with the vapour

After a monolayer is formed, the subsequent layers can be treated as if the vapour phase is interacting with a bulk liquid phase, giving the following equation:

$$\frac{V}{V_{mono}} = \frac{cz}{(1-z)[1-(1-c)z]} \text{ where } z = \frac{p}{p^*}$$

Equation 22 – Relationship between multilayer adsorption and partial pressure

Where V is the total volume of adsorbate, V_{mono} is the monolayer volume and c is the BET constant as shown in Equation 23 and z is the relative pressure of the vapour phase.

Chapter 4 – Analytical and characterisation techniques

$$c = e^{\left(\frac{\Delta_{Ads}H^{\circ} - \Delta_{Cond}H^{\circ}}{RT}\right)}$$

Equation 23 - BET constant, c.

Where c relates the enthalpy of desorption of the monolayer and the enthalpy of condensation of adsorbate. Equation 22 can then be rearranged, as shown above in Equation 19 for the Langmuir isotherm to give a form consistent with the equation of a straight line.

$$\frac{z}{(1-z)V} = \frac{(c-1)z}{c V_{mono}} + \frac{1}{c V_{mono}}$$

Equation 24 - BET Equation in form equivalent to y=mx + c

However, in cases where $c \gg 1$, this can be further simplified to give Equation 25.

$$\frac{1}{(1-z)} = \frac{V}{V_{mono}}$$

Equation 25 - Simplified form of BET equation when $c \gg 1$

Therefore by plotting a graph with total quantity adsorbed ($\frac{z}{(1-z)V}$) against z, the gradient of the line is equal to $\frac{(c-1)}{c V_{mono}}$, and the y-intercept is equal to $\frac{1}{c V_{mono}}$.

The total surface area can then be found, in a method similar to the Langmuir Isotherm as $\frac{z}{(1-z)V}$ is equal to the total number of moles of gas adsorbed.

$$A_{(BET)} = \frac{z}{(1-z)V} N_A A_m$$

Equation 26 - Total BET surface area

The simplification of the BET equation that occurs when $c \gg 1$ as shown in Equation 25 is useful when an unreactive gas is adsorbed onto a surface with high bonding energy, for instance a polar surface. When this occurs, the value of the enthalpy of adsorption is considerably larger than the enthalpy of condensation allowing this simplification.

As with the Langmuir Isotherm, this model is limited by a number of factors. The BET Isotherm is best suited to Type II and IV isotherms, but not for Type I isotherms, where the Langmuir Isotherm model should be used. This is due to the BET Isotherm not accounting for the adsorption only at higher energy sites when at low pressures, whereas the BET isotherm assumes all sites as being of equal energies.. Therefore, the key assumption is that the total volume of adsorbate varies linearly with partial pressure. This does not hold true for low partial pressures ($\frac{p}{p^*} < 0.05$) as surface sites are not homogenous and the driving force applied by the partial pressure at this point will only allow for adsorption to higher energy sites within a material. Further, the assumption that “Other than the monolayer, interaction energy is equal to the heat of condensation” will not hold true in experiments, with the surface having a decreased effect with more layers rather than no effect. Therefore, in addition to the potential issues at low partial pressures, at higher partial pressures ($\frac{p}{p^*} > 0.35$) the system will deviate from the assumption that the heats of adsorption for layering out with the monolayer are equal to the enthalpy of condensation. The BET constant is considered constant due to the assumptions made, but in actual fact will vary with partial pressure. As outwith this region the variation is not generally linear, therefore the general range of the BET equation is $0.05 < \frac{p}{p^*} < 0.35$ ⁸.

As the BET isotherm accounts for both monolayer formation and pore filling, it is generally the most commonly reported method for approximating the surface area of a material.

4.4.9 Barrett, Joyner and Halenda (BJH) Theory

While Langmuir and BET isotherms allow for determination of the available surface area of a material, either monolayer or including condensation within pores, it is important to know the size of pores as this can greatly affect the possible applications of these materials. This method uses the Kelvin model for pore filling and so only applies to mesoporous and the lower end of macroporous pore sizes. The Kelvin model relates the width of pores to the pressure required to fill the pore¹⁰⁵.

$$\ln\left(\frac{P_C}{P_O}\right) = \frac{-2\sigma_N}{RT\rho_N H}$$

Equation 27 - Kelvin Model describing width of pore to bulk adsorbate pressure

Where P_c and P_0 represent the pressure at which a pore of width H fills and the bulk saturation pressure of Nitrogen. σ_N and ρ_N represent the surface tension and density of liquefied adsorbate at temperature, T , respectively. The Kelvin model relies upon the assumption that pore filling and emptying will occur in a step-wise manner consistent with Figure 57.

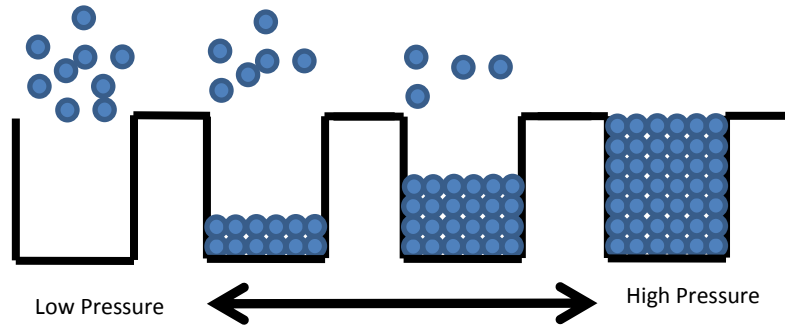


Figure 57 - Visual representation of Kelvin model of pore filling

The BJH model builds upon this theory based on a number of assumptions¹⁰⁶.

Firstly, in all pores the thickness of the adsorbed layer is considered constant. Pore sizes will follow a Gaussian distribution. Adsorption only occurs via physisorption or capillary condensation. All pores are cylindrical and open-ended, and therefore have equal radii and changes to relative pressure will fill and empty pores as shown in Figure 57.

$$r_K = \frac{2\sigma^{lg}V_m^l}{RT \log\left(\frac{p}{p^*}\right)} = \frac{4.14}{\log\left(\frac{p}{p^*}\right)}$$

Equation 28 - General Equation for Kelvin Radius, with the Kelvin Radius for Nitrogen at 77K given to the right

Where r_K is the calculated Kelvin radius, V_m^l is the molar volume of the liquid condensate and σ^{lg} is the surface tension of the liquid condensate. For nitrogen, this can be simplified to give the Kelvin radius in terms only of $\frac{p}{p^*}$. Therefore by knowing the total adsorption of gas into pores for a given partial pressure, we can correct the Kelvin model to also include monolayer formation, determined as described previously.

$$r_p = r_K + \text{monolayer thickness}$$

Where r_p is the radius of the pore accounting for both Kelvin adsorption and monolayer formation.

The desorption isotherm for the material, rather than the adsorption isotherm due to not being completely saturated, can then be used to computationally determine the pore size distribution.

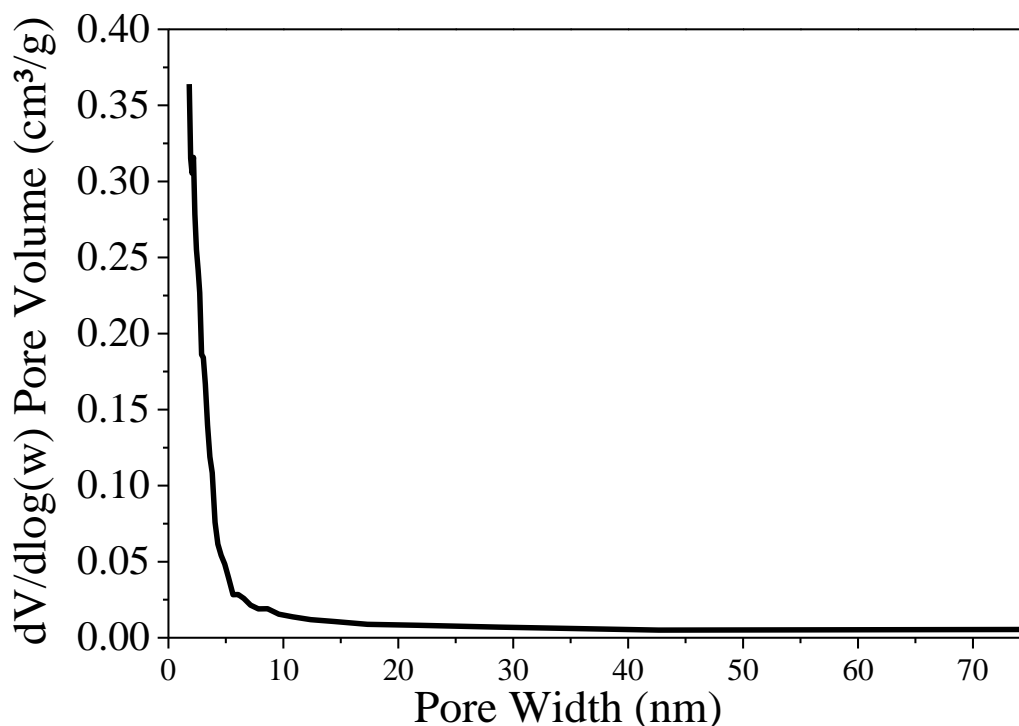


Figure 58 - Pore size distribution of MOF-5, produced continuously as part of this thesis.

However, for the N_2 sorption equipment used within this project, the lower bound is 1nm, above or on the borderline of the expected pore size of the materials we intend on producing as can be seen in Figure 58 where the peak of the data for MOF-5, with pore width of 0.6 nm^{49} , cannot be seen due to the lower limit of the equipment.

For analysis, samples were degassed (or activated) by heating to a high temperature under vacuum conditions in order to remove all volatile materials from the pores. A tube is used for both degas and analysis. The weight of this tube, when clean and empty must be recorded. The sample is then added to the tube, taking care to prevent sample from sticking to the sides of the tubes. As only the base of the tubes is heated, it is important at this point to ensure as little powder remains stuck to the walls of the tubes as this may not be sufficiently heated or cooled during the degas and analysis steps.. The sample and tube are then re-weighed, giving the weight of the degassed sample. This weight serves as

the basis for the true mass of material present, and has a large impact upon the specific surface area. For analysis, the tubes are jacketed to allow capillary action to draw liquid nitrogen to a set point on the tube regardless of the level of liquid nitrogen. Samples are then cooled and nitrogen is dosed onto the material at a given pressure until equilibration, at which point the pressure is increased. The data is logged automatically and then requires processing to give the reported values.

4.5 TGA-DSC

Thermogravimetric Analysis (TGA) is an analytical technique based upon highly accurate measurements of the rate of change of weight of a substance with varying temperature. The heat flux of the sample can also be measured, allowing in depth knowledge of what is occurring within the sample. This is of particular use to identify endothermic or exothermic processes that may occur without any temperature or weight change, such as melting or phase changes occurring due to decomposition of the sample or removal of solvents present within pores. The derivative of the weight peak is often taken to allow for a clearer positioning of where the weight loss is occurring. TGA can be carried out under N_2 or O_2 based on desired effect e.g., if oxidation is required then O_2 atmosphere would be selected. The TGA data can show a number of important details. The overall thermal stability of a compound can be analysed by determining structure before heating and then re-analysing after. Using the heat flux and the derivative of the weight at given time, the point at which a compound begins to thermally degrade can be found. The level of molecular, absorbed and adsorbed water can also be very accurately calculated using TGA.

4.6 Scanning electron microscopy (SEM)

Scanning electron microscopy (SEM) uses the interaction of electrons with a material in order to generate information from these interactions such as the surface topography and can provide insight into the overall composition of the material. This allows for images to be generated without relying on the interaction of light with the material and so can be used to investigate materials to extents that would not be possible with optical microscopy due to the diffraction limit¹⁰⁷. Beyond the diffraction limit it becomes very difficult to obtain useful information at resolution below the wavelength of

Chapter 4 – Analytical and characterisation techniques

incidence light, though this can be avoided in some cases¹⁰⁸. An electron beam is aimed at the material that is being probed. As these electrons interact with the material this causes excitation of electrons within the material, causing a variety of outputs such as secondary electrons, scattering of incidence electrons and release of electromagnetic radiation. The secondary electron output can be used to generate very high resolution images of the material being probed.

Importantly, the sample must be pre-treated to avoid the build-up of charge on the material surface. This is most commonly done by vaporising a small quantity of a conductive, unreactive metal such as gold within a vacuum chamber in order to give a coating in the order of microns thick.

Chapter 5 – Results and Analysis for MOF-5

5.1 Understanding the formation mechanism of MOF-5 and key parameters affecting batch synthesis

While MOF-5 has a large body of scientific literature related to synthesis, characterisation and applications of this material, few papers have covered in detail the effect of changing a single synthesis parameter and no work has been published concerning solid phase formation as a function of time and temperature. By understanding the solid phase output of a time-temperature space for this material, new insights into the formation mechanism of MOF-5 were gained.

For these experiments, the M:L ratio was kept at 3:1 and 1% solids. The temperature and reaction duration were varied and both stirred and unstirred conditions were varied. When operating at 140 °C, under stirred conditions, the reaction mechanism was found to follow the simplest pathway of the conditions analysed. At these conditions, MOF-5 is formed in 1.5 h although an intermediate phase, identified as MOF-69c, was shown to be formed before MOF-5 before gradually transforming into MOF-5 at longer timeframes. When the reaction temperature is lowered to 130 °C, the reaction pathways appear to become considerably more complex with multiple crystalline metastable intermediate phases present before the formation of MOF-5. As these phases are metastable and multiple phases co-exist within the system, it was not possible to isolate and characterize these intermediate phases. As a result, we have characterised all metastable intermediates together as “intermediates” with the exception of MOF-69c.

Figure 59 shows the PXRD patterns of solid phases formed at 140 °C under stirred conditions. MOF-5 in a pure phase, as confirmed by PXRD to be consistent with crystallographic data published by Yaghi *et al*⁴⁹, was formed when the reaction time was ≥ 1.5 h.

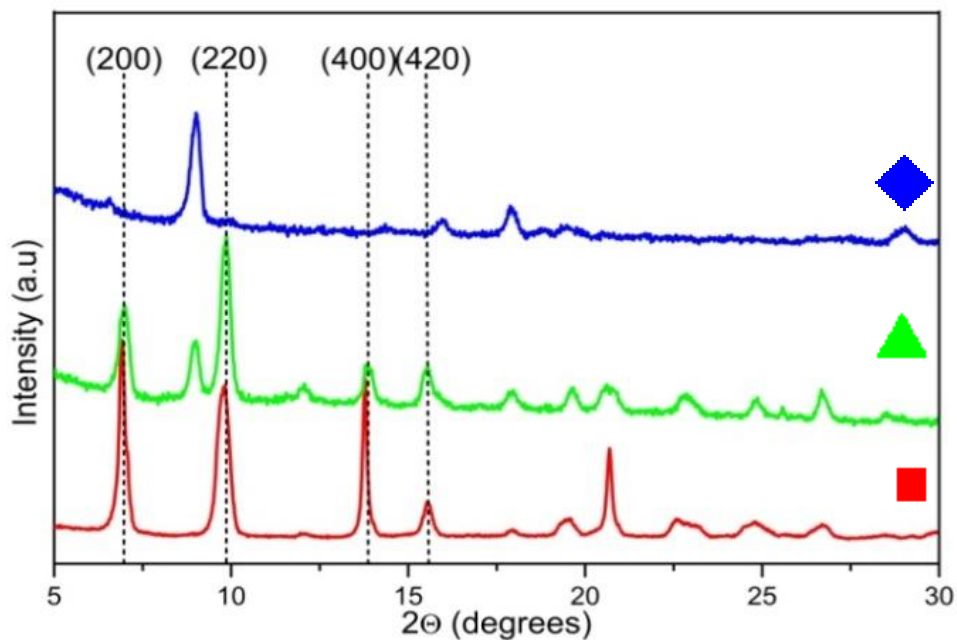


Figure 59 - PXRD results for single step synthesis showing: ◆ - MOF-69c(desolv) (main peak at 8.9°), ▲ MOF-5 + MOF-69c(desolv), ■ MOF-5.

MOF-69c(desolv) observed under these conditions is isostructural with phases described by Hausdorf *et al.*⁷⁰ and Kaye *et al.*^{34c}. Though MOF-69c is reported within the literature as a breakdown product of MOF-5 when exposed to sufficient humidity^{34c}, MOF-69c had never been shown to be present as solid precursor phase in the direct synthesis of MOF-5. MOF-69c was first synthesized by Rosi *et al.*⁷⁵ by adding water to the MOF-5 synthesis route, producing a layered structure with low porosity and composition $Zn_3(OH)_2(BDC)_2$.

In our system, the reaction scheme for conversion between MOF-69c (desolv) and MOF-5 is hypothesised as follows:



Further evidence that this transitional mechanism occurs was found from FT-IR results, shown in Figure 60, which show increased intensity of the peak of the Zn:ligand framework located at 1650 and 1435 cm^{-1} . The presence of a peak at 1650 cm^{-1} represents a characteristic shift of uncoordinated

terephthalic acid from 1610 cm^{-1} to 1650 cm^{-1} when coordinated with the Zn_4O tetrahedra^{73r}. The peak located at 1435 cm^{-1} has also been reported as indicating the presence of deprotonated carboxylates bonded to the metal centre, suggesting a greater degree of metal:ligand bonding in pure phase MOF-5 compared to MOF-69c^{73i, 73j, 109}. The $3000\text{--}3600\text{ cm}^{-1}$ region, generally indicative of the presence of hydroxyl groups within the material is also significantly more intense for MOF-69c relative to pure phase MOF-5, further evidencing this hypothesis.

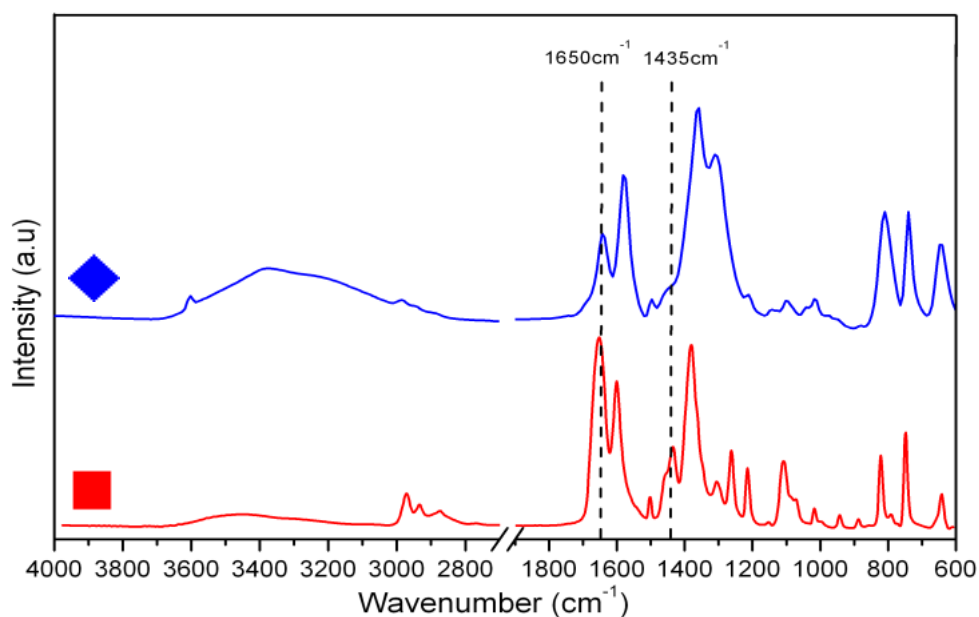


Figure 60 - FT-IR for \blacklozenge MOF-69c(desolv) and \blacksquare MOF-5. The series of peaks located at $2800\text{--}2900\text{cm}^{-1}$ are indicative of the formic acid formed due to the breakdown of the DEF solvent. The two peaks characteristic of metal-ligand bonding have been highlighted.

In order to gain further insight into the complex mechanisms involved in formation of MOF-5 from solution, a range of times and temperatures were analysed in order to map the solid state outputs of this system. Figure 61 shows a map of the solid state output of MOF-5 synthesis conditions within a period of 6 h at 4 different temperatures between $110\text{--}140\text{ }^{\circ}\text{C}$. MOF-5 was shown to form within the 6 h timeframe when operating at temperatures $\geq 120\text{ }^{\circ}\text{C}$. This mapping of the t-T space also highlights the complexity of the formation mechanisms occurring within MOF-5 synthesis as in every case analysed, crystalline metastable intermediates were present before MOF-5 was formed. This mapping

also delineates the conditions best suited for MOF-5 production. Where no solids were visible to the naked eye, the solution was deemed to have not yet produced any solid mass.

By performing multiple, parallel runs synthesis progress could be followed *ex situ* as a function of reaction time in order to prevent disturbing or artificially altering the reaction mixtures during synthesis, as would be required by removal of aliquots. Further, this technique presents the additional benefit of being able to provide a reasonable estimate of yield at each point. At all temperatures, no solid material was observed to have formed within the first 0.5 h of heating. After solid mass was observed to have formed various intermediate phases were observed in reaction samples. At temperatures ≥ 130 °C the intermediate phases were observed to be eliminated with only MOF-5 as a pure phase as a single crystalline phase product, after sufficiently long reaction times.

At temperatures below 130 °C, lower reaction temperatures resulted in a significant increase in the time required for formation of the first crystalline solids, with the solid product noted at approximately 3 h for 110 – 120 °C, compared to 1 h when operating at ≥ 130 °C. Further, the length of time that intermediate solid phases persist within the system increases greatly when operating at lower temperatures, as well as mixtures of two or more solid phases persisting for longer times, extending up to at least 6 h at 110 °C. When considering the full range of outputs from this system, the number of phases present increases to five from the two described above for the stirred system at 140 °C.

Stirring was shown to have significant effect upon the reaction process, especially at temperatures of 110 -120 °C. Within this region, both the stirred and unstirred reactions do not produce any visible solid material for a period of 2.5-3 h. After this period, the stirred reaction mixture produces MOF-69c with other intermediate phases present, and MOF-5 is not formed in pure or impure states over the 6 h analysis period. For unstirred reactions operating at otherwise identical conditions, the solid output of the system showed a mixture of MOF-69c, various metastable intermediates and MOF-5, though pure phase MOF-5 was only observed at 120 °C after 6 h, and was not formed as a single pure phase at 110 °C. This suggests that agitation of the reaction solution either stabilises the intermediate

phases or otherwise hinders the formation of MOF-5. Further, the formation of MOF-5 in unstirred reactions may be helped by inhomogeneity within the system, promoting MOF-5 formation in regions where reactant concentrations differ from the bulk.

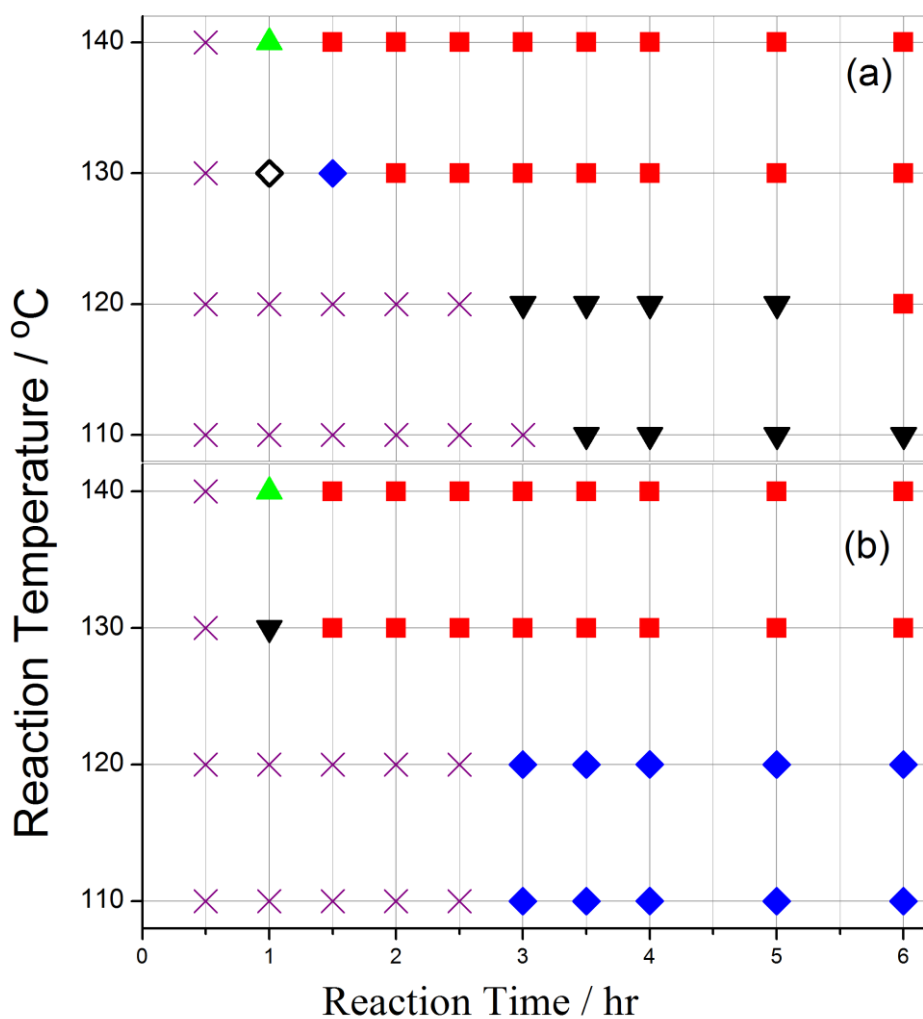


Figure 61 - Synthesis parameter space for (a) unstirred and (b) stirred conditions. X no solid mass as visible to the naked eye, ◇ intermediate phase, ◆ MOF-69c(desolv) with other intermediate phases, ▼ MOF-5 + MOF-69c(desolv) and other intermediates, ▲ MOF-5 + MOF-69c(desolv), ■ pure MOF-5.

From the phase matrix seen in Figure 61 we can show approximate pathways for formation of MOF-5 from solution at these conditions, although the 0.5 h resolution ($0 \leq t \leq 4$ h) and 1 h resolution ($4 < t \leq 6$ h) may allow the formation and subsequent transformation of certain metastable intermediates before collection. It is important to reiterate here that the transient, metastable nature of these solids

dramatically increases the difficulty in isolating these phases for further analysis and, as such, it is beyond the scope of this project to attempt to isolate and identify these species.

The reaction scheme and phase transitions observed in both stirred and unstirred solutions are shown below (Figure 62).

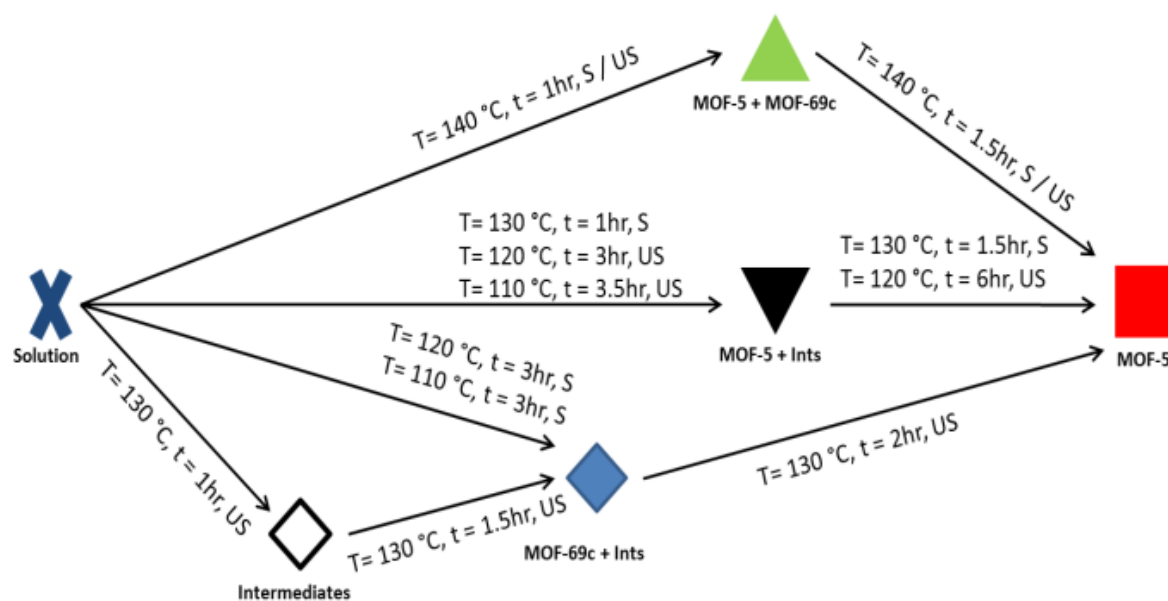


Figure 62 - MOF-5 formational phase transitions. X no solid mass as visible to the naked eye, \diamond intermediate phase, \blacklozenge MOF-69c(desolv) with other intermediate phases, \blacktriangledown MOF-5 + MOF-69c(desolv) and other intermediates, \blacktriangle MOF-5 + MOF-69c(desolv), \blacksquare pure MOF-5. Key (Temperature, Time phase transition occurs, S = Stirred, US = Unstirred, S / US = Occurs both in Unstirred and Stirred reactions).

Under every condition investigated within this temperature range, under both stirred and unstirred conditions, at least one intermediate phase is observed prior to formation of pure MOF-5. The system appears to transition through metastable states until pure phase MOF-5 is formed, in agreement with Ostwald's rule of stages, whereby the system passes through metastable intermediate(s) with stability nearest to the original state before reaching the most stable phase^{110,111}. The further implications of this suggest that when using techniques in situ to monitor formation of MOF-5 from solutions⁶³, the presence of the various intermediate phases must be taken into account in order to accurately describe the synthesis.

The results shown also suggest that the MOF-5 formation mechanism is considerably more complex than has often been assumed in the past and suggests that formation of MOF-5, possibly along with other metal-organic frameworks, occurs as part of a complex and extensive landscape of metastable intermediate phases that may be influenced by many process parameters, such as composition, reaction time, reaction temperature and agitation. Crucially, the adverse effects of stirring upon the formation of MOF-5 are significantly reduced at temperature ≥ 130 °C, thus stirred conditions still have the possibility to be utilised in order to increase heat and mass transfer, potentially facilitating efficient scale up for production of large quantities of MOF-5. Further, given MOF-69c with composition $(\text{Zn}_3(\text{OH})_2(\text{BDC})_2)$, is generally amongst the last impurities observed, this suggests that the complex Zn_4O^{6+} cation is one of the last structural aspects to form. While cost prohibits the use of basic zinc acetate, which already contains this cation, use of this zinc salt may allow for a significant reduction in the time to form MOF-5 at these conditions.

The results generated allow speculation into the actual formation mechanisms of MOF-5 but does not yield data on the specifics of how the material forms. As this MOF is isoreticular with many other MOFs, further insight into the formation mechanisms may allow transferability to this knowledge to others based around the Zn_4O^{6+} cation. Future work to isolate and identify many of the metastable intermediates, where this is possible, combined with modeling may allow for the true formation mechanisms that underlie MOF-5 production to be discovered, and may overlap with the formation mechanisms of other MOFs within the same group.

5.2 Understanding the effects of salt hydration on MOF-5 formation

Due to the possible impact of increased water concentration on the system due to MOF-69c forming when water concentration is sufficiently high⁷⁵, MOF-5 was synthesised by using either tetrahydrate and hexahydrate of zinc nitrate.

Based on the results shown in Figure 61, we selected 130 °C and 3 h as standard conditions, as these conditions have consistently shown formation of pure phase MOF-5 when using tetrahydrate salt. M:L ratio was maintained at 3:1 and 1% solids. In Figure 63 we show that while MOF-5 is formed

and is the most prevalent phase, a small number of low intensity Bragg peaks that are not due to the presence of MOF-5 occur, suggesting crystalline impurities occur in this sample.

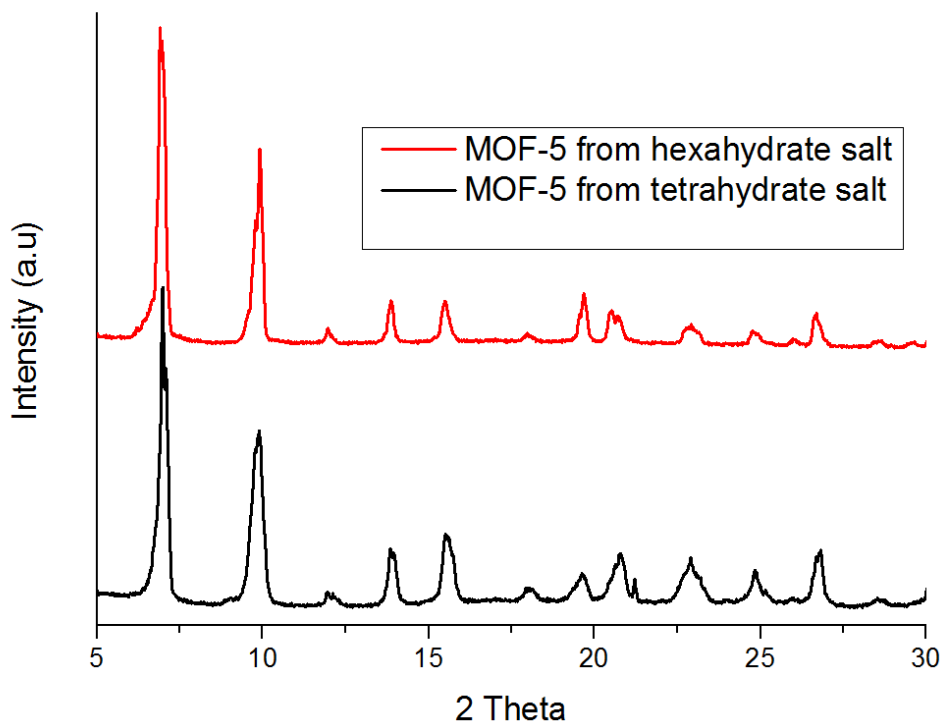


Figure 63 - Comparison of the effect of precursor salts with different hydrations after heating to 130 °C for 3 h. Tetrahydrate salt results in fewer impurities compared to the hexahydrate salt.

5.3 Understanding the effect of metal:ligand ratio on MOF-5 formation

Variation of the metal/ligand ratio (M/L) was studied over the range 3 to 0.67. The systems all had maximum theoretical yield set (1%) and kept identical over all samples. Samples with $M:L \geq 1.33$ produce MOF-5 on timescale comparable to those shown in Figure 61. When the M:L is below 1.33, the ligand is in excess which appears to prevent MOF-5 formation, though other reaction conditions have shown MOF-5 to be formed when ligand is in excess, as was shown in Figure 19. MOF-5 formed at $M:L = 1.33$ shows superior crystallinity to MOF-5 formed with $M:L = 3$, with narrower Bragg peaks.

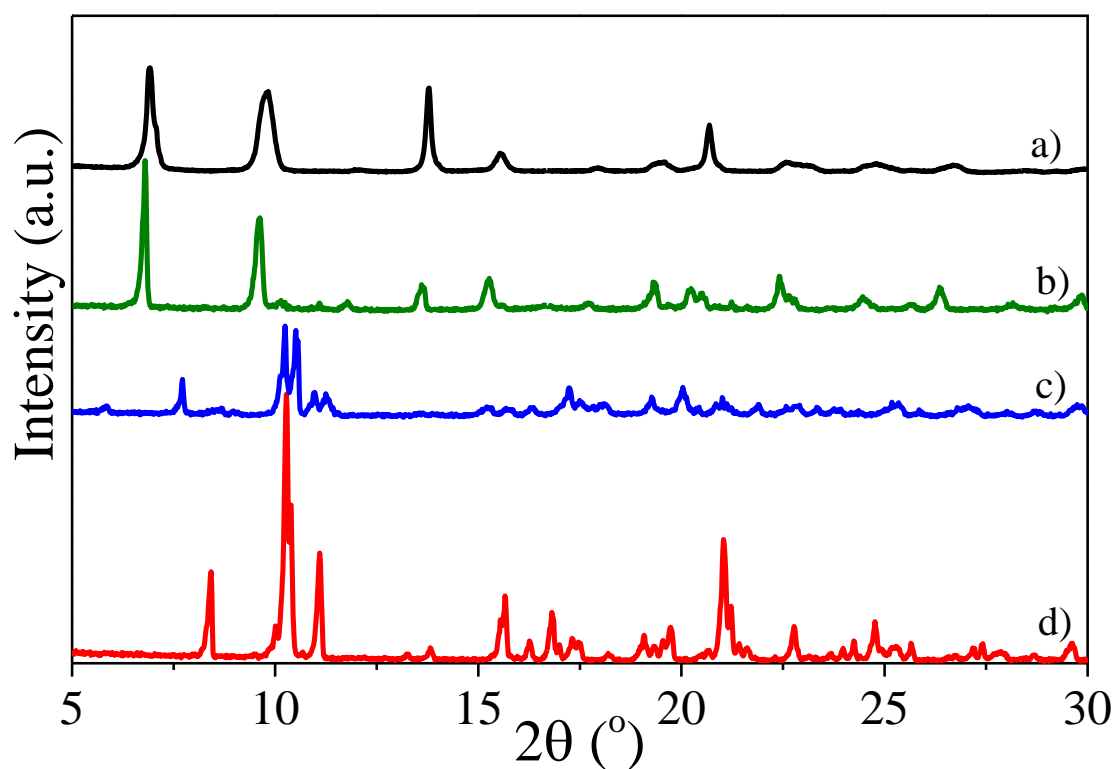


Figure 64 - Comparison of the effect of altering metal/ligand ratio. Samples were heated at 130 °C for 3 h. M/L was as follows: a) 3, b) 1.33, c) 1, d) 0.67.

However, while the yield of the successful MOF-5 Syntheses ($M/L = 3$ and $M/L = 1.33$) were almost identical, N_2 sorption studies show alteration of the ratio of metal salt and ligand used will have considerable impact upon the final accessible surface area of the material.

Table 13 - Comparison of surface areas at two solid concentrations, with M/L ratio varied between stoichiometric (1.33) and excess metal (3)

	M/L = 1.33	M/L = 3
1% Solids	469	2516
10% Solids	394	525

When solid concentration is set as 1% solids equivalent, using excess zinc results in a surface area comparable to many published papers on MOF-5 synthesis, with Langmuir SSA of around $2500 \text{ m}^2 \text{ g}^{-1}$. Increasing this concentration 10 fold results in the yield increasing by approximately the same magnitude, while the surface area drops to around $500 \text{ m}^2 \text{ g}^{-1}$, equivalent to a factor of 5. More revealing is the importance of M/L ratio. Even at 1% solids without the presence of excess zinc, the surface area of MOF-5 formed in short time at reasonably high temperatures such as used here will have a low surface area compared to those formed with a presence of excess zinc. Although atom efficiency is an aim, the reduction in surface area would likely reduce the sale price considerably more than would make this trade-off effective.

5.4 Process Intensification of Batch MOF-5 Formation

In order to probe the upper limit of reactant concentration we analysed a number of concentrations between 3 – 30% solids, while keeping a M:L of 3:1, and using $130 \text{ }^\circ\text{C}$ and 3 h as reaction time and temperature as these conditions had previously produced high quality MOF-5.

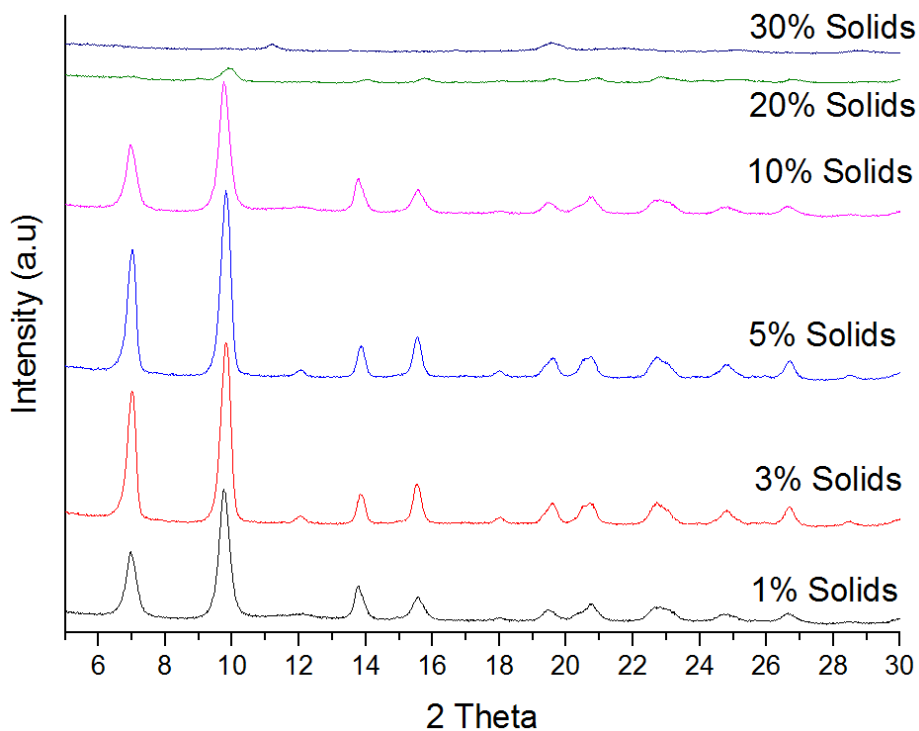


Figure 65 - Final products produced at 130 °C for 3 h. 1%, 3%, 5% and 10% show MOF-5 in high quality. 20% solids show that MOF-5 is formed, but with low crystallinity and high amorphous content. 30% solids show MOF-5 is not formed

MOF-5 is shown to form with high crystallinity in all samples up to 10% solids. 20% solids shows MOF-5 with significantly reduced crystallinity with broad, low intensity peaks. This is ascribed to the likely presence of amorphous solids. 30% solids, as shown in Figure 65 does not produce MOF-5. Further to this, the kinetics of the reaction appear to be significantly improved at higher concentrations, as would be expected, with MOF-5 formed in higher yields at shorter times relative to lower concentrations, though the time for MOF-5 to form did not appear to be reduced. As expected when understanding the potential implications related to interpenetration of MOFs when operating at concentrations above a critical point, we see significant drop off in the gas adsorption capabilities of MOF-5, with the available surface area reduced by a factor of 5 (as shown in Table 14) with the benefit of yield close to 10 times greater for the same solvent requirement.

Table 14 - Gas adsorption analysis of 1% and 10% solids, along with approximate dry yield.

Concentration	Langmuir SSA ($\text{m}^2 \text{g}^{-1}$)	Yield ($\%_{\text{theoretical}}$)
1% Solids	2516	~80
10% Solids	525	~80

Higher concentrations of precursors are more likely to form interpenetrated MOF structures, as supported by the observed reduction in Langmuir Specific Surface Area with solids content showing an 80% reduction in SSA when moving from 1% to 10% solids while maintaining very similar yield as shown in Table 14.

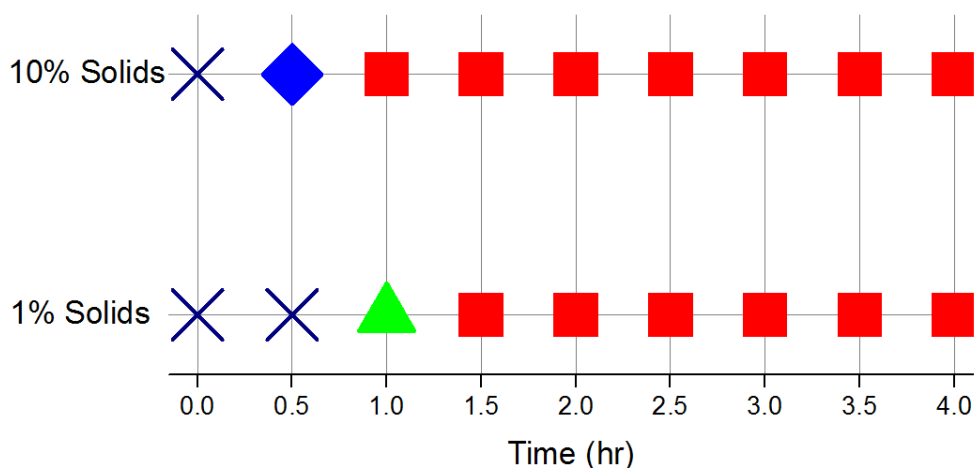
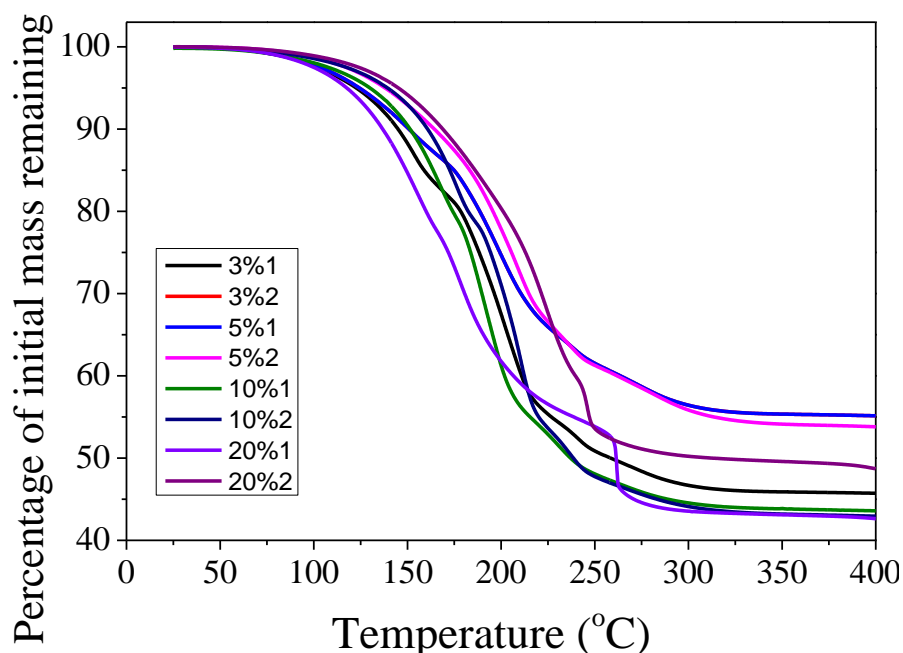


Figure 66 - Evolution of crystalline solids with top - 10% solids, bottom 1% solids, heated at 140 °C. ◆ - MOF-69c(desolv), ▲ MOF-5 + MOF-69c(desolv), ■ MOF-5. Increased concentration reduced both the time for first solid formation and the time to produce MOF-5 at 140 °C.

Crystal structures were determined by PXRD before and after TGA studies. For samples at 3, 5 and 10% solids content, amorphous species were found to be present at very low levels, by calculation based on decomposition of samples, via heating, to ZnO, and high degrees of crystallinity coupled with an absence of broad peaks in the PXRD spectra obtained. At 20% solids, expansion of MOF-5 crystals formed prevents full mixing from occurring, resulting in reduced crystallinity and high

amorphous content. Increasing solid concentrations also increases the yield of crystals produced, from ~70% yield (after solvent extraction) at 1% solids to over 90% yield for 10% solids, over the same duration at the same temperature – 130 °C, 3 h producing 0.007g MOF-5 per ml solvent at 1% solids and increasing by a factor greater than 10 to 0.09g per ml of solvent at 10% solids. This decreases solvent used per unit mass of MOF-5 synthesized by 10 times.

Interestingly, TGA results show that the proportional mass loss of each sample over the analysis temperatures is approximately the same for all samples, suggesting that the level of solvent and volatile organics within the pores is unaffected by the interpenetration that is likely occurring at these concentrations.



5.5 Continuous Synthesis of MOF-5

Using the data from batch synthesis shown in Figure 61 we elected to operate at 140 °C as the basis for a continuous reaction system. The reduced surface area due to high temperature synthesis is compromised with the significant decrease in reaction time while still providing high yields. Initial experiments were carried out with a residence time of 2 h, M:L = 3, 1% solids and 140 °C.

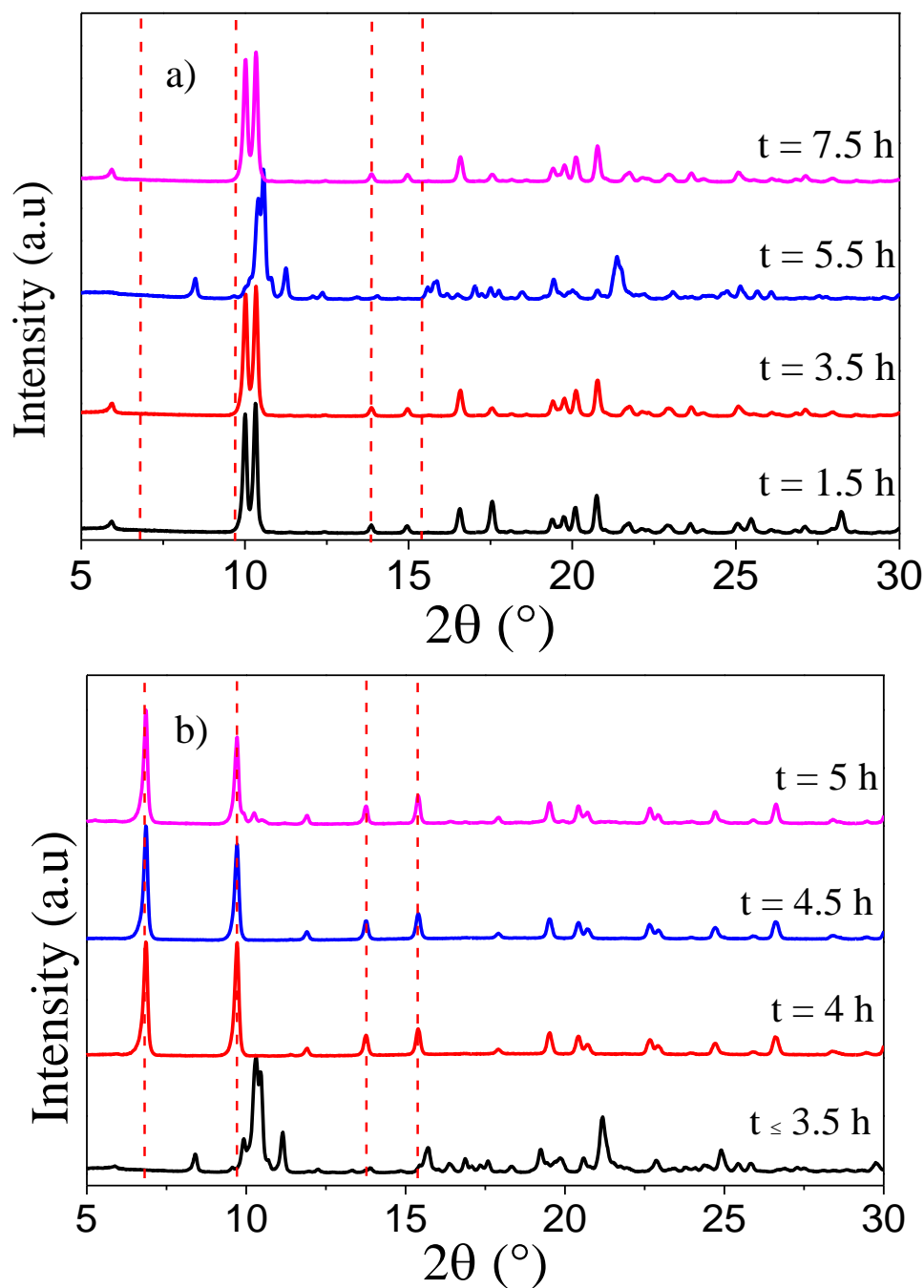


Figure 67 - PXRD results for samples collected at various time intervals with (a) 2 h and (b) 4h residence time. The collection time for each sample was 30 minutes and samples were labelled by the time when collection started. Dashed lines indicate the first 4 locations of MOF-5 Bragg peaks.

Figure 67a shows PXRD results for the continuous system operating at 2 h residence time, with no MOF-5 being formed over the 8 h observation window. Two intermediate phases that were also observed during the batch synthesis before MOF-5 forms are formed instead suggesting the residence time was insufficient to enable the formation of MOF-5 in a pure phase. It is likely that the

Chapter 5 – Results and Analysis for MOF-5

concentration of specific species, such as diethylamine, a known breakdown product of the DEF⁷⁰ solvent that is essential to the MOF-5 production reaction, is too low early on in the experiment. For the MOF-5 to form, amine concentration must be allowed to build up, therefore the removal of partially decomposed DEF and replacement with fresh DEF may cause the conditions to take significantly longer before being suitable for MOF-5 formation. This results in the continuous process requiring longer to form MOF-5 at these conditions than the comparable batch system^{73a, 112}. Therefore we increased the residence time of the system from 2h to 4h while maintaining the same temperature and precursor concentrations as above.

Figure 67b shows that when operating at a 4 h residence time intermediate phases, appearing identical to one of those seen in Figure 67a, are collected until a time of 3.5 h. For $t > 3.5$ h we see pure phase MOF-5 formed consistently with the exception of the sample taken at $t = 5$ h which shows the presence of a slight impurity. The theoretical yield of this system was 0.25 g h^{-1} , with actual output averaging at 0.21 g h^{-1} (84% yield) at steady state giving a space-time yield (STY) of $50 \text{ kg m}^{-3} \text{ day}^{-1}$.

In order to further corroborate the presence of MOF-5, FT-IR was completed on selected samples.

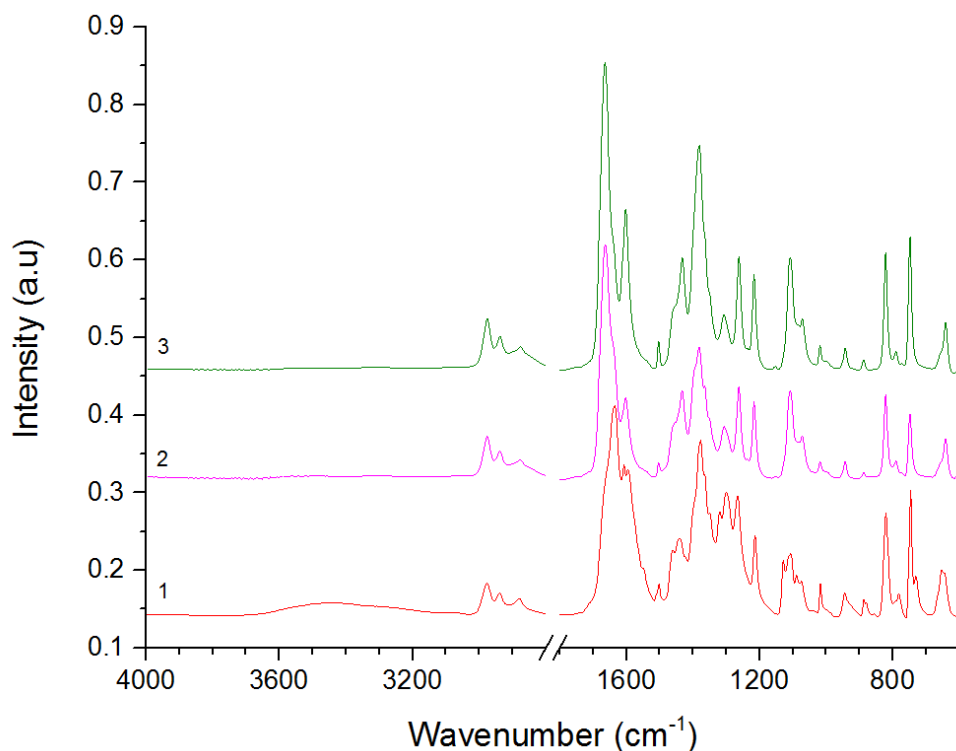


Figure 68 - FT-IR of a selection of solid products.

Figure 68 shows FT-IR spectra from typical solid products samples. Sample 1 is typical of the intermediate phase seen in the early stages of the reaction. The reduction in the peaks present at 3000-3600 cm^{-1} , from sample 1 to 2 and 3 indicates the presence of water or hydroxyl groups is due to the structure formed likely being a zinc hydroxyl based MOF. The three peaks at 2978, 2939 and 2879 cm^{-1} indicate the presence of amine groups from the decomposition of DEF during the reaction and are present in the wet sample but not the desolvated sample. The peak present at 1650 cm^{-1} indicates a characteristic shift in the peak location for the carboxylate group from 1610 cm^{-1} due to interaction with the Zn_4O tetrahedra^{73f}. The peak present at 1435 cm^{-1} also indicates deprotonated carboxylic acid bonded to the MOF-5 metal centre^{73j}.

Gas adsorption measurements for a sample collected at steady state for this reactor running with excess zinc (3:1 Zn:BDC ratio) shows an average Langmuir SSA of $2302 \pm 286 \text{ m}^2 \text{ g}^{-1}$ further suggesting that MOF-5 had been produced as a single phase and also highlighting the consistency of the output from this reaction system.

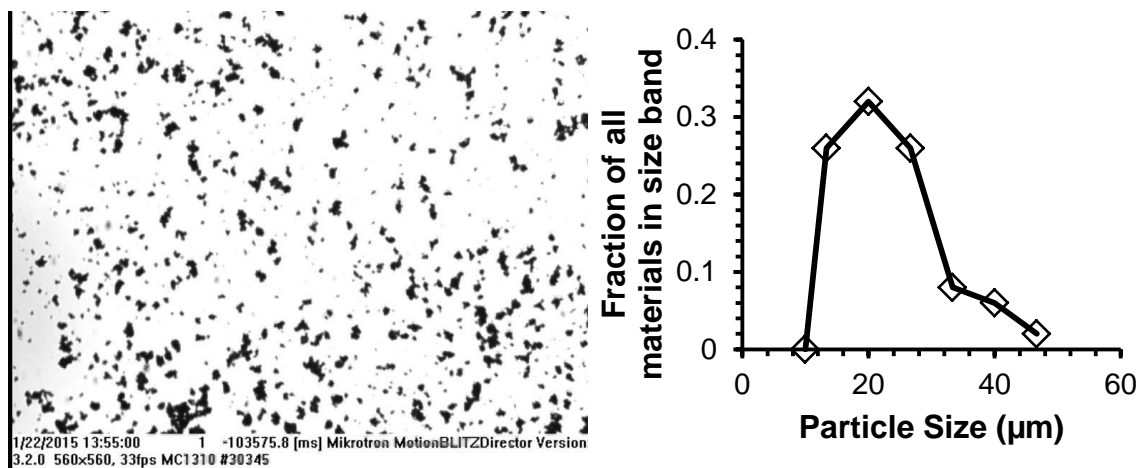


Figure 69- Optimal microscopy showing: Left - MOF-5 particle sizes from continuous system running at 4 h residence time and 1% solids. Right - particle size distribution.

Optical microscopy was performed to determine the range of particle size produced from the system with the general range appearing to fall within 10-40 µm. SEM shows distinctive cubic shaped crystal particles similar to those shown for batch synthesis of high quality MOF-5⁶⁵.

In order to investigate the duration of the start-up phase of the reactor system at these conditions, the system was reset and multiple repetitions were carried out at identical conditions: residence time of 4 h, M:L = 3, 1% solids and 140 °C. Analysis of the PXRD results collected were used to determine if any crystalline material was present and if MOF-5 was formed. Samples were classified into 3 categories: no crystalline material present, MOF-5 as a pure phase and any crystalline material showing the presence of intermediate phases which includes samples of MOF-5 with impurities. 6 runs were completed and the fraction of samples showing each of these conditions as a function of time is shown in Figure 70.

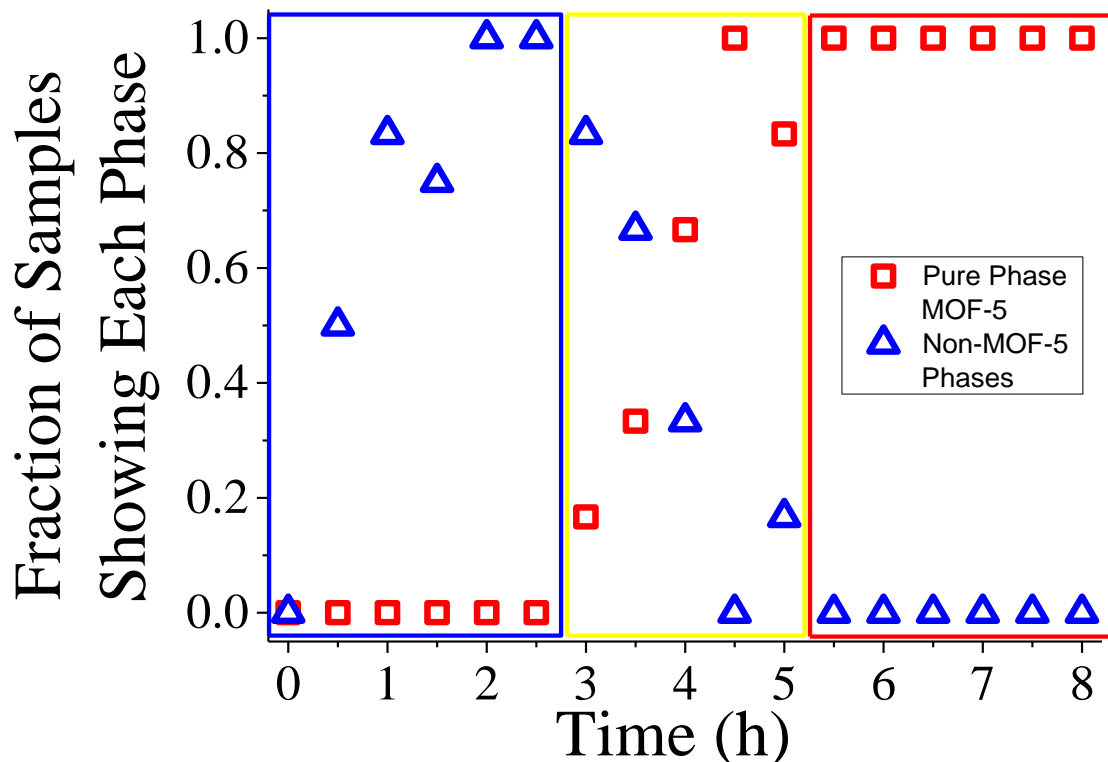


Figure 70 - Diagram showing general trend with system to have a start-up phase and a MOF-5 steady state production phase. ◆ non-MOF-5 phases; ■ pure MOF-5. Data collected over multiple repeat runs with 4 h residence time.

Three distinct phases appear to be present over the 8 h operating window for the reactor. Steady state production of MOF-5 occurs when $t \geq 5.33$ h as only pure phase MOF-5 is observed after this time period, and surface areas of samples at this point are tightly banded (for 1% solids, Langmuir SSA of $2302 \pm 228 \text{ m}^2 \text{ g}^{-1}$). The start-up phase runs from 0 – 5.33 h and can be further split into two regions. From start-up until $t = 2.67$ h we only see no significant solid production or low yields of metastable intermediate phases. Between 2.67-5.33 h the system enters a transitional region where both MOF-5, intermediate phases and mixtures thereof were observed. The fraction of samples showing intermediate phases decreases as the time for steady state is reached. It is important to note that through all analyses, no crystalline intermediate phases in the steady state region, which has interesting applications when considering formation of MOF-5 through continuous processing where steady state operation will occur for most of the reactor run.

5.6 Process Intensification of Continuous MOF-5 Synthesis

Process intensification with respect to the concentration of precursors in the feed supply and initial reactor concentration were then considered in an aim to increase the STY of this reactor system. The concentrations analysed were 5 and 10% solids based on 100% theoretical yield while all other parameters were kept identical (residence time of 4 h, M:L = 3 and T = 140 °C). While greater concentration of reactant species is likely to cause interpenetration and reduce the surface area of the MOFs, in a potential scale-up this may be a compromise to reduce the costs of solvents.

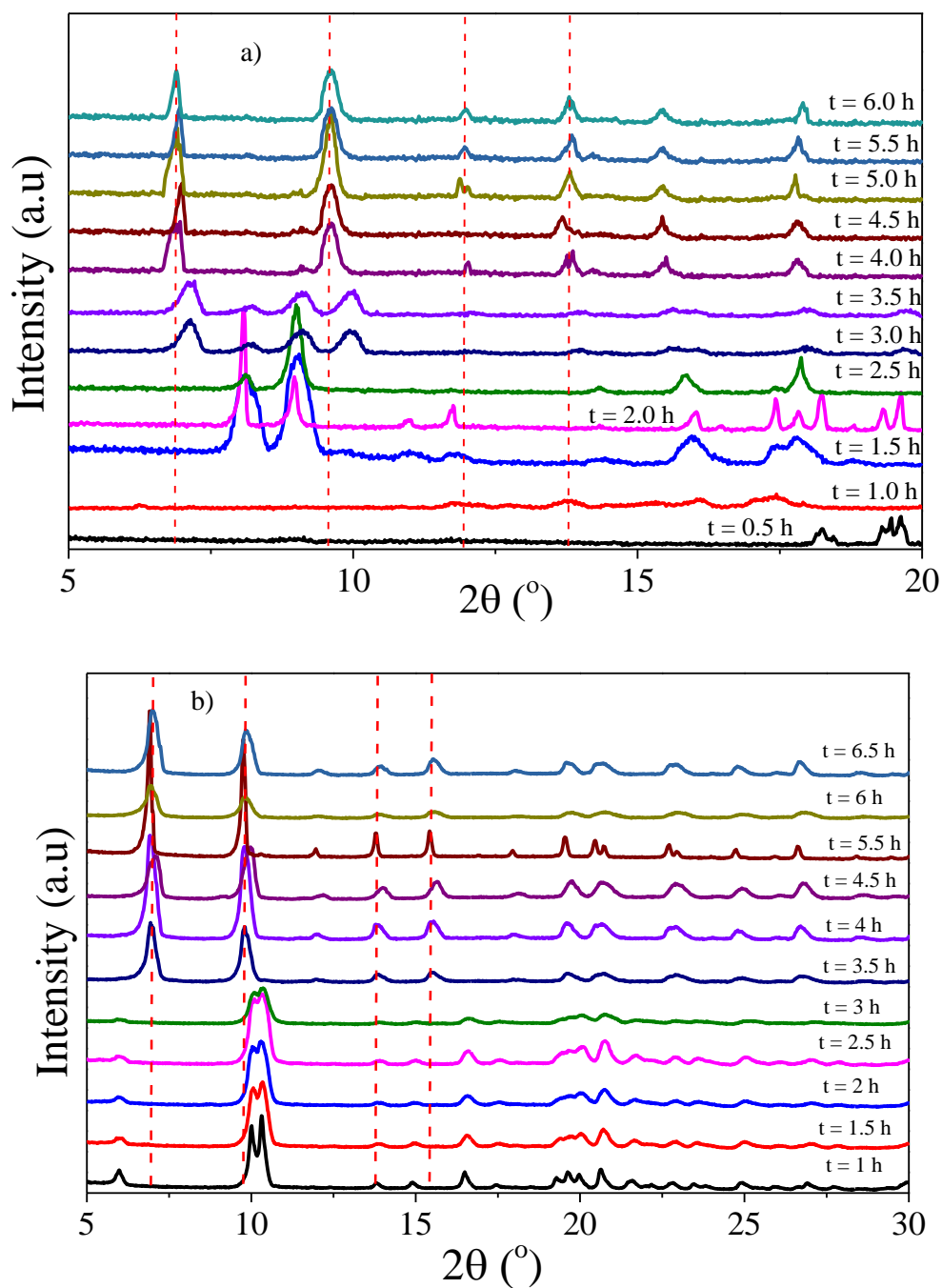


Figure 71 - PXRD results for samples produced at a) 5% and b) 10% solids concentration and collected over a wide time interval.

At 10% solids, Figure 71 shows an almost identical formation route to the pathway observed for 1% solids despite the 10 fold increase in reactant concentration. Intermediate phases are formed for $t < 3.5$ h while all samples collected at $t \geq 3.5$ h show MOF-5 as the only crystalline phase formed. Although

the increase in % solids and the similar yield to the 1% system allows MOF-5 to be formed with STY of approximately $500 \text{ kg m}^{-3} \text{ day}^{-1}$, nitrogen adsorption showed a significant reduction in the Langmuir SSA of this system, showing only $525 \text{ m}^2 \text{ g}^{-1}$ compared to the $2302 \text{ m}^2 \text{ g}^{-1}$ recorded for the 1% solids system. This is expected due to the formation of an interpenetrated structure¹¹³ and/or the presence of amorphous impurities within the crystal structure⁴⁶. The reaction with 5% solid concentration shows similar results and produced solid outputs, confirmed to be MOF-5 by PXRD with Langmuir Specific Surface Area of $759 \text{ m}^2 \text{ g}^{-1}$.

5.7 Optimisation of Continuous Flow Process Chemistry

Due to the presence of three distinct regions present during MOF-5 production (see Figure 70) at 140°C and 4 h residence time, we investigated if the reactor system could be left to run until reaching steady state at 4 h residence time after which the flow rates would be doubled, equivalent to a 2h residence time. For this, the other key reactor parameters were kept identical to previous experiments with residence time of 4 h, M:L = 3 and $T = 140^\circ\text{C}$.

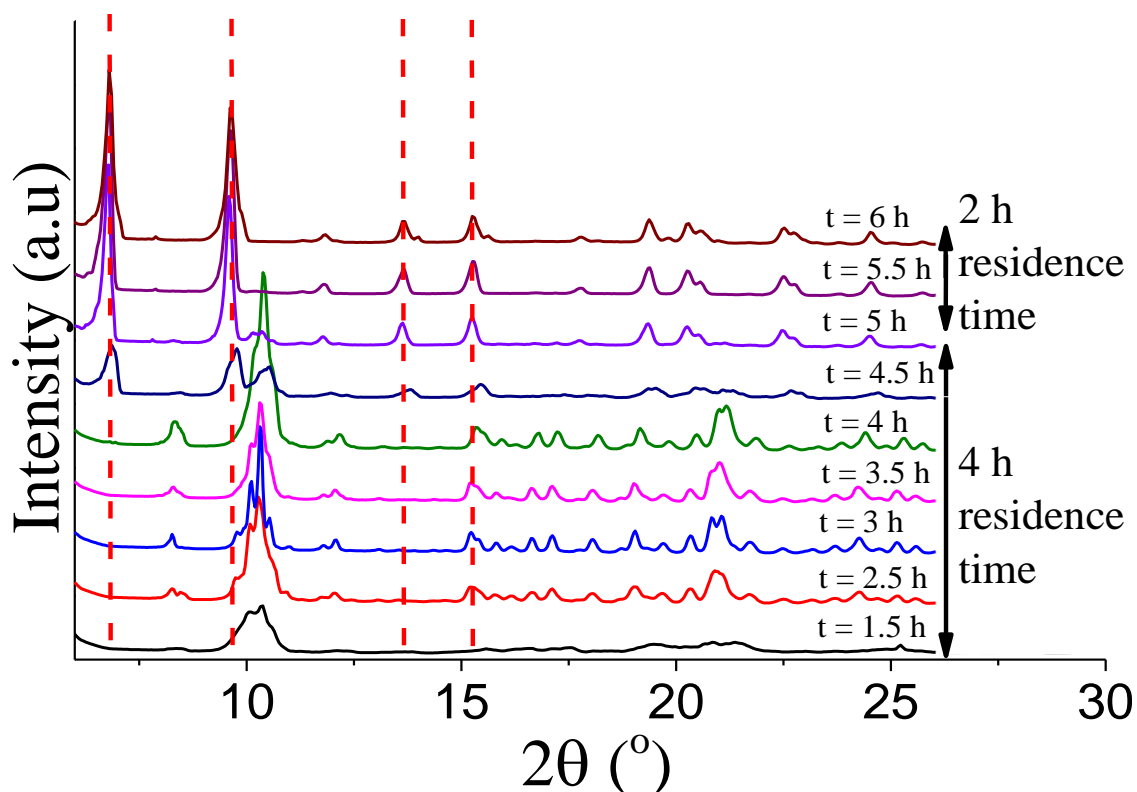


Figure 72 - PXRD showing samples collected from variable residence time reactor run at 10% solids (M:L 4:3). Dashed lines indicate the location of the first 4 Bragg peaks of MOF-5.

PXRD of sample collected show the presence of metastable intermediate phases beginning at $t = 1.5$ h until 4 h. The sample collected between 4.5 and 5 h shows the final remnants of the transient phase with MOF-5 and intermediates present. At $t = 5$ h, at which point the system produces pure phase MOF-5, the flow rates were doubled in order to reduce the residence time by 2 samples collected after this point continue to show MOF-5 until observation was ceased. However, it is unclear if this effect would be sustainable over a longer period of time, if this effect was sustainable it would effectively double the STY of the reactor, assuming yield was not adversely affected.

The theoretical yield of this system at steady state is 5 g h^{-1} , with actual output averaging at 4.1 g h^{-1} (82%) at steady state giving a STY of $984\text{ kg m}^{-3}\text{ day}^{-1}$ demonstrating the possibility of increasing the reactor output by understanding and optimisation of the process mechanisms.

5.8 Use of DMF as alternative solvent for MOF-5 production

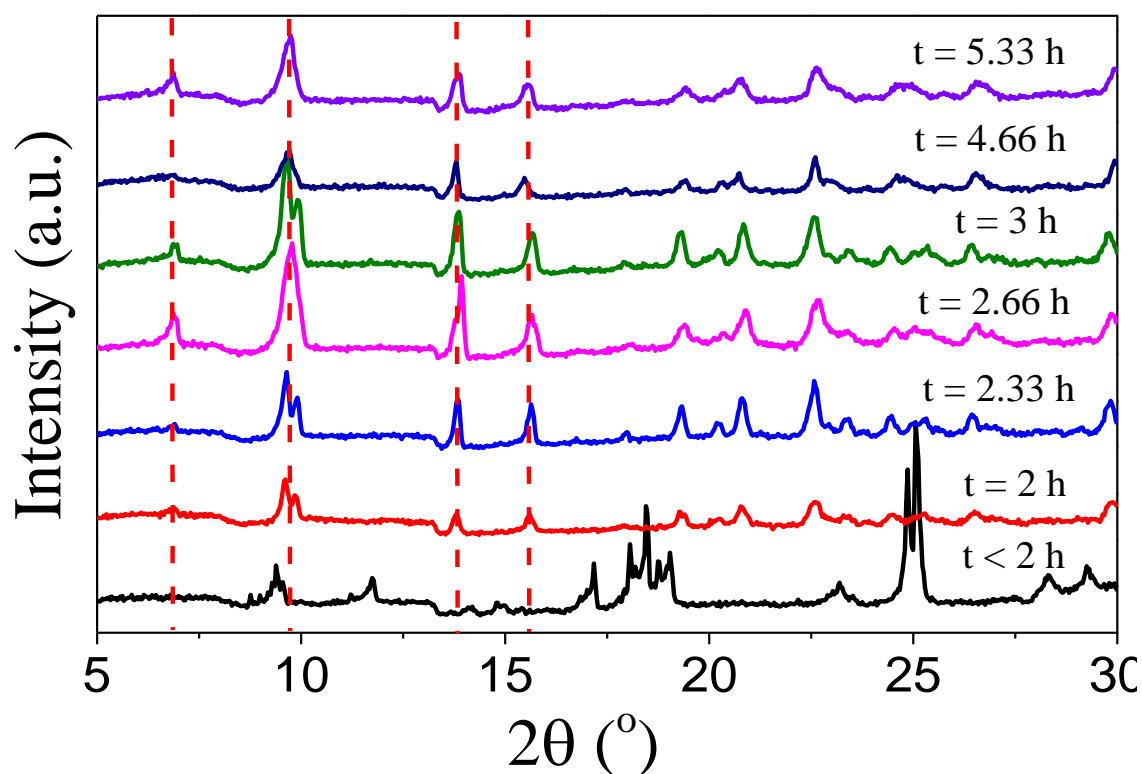


Figure 73 - PXRD results of samples prepared in DMF with 4 h residence time collected at selected time periods. Dashed lines indicate the position of peaks due to the presence of MOF-5, see here at $t \geq 2.66$ h.

Chapter 5 – Results and Analysis for MOF-5

Due to the high cost of DEF and potential likelihood of it being difficult to source in large quantities to allow significant scale up, DMF was used as a comparison using the same conditions. While DMF is noted to generally produce MOF-5 with a lower SSA than DEF, the approximate order of magnitude difference in the price along with the widespread availability of the solvent at manufacturing scale may provide benefit to this process. For this experiment, the conditions of the reactor were kept identical to those described in Chapter 5.5 initially. The reaction temperature here is 140 °C, residence time of 4 h, M:L 3:1 and % solids = 1%, though this parameter was varied similar to the way described in Chapter 5.6.

Figure 73 shows samples collected in the early phase of the reactor (<2.66 h) show only the intermediate phase and no indication of the formation of MOF-5. Samples collected over the time region 3 – 6 h show the formation of MOF-5. Relative to the PXRD of samples synthesised in DEF solvent, The crystallinity of the MOF-5 produced is reduced and appears to have greater variability between samples. MOF-5 produced using DMF shows a greatly reduced surface area with an average Langmuir SSA of $992 \pm 227 \text{ m}^2 \text{ g}^{-1}$ (Table S1) when operating at 1% solids. This value drops to $676 \pm 241 \text{ m}^2 \text{ g}^{-1}$ when the concentration is increased to 5% solids. When the reactor is run at the maximum concentration investigated here, 10% solids, and the surface area of steady state MOF-5 produced is further reduced to $459 \pm 115 \text{ m}^2 \text{ g}^{-1}$. While the surface area drop is expected, the relatively tight banding on the associated errors shows that the system still produces consistent quality MOF-5 when operating at steady state. Along with the reduction in surface area it must also be considered that DMF is also harder to remove from the final product, with solvent exchange usually being required to maximise available surface area^{73d}.

5.9 Comparison of Continuous MOF-5 Output of DMF and DEF solvent systems

A comparison of selected DEF and DMF based MOF-5 is shown below. Both reactors ran for identical periods of time and samples were treated identically after collection.

Table 15 - The results of each of the synthesis conditions are tabulated below. All reactions had 4 h residence time at 140 °C.

Solvent	% Solids	Zn:BDC	Yield (at Steady state)		STY (kg m ⁻³ day ⁻¹)	Average Langmuir SSA (m ² g ⁻¹)	Surface Area Production x10 ⁶ (m ² m ⁻³ reactor day ⁻¹)
			g hr ⁻¹	%			
DEF	1	4:3	0.2	80	48	600	2.9
DEF	5	4:3	0.8	64	196	469	92
DEF	10	4:3	2.1	84	504	270	14
DEF	1	3:1	0.21	84	50	2302	12
DEF	5	3:1	0.8	64	196	759	14
DEF	10	3:1	2.1	84	504	525	26
DMF	1	3:1	0.18	72	43	992	4.3
DMF	3	3:1	0.43	57	104	676	12
DMF	5	3:1	1.85	74	218	671	20

As expected from the literature, the DMF based reaction produces MOF-5 with a lower surface area; the surface area drops by around 60% when switching from DEF to DMF even after activation at 200 °C for 24 h under vacuum. While a reduction in surface area is to be expected, this difference could be reduced by removing solvent through solvent exchange.

The Zn:BDC ratio used has a large impact upon the surface area of the MOF-5 produced as was the case with batch synthesis, as shown in Table 13. PXRD of both phases shows pure phase MOF-5, however we see the Langmuir SSA of MOF-5 formed with excess zinc (M:L = 3:1) is 2302 m² g⁻¹, whereas the same conditions with stoichiometric quantities of precursor (4:3 Zn:BDC ratio) is 600 m² g⁻¹. Both values are also very similar to the equivalent values for batch synthesis using these conditions. While with a view to green chemistry and high atom efficiency an excess of a feed

Chapter 5 – Results and Analysis for MOF-5

component is not desirable¹¹⁴, in this case the reduction in surface area meant that running stoichiometric feed quantities would not be viable for further scale up.

Further, the total surface area production is seen to increase with increased solid content for all systems here, highlighting the potential for running these systems with high solid contents resulting in reduced surface areas being potentially interesting when considering scaling up synthesis to an industrial scale. However, it is important to note that for each series at M:L ratio of 3:1, increasing the reactant concentration of the system results in a significant increase in the total surface area production, the surface area of these materials shows a significant drop off over the same period. As described in Chapter 1.6.4, this may in effect result in a process that does not produce MOF of high enough quality to merit their use over more conventional, cheaper products.

Chapter 6 – Results and Analysis for HKUST-1

6.1 HKUST-1 Formation and Mechanistic Study

As analysis of samples drawn over a fine resolution of times did not show any intermediates, we decided to assume that unlike some other MOFs such as MOF-5¹¹², HKUST-1 does not transform through any metastable intermediates and instead forms directly from solution. For this reaction, we used a temperature of 60 °C, M:L of 1.8, and 3% solids. Figure 74 shows FT-IR spectra for samples taken at various time periods.

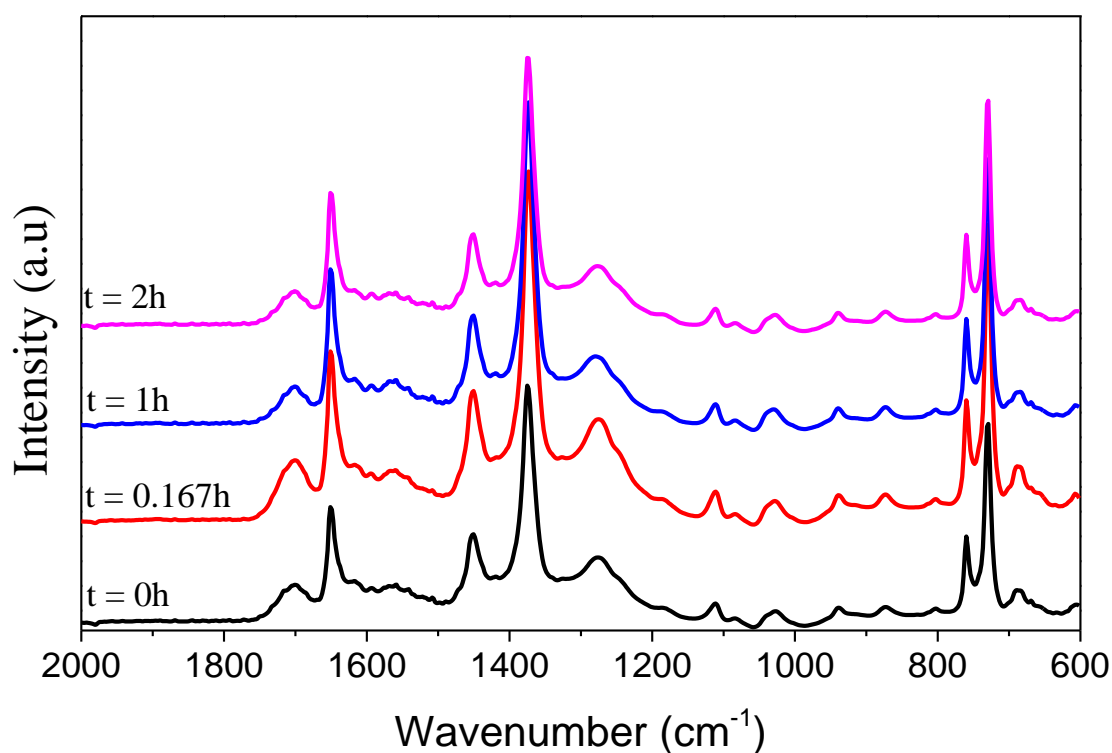


Figure 74 - FT-IR Spectra of samples from the kinetic study at various time periods.

All 4 samples show bonding indicative of HKUST-1 having formed from the structure. The sample at $t=0$ was taken immediately after the two solutions were mixed suggesting that the formation of HKUST-1 will occur almost instantly to some degree. The FT-IR spectra also shows significant area related to peaks showing unbonded ligand at 1700 and 1275 cm^{-1} . The other major peaks present, are all in good agreement with the peak locations and associated vibrational modes previously published^{85, 115}.

6.2 Comparison of batch syntheses

As outlined in section 2.11, the synthesis described by Huo *et al.*⁸⁹ was of considerable interest due to reports of high quality, high yield HKUST-1 times at ambient conditions using water the only solvent.

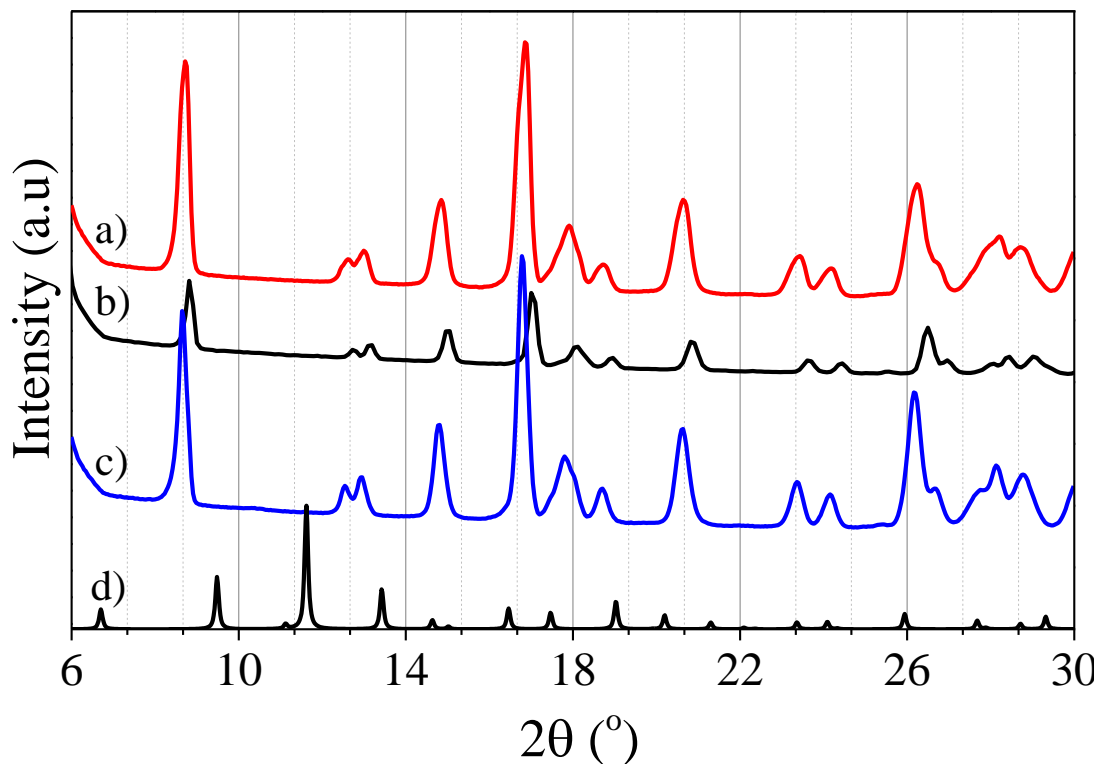


Figure 75 - PXRD results of typical samples of HKUST-1 synthesised using water as only solvent. a) - PXRD of typical synthesis at room temperature. b) PXRD of typical sample heated (80 °C) and stirred. c) Sample sonicated in ethanol after drying d) Simulated XRD for HKUST-1 for crystallographic data¹¹⁶.

Multiple repetitions at each temperature (8, 8 and 4 for room temperature, heated and sonicated samples respectively) yielded consistent results, but none show HKUST-1. PXRD shows all samples forming a crystalline phase, though comparison to the powder pattern generated from crystallographic data shows HKUST-1 is not present in any sample but instead it appears that $\text{Cu}_2\text{OH}(\text{BTC})(\text{H}_2\text{O})_n \cdot 2n \text{H}_2\text{O}$ is formed instead¹¹⁷. This phase has also been previously reported as forming from the same precursors as HKUST-1 when the solvent is completely replaced with water¹¹⁸. Due to issues replicating this work, we decided to switch focus to more conventional syntheses.

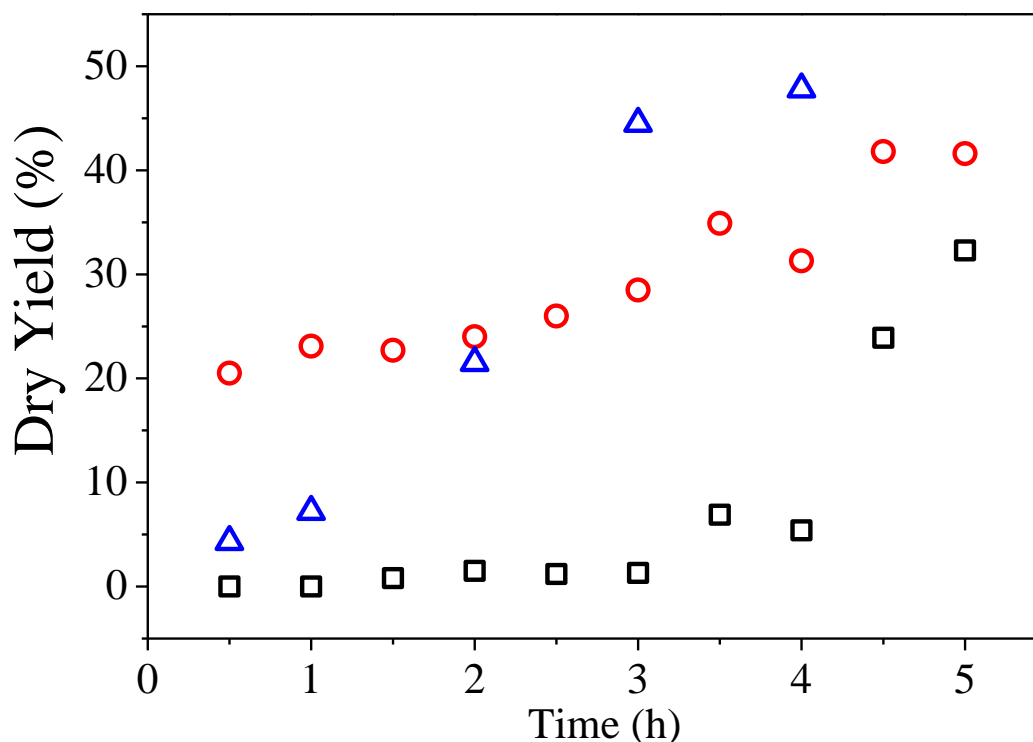


Figure 76 - Comparison of yields of batch systems as a function of time. Squares - Ethanol only synthesis at 60°C. Circles - Ethanol only synthesis at 79°C. Triangles – DMF/water/ethanol synthesis at 60°C.

Ethanol is a suitable solvent and is cheaper than DMF and much less hazardous, however the kinetics are rather slow. DMF/water/ethanol appears to have considerably faster kinetics than ethanol only synthesis when both are run at 60°C, likely due to the breakdown of the DMF to form amine species. However, it also appears that ethanol alone, with all other parameters staying identical, forms a material with higher surface area. In order to determine which process would likely be the most viable, we must consider a number of metrics. For instance, the faster kinetics of the DMF/water/ethanol based product allows for higher yields, which may be more desirable than a higher surface area product formed by ethanol alone with a low yield. In order to fully compare which route would be most effective, we undertook several experiments and the results are reported in Table 16. The DMF/ethanol/water system shows the highest yield overall and also shows HKUST-1 forming faster than the ethanol only solutions. The mixed solvent system shows 20% yield at 2 hours, increasing to 45% yield at 4 hours. Comparatively, the ethanol system run at 60°C shows very low yield, typically less than 10% before increasing to 23% at 4.5h and 33% at 5h. While the yields of

DMF/Ethanol/Water are generally superior, we also analysed the output by gas adsorption in order to determine which system produces the highest quality crystals. After repeating the experiment using ethanol as the only solvent at a higher temperature (79°C rather than 60°C) we see that increasing the temperature of the ethanol only synthesis increases the rate of formation of the HKUST-1, showing 20% yields at times as low as 0.5h and increasing to a little over 40% by 5h. This shows significant improvement over the same system at 60 °C which produced only 32% yield at 5h. The largest difference between the two systems is that operating at full reflux temperature increases the yield at times under 3 h to be increased by a large margin, approximately 25%.

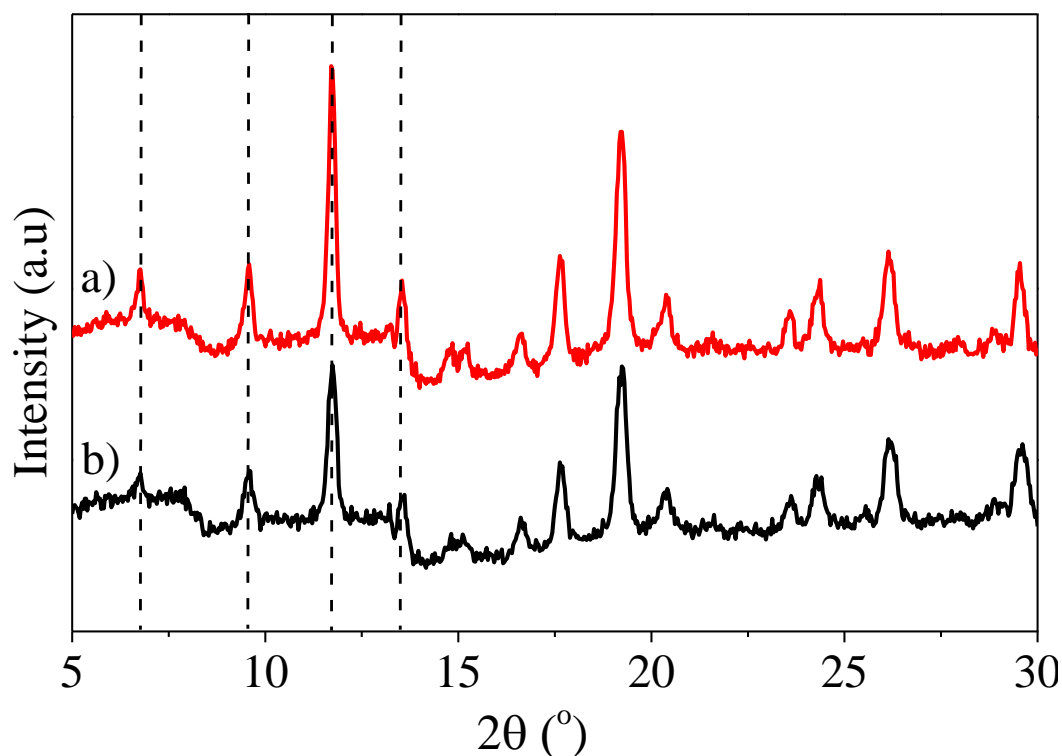


Figure 77 - PXRD showing HKUST-1 as synthesized in 4 h at 60 °C in a)DMF/ethanol/water, b) ethanol only. Both samples show HKUST-1 with a variation in crystallinity between the samples.

Figure 77 shows that after 4hr both systems will produce HKUST-1, with locations of expected Bragg peaks matching the powder pattern generated from single crystal data. HKUST-1 produced using ethanol as the only solvent has higher crystallinity, with more intense, narrow Bragg peaks.

Gas adsorption studies show that the DMF/ethanol/water system produces crystals with a Langmuir Specific Surface Area of $1100 \pm 50 \text{ m}^2/\text{g}$ at 4 h synthesis time. Both ethanol systems show a higher

Chapter 6 – Results and Analysis for HKUST-1

Langmuir SSA with surface areas in the region of $2000 \pm 200 \text{ m}^2/\text{g}$. As a determining factor for deciding which system to use as the basis for the continuous reactor system, the yield, cost and availability of solvents and the surface areas of the products must be considered.

Table 16 - Comparison of batch synthesis routes for HKUST-1 and the key parameters related to synthesis

Solvents		DMF/Water/Ethanol	Ethanol (60C)	Ethanol (Reflux)
Reaction Temperature (°C)		60	60	78
Dry Yield (%)	3hr	45	1.3	28.5
	4hr	47	5.4	31.3
	5hr	-	32.3	41.6
Average Langmuir SSA m^2g^{-1}		1100	2200	2100
Solvent Cost (£/ g _{HKUST-1})		3.60	8.95	6.81
STY (best from above) $\text{kg m}^{-3} \text{ day}^{-1}$		1.67	0.9	1.2
Surface Area Produced ($\text{m}^2 \text{ m}^{-3}_{(\text{reactor})} \text{ day}^{-1}$)		1.84×10^6	1.98×10^6	2.52×10^6
Rough Cost	(£/m ²)	0.003273	0.0040	0.003243
	Relative Cost	0.804	1	0.797

Table 16 shows yield increasing with time although no synthesis appears to produce more than 50% yield. The clear differences between kinetics and product quality are highlighted when comparing DMF/water/ethanol synthesis to ethanol only synthesis. The HKUST-1 from the DMF/water/ethanol synthesis shows similar yield at $t = 0.5 \text{ h}$, however the kinetics are considerably faster beyond this point with 7.2 and 21.5% yield at 2 and 3h respectively, compared to approximately 1% yield at both time points for ethanol only synthesis at the same temperatures. Increasing the temperature of the ethanol only system to $79 \text{ }^\circ\text{C}$ increases the yield significantly, with 20% yield after 0.5 h. However, product quality, in terms of surface area must also be considered. The ethanol only system at $79 \text{ }^\circ\text{C}$

has a slightly lower average surface area of $2100 \text{ m}^2\text{g}^{-1}$, likely due to the faster formation. We then considered the total surface area produced, by combining the space-time yield and the surface area. All 3 systems analysed here show similar surface area production (SAP). The high yield and lower surface area of the DMF/water/ethanol provides slightly lower SAP compared to the low yield, high surface area material produced from ethanol only synthesis, however the difference in SAP is minimal. However, as discussed previously this situation is unlikely and is mentioned for completeness. For applications where the absolute highest possible surface area is desirable, ethanol at reflux temperature provides the highest SAP and highest overall average surface area. Due to the relatively high yield of the ethanol system at $79 \text{ }^\circ\text{C}$, and the small reduction in surface area compared to the ethanol system at $60 \text{ }^\circ\text{C}$ we see an increase of about 25% to the SAP of the system.

It is important to note that for the above, we consider only the approximate costs for the solvents here and without any form of recycling and are based on the costs of small scale synthesis.

6.3 Process Intensification of HKUST-1 Batch Syntheses

When considering process intensification, one of the areas for improvement is to increase the concentration of precursors in the feed in order to produce more material in the same quantity of solvent. However, due to the formation mechanisms of MOFs this can often result in interpenetration or increased presence of unreacted ligand or other components blocking pores which will greatly reduce the surface areas. The system described above produces 3% solids at 100% theoretical yield. In order to access the possibility of increasing the solids output we repeated the batch experiments to produce solutions at the equivalent of 6, 9 and 15% solids.

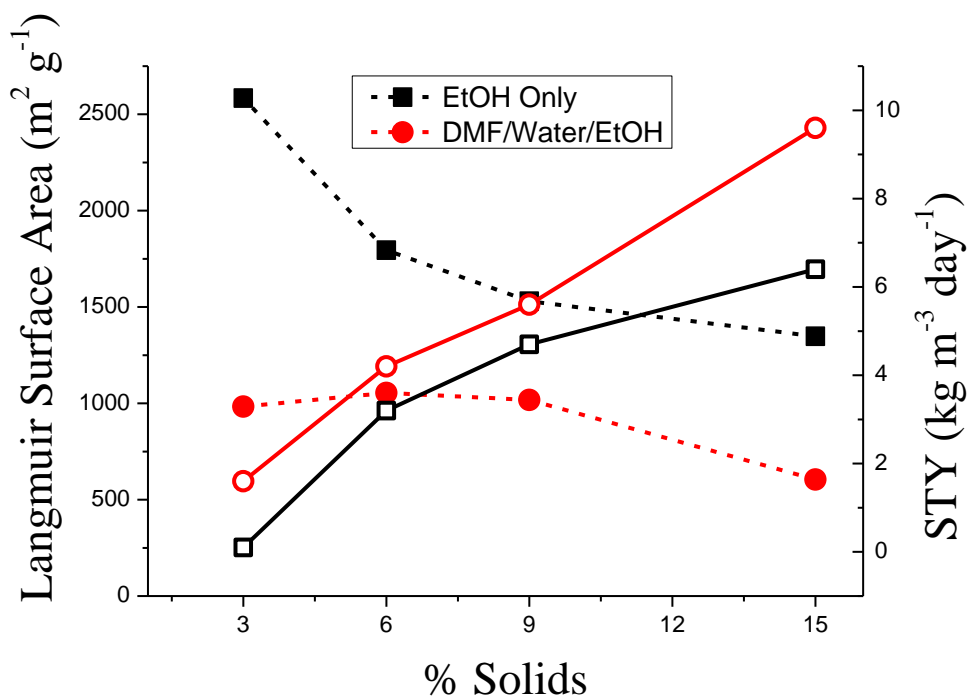


Figure 78 - Comparison of Surface Area and STY as a function of % solids. Red circles indicated DMF/water/ethanol system. Black squares indicates ethanol only. Hollow shapes represent STY and full shapes represent Langmuir surface area.

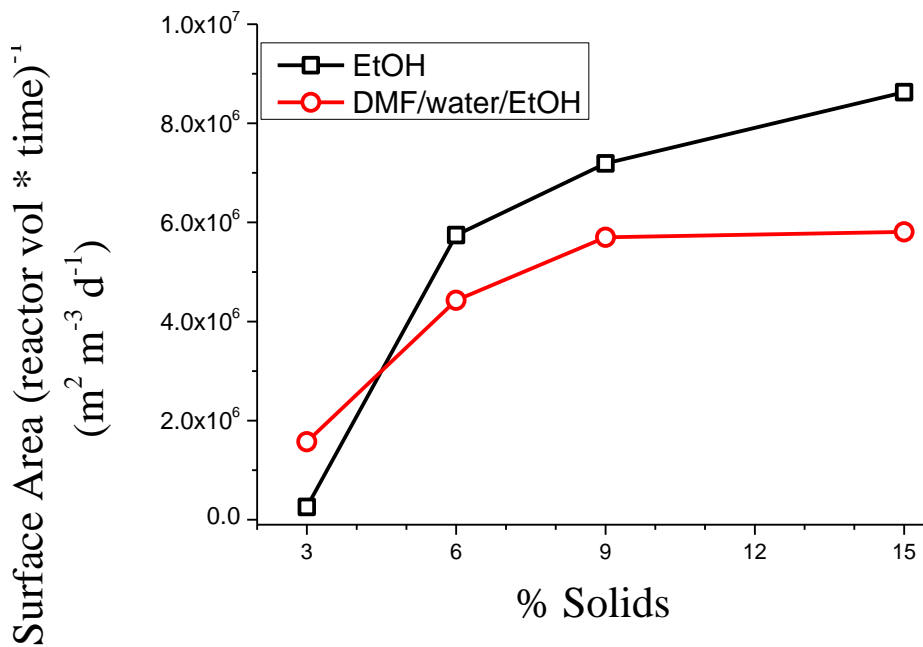


Figure 79 - The surface area of material produced per unit of reactor volume per day. Black line with squares shows ethanol only synthesis. Red line with circles shows DMF/water/ethanol solution synthesis.

Chapter 6 – Results and Analysis for HKUST-1

It is important to note that at low concentrations, the DMF/water/ethanol synthesis produces more surface area of material per unit volume of reactor per unit time. However, when intensifying the process, the reduction in surface area of the DMF/water/ethanol system results in the ethanol only synthesis being favourable in terms of surface area output.

The important factors are all linked together, but essentially the most important metrics are the reaction time, the yield and the average surface area. Importantly, the approximate costs per square metre of surface area are almost identical between the DMF/water/ethanol system and the ethanol system at reflux. However, when scaling this process up the changes in the process chemistry will have more important effects on the quality of the final product. Ethanol does not break down in the process and so can theoretically be almost infinitely recycled with only minimal losses. DMF is known to breakdown when exposed to water and heat and hence cannot be easily recycled. The amines produced from this breakdown also present an environmental risk. Furthermore the heat capacity of each solvent must be considered. Ethanol has an approximate heat capacity of 2.3 kJ/kg K compared to 4.2 and 2.0 kJ/kg K for water and DMF respectively. While DMF actually has a lower heat capacity, the addition of water also increases the heat capacity of a DMF/water/ethanol solution to approximately 2.8 kJ/kg K. When the energy usage is compared to the pure ethanol synthesis, and is scaled up this will be a significant amount of energy. Therefore we have elected to design this plant with a mind toward the pure ethanol synthesis.

The ethanol systems show higher starting surface areas, though also a more significant drop off in available surface area. While both solvent choices show a drop off in surface area with increasing % solid loading, it is also important to account for the increased solid throughput. While 3% solid may produce materials with surface areas close to the maximum recorded, an economically viable scaled up process may have to compromise surface area for high STY. Interestingly, the DMF/water/ethanol solution produces HKUST-1 with similar surface areas at 3, 6 and 9 % solids suggesting that a DMF/water/ethanol system can be run at 9% solids without any significant reduction in the quality of the MOF. However, the surface area of these MOFs are still below the ethanol only synthesis which falls from 2600 m² g⁻¹ to 1550 m² g⁻¹ when increasing solid loading from 3 to 15%.

6.4 Solvothermal Continuous Synthesis of HKUST-1

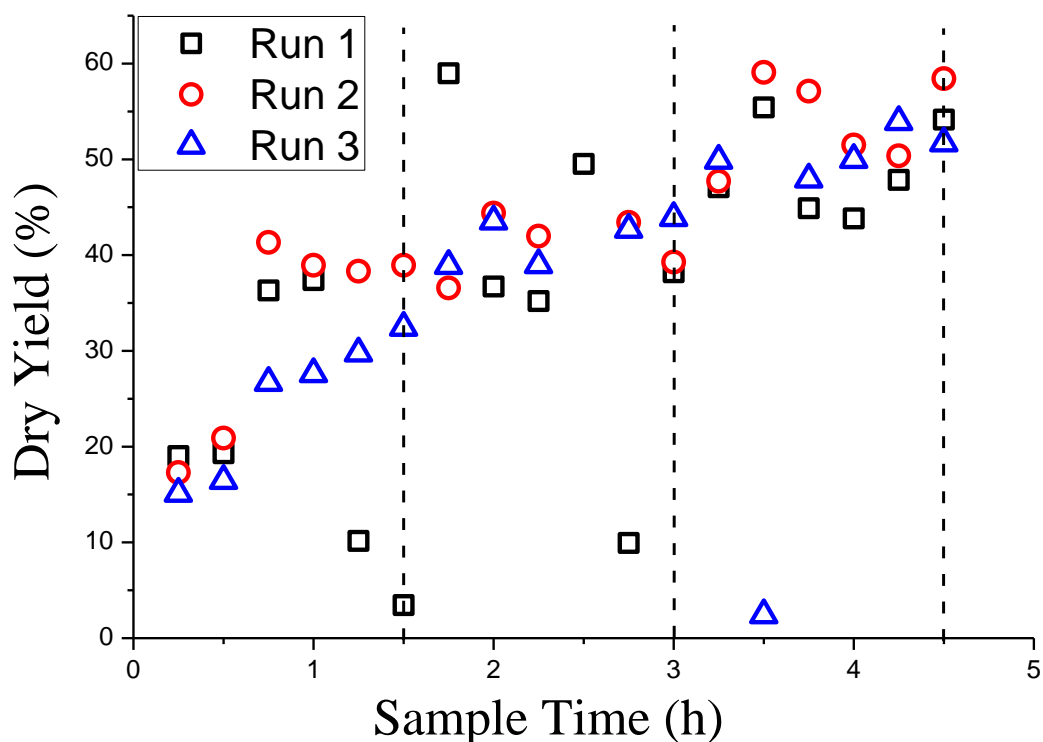


Figure 80 - Dry Yield for samples collected from the continuous HKUST-1 reactor. Dashed lines indicate the end of the 1st, 2nd and 3rd residence times of the reactor.

The system, run at residence time of 1.5 h, M:L = 1.8, 3% solids and 79 °C, shows yields favourably comparable to the equivalent batch testing. This is likely an effect of the system self-seeding itself and being in a state favourable to producing HKUST-1, highlighting one of the key benefits to continuous synthesis. It should be noted that the solids in the output stream can often form slugs and so this often results in a low yield at one collection point followed by a high yield in the next collection period when the slug moves through the system. This is particularly common in the first run.

This experiment was then repeated with the volumes of feed increased by a factor of two, with all concentrations kept constant, and was run for 9 hours total, giving 6 full residence times for this reaction in order to determine if the steady state yield had been reached.

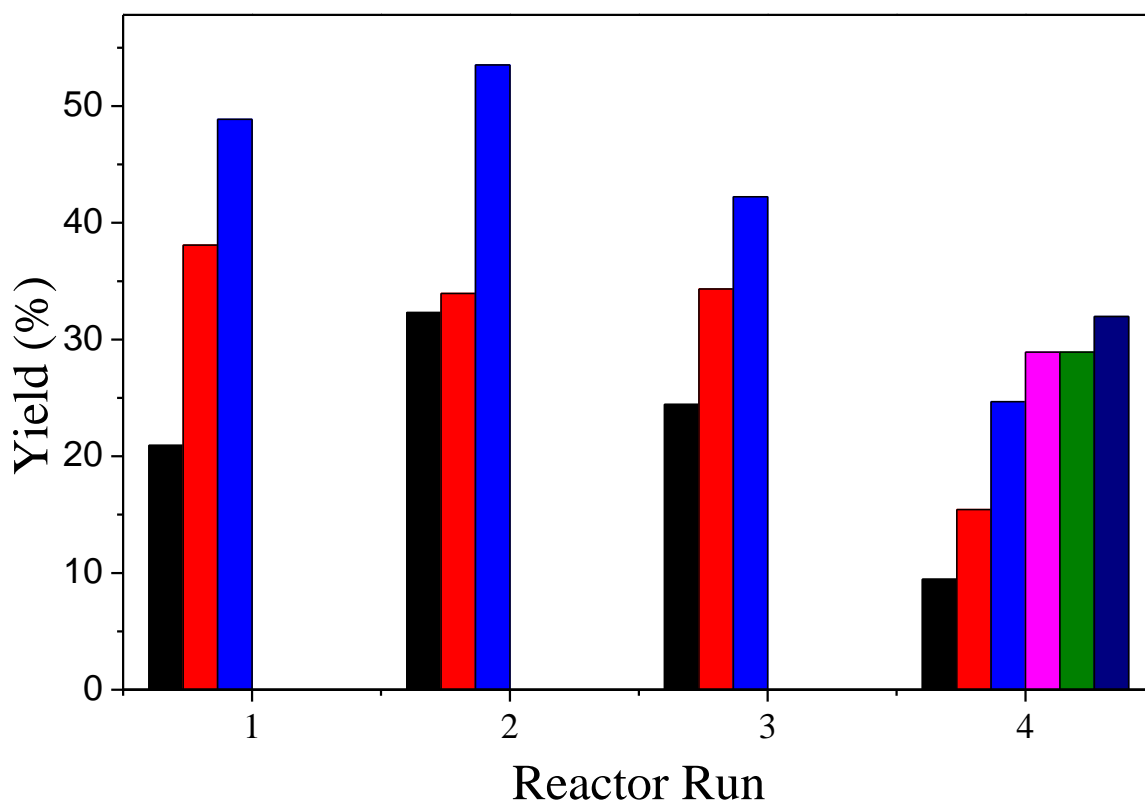


Figure 81 - Average yield over consecutive residence times for each reactor run, showing a steady increase in yield over the first 3 residence times before levelling off at longer residence times.

As Figure 81 shows, the yield per residence time increases significantly over the first 3 residence times but levels off with residence times of 4 or more ($t > 4.5\text{hr}$) suggesting steady state has been reached by this point. The system produces HKUST-1 with a yield of 36% over the 3 residence time period the system was operated for. However, when analysing the average yield over a single residence time, the first residence time produces an average yield of 26% ($\pm 6\%$), this increases to 40% ($\pm 2\%$) during the second residence time and increases further to 48% ($\pm 6\%$) in the third residence time. The yield within the first residence time is similar to the yield seen for the same reactor set-up running a batch reaction for 1.5 h. In the second and third residence times, the continuous system is able to produce a higher yield than the batch system demonstrating the benefits of continuous processing to HKUST-1 production. Subsequently, the average STY of the system is $172\text{ kg m}^{-3}\text{ day}^{-1}$, while this is 101, 182.4 and $235.2\text{ kg m}^{-3}\text{ day}^{-1}$ for the first, second and third residence times respectively showing the need to give output at steady state.

Chapter 6 – Results and Analysis for HKUST-1

The HKUST-1 produced by the system has an average Langmuir Surface Area of $1857 \pm 138 \text{ m}^2 \text{ g}^{-1}$, BET Surface Area of $1270 \text{ m}^2 \text{ g}^{-1}$ and c-value of -44. The negative c value highlights why this type of analysis is unsuitable due to the nature of pore filling in MOFs as discussed in Chapter 4.. The surface area of the solid outputs is very consistent with samples from multiple repeats all conforming to the same tight banding as shown in Figure 82.

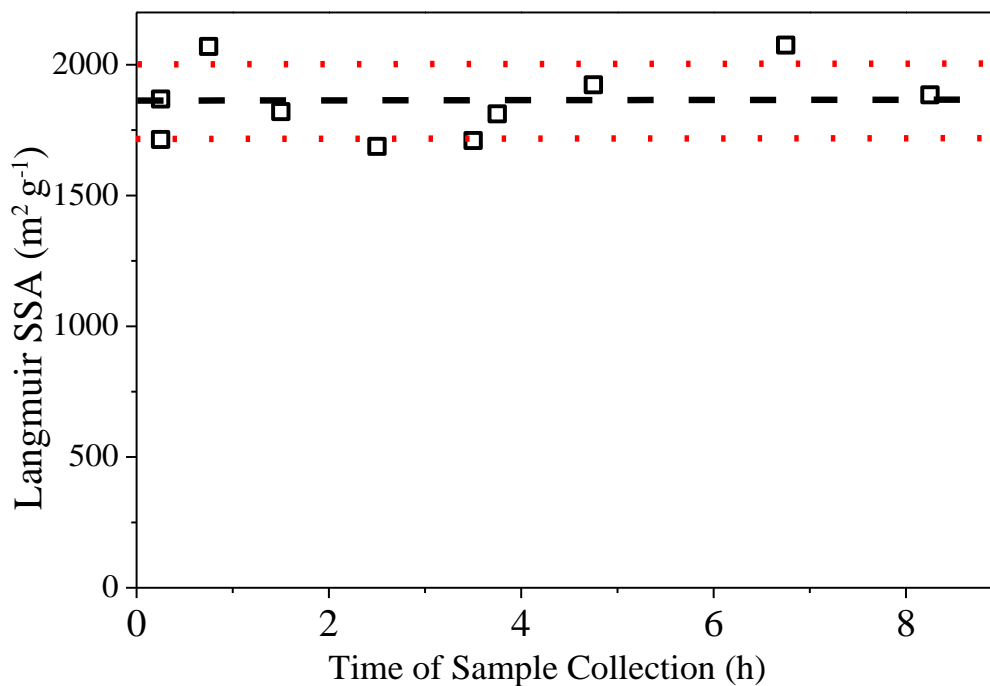


Figure 82 - Langmuir Specific Surface Area results from 4 different runs at various time collection times. The black dashed line reflects the average specific surface area, and the red dotted lines indicate 1 standard deviation from the mean.

PXRD confirmed the solid outputs were HKUST-1 as shown in Figure 83 showing that HKUST-1 is present even during the first collection period of 0-0.25h after start up.

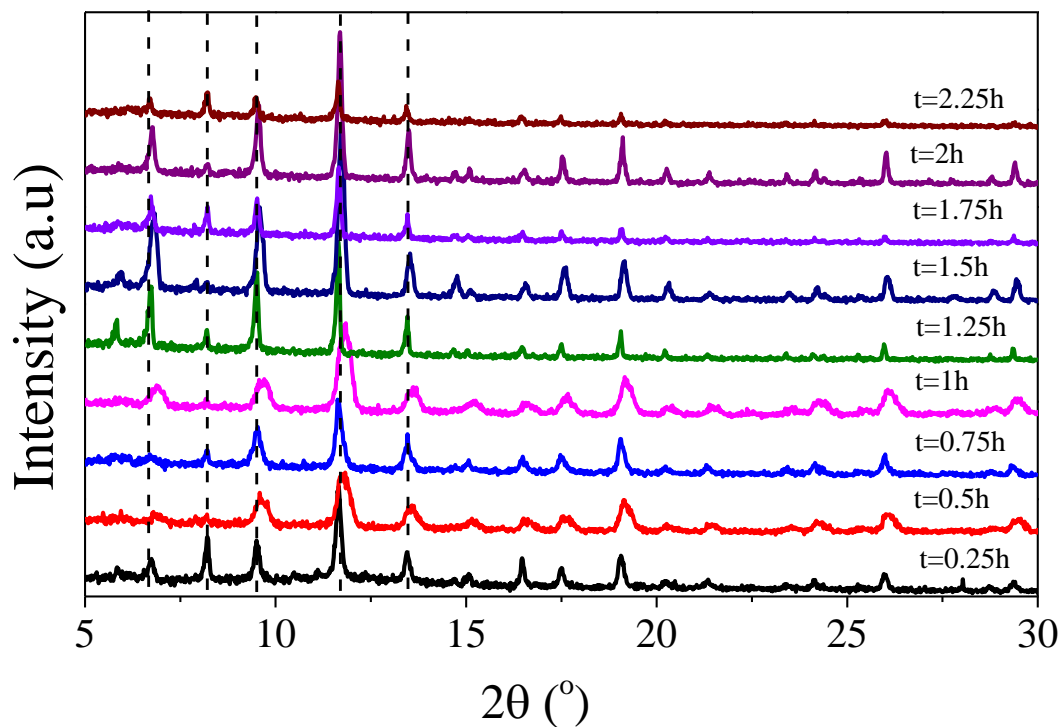


Figure 83 - PXRD results showing output of solid content from continuous reactor at various times. Dashed lines indicate the location of Bragg peaks for HKUST-1

Although it was expected that the continuous reaction system will produce HKUST-1 with reduced surface areas when increasing solid concentration, it may be possible that for a scaled up process a compromise between increased STY and reduced surface area is possible. As such, this experiment was then repeated at 9 and 15% solids, while the other reactor parameters were kept as set in the previous experiment (residence time of 1.5 h, M:L = 1.8 and 79 °C).

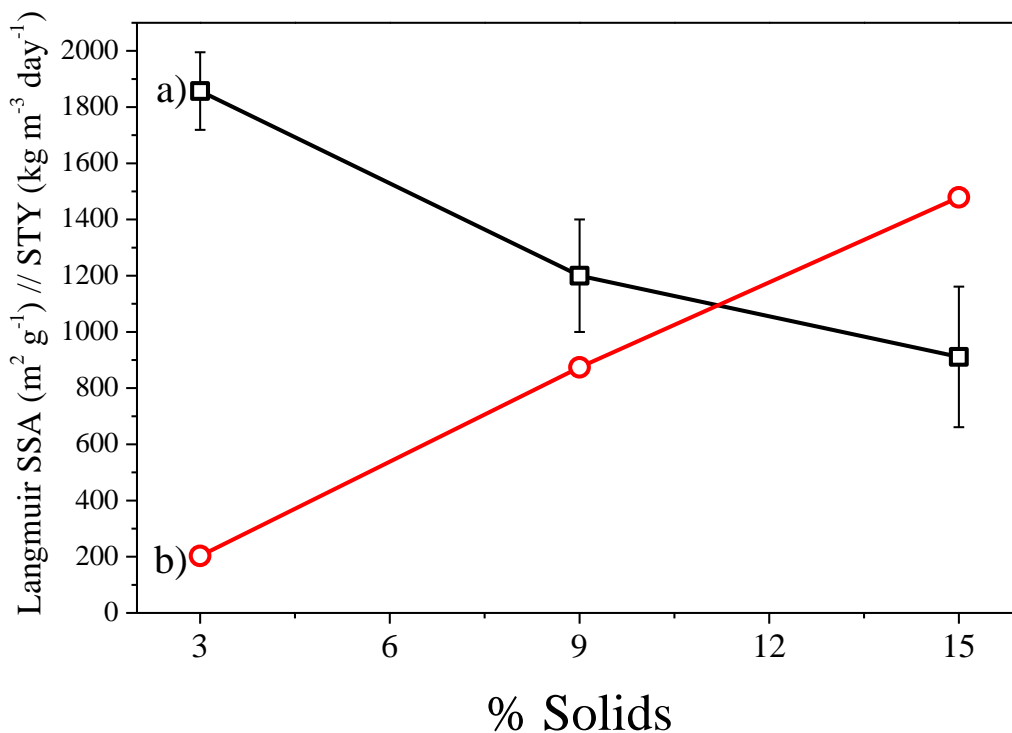


Figure 84 - a) The average Langmuir SSA ($\text{m}^2 \text{g}^{-1}$) b) the calculated space time yield ($\text{kg m}^{-3} \text{day}^{-1}$) showing the general trend of increasing STY resulting in a reduction in surface area of the material.

One of the most vital changes observed when increasing the reactant concentrations was the increase in % theoretical yield from approximately 40% at 3% solids increasing to approximately 60% yield at 9 and 15% solids. The average surface area produced shows a decrease with increasing solid concentrations that appear to be very similar to what is seen with the batch processing experiments above.

Table 17 - Comparison of yield, SSA and total surface area produced by the continuous system at steady state.

% Solids	Steady State Yield		Average Langmuir SSA ($\text{m}^2 \text{g}^{-1}$)	Surface Area Production $\times 10^6$ ($\text{m}^2 \text{m}^{-3}_{(\text{reactor})} \text{day}^{-1}$)
	(% theoretical)	Space Time Yield ($\text{kg m}^{-3} \text{day}^{-1}$)		
3	39	203	1857 ± 138	377
9	58	874	1046 ± 118	914
15	60	1479	911 ± 250	1347

Chapter 6 – Results and Analysis for HKUST-1

However, in June 2014 a continuous reactor system for producing HKUST-1 had results published which we compare to here¹¹⁹. Unlike the system described above, the reactor used is a tubular reactor vessel, though importantly it was operated at 80 °C using ethanol as the only solvent at similar concentrations to those described above. The material produced from both reactors is similar in surface area ($> 1800 \text{ m}^2 \text{ g}^{-1}$) however; the yield of the tubular reactor system varies between 60-90% yield, with 60% being equivalent to the upper yield of the system we have developed. Further, the tubular system appears to allow for significantly higher yield per unit time, which directly impacts the STY of the product. For comparison, operating a tubular reactor at 80°C with residence time of 1.2 and 10 min forms HKUST-1 with surface area ($> 1800 \text{ m}^2 \text{ g}^{-1}$) and STY of 4533 and 692 $\text{kg m}^{-3} \text{ day}^{-1}$ respectively. This represents a significant increase from the STY values determined here for a tank reactor, which produces similar quality of material but requires 90 min residence time and only produces an overall STY of 377 $\text{kg m}^{-3} \text{ day}^{-1}$.

6.5 Post Processing of HKUST-1

As MOFs are generally produced as bulk powders, for applications it is more likely that the material would be pelletised before use. The results of these tests are tabulated in Table 18. Though Langmuir SSA has generally been used to report surface areas within this thesis, only the BET surface areas are given by Peterson *et al.* who have similarly compressed HKUST-1.

Table 18 - Surface Area measurements for HKUST-1 compressed at various degrees

Sample Compression	Work completed within			Reported Peterson <i>et al</i> ¹²⁰ .	
	Langmuir SSA ($\text{m}^2 \text{ g}^{-1}$)	BET Surface area ($\text{m}^2 \text{ g}^{-1}$)	Micropore Volume ($\text{cm}^3 \text{ g}^{-1}$)	BET Surface area ($\text{m}^2 \text{ g}^{-1}$) 1)	Micropore Volume ($\text{cm}^3 \text{ g}^{-1}$)
Bulk Powder	2048 (100%)	1406 (100%)	0.616 (100%)	1698 (100%)	0.75 (100%)
Compression to 1000	N/A	N/A	N/A	1045	0.61

psi (equivalent to 68 atm)				(61.5%)	(81.3%)
Compression to 1000 psi (equivalent to 680 atm)	N/A	N/A	N/A	892 (52.5%)	0.52 (69.3%)
Compressed at 1 tonne (equivalent 740 atm)	1324 (64.6%)	908 (64.6%)	0.415 (67.4%)	N/A	N/A
Compressed at 2 tonne (equivalent 1480 atm)	1009 (49.3%)	693 (49.3%)	0.317 (51.4%)	N/A	N/A

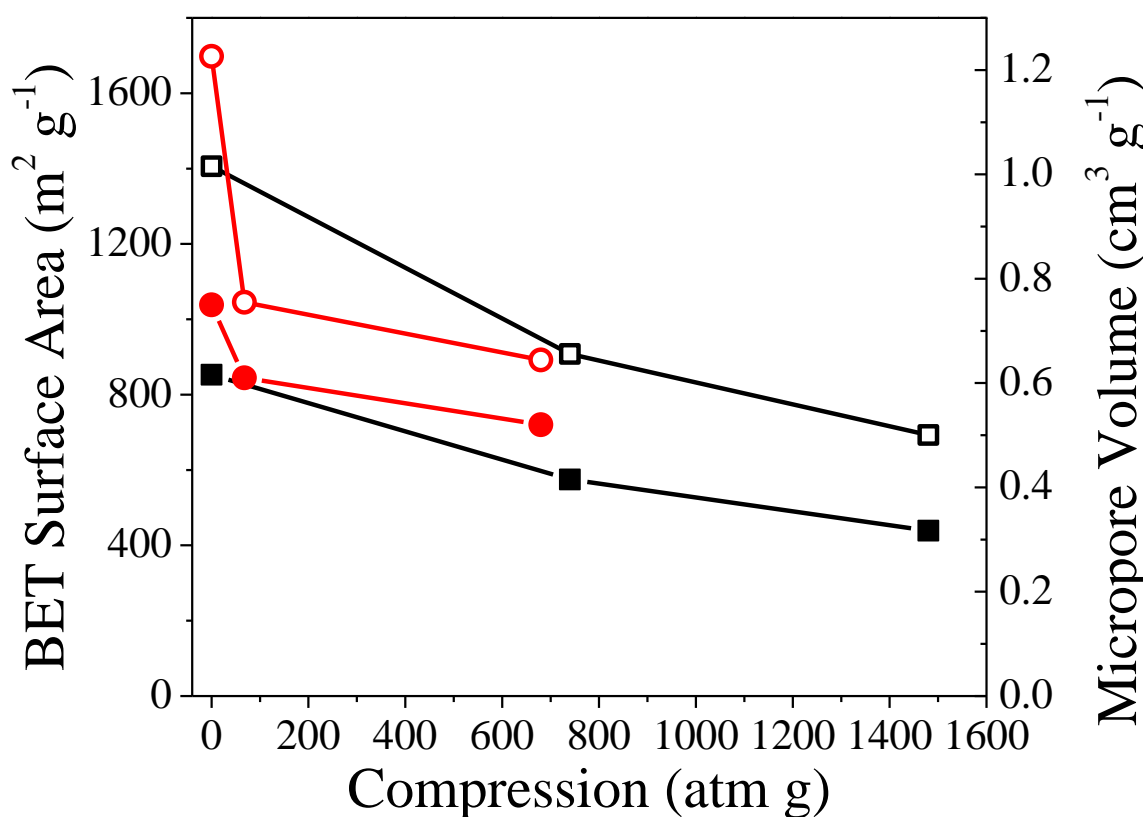


Figure 85 - Comparison of HKUST-1 compression tests to values given by Peterson *et al.* Squares indicate work completed as part of this project, Circles represent reported values from literature by Peterson *et al.*¹²⁰. Filled symbols indicates micropore volume, hollow symbols indicates BET surface area.

These results are comparable to those published by Peterson *et al.*¹²⁰, though the bulk powder synthesised has slightly higher BET surface area, both sample show similar loss when compressed to 680 and 740atm. Differences between the two results are likely due to the initial difference in bulk powder surface area and the pellet diameter, and overall thickness differences between the two samples.

FT-IR and PXRD were used to check for structural changes within the crystal that may have occurred during pressing.

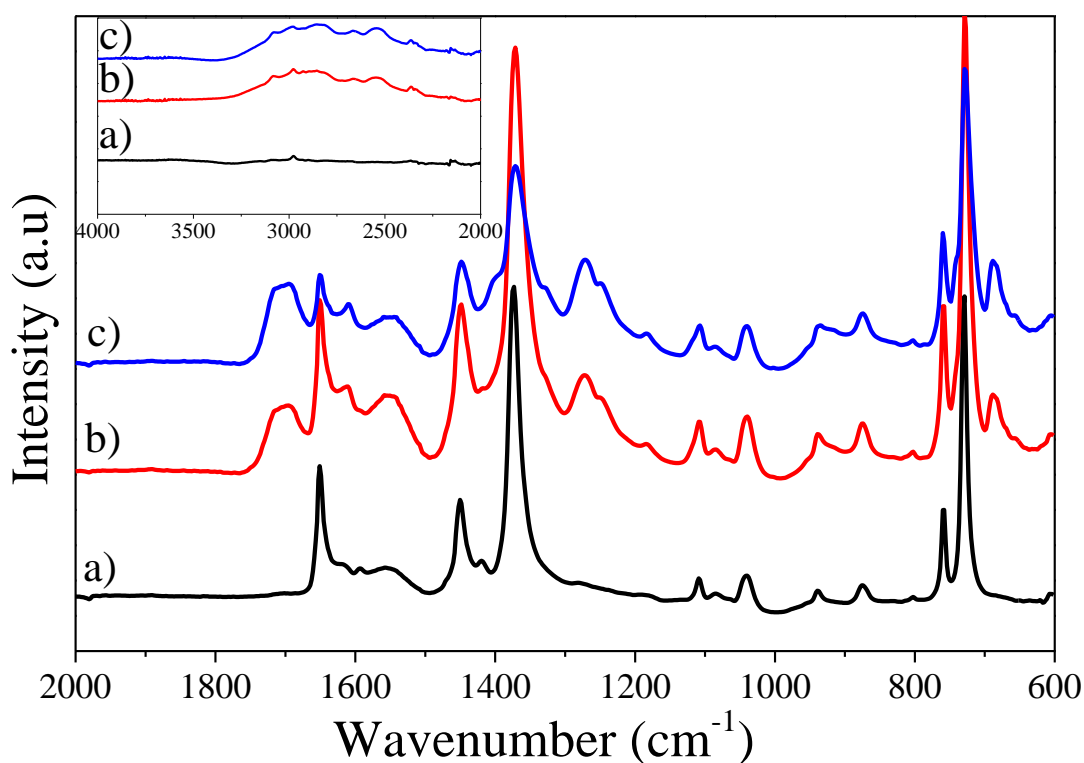


Figure 86 - FT-IR results of compressed HKUST-1 samples. a) no compression, b) compressed at 740 atm, c) compressed at 1480 atm.

Figure 86 shows that while HKUST-1 bonding is still in place, we see some breakdown with the peaks for unbonded ligand being present in samples that underwent compression, however the framework structure does appear to be intact still.

Chapter 7 – Use of Microwave Heating for MOF Synthesis

7.1 Testing of Microwave for Potential Use for MOF Synthesis

The microwave system was initially tested using 100ml DEF with no reactive precursors in order to find the approximate temperature profiles of the microwave at different power levels for this solvent. Further to establishing an approximate heating rate, the steady state temperature of the system is of great importance.

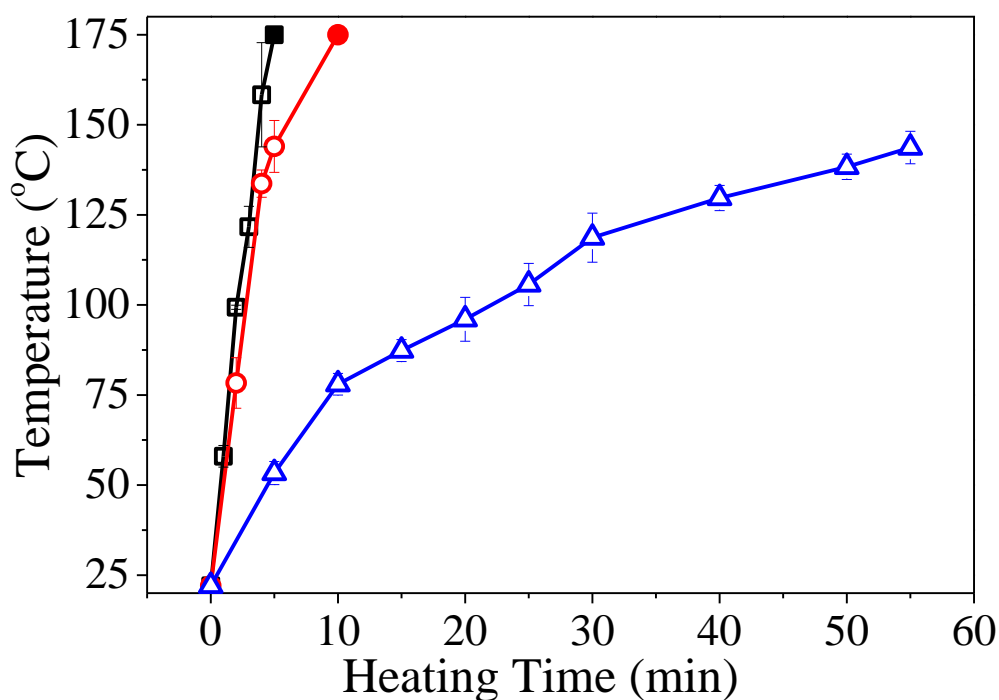


Figure 87 - Heating profiles for 100ml DEF solvent, Squares indicate 50% power, Circles represent 30% power, and Triangles represent 10% power. Filled symbols indicate the DEF superheated at this time, rather than being an indication of the true temperature.

Heating at 50% power forces the system into superheating very quickly. At 30% power, we see a similar trend though with a slightly longer time. Reducing power to 10%, the minimum available on our domestic microwave, we see the solution heat more slowly. Though it does not reach steady state until a temperature above our preferred operating window, this will be the power level used for flow experiments as it still allows us a wider operating time within the 110-140°C range. However, for 30

min exposure to microwaves at 10% power, the temperature is approximately 125°C which is close to the temperatures anticipated to provide the simplest reaction pathway, as shown in Figure 62.

Bulk temperature as a function of time was then monitored with a slight variation of conditions. The pure solvent system was flowed at 30min residence time. Secondly, the system was not under flow conditions but has the precursor materials for the reaction included. These allow the effect of adding the precursors to the solvent and the effects of flow to be observed independently. Finally, we combine the experiments and record temperature against time for a system under flow conditions with the reaction precursors included.

An internal reactor volume was created using tubing of 8mm d_i giving an overall reactor volume of 200 ml. This is a similar scale to that used within the conventionally heated continuous system detailed in Chapter 5.5. While the output temperature of the coil was monitored, further analysis showed the system tended to be very prone to heating in specific locations. The approximate profile of this is shown in Figure 88.

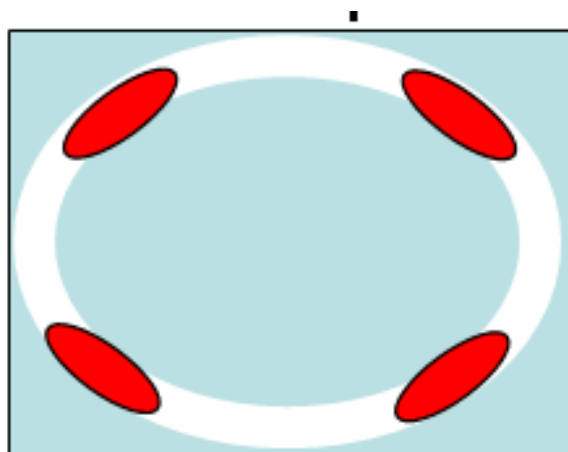


Figure 88 - Location of distinct hot spots in the reaction tubing. Tubing indicated by white circle, the marked red regions were considerably hotter than other locations on the tubing.

The hotspots disperse easily however when the system is under flow conditions of a reasonable rate, though are still noticeable at residence time of 30 min.

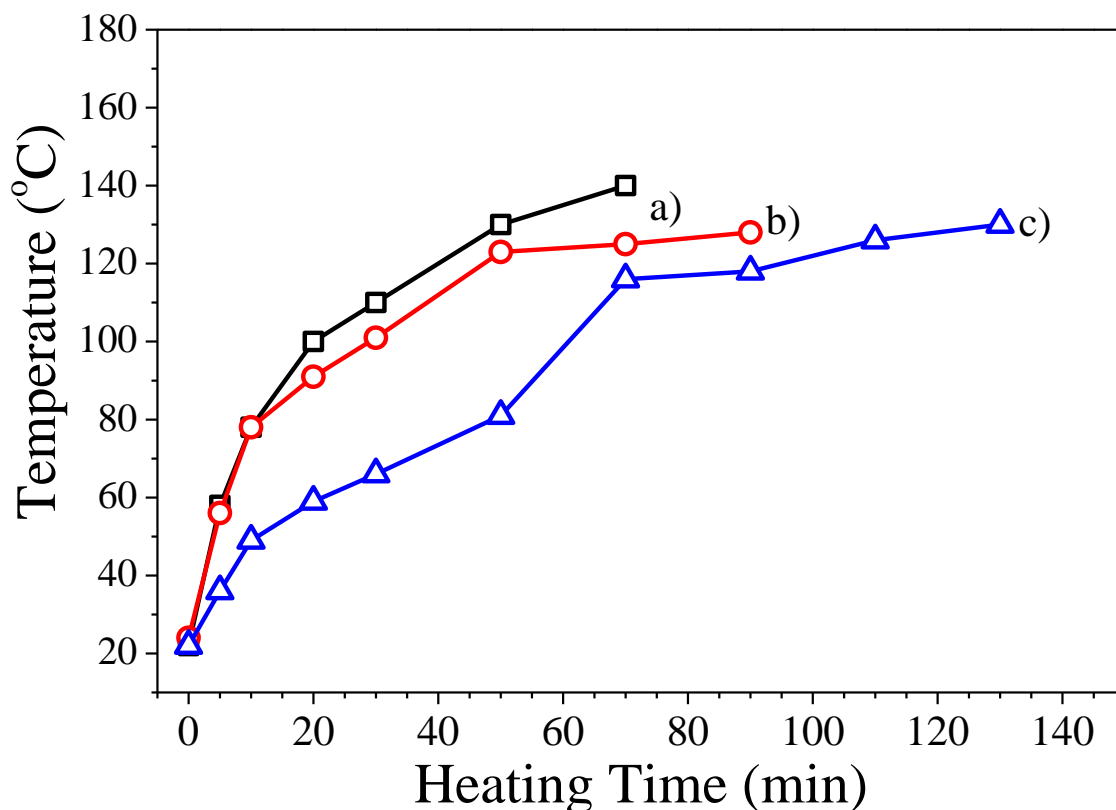


Figure 89 - Comparison of temperature profiles from various conditions. a) Solvent only, no flow. b) Solvent only, residence time = 30 min, 10% power, c) Reaction Mixture, no flow.

The system was first tested with only DEF solvent present shown as Figure 89a). The temperature is slowly built up however, the system will eventually overheat. This experiment was then repeated with DEF solvent only under flow conditions, giving a residence time of 30 min, resulting in the temperature reaching an approximate steady state at a temperature of 125 ± 5 °C, approximately the temperature range deemed optimal based on results shown in Chapter 5. In order to test the effect of including reaction precursors in the solvent, a batch solution of DEF with reaction precursors was heated. This showed a lower heating rate than the equivalent test without reaction precursors, and reaching a stable temperature in approximately the same time.

7.2 MOF-5 Continuous Synthesis using Microwaves

The next step in testing of the microwave system was to attempt to monitor the temperature profile of continuous MOF-5 production reactions, heating the reaction mixture under flow conditions giving a residence time of 30 min shown in Figure 90. Heating the reaction solution at 10% solids shows a rapid heating profile over the first 5 min, though the temperature profile levels off at approximately 90

± 5 °C. Repeating this experiment with new solvent, at 20% power level shows more rapid heating in the first 5 minutes, before the temperature appears to begin to level off at 130 ± 5 °C, however, the system then appeared to over-pressurise and the experiment was terminated. Due to this overheating at 20% power, 10% power had to be used for further continuous MOF-5 production using microwave heating testing.

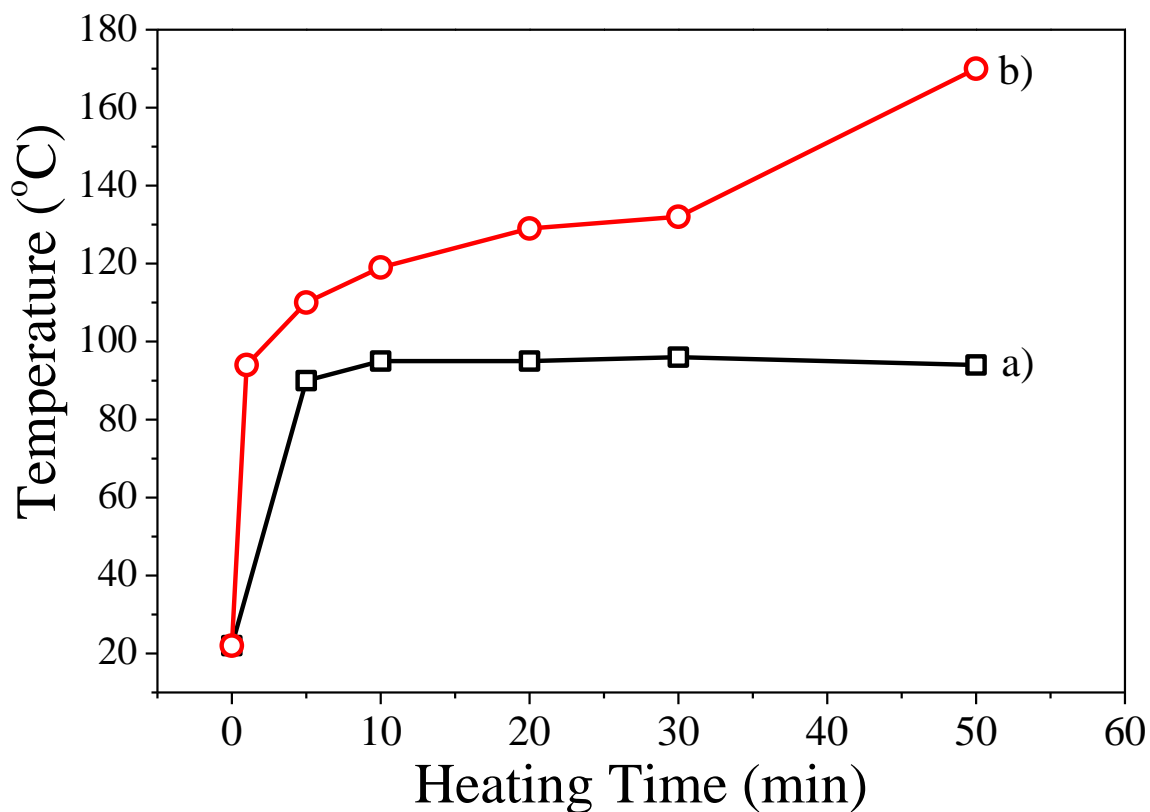


Figure 90 - a) Reaction mixture, residence time = 30 min, 10% power. b) Reaction mixture, residence time = 30 min, 20% power.

The Powder X-Ray Diffraction (PXRD) results for the system at 10% power are as follows:

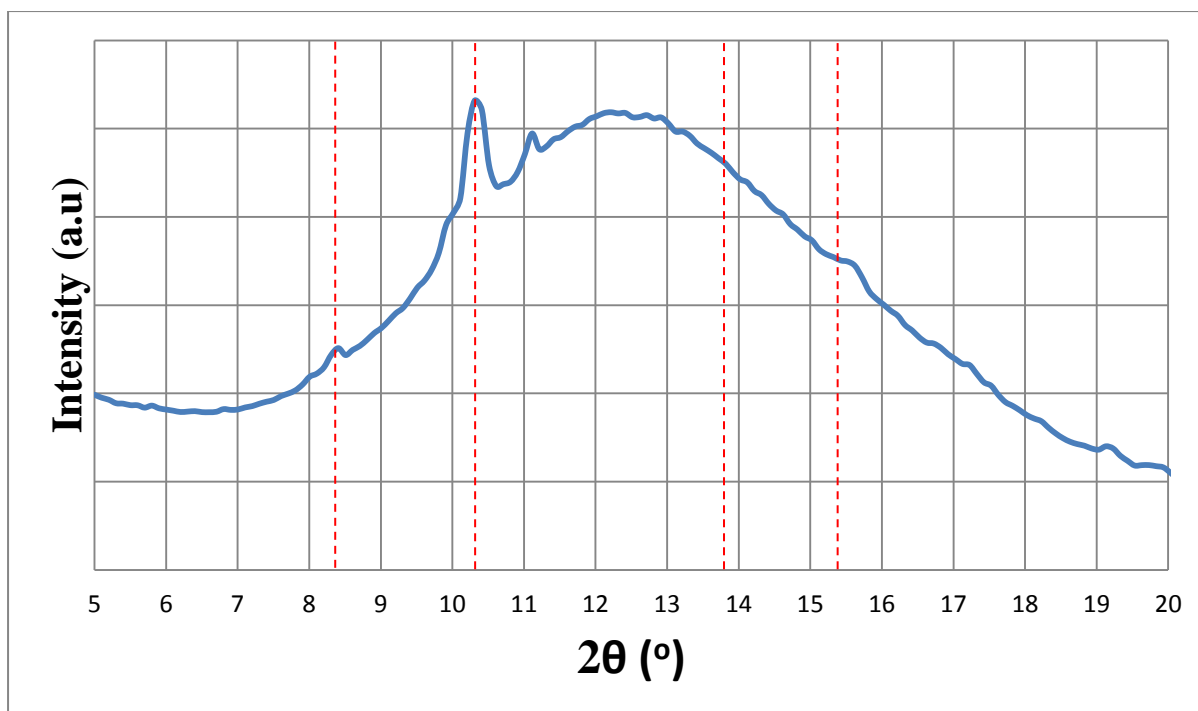


Figure 91 - PXRD Result showing no presence of MOF-5, reaction conditions were: Residence Time = 0.5 h, 10% power level.

The PXRD results show that MOF-5 is not formed at these conditions. MOF-5 being present would result in a number of known Bragg peaks being present at the angles marked by the red lines in Figure 91. The presence of the large broad Bragg peak is due to the polypropylene sample holder.

The most likely reason for the system to not produce MOF-5 is the temperature not being high enough in order for the reaction to occur. As a result, the system was repeated with the conditions identical except with the power level increased to 20% power.

This system produced a sample with the following PXRD pattern when operating at 20% power:

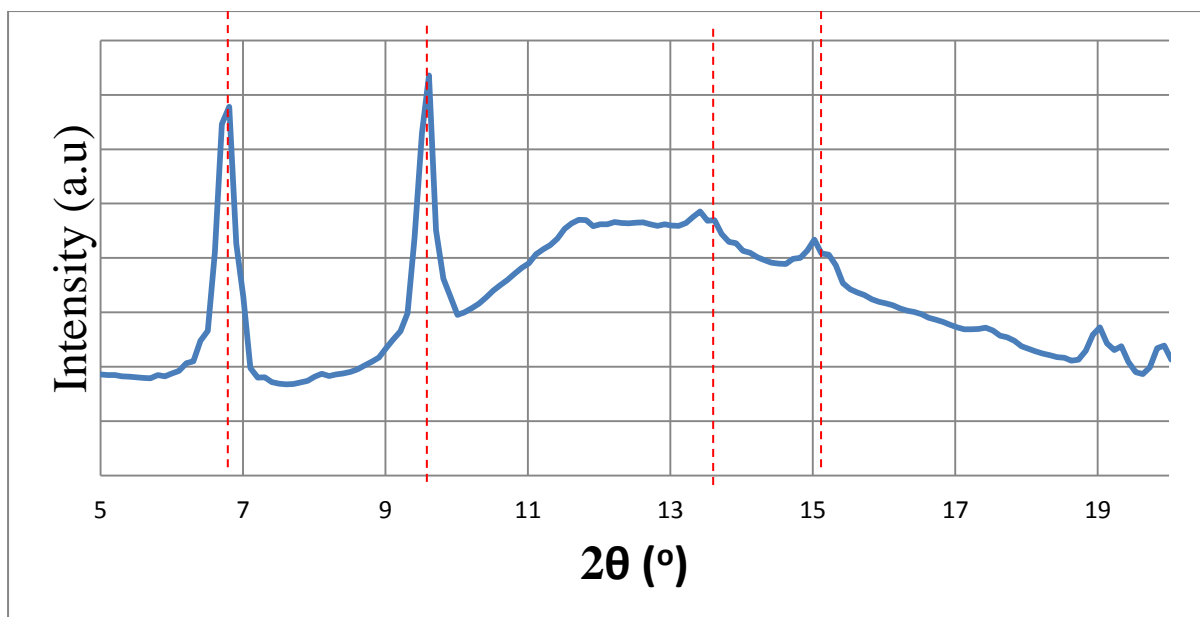


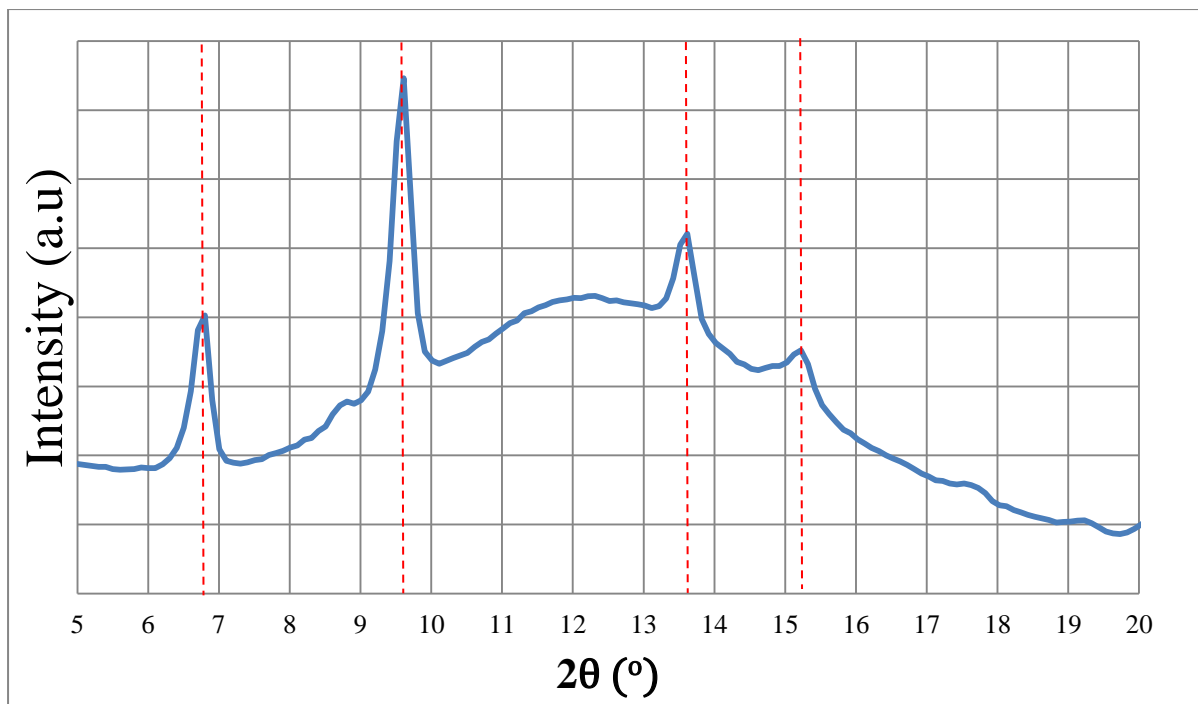
Figure 92 - PXRD Result showing no presence of MOF-5, reaction conditions were: Residence Time = 0.5 h, 20% power level

The PXRD confirms the production of MOF-5 due to the presence of Bragg peaks at the locations marked by the red lines. The phase purity is not completely MOF-5 as seen by the presence of Bragg peaks due to other crystalline materials. The large broad peak is due to the polypropylene holder.

This system however, eventually overheated and built up enough pressure to force one of the connections between the large bore tubing and the small bore tubing out.

As a result, with the sample that had already been heated to 95°C, the power level was increased to 20% to attempt to instigate the MOF-5 reaction. At the end of the 10% power section, no solids were seen in the reaction vessel. Between this time and the termination point, crystals began to form. The reaction was terminated due to consistent superheating.

The PXRD results for this sample are as follows:



The Bragg peaks of the sample match up with the dashed red lines indicating the Bragg peaks from MOF-5 showing the MOF-5 has formed in this case, with good crystallinity. Though some peak shouldering and small peaks not associated with the MOF-5 peaks are present this sample shows that MOF-5 of reasonable purity can be formed in this reactor type.

7.3 Microwave-assisted Batch Synthesis of HKUST-1

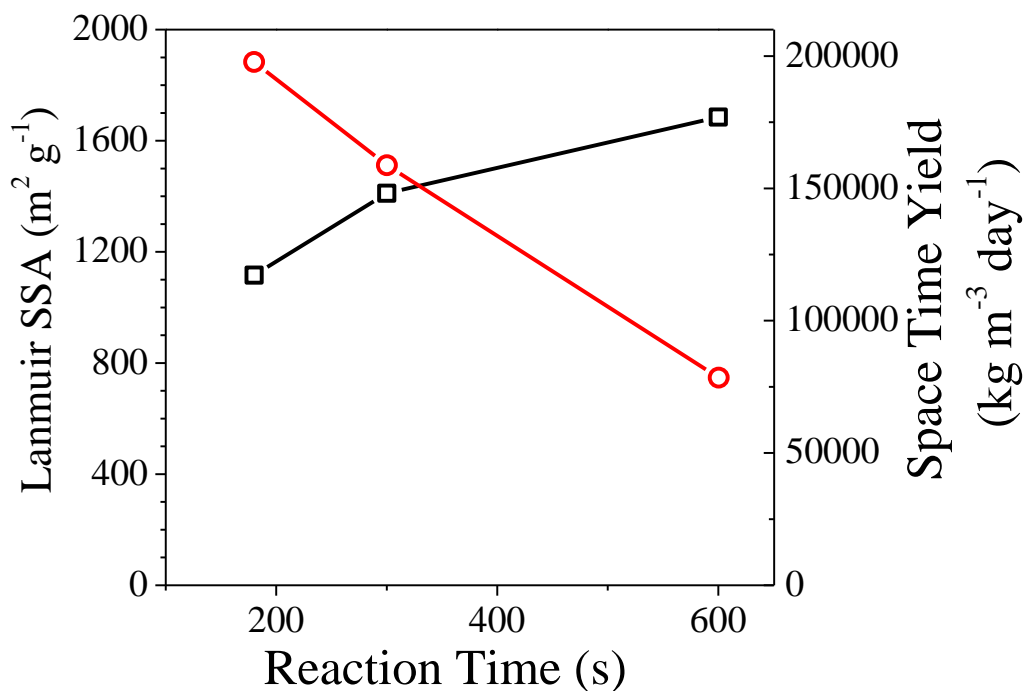


Figure 93 - Trends in surface area and space time yield. Squares indicate SSA, Circles represent STY.

Samples collected at 10% power with a reaction time of 180 seconds showed an average final solution temperature for these samples was 53°C. This system produced an average dry theoretical yield of 24%, which is comparable to the yield expected from the equivalent solvothermal system running at 60C for over 4 hours. However, the available surface area of these samples is reduced to an average Langmuir SSA of $1116 \pm 680 \text{ m}^2 \text{ g}^{-1}$ showing a very large variability in the output. The repetition of this experiment with longer reaction times of 300 and 600s showed slightly higher yields of 32 and 31% of theoretical. Increasing reaction time to 300s or 600s shows an increase in average Langmuir SSA, and also a reduction in the associated error with 180s giving a value of $1411 \pm 393 \text{ m}^2 \text{ g}^{-1}$ and $1685 \pm 299 \text{ m}^2 \text{ g}^{-1}$ for 300 and 600 s respectively. Due to the inherent “randomness” introduced by the variability of the electric field within a domestic microwave, this surface area increasing and the error on them decreasing is expected. Further, this suggests that while it may be possible to produce HKUST-1 in short times, it is likely to prove beneficial to compromise between reaction time and crystal quality.

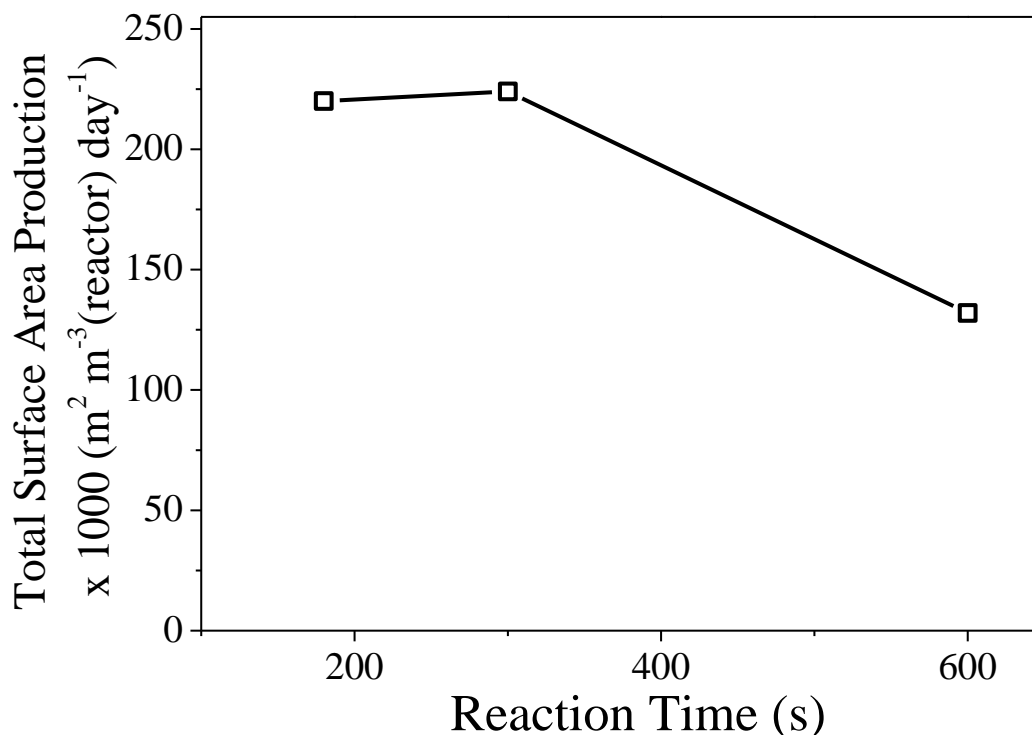


Figure 94 – Total surface area production of HKUST-1 using microwave heating with varying reaction time.

The total surface area produced (the space-time yield multiplied by the average surface area per unit mass) from each of these samples shows that running at 300s residence time provides the highest surface area output per cubic meter of reactor volume per day, despite having similar yields to the longer residence time and lower surface area as shown in Figure 93.

We then investigated how the system behaves when a greater heating rate was applied. For this we increased the operating power to 20% for 180s. When compared to samples heated for the same length of time at 10% power, we see almost identical average yields, with both conditions producing 24% yields. However, the larger difference when altering the heating rate is that the final temperature increased by a reasonably large margin ($\Delta T = 17\text{ }^{\circ}\text{C}$) which results in a significantly higher average surface area being produced – $1880 \pm 271\text{ m}^2\text{ g}^{-1}$, and featuring the lowest error of the samples analysed so far.

Finally, we looked at process intensification, repeating the running a sample at 10% power for 300s with the solutions at 3% solids and 9% solids. At 3% solids, an average yield of 32% was achieved.

Interestingly, this drops to 14% when increasing the reactant concentration by a factor of 3, which we believe to be related to the lack of direct mixing within the vessel during the reaction. The average surface area of the samples formed from the 9% solids solution is significantly higher than that formed from the 3% solids solution, increasing to $1664 \pm 595 \text{ m}^2 \text{ g}^{-1}$ from $1116 \pm 680 \text{ m}^2 \text{ g}^{-1}$. This is much unexpected as generally an increase in solids beyond a critical level will begin to reduce surface area of a MOF via the presence of unwanted ligand or other species trapped within the pores and other defects within the crystal structure. This effect has both been reported in literature and also appears to be true under conventional heating as was shown in Figure 95.

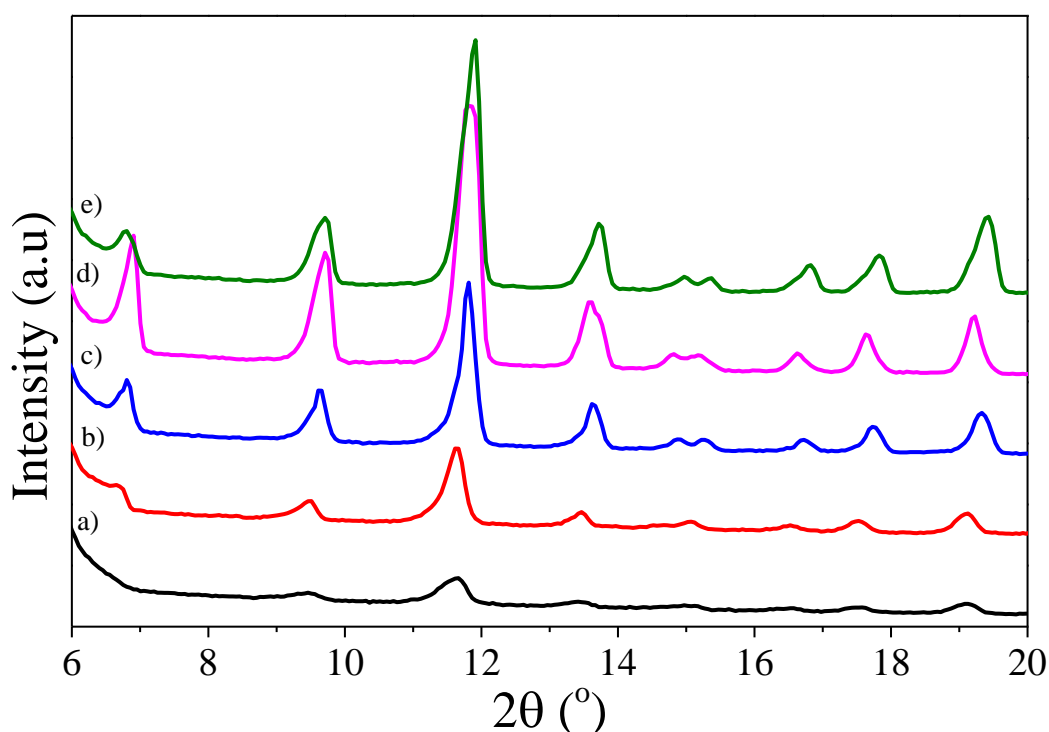


Figure 95 - Example PXRDs of the 5 conditions analysed here. Details given in form of [Power Level (%), Reaction Time (s), Solids (%)]. a) 10%, 180s, 3%. b) 10%, 300s, 3%. c) 10%, 600s, 3%. d) 20%, 180s, 3%. e) 10%, 300s, 9%.

PXRD in Figure 95 shows phase pure HKUST-1 forms in all cases, however the relative crystallinity of the sample marked a) is far poorer than the alternative samples with low intensity, wide Bragg peaks. Crystallinity appears to increase with reaction time (a), b) and c)) which also corresponds to an increase in surface area as described above. Figure 95d) shows the highest crystallinity of the 5 conditions analysed and also produced the highest average surface area.

7.4 Continuous Microwave Enhanced Synthesis of HKUST-1

Outputs from the single pass microwave system were analysed. The residence time was first set at 6 minutes, allowing the reaction mixture to be heated to a temperature of 45 ± 5 °C. Due to the inherent variability of a multimodal cavity and limited options for manipulating power input to the system, the temperature could not be controlled to a more fine degree.

This system was run at 3% solids using ethanol as the only solvent. Crystal output was analysed by PXRD, FT-IR and gas adsorption. Gas adsorption showed that the system produced HKUST-1 with an average surface area of 1930 ± 90 m² g⁻¹, similar to the surface areas found during the batch work and within the same range as continuous synthesis with conventional heating. The dry yield of crystals with these conditions is only 26%, however due to the very short residence time this still results in a STY of 2660 kg m⁻³ day⁻¹ as we found HKUST-1 to be formed in less than 7 minutes using the microwave technology compared to greater than 2.5 hours required for similar yields with the conventionally heated batch systems.

When swapping to the higher flow rate of 550 ml h⁻¹ and reducing the reactor volume to 2 ml from the 25ml previous used, HKUST-1 was still found to form with residence time 13 seconds, albeit with a relatively low yield of 27%. The temperature was found to average at 60 ± 5 °C for this system.

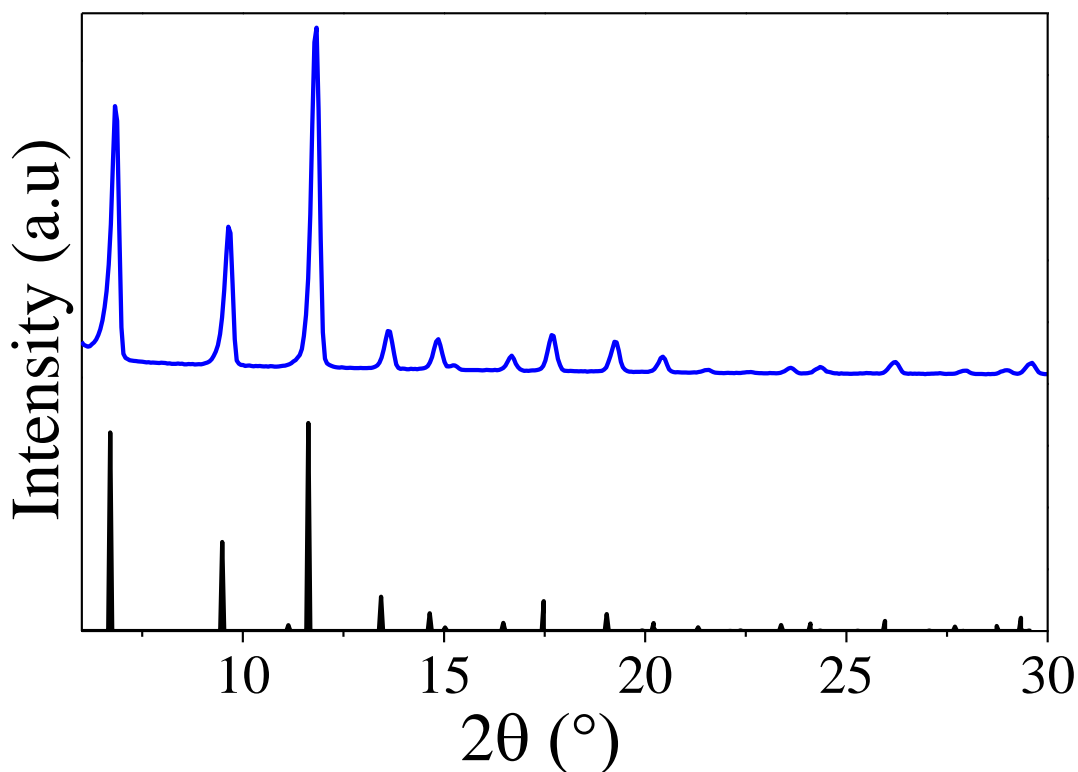


Figure 96 - Powder x-ray diffraction data for typical HKUST-1 formed using microwave heating with residence time of 13 seconds. Black line shows Bragg peak locations as generated by the crystallographic information for HKUST-1.

Figure 96 shows that HKUST-1 is formed in this short reaction time. The product has an average Langmuir Specific Surface area of $1550 \text{ m}^2 \text{ g}^{-1}$, suggesting that the rapid formation within the microwave system may cause quantities of metal or ligand to be retained within the pores. When increasing the concentration of the feed to 15% solids, HKUST-1 was still formed, though the Langmuir surface area drops to $575 \text{ m}^2 \text{ g}^{-1}$. The yields of both products are approximately 30%, resulting in STY of $\sim 80,000$ and $\sim 400,000 \text{ kg m}^{-3} \text{ day}^{-1}$ for the 3% and 15% samples respectively. Due to the reduction in residence time, this allows the STY to be greatly increased despite suffering from lower yields overall.

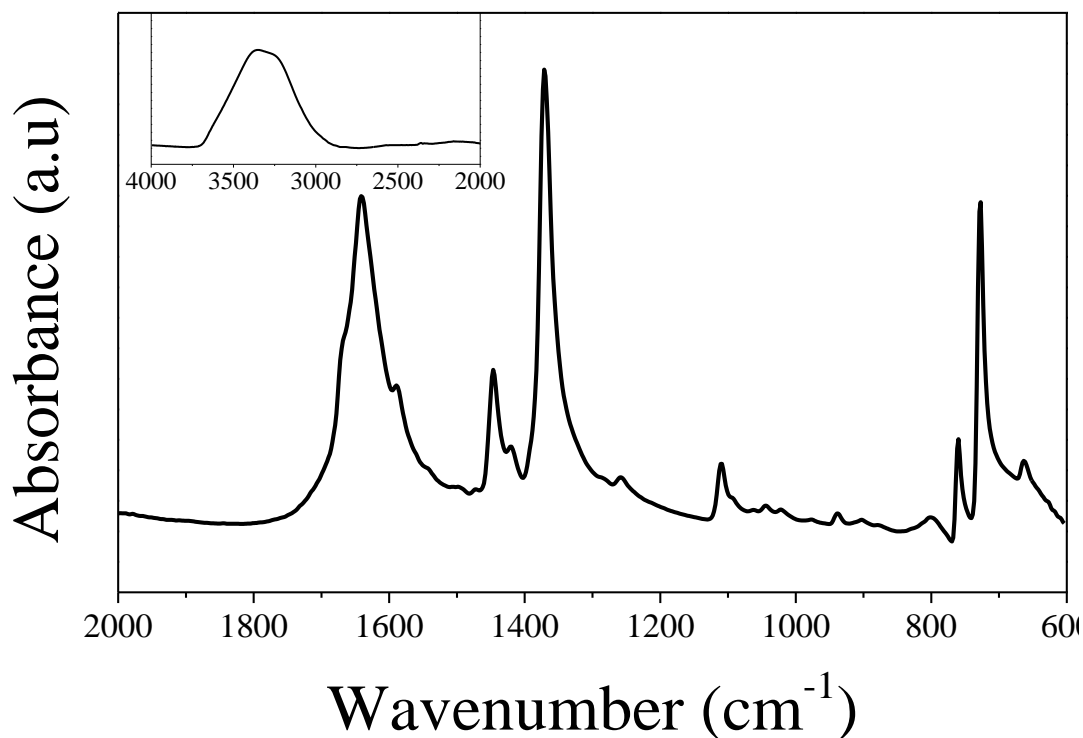


Figure 97 - FT-IR spectra for typical HKUST-1 sample, produced using the continuous microwave heated system

Figure 97 shows the FT-IR spectra for a typical HKUST-1 sample. As HKUST-1 will quickly absorb water from the atmosphere, a large peak is present in the 3000-3600 cm^{-1} region which is shown only in the inset image above and has generally otherwise been excluded from other FT-IR spectra shown. We are unable to see the vibrational mode involving the Copper centre which occurs at 493cm^{-1} ,¹¹⁵ out with the range of our equipment. We see peaks at 1645, 1616, 1554, 1455, 1375 in good agreement with published sources^{85, 115}.

Chapter 8 – Economical Potential of Scale Up of MOF synthesis

In this section we consider if the processes developed in previous chapters are likely to be applicable at large scale with the ability to compete with other materials both in terms of production at high capacity and economic viability. At this point, considerably more information is required in order to accurately determine the feasibility of these products. The market for MOFs is currently rather unclear, due to the lack of large scale availability, and the constant progression of MOF chemistry resulting in a landscape where the best material for an application can become out-dated rather quickly. Thusly, this serves only as a very rough estimate. In order to determine the costs with more accuracy, with a deeper understanding of the kinetics and issues affecting synthesis the full detailed design of the MOF-5 and HKUST-1 process would need to be undertaken in conjunction. It is possible that without this complex understanding both experimentally and from modelling, the economic viability would be inaccurate due to the changes in many factors when considering scale up. Further the separation and activation processes required for the product to meet sale criteria would need to be considered and could result in a large change in the break-even price of the materials due to the energy costs involved. At this stage, we simply complete basic estimations of the costs of these products and the ability to produce at scale in order to determine if further work is likely to be beneficial in the longer term.

8.1 Initial Study into Feasibility of MOF-5 Manufacturing

For the continuous synthesis of MOF-5, we elected to base our results on the continuous syntheses experiments carried out earlier in this project.

Solvent	% Solids	STY (kg m ⁻³ day ⁻¹)	Average Langmuir SSA (m ² g ⁻¹)	Surface Area Production x 10 ⁶ (m ² m ⁻³ _{reactor} day ⁻¹)
DEF	1	50	2302	12
DEF	5	196	759	14

Chapter 8 – Feasibility of scale up of MOF synthesis

DEF	10	504	525	26
DMF	1	43	992	4.3
DMF	5	444	671	20

We are only considering reaction running with excess zinc, and all of them have residence time of 4 hours. Firstly, we consider the solvent cost here. DMF is a widely available bulk chemical and can be purchased at large scales that would be required for industrial use. DMF costs approximately £30/litre at large scales. DEF is considered a lab grade chemical and is generally unavailable at large scales and so a price can only be found for small scales which are obviously more expensive than large scale bulk chemicals and has been approximated as £300/litre.

Given these costs, we can estimate the price required for 1kg of MOF to be formed, excluding energy or capital costs to be as shown in Table 19.

Table 19 - Estimated cost per kg for each selected syntheses

Solvent	% Solids	Solvent Costs (£/kg)	Average Langmuir SSA ($\text{m}^2 \text{g}^{-1}$)	Cost per m^2 surface area produced	Relative Cost
DEF	1	35710	2302	0.0155	100.00%
DEF	5	9380	759	0.0124	79.61%
DEF	10	3570	525	0.0068	43.85%
DMF	1	4170	992	0.0042	27.07%
DMF	5	810	671	0.0012	7.79%

The most expensive product, formed using DEF solvent at 1% solids would have to be sold for a minimum of £35710 per kg in order to cover raw material costs alone. While DMF solvent can be used at 5% solids to bring this cost down to approximately £800 per kg, it is considered unlikely that the product would hold sufficient value at such low surface areas. Due to issues with procuring large

scale quantities of DEF, and the issue of solvent breakdown and the storage and disposal of large quantities of amine species, MOF-5 synthesis is probably not viable at larger scale.

8.2 Initial Study into Feasibility of HKUST-1

Synthetic routes for solvothermal synthesis make use of 3 main solvents, in differing amounts from a single pure solvent to a combination of all of them. The three solvents used are dimethylformamide (DMF), water and ethanol. A room temperature synthesis using water as the only solvent has been published, however we had severe issues in attempting to replicate this process, even when subjected to heating. Literature suggests that the two main solvent mixtures used are an equal mixture of DMF/water/ethanol or simply to use pure ethanol as the only solvent. DMF appears to allow decomposition of the solvent to form an amine which increases the rate of formation of the MOF, but DMF is expensive compared to water and ethanol. Water serves the purpose of being a cheap bulk solvent in order to reduce the overall concentration without adding too much cost. After a point, the presence of water begins to affect the system. Ethanol is a suitable solvent and is cheaper than DMF and much less hazardous, however the kinetics are rather slow. DMF/water/ethanol appears to have considerably faster kinetics, likely due to the breakdown of the DMF to form amine species. However, it also appears that ethanol alone forms a material with higher surface area. In order to determine which process would likely be the most viable, we must consider a number of metrics. For instance, the faster kinetics of the DMF/water/ethanol based product allow for higher yields, which may be more desirable than a higher surface area product formed by ethanol alone with a low yield. In order to fully compare which route would be most effective, we undertook several experiments and produced the shown as Table 16.

It is important to note also that HKUST-1 is currently produced at medium scale for sale as a lab chemical by Sigma Aldrich. This material is produced using an electrochemical route and has a surface area of around $1650\text{m}^2\text{ g}^{-1}$. As of July 2014, the approximate price per kg of this material is £12500, though this is based on a 500g package size and is, in effect, a high grade laboratory material. In order to be economically viable for use at the scales likely required for industrial use, we would aim to bring this price down by around an order of magnitude at minimum.

8.2.1 Provisional Material Balances, Energy Balances and Economic Analysis for HKUST-1

To begin, we set the total HKUST-1 output to be 100 tonnes per year (~275kg/day). This serves as a basic overview of the process economics and is not in depth, therefore the values all scale linearly. The methodology used is an ethanol only synthesis running at reflux temperatures. The conversion of this process is relatively low (~25%) and so we will consider two situations, one with a recycle loop and one without. It is very unlikely the process would be carried out without recycle, given the economic potential in recycling with this low a conversion. With the %solids also set at 3%, we can therefore determine the total volume of ethanol that must be passed through the reactor system per year.

$$\text{Ethanol required} = 3.33 * 10^6 \text{ litres} = 2365 \text{ tonnes}$$

The number of moles of HKUST-1 produced each year is given by:

$$HKUST-1_{mols} = \frac{\text{molecular weight HKUST-1}}{HKUST-1_{mass}} = 1.985 * 10^6 \text{ mols}$$

From this we can calculate the number of mols and masses of each of the precursor species required. However, at this point we must also take into account the conversion is only 25%, and so the feeds must be scaled up to the point they will produce 100 tonnes per year.

Table 20 - Required Consumption of reactants and solvents over 1 year.

	mols	kg
Copper Salt	19.9 x 10 ⁶	462531
Ethanol	5.1 x 10 ⁶	2363333
Trimesic Acid	1.3 x 10 ⁶	278048

At this point, we can calculate the raw materials costs for the system.

Chapter 8 – Feasibility of scale up of MOF synthesis

Table 21 - Raw material costs of reactants and solvents over 1 year.

Component	Cost Per kg (£/kg)	Cost Per Year (£)	Fractional of total raw material Cost
Copper Salt	114	52.7×10^6	0.319
Ethanol	0.38	0.89×10^6	0.0054
Trimesic Acid	400	1.11×10^8	0.674

Given the total output of HKUST-1 set at $100 \text{ tonne year}^{-1}$, we can calculate the total material costs and determine initially the approximate sale value of HKUST-1 that will be required in order to break even. At this point, the total material cost is approximately £165 million. At this price point, the HKUST-1 would need to be sold for approximately £1650 per kg. It is important to reiterate that this value represents covering costs when the system has no recycling. At this price point, the sale value is still considerably below the value Sigma Aldrich charge for their HKUST-1.

The energy requirement of the system can be summarised by considering two factors. Heating the ethanol for the system (this is the major heat sink of the system) and the energy required to form the HKUST-1 crystals. The heat of formation of HKUST-1, taken from Bhunia *et al*²⁸, is 158.1 kJ/mol or 0.261 kJ/g. Therefore the total energy required to form the MOF is 26.15GJ per year. The energy required to heat the solution from 10°C to 80°C must also be considered. 10°C is set as the ambient temperature here as this allows storage to be below the flashpoint of ethanol. Ethanol has a heat capacity of 111.5 J/ mol K. Therefore the total energy required to heat the ethanol is 400.13GJ. Based on an energy cost of 12p per kilowatt hour equal to 0.0333 £ per MJ, the total energy input required would cost £164,000 per year. The energy cost is minimal compared to the raw material cost and so the break-even price remains £1650 per kg.

Beyond this, we can see that this system will output almost 100% of the ethanol input (some losses due to ethanol in the structure and general losses). However, most of the copper salt and trimesic acid

Chapter 8 – Feasibility of scale up of MOF synthesis

will also be left unreacted. Assuming a constant conversion at steady state, the reactor will output the following:

Table 22 - Level of recycling anticipated for lowest cost of raw materials.

Component	Kg/yr	Total Recycled
HKUST-1	100,000	0
Ethanol	236,000	236,000
Copper Salt	115,000	0
Trimesic Acid	69,500	0

Although a full, complete provisional design is beyond the scope of this project, it is possible to estimate the capital costs in order to further approximate if the overall project will be economically viable at large scale. The cost of unit operations can be estimated as 3 core units, the MOF reaction vessel, the separation of HKUST-1 from solution and the activation of the material. Based on the scale, we can anticipate the following:

Table 23 - Capital Cost Estimations

Cost	Number of Units	Per Unit (x 10 ⁶ £)	Total (x 10 ⁶ £)
Unit operations	3	2	6
Pumps Required	8	0.25	2
Storage Vessels	3	1	3
Heat Exchangers	3	0.25	0.75

Therefore an approximate value of £11.75 million on unit operations, at best case scenario is estimated from data given⁵³.

Chapter 8 – Feasibility of scale up of MOF synthesis

Table 24 - Factors for estimation of total operating costs

Plant Costs	Estimated Costs (x10⁶ £)	Notes
Total Capital Cost with safety factor	1.47	25% added on to cover errors in estimation
Working Capital	0.29	20% (upper limit)
Raw Material Costs	164.9	With no recycle
Raw Material Costs	41	With recycle of ethanol
Maintenance	0.22	15% of Capital Costs
Staffing	2.47	15% of Raw Materials Cost
Staff Needs and Overheads	2.47	Equal to Staffing Costs
Energy Costs	0.003	Double the energy estimated for the reaction
Fixed Costs	2.47	15% of Raw Material Costs
Total Operating Cost	7.64	

Thus we can calculate the net present value (NPV) of the plant based on the above approximations. Here we consider recycle and non-recycle loops in order to evaluate the importance of recycling further. The NPV allows us to evaluate project costs spanning multiple years in order to determine the quality of an investment.

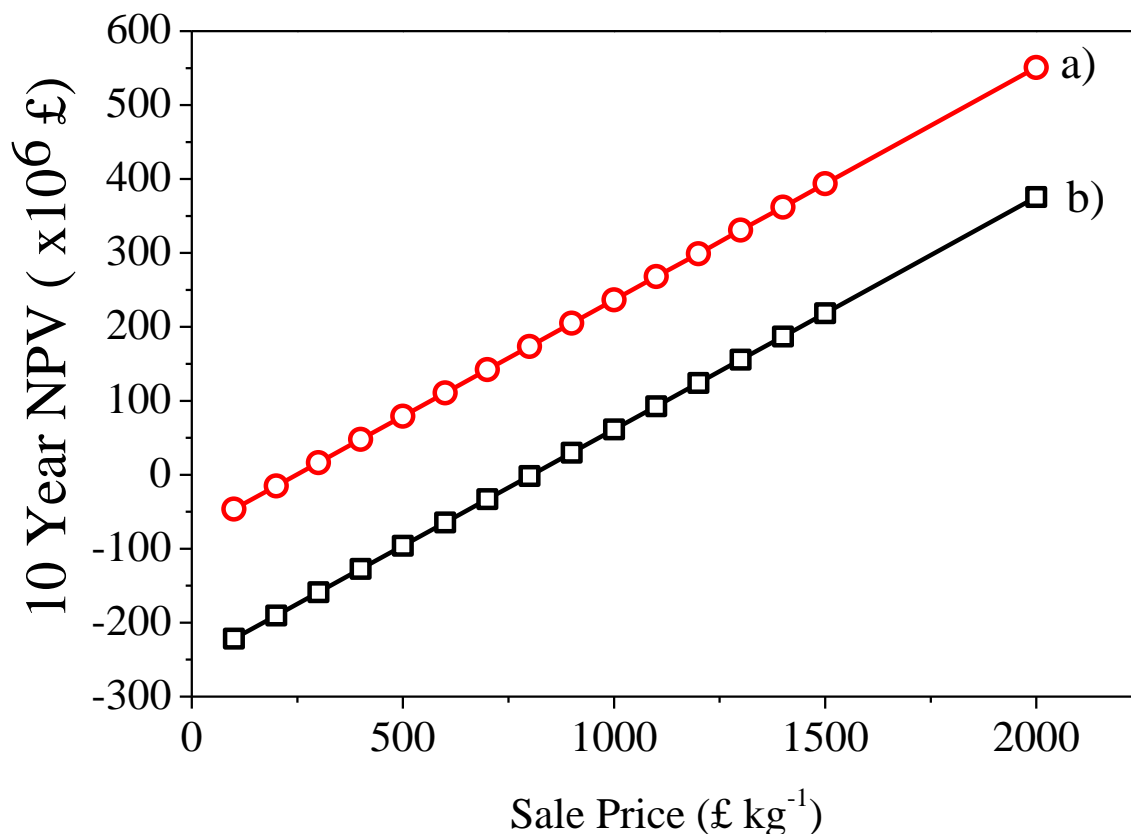


Figure 98 - Net Present Value over 10 years for a) HKUST-1 with ethanol recycled and b) no recycle. Recycling ethanol shows significant benefit with a positive NPV within 3 years, compared to 9 years for the system without recycle.

NPV analyses show that when operating with a complete recycle stream, the product will break even at a sale price above £250/kg, whereas without recycle the material would need to be sold for approximately £750/kg in order to show a positive NPV over the 10 year analysis period considered here. As this evaluation only considers two of the largest on-going costs and estimates a number of other costs the plant would be required to pay, the actual break-even point will likely lie between the £250/kg and £750/kg values. As both projects show positive NPV over a long enough timescale, this suggests that if HKUST-1 is able to be produced at large enough scale and the market consumption is sufficient, HKUST-1 synthesis at large scale may be a lucrative business.

Chapter 9 – Conclusions

9.1 Conclusions concerning MOF-5 formation with conventional heating

In conclusion, MOF-5 synthesis within the temperatures ranges and reactant compositions investigated here appears to invariably involve formation of metastable intermediate solids phases as a precursor to MOF-5 formations. Longer reaction times shown MOF-5 will form from these intermediate phases given continued treatment, as shown by analysis of the solid phases formed using PXRD and FT-IR analyses. The reaction pathways over the 110-140 °C window also shows a number of interesting outcomes. At 140 °C, under stirred conditions, a single intermediate phase, isostructural to MOF-69c(desolv) is shown to form initially before transitioning into pure phase MOF-5 in by 1.5 h. While the pathways for unstirred reactions at 140 °C and for both stirred and unstirred reactions at 130 °C show similar reaction pathways, operating below this temperature we see a significant change.

At 120 °C and below, we see evidence that stirring of the syntheses adversely affected the formation of MOF-5, with metastable intermediate phase(s) persisting for considerably longer time periods relative to operating at 130 °C and above, with MOF-5 only being formed at longer times. This suggests that operating at a temperature of ≥ 130 °C will present a benefit when considering scale up and continuous manufacturing processes.

Process intensification attempts showed that MOF-5 can be formed at higher concentrations than previously reported in the literature surveyed. This allows MOF-5 to be formed using considerably less solvent per gram of product and showing improved kinetics. However, this, as expected, shows a drop off in available surface area of the final product due to interpenetration of the structure or the presence of unreacted metal or ligand within the pores. The drop off in surface area is reduced by an approximate factor of 5 with an approximate increase in yield of a factor of 10, therefore showing an overall increase in the total surface area production of the system.

Chapter 9 – Conclusions and Future Work

Varying the metal:ligand ratio from excess metal (3:1) to stoichiometric quantities (1.33:1) shows no obvious alteration to the yield of MOF-5, but does result in a considerable reduction of the surface area of the product formed, with SSAs of 2516 and 469 m² g⁻¹ for 3:1 and 1.33:1 respectively.

When considering continuous solvothermal processes for production of MOF-5, we have shown that MOF-5 can be formed with high yields and high surface area, one of the key quality factors of the material. The system was optimised by systematic variation of key process parameters as well as forming an understanding of underlying process chemistry. Further, the number of intermediate phases seen during synthesis is reduced relative to the equivalent batch process, highlighting another benefit of continuous MOF-5 production.

As DMF is a considerably cheaper solvent, we compared the quality of MOF-5 formed using DMF to that formed using DEF. In order to understand the variations in product quality that occur with increased solid concentration, MOF-5 was synthesised at various reactant concentrations leading to a range of 1-10% solids with DEF and 1-5% solids using DMF, as MOF-5 was not found to form at 10% solids in DMF solvent. The highest surface area MOF-5 was formed using a 3:1 M:L ratio using DEF as a solvent. The equivalent product formed with DMF as the solvent had surface area around 40% of the DEF synthesised material. Increasing solids concentrations showed comparable results for the DEF and DMF batch systems with a significant decrease in surface area. DMF solvent systems showed similar surface areas at 1-3% before significantly reducing when operating at 5% solids.

The process intensification method used also requires more work in order to determine its long term viability. Though we have shown that MOF-5 will form when the throughput is doubled after reaching steady state, it is unclear if this would continue long term as the experiment within only continues for a single residence time which may be insufficient to show the system reverting to the conditions prior to steady state which do not produce MOF-5.

For increased viability of the system for large scale use, the STY of the system should be optimized. The start-up phase lasts only about one residence time after which the system can reach steady state. We have shown here that it is possible to produce a continuous reaction system for producing MOF-5.

We have optimised the system and shown that high purity, high surface area MOF-5 can be produced but the STY of a system would be limited to approximately $50 \text{ kg/m}^3 \cdot \text{day}$. We have shown methods for intensification allowing the STY of the system can be significantly increased to a value close to $1000 \text{ kg/m}^3 \cdot \text{day}$, however, this also results in changes to the properties of the system, such as reducing surface area, which may affect the economic viability of a potential scale-up of this system.

9.2 Conclusions concerning MOF-5 Formation with Microwave Heating

We have shown that MOF-5 can be formed using microwave heating techniques. However, the long duration required resulted in significant issues with temperature control, leading to cessation of study of this system. However, this type of reactor system will produce MOF-5 using microwave energy as the heating source with the reaction time required around 1hr, compared to approx. 4hr for a conventionally heated system. Further characterisation and optimisation of this system was not possible due to the temperature control issues, though microwave heating still appears to be one of the important factors to be considered for improving STY of the MOF-5 reaction, as use of this heating technique should allow for MOF-5 to be formed considerably faster. However, without complete characterisation and optimisation of the quality of material formed, it is unclear if this reaction system will show improvement on the continuous system using conventional heating techniques.

9.3 HKUST-1 Conclusions

It is interesting to note that MOF-5 was always observed to transition through a metastable crystalline intermediate phase before producing MOF-5, while HKUST-1 is the only product observed in any outputs from these reactions, suggesting that the formation pathway for HKUST-1 is much simpler, with the Cu-Cu dimer forming and then bonding to the ligand without any intermediate phases forming between. We were able to find evidence of the presence of HKUST-1 crystals essentially immediately after mixing metal and ligand solutions, suggesting either HKUST-1 does not transition through metastable intermediates or that the intermediates are only present for a minute period of time.

Chapter 9 – Conclusions and Future Work

Further we have shown that HKUST-1 can be produced solvothermally in a continuous reaction vessel in both CSTR and tubular reactor forms and shown intensification of these reactors which reduces the Langmuir SSA of the materials but allows far higher production per unit volume.

In conclusion, we established a scalable procedure for producing high quality HKUST-1 in a batch process by in depth analysis of yields and how desirable properties, such as surface area, are affected.

We have shown that a conventionally heated continuous reaction system can be used to produce HKUST-1 in a relatively short period of time while maintaining surface areas in $>2000 \text{ m}^2 \text{ g}^{-1}$, increasing the potential output by a factor of approximately 100 times from a batch STY of $1.4 \text{ kg m}^{-3} \text{ day}^{-1}$ to $172 \text{ kg m}^{-3} \text{ day}^{-1}$. This system was then optimised and the properties, yields and STY of materials produced at higher concentrations were considered. There appears to be a compromise between solid output and surface area of the MOF as higher concentrations of precursors resulted in a reduction of surface area available within the MOF, while producing more MOF per unit volume of reactor. This should allow potential scale up to be able to consider an operating point that allows a suitable compromise between steady state output and surface area. We then showed that microwave heating can be used to improve the yield output of this system while maintain a surface area similar to the conventionally heated process with a STY of $2700 \text{ kg m}^{-3} \text{ day}^{-1}$ and average Langmuir surface area of $1930 \text{ m}^2 \text{ g}^{-1}$ and that through microwave heating applications space time yields can be increased orders of magnitude.

Table 25 - Comparison of collected data for HKUST-1 Synthesis. All systems barring the commercially available product formed using ethanol as the only solvent. Conventionally heated samples heated to 79 °C, Microwave system with 7 min residence time heated to 45 °C, 13 s residence time heated to 35 °C.

System	% Solids	Yield		Langmuir	Surface area
		% _{theoretical} (dry basis)	STY ($\text{kg m}^{-3} \text{ day}^{-1}$)	Surface Area ($\text{m}^2 \text{ g}^{-1}$)	production ($\text{m}^2 \text{ m}^{-3}_{(\text{reactor})} \text{ day}^{-1}$)
Batch	3	20-25	1.4	2000 ± 200	0.28×10^6
	15	55-80	11.5	1090 ± 110	6.9×10^6
Continuous	3	35	172	1950 ± 100	335.4×10^6
	9	58	874	1046 ± 120	914×10^6

Chapter 9 – Conclusions and Future Work

	15	60	1479	910 ± 250	1347 x 10 ⁶
Microwave System (7 min)	3	20-30	2700	1930 ± 90	5211 x 10 ⁶
Microwave System (13 seconds)	3	20-25	~80,000	1530 ± 120	122400 x 10 ⁶
	15	10-15	~400,000	600 ± 100	240000 x 10 ⁶
Commercially Available Product*	-	-	225	1680	378 x 10 ⁶

* Basolite C300, produced by BASF

In conclusion, we established a scalable procedure for producing high quality HKUST-1 in a batch process by in depth analysis of yields and how desirable properties, such as surface area, are affected. We have shown that a conventionally heated continuous reaction system can be used to produce HKUST-1 in a relatively short period of time while maintaining surface areas in >2000 m² g⁻¹, increasing the potential output by a factor of approximately 100 times from a batch STY of 1.4 kg m⁻³ day⁻¹ to 172 kg m⁻³ day⁻¹. This system was then optimised and the properties, yields and STY of materials produced at higher concentrations were considered. There appears to be a compromise between solid output and surface area of the MOF as higher concentrations of precursors resulted in a reduction of surface area available within the MOF, while producing more MOF per unit volume of reactor. This should allow potential scale up to be able to consider an operating point that allows a suitable compromise between steady state output and surface area. We then showed that microwave heating can be used to improve the yield output of this system while maintain a surface area similar to the conventionally heated process with a STY of 2700 kg m⁻³ day⁻¹ and average Langmuir surface area of 1930 m² g⁻¹ and that through microwave heating applications space time yields can be increased orders of magnitude.

9.4 Comparison of MOF-5 and HKUST-1

One of the key differences in the outputs of the two MOFs is the timeframe required to form the MOF. At temperatures of 140°C, it takes >1.5h in order to form the structure of MOF-5. For HKUST-1, operating at 79°C the structure begins to form almost instantly. This is likely due to the fundamental differences in the metal cation required to form these MOFs. HKUST-1 requires the formation of Cu-Cu dimer, whereas MOF-5 requires the formation of the considerably more complex Zn_4O^{6+} cation, which appears to be the rate limiting step as several complexes that form previous to this feature carboxylate-metal bonding to zinc hydroxide and zinc complexes.

The requirement to heat for longer and traverse through this region of metastable states likely limits the maximum rate that MOF-5 can be formed at, and therefore it is likely that the maximum STY of MOF-5 will be lower than the equivalent for HKUST-1. This also impacts the ability of microwaves to be used to form MOF-5. Due to the lack of true fine control on the applied power to the microwave system, the extended timeframes required with the MOF-5 system increase the likelihood of the system leaving its stable zone and overheating or causing significant pressure build up.

While both materials are archetypal MOFs, the solvents required for MOF-5 formation also have issues with degradation, recycling and disposal, whereas the HKUST-1 system can be used with only ethanol which does not undergo any breakdown to form the MOF. HKUST-1 is also considerably easier to work with due to the fact it does not undergo an irreversible reaction with water. HKUST-1 takes in water by physisorption only and so the material can be easily regenerated, whereas MOF-5 undergoes structural changes when water is adsorbed and requires a considerably more complex process to regenerate it, as seen in Figure 23.

9.5 Future Work

Future work concerning this project can be considered on two main fronts. While we have shown the ability to produce two archetypal MOFs using continuous reactor systems at 100 mL scale, further testing at at least litre scale would add value to the project. In order to truly scale up, the MOF systems would likely need to be accurately modelled which would also require accurate data

Chapter 9 – Conclusions and Future Work

collection on the system at small scales in order to fully understand the implications of scale up. Data particularly regarding the kinetics of MOFs is challenging, especially for MOFs that undergo multiple phase transitions between metastable intermediate crystalline materials which also pose a challenge in isolation and identification. Further, issues such as mixing would need to be considered and the potential effect in having to increase rotation speed or having to alter impeller shape and size in order to mix fully at large scale represent potential issues. After this, a deeper, more detailed design of a potential MOF production facility would be required in order to determine the potential economic viability of large scale production of MOFs. Further, it may also be of interest to determine the potential transferability of the data collected here. MOF-5 and HKUST-1 do not necessarily represent ideal MOFs to produce, but serve instead as model systems for determining various process variables of importance and showing that continuous MOF production is viable. To fully scale up the MOF-5 process, a more complete understanding of the kinetics and thermodynamics of the process would need to be completed. By marrying a more in-depth consideration of the products formed, as well as attempting to isolate and identify the intermediate stages formed using both experimental and simulation techniques, the process can be more completely understood. This will affect the viability of the MOF for large scale production and may also allow insights that can increase the space time yield without the significant penalties to the surface area shown here. A potential further benefit would be if there is a significant overlap in behaviour of MOF-5 to other MOFs using the Zn_4O cation and ligands with carboxylate functional groups, which would represent a cross over with a large number of MOFs.

With respect to microwave enhanced syntheses of MOFs, domestic microwaves allow for inexpensive access to microwave technology in the laboratory, but suffer from variability in the electric field resulting in temperature profiles varying significantly between repetitions of experiments. In terms of microwave based synthesis of MOFs, although promise has been shown for HKUST-1 the current state of technology limits progress in this area. The use of domestic microwave allows a relatively large cavity to be heated and can be simply modified to allow continuous flow system to be operated within it. However, the domestic microwave lacks the ability to control the temperature of the system to a fine degree, which would be required if this system was considered as viable for scale up.

Chapter 9 – Conclusions and Future Work

Tracking temperature via a method like IR, and the ability to rapidly control the applied power of the microwave system in order to maintain and control the temperature of the material. In order to fully evaluate the system the microwave field would need to be more homogenous, which is obtainable when considering specially designed equipment. Continuous flow reactors with microwave heating capabilities exist but are expensive, though it is likely that the benefits of microwaves for MOF synthesis we have shown here could be significantly improved upon with this technology.

References

1. Farha, O. K.; Eryazici, I.; Jeong, N. C.; Hauser, B. G.; Wilmer, C. E.; Sarjeant, A. A.; Snurr, R. Q.; Nguyen, S. T.; Yazaydin, A. Ö.; Hupp, J. T., Metal–Organic Framework Materials with Ultrahigh Surface Areas: Is the Sky the Limit? *Journal of the American Chemical Society* **2012**, *134* (36), 15016-15021.
2. Peralta, D.; Chaplais, G.; Simon-Masseron, A.; Barthelet, K.; Chizallet, C.; Quoineaud, A. A.; Pirngruber, G. D., Comparison of the Behavior of Metal–Organic Frameworks and Zeolites for Hydrocarbon Separations. *Journal of the American Chemical Society* **2012**, *134* (19), 8115-8126.
3. Wang, S. Y.; Yang, Q. Y.; Zhong, C. L., Adsorption and separation of binary mixtures in a metal-organic framework Cu-BTC: A computational study. *Sep. Purif. Technol.* **2008**, *60* (1), 30-35.
4. Xiao, J. S.; Hu, M.; Benard, P.; Chahine, R., Simulation of hydrogen storage tank packed with metal-organic framework. *Int. J. Hydrog. Energy* **2013**, *38* (29), 13000-13010.
5. Silva, B.; Solomon, I.; Ribeiro, A. M.; Lee, U. H.; Hwang, Y. K.; Chang, J. S.; Loureiro, J. M.; Rodrigues, A. E., H-2 purification by pressure swing adsorption using CuBTC. *Sep. Purif. Technol.* **2013**, *118*, 744-756.
6. DeCoste, J. B.; Peterson, G. W., Metal-Organic Frameworks for Air Purification of Toxic Chemicals. *Chem. Rev.* **2014**, *114* (11), 5695-5727.
7. Subject Index. In *Adsorption by Powders and Porous Solids*, Rouquerol, F.; Rouquerol, J.; Sing, K., Eds. Academic Press: London, 1999; pp 460-467.
8. Rouquerol, J.; Avnir, D.; Fairbridge, C. W.; Everett, D. H.; Haynes, J. M.; Pernicone, N.; Ramsay, J. D. F.; Sing, K. S. W.; Unger, K. K., Recommendations for the characterization of porous solids (Technical Report). In *Pure and Applied Chemistry*, 1994; Vol. 66, p 1739.
9. Chae, H. K.; Siberio-Perez, D. Y.; Kim, J.; Go, Y.; Eddaoudi, M.; Matzger, A. J.; O'Keeffe, M.; Yaghi, O. M., A route to high surface area, porosity and inclusion of large molecules in crystals. *Nature* **2004**, *427* (6974), 523-527.
10. Kresge, C. T.; Leonowicz, M. E.; Roth, W. J.; Vartuli, J. C.; Beck, J. S., Ordered mesoporous molecular sieves synthesized by a liquid-crystal template mechanism. *Nature* **1992**, *359* (6397), 710-712.
11. Nijkamp, M. G.; Raaymakers, J.; van Dillen, A. J.; de Jong, K. P., Hydrogen storage using physisorption - materials demands. *Appl. Phys. A-Mater. Sci. Process.* **2001**, *72* (5), 619-623.
12. Aitken, R. J.; Chaudhry, M. Q.; Boxall, A. B. A.; Hull, M., Manufacture and use of nanomaterials: current status in the UK and global trends. *Occup. Med.-Oxf.* **2006**, *56* (5), 300-306.
13. Kinoshita, Y. M., I. ; Higuchi, T. ; Saito, Y. , *Bulletins of the Chemical Society of Japan* **1959** 32 1221-1226.
14. Tomic, E. A., Thermal stability of coordination polymers. *J. Appl. Polym. Sci.* **1965**, *9* (11), 3745-3752.
15. James, S. L., Metal-organic frameworks. *Chem. Soc. Rev.* **2003**, *32* (5), 276-288.
16. Farha, O. K.; Hupp, J. T., Rational Design, Synthesis, Purification, and Activation of Metal–Organic Framework Materials. *Accounts Chem. Res.* **2010**, *43* (8), 1166-1175.
17. Czaja, A. U.; Trukhan, N.; Muller, U., Industrial applications of metal-organic frameworks. *Chem. Soc. Rev.* **2009**, *38* (5), 1284-1293.
18. Tranchemontagne, D. J. H., J. R.; Yaghi, O. M, Room temperature synthesis of metal-organic frameworks: MOF-5, MOF-74, MOF-177, MOF-199, and IRMOF-0. *Tetrahedron* **2008**, *64*, 8553-8557.
19. Xiang, Z.; Cao, D.; Lan, J.; Wang, W.; Broom, D. P., Multiscale simulation and modelling of adsorptive processes for energy gas storage and carbon dioxide capture in porous coordination frameworks. *Energy & Environmental Science* **2010**, *3* (10), 1469-1487.
20. Garibay, S. J.; Wang, Z. Q.; Tanabe, K. K.; Cohen, S. M., Postsynthetic Modification: A Versatile Approach Toward Multifunctional Metal–Organic Frameworks. *Inorg. Chem.* **2009**, *48* (15), 7341-7349.

References

21. Shultz, A. M.; Sarjeant, A. A.; Farha, O. K.; Hupp, J. T.; Nguyen, S. T., Post-Synthesis Modification of a Metal-Organic Framework To Form Metallosalen-Containing MOF Materials. *J. Am. Chem. Soc.* **2011**, *133* (34), 13252-13255.
22. Cheng, S. J.; Liu, S. B.; Zhao, Q.; Li, J. P., Improved synthesis and hydrogen storage of a microporous metal-organic framework material. *Energ. Convers. Manage* **2009**, *50* (5), 1314-1317.
23. Lu, C. M.; Liu, J.; Xiao, K. F.; Harris, A. T., Microwave enhanced synthesis of MOF-5 and its CO₂ capture ability at moderate temperatures across multiple capture and release cycles. *Chem. Eng. J.* **2010**, *156* (2), 465-470.
24. Kleist, W.; Maciejewski, M.; Baiker, A., MOF-5 based mixed-linker metal-organic frameworks: Synthesis, thermal stability and catalytic application. *Thermochim. Acta.* **2010**, *499* (1-2), 71-78.
25. McKinlay, A. C.; Morris, R. E.; Horcajada, P.; Ferey, G.; Gref, R.; Couvreur, P.; Serre, C., BioMOFs: Metal-Organic Frameworks for Biological and Medical Applications. *Angew. Chem. Int. Edit.* **2010**, *49* (36), 6260-6266.
26. Wood, P. Highly Holey: MOFs with Record-Breaking Surface Areas. <https://www.ccdc.cam.ac.uk/Community/Blog/pages/BlogPost.aspx?bpid=21>.
27. Yaghi, O. M.; O'Keeffe, M.; Ockwig, N. W.; Chae, H. K.; Eddaoudi, M.; Kim, J., Reticular synthesis and the design of new materials. *Nature* **2003**, *423* (6941), 705-714.
28. Bhunia, M. K.; Hughes, J. T.; Fetting, J. C.; Navrotsky, A., Thermochemistry of Paddle Wheel MOFs: Cu-HKUST-1 and Zn-HKUST-1. *Langmuir* **2013**, *29* (25), 8140-8145.
29. Gao, S. X.; Zhao, N.; Shu, M. H.; Che, S. N., Palladium nanoparticles supported on MOF-5: A highly active catalyst for a ligand- and copper-free Sonogashira coupling reaction. *Appl. Catal. A-Gen.* **2010**, *388* (1-2), 196-201.
30. Schröder, F.; Esken, D.; Cokoja, M.; van den Berg, M. W. E.; Lebedev, O. I.; Van Tendeloo, G.; Walaszek, B.; Buntkowsky, G.; Limbach, H.-H.; Chaudret, B.; Fischer, R. A., Ruthenium Nanoparticles inside Porous [Zn₄O(bdc)₃] by Hydrogenolysis of Adsorbed [Ru(cod)(cot)]: A Solid-State Reference System for Surfactant-Stabilized Ruthenium Colloids. *Journal of the American Chemical Society* **2008**, *130* (19), 6119-6130.
31. Schlichte, K.; Kratzke, T.; Kaskel, S., Improved synthesis, thermal stability and catalytic properties of the metal-organic framework compound Cu₃(BTC)₂. *Microporous and Mesoporous Materials* **2004**, *73* (1-2), 81-88.
32. Dhakshinamoorthy, A.; Alvaro, M.; Chevreau, H.; Horcajada, P.; Devic, T.; Serre, C.; Garcia, H., Iron(III) metal-organic frameworks as solid Lewis acids for the isomerization of [small alpha]-pinene oxide. *Catalysis Science & Technology* **2012**, *2* (2), 324-330.
33. Schlapbach, L.; Züttel, A., Hydrogen-storage materials for mobile applications. *Nature* **2001**, *414* (6861), 353-358.
34. (a) Rowsell, J. L. C. M., A. R.; Park, K. S.; Yaghi, O. M., Hydrogen Sorption in Functionalized Metal-Organic Frameworks. *J. Am. Chem. Soc.* **2004**, *126*, 5666-5667; (b) Rosi, N. L. E., J.; Eddaoudi, M.; Vodak, D. T.; Kim, J.; O'Keeffe, M.; Yaghi, O. M., Hydrogen storage in microporous metal-organic frameworks. *Science* **2003**, *300* (5622), 1127-1129; (c) Kaye, S. S.; Dailly, A.; Yaghi, O. M.; Long, J. R., Impact of preparation and handling on the hydrogen storage properties of Zn₄O(1,4-benzenedicarboxylate)₃ (MOF-5). *J. Am. Chem. Soc.* **2007**, *129* (46), 14176-+; (d) Han, S. S.; Mendoza-Cortes, J. L.; Goddard Iii, W. A., Recent advances on simulation and theory of hydrogen storage in metal-organic frameworks and covalent organic frameworks. *Chem. Soc. Rev.* **2009**, *38* (5), 1460-1476.
35. Vitillo, J. G.; Regli, L.; Chavan, S.; Ricchiardi, G.; Spoto, G.; Dietzel, P. D. C.; Bordiga, S.; Zecchina, A., Role of exposed metal sites in hydrogen storage in MOFs. *J. Am. Chem. Soc.* **2008**, *130* (26), 8386-8396.
36. Sagara, T.; Klassen, J.; Ortony, J.; Ganz, E., Binding energies of hydrogen molecules to isorecticular metal-organic framework materials. *The Journal of Chemical Physics* **2005**, *123* (1), 014701.
37. Romeo, L. M.; Espatolero, S.; Bolea, I., Designing a supercritical steam cycle to integrate the energy requirements of CO₂ amine scrubbing. *International Journal of Greenhouse Gas Control* **2008**, *2* (4), 563-570.

References

38. Liu, Y.; Wang, Z. U.; Zhou, H.-C., Recent advances in carbon dioxide capture with metal-organic frameworks. *Greenhouse Gases: Science and Technology* **2012**, 2 (4), 239-259.
39. Lee, K. B.; Sircar, S., Removal and recovery of compressed CO₂ from flue gas by a novel thermal swing chemisorption process. *AIChE Journal* **2008**, 54 (9), 2293-2302.
40. Li, Y.; Yang, R. T., Gas Adsorption and Storage in Metal–Organic Framework MOF-177. *Langmuir* **2007**, 23 (26), 12937-12944.
41. Yazaydin, A. Ö.; Snurr, R. Q.; Park, T.-H.; Koh, K.; Liu, J.; LeVan, M. D.; Benin, A. I.; Jakubczak, P.; Lanuza, M.; Galloway, D. B.; Low, J. J.; Willis, R. R., Screening of Metal–Organic Frameworks for Carbon Dioxide Capture from Flue Gas Using a Combined Experimental and Modeling Approach. *J. Am. Chem. Soc.* **2009**, 131 (51), 18198-18199.
42. Khan, N. A.; Haque, E.; Jhung, S. H., Rapid syntheses of a metal-organic framework material Cu₃(BTC)₂(H₂O)₃ under microwave: a quantitative analysis of accelerated syntheses. *Physical Chemistry Chemical Physics* **2010**, 12 (11), 2625-2631.
43. Yang, S. L., X.; Lewis, W.; Suyetin, M.; Bichoutskaia, E; Parker, J. E.; Tang, C. C.; Allan, D. R.; Rizkallah, P. J.; Hubberstey, P.; Champness, N. R.; Thomas, K. M.; Blake, A. J.; Schröder, M., A partially interpenetrated metal–organic framework for selective hysteretic sorption of carbon dioxide. *Nature Materials* **2012**, 11, 710-716.
44. Prasad, T. K. S., M. P., Control of Interpenetration and Gas-Sorption Properties of Metal-Organic Frameworks by a Simple Change in Ligand Design. *Chemistry - A European Journal* **2012**, 18 (28), 8673-8680.
45. Liu, B. T., L. X. ; Lian, Y.H. ; Li, Z. ; Sun, C.Y. ; Chen, G.J., Study on Separation Performance of Metal-organic Frameworks with Interpenetration and Mixed-ligand. *Acta Chimica Sinica* **2013**, 71 (6), 920-928.
46. Hafizovic, J.; Bjorgen, M.; Olsbye, U.; Dietzel, P. D. C.; Bordiga, S.; Prestipino, C.; Lamberti, C.; Lillerud, K. P., The inconsistency in adsorption properties and powder XRD data of MOF-5 is rationalized by framework interpenetration and the presence of organic and inorganic species in the nanocavities. *J. Am. Chem. Soc.* **2007**, 129 (12), 3612-3620.
47. Férey, G., Hybrid porous solids: past, present, future. *Chem. Soc. Rev.* **2008**, 37 (1), 191-214.
48. Loiseau, T.; Serre, C.; Huguenard, C.; Fink, G.; Taulelle, F.; Henry, M.; Bataille, T.; Férey, G., A Rationale for the Large Breathing of the Porous Aluminum Terephthalate (MIL-53) Upon Hydration. *Chemistry – A European Journal* **2004**, 10 (6), 1373-1382.
49. Li, H.; Eddaoudi, M.; O'Keeffe, M.; Yaghi, O. M., Design and synthesis of an exceptionally stable and highly porous metal-organic framework. *Nature* **1999**, 402 (6759), 276-279.
50. Bosch, M.; Zhang, M.; Zhou, H.-C., Increasing the Stability of Metal-Organic Frameworks. *Advances in Chemistry* **2014**, 2014, 8.
51. Küsgens, P.; Rose, M.; Senkovska, I.; Fröde, H.; Henschel, A.; Siegle, S.; Kaskel, S., Characterization of metal-organic frameworks by water adsorption. *Microporous and Mesoporous Materials* **2009**, 120 (3), 325-330.
52. Mustafa, D.; Breynaert, E.; Bajpe, S. R.; Martens, J. A.; Kirschhock, C. E. A., Stability improvement of Cu₃(BTC)₂ metal-organic frameworks under steaming conditions by encapsulation of a Keggin polyoxometalate. *Chem. Commun.* **2011**, 47 (28), 8037-8039.
53. Sinnott, R. K., CHAPTER 6 - Costing and Project Evaluation. In *Coulson and Richardson's Chemical Engineering*, Sinnott, R. K., Ed. Pergamon: Amsterdam, 1993; pp 209-244.
54. Harmsen, J., Chapter 7 - Scale-Up of Unit Operations. In *Industrial Process Scale-up*, Harmsen, J., Ed. Elsevier: Amsterdam, 2013; pp 59-71.
55. Donati, G.; Paludetto, R., Scale up of chemical reactors. *Catalysis Today* **1997**, 34 (3–4), 483-533.
56. Vogel, H., Development of Chemical Processes. In *Chemical Engineering and Chemical Process Technology*, Vol. IV.
57. Harmsen, J., Chapter 4 - Development Stage. In *Industrial Process Scale-up*, Harmsen, J., Ed. Elsevier: Amsterdam, 2013; pp 45-51.
58. Lipworth, D. S. *Scale up of Chemical Reactions*; Royal Society of Chemistry: 2013.
59. Frankie, W.-B., Considerations for Scale-Up ? Moving from the Bench to the Pilot Plant to Full Production. In *Academia and Industrial Pilot Plant Operations and Safety*, American Chemical Society: 2014; Vol. 1163, pp 37-45.

References

60. Fogler, H. S., *Elements of chemical reaction engineering*. 4th ed.; Prentice-Hall: 1986.
61. Tsao, C. S.; Yu, M. S.; Chung, T. Y.; Wu, H. C.; Wang, C. Y.; Chang, K. S.; Chent, H. L., Characterization of pore structure in metal-organic framework by small-angle X-ray scattering. *J. Am. Chem. Soc.* **2007**, *129* (51), 15997-16004.
62. Lock, N.; Wu, Y.; Christensen, M.; Cameron, L. J.; Peterson, V. K.; Bridgeman, A. J.; Kepert, C. J.; Iversen, B. B., Elucidating Negative Thermal Expansion in MOF-5. *J. Phys. Chem. C* **2010**, *114* (39), 16181-16186.
63. Hermes, S.; Witte, T.; Hikov, T.; Zacher, D.; Bahnmuller, S.; Langstein, G.; Huber, K.; Fischer, R. A., Trapping metal-organic framework nanocrystals: An in-situ time-resolved light scattering study on the crystal growth of MOF-5 in solution. *J. Am. Chem. Soc.* **2007**, *129* (17), 5324-5325.
64. Choi, J. Y. K., J; Jhung, S. H; Kim, H; Chang, J.;Chae, H. K., Microwave Synthesis of a Porous Metal-Organic Framework, Zinc Terephthalate MOF-5. *Bulletins of the Korean Chemical Society* **2006**, *27* (10), 1523-1524.
65. Sabouni, R.; Kazemian, H.; Rohani, S., A novel combined manufacturing technique for rapid production of IRMOF-1 using ultrasound and microwave energies. *Chem. Eng. J.* **2010**, *165* (3), 966-973.
66. Jia, Z.; Li, H. B.; Yu, Z. X.; Wang, P.; Fan, X. L., Densification of MOF-5 synthesized at ambient temperature for methane adsorption. *Mater. Lett.* **2011**, *65* (15-16), 2445-2447.
67. Hausdorf, S. M., O. R. L.; Baitalow, F.; Bohle, T.; Rafaja, D., Main-Group and Transition-Element IRMOF Homologues. *J. Am. Chem. Soc.* **2010**, *132*, 10978-10981.
68. (a) Yoo, Y.; Lai, Z. P.; Jeong, H. K., Fabrication of MOF-5 membranes using microwave-induced rapid seeding and solvothermal secondary growth. *Micropor. Mesopor. Mat.* **2009**, *123* (1-3), 100-106; (b) Blanita, G.; Ardelean, O.; Lupu, D.; Borodi, G.; Mihet, M.; Coros, M.; Vlassa, M.; Misan, I.; Coldea, I.; Popeneciu, G., Microwave Assisted Synthesis of MOF-5 at Atmospheric Pressure. *Rev. Roum. Chim.* **2011**, *56* (6), 583-+.
69. (a) Ma, M.; Zacher, D.; Zhang, X. N.; Fischer, R. A.; Metzler-Nolte, N., A Method for the Preparation of Highly Porous, Nanosized Crystals of Isorecticular Metal-Organic Frameworks. *Cryst. Growth. Des.* **2011**, *11* (1), 185-189; (b) Li, J. P.; Cheng, S. J.; Zhao, Q.; Long, P. P.; Dong, J. X., Synthesis and hydrogen-storage behavior of metal-organic framework MOF-5. *Int. J. Hydrogen Energ.* **2009**, *34* (3), 1377-1382.
70. Hausdorf, S. W., J.; Mossig, R.; Mertens, O. R. L., Proton and Water Activity-Controlled Structure Formation in Zinc Carboxylate-Based Metal Organic Frameworks. *J. Phys. Chem. A* **2008**, *112*, 7567-7576.
71. Biemmi, E.; Bein, T.; Stock, N., Synthesis and characterization of a new metal organic framework structure with a 2D porous system: (H₂NEt₂)₂[Zn₃(BDC)₄]-3DEF. *Solid State Sciences* **2006**, *8* (3-4), 363-370.
72. Biemmi, E.; Christian, S.; Stock, N.; Bein, T., High-throughput screening of synthesis parameters in the formation of the metal-organic frameworks MOF-5 and HKUST-1. *Microporous Mesoporous Mater.* **2009**, *117* (1-2), 111-117.
73. (a) Zhao, Z. X.; Li, Z.; Lin, Y. S., Adsorption and Diffusion of Carbon Dioxide on Metal-Organic Framework (MOF-5). *Ind. Eng. Chem. Res.* **2009**, *48* (22), 10015-10020; (b) Saha, D.; Deng, S., Ammonia adsorption and its effects on framework stability of MOF-5 and MOF-177. *J Colloid Interface Sci* **2010**, *348* (2), 615-20; (c) Yang, S. J.; Cho, J. H.; Lee, K.; Kim, T.; Park, C. R., Concentration-Driven Evolution of Crystal Structure, Pore Characteristics, and Hydrogen Storage Capacity of Metal Organic Framework-5s: Experimental and Computational Studies. *Chem. Mater.* **2010**, *22* (22), 6138-6145; (d) Zhang, L.; Hu, Y. H., Desorption of dimethylformamide from Zn₄O(C₈H₄O₄)(₃) framework. *Appl. Surf. Sci.* **2011**, *257* (8), 3392-3398; (e) Calleja, G.; Botas, J. A.; Orcajo, M. G.; Sanchez-Sanchez, M., Differences between the isostructural IRMOF-1 and MOCPL porous adsorbents. *J. Porous Mater.* **2010**, *17* (1), 91-97; (f) Buso, D.; Nairn, K. M.; Gimona, M.; Hill, A. J.; Falcaro, P., Fast Synthesis of MOF-5 Microcrystals Using Sol-Gel SiO₂ Nanoparticles. *Chemistry of Materials* **2011**, *23* (4), 929-934; (g) Hausdorf, S.; Baitalow, F.; Seidel, J.; Mertens, F., Gaseous species as reaction tracers in the solvothermal synthesis of the zinc oxide terephthalate MOF-5. *J. Phys. Chem. A* **2007**, *111* (20), 4259-4266; (h) Choi, K. M.; Jeon, H. J.; Kang, J. K.; Yaghi, O. M., Heterogeneity within Order in Crystals of a Porous Metal-Organic

References

- Framework. *J. Am. Chem. Soc.* **2011**, *133* (31), 11920-11923; (i) Saha, D. P.; Wei, Z. J.; Deng, S. G., Hydrogen adsorption equilibrium and kinetics in metal-organic framework (MOF-5) synthesized with DEF approach. *Sep. Purif. Technol.* **2009**, *64* (3), 280-287; (j) Saha, D. P. D.; Deng, S. G.; Yang, Z. G., Hydrogen adsorption on metal-organic framework (MOF-5) synthesized by DMF approach. *J. Porous Mater.* **2009**, *16* (2), 141-149; (k) Hirscher, M. P., B., Hydrogen Physisorption in Metal-Organic Porous Crystals. *Adv. Mater.* **2005**, *17*, 538-541; (l) Hermes, S.; Schroder, F.; Amirjalayer, S.; Schmid, R.; Fischer, R. A., Loading of porous metal-organic open frameworks with organometallic CVD precursors: inclusion compounds of the type LnM (a)@MOF-5. *J. Mater. Chem.* **2006**, *16* (25), 2464-2472; (m) Choi, J. S., W; Kim, J; Ahn, W, Metal Organic Framework MOF-5 prepared by microwave heating: Factors to be considered. *Micropor. Mesopor. Mat.* **2008**, *116*, 727-731; (n) Mueller, U.; Schubert, M.; Teich, F.; Puetter, H.; Schierle-Arndt, K.; Pastre, J., Metal-organic frameworks - prospective industrial applications. *J. Mater. Chem.* **2006**, *16* (7), 626-636; (o) Phan, N. T. S.; Le, K. K. A.; Phan, T. D., MOF-5 as an efficient heterogeneous catalyst for Friedel-Crafts alkylation reactions. *Appl. Catal. A-Gen.* **2010**, *382* (2), 246-253; (p) Sabo, M.; Henschel, A.; Froede, H.; Klemm, E.; Kaskel, S., Solution infiltration of palladium into MOF-5: synthesis, physisorption and catalytic properties. *J. Mater. Chem.* **2007**, *17* (36), 3827-3832; (q) Chuang, S. S. C. C., A. C., Static and dynamic hydrogen adsorption on PtAC and MOF-5. *Int. J. Hydrogen Energ.* **2011**, *36*, 6022-6030; (r) Chen, B.; Wang, X. J.; Zhang, Q. F.; Xi, X. Y.; Cai, J. J.; Qi, H.; Shi, S.; Wang, J.; Yuan, D.; Fang, M., Synthesis and characterization of the interpenetrated MOF-5. *J. Mater. Chem.* **2010**, *20* (18), 3758-3767; (s) Huang, L. M.; Wang, H. T.; Chen, J. X.; Wang, Z. B.; Sun, J. Y.; Zhao, D. Y.; Yan, Y. S., Synthesis, morphology control, and properties of porous metal-organic coordination polymers. *Micropor. Mesopor. Mat.* **2003**, *58* (2), 105-114.
74. Hughes, J. T.; Navrotsky, A., MOF-5: Enthalpy of Formation and Energy Landscape of Porous Materials. *J. Am. Chem. Soc.* **2011**, *133* (24), 9184-9187.
75. Rosi, N. L. K., J.; Eddoudi, M.; Chen, B.; O'Keeffe, M.; Yaghi, O. M., Rod Packings and Metal-Organic Frameworks Constructed from Rod-Shaped Secondary Building Units. *J. Am. Chem. Soc.* **2005**, *127*, 1504-1518.
76. Rosi, N. L.; Eddaoudi, M.; Kim, J.; O'Keeffe, M.; Yaghi, O. M., Infinite Secondary Building Units and Forbidden Catenation in Metal-Organic Frameworks. *Angewandte Chemie International Edition* **2002**, *41* (2), 284-287.
77. Loiseau, T. M., H.; Ferey, G.; Haouas, M.; Taulelle, F., Synthesis and Structural characterisation of a new open framework zinc terephthalate Zn₃(OH)₂(BDC)₂ * 2DEF, with infinite Zn-(μ₃-OH)-Zn chains. *Journal of Solid State Chemistry* **2005**, *178*, 621-628.
78. Farrusseng, D. R., U.; Savonnet, M.; Aguado, S.; Dominie, M. E., Janneau, E., Engineering of coordination polymers for shape selective alkylation of large aromatics and the role of defects. *Micropor. Mesopor. Mat.* **2010**, *129*, 319-329.
79. Greathouse, J. A. A., M. D., The Interaction of Water with MOF-5 Simulated by Molecular Dynamics. *J. Am. Chem. Soc.* **2006**, *128*, 10678-10679.
80. Bellarosa, L. C., S.; Lopez, N., Early stages in the degradation of metal organic frameworks in liquid water from first principles molecular dynamics. *Physical Chemistry Chemical Physics* **2012**, *14*, 7240-7245.
81. Walton, K. S. S., P. M., Carson, C. G.; Jasuja H.; Flemming, C. J. J., Effect of Water Adsorption on Retention of Structure and Surface Area of Metal Organic Frameworks. *Ind. Eng. Chem. Res.* **2012**, *51*, 6513-6519.
82. Ma, D. Y.; Li, Y. W.; Li, Z., Tuning the moisture stability of metal-organic frameworks by incorporating hydrophobic functional groups at different positions of ligands. *Chem. Commun.* **2011**, *47* (26), 7377-7379.
83. Masel, R. I. W., T; Shen, L; Luebbers, M.; Hu, C.; Chem, Q.; Ni, Z., Enhancing the stability of metal organic frameworks in humid air by incorporating water repellent functional groups. *Chem. Commun.* **2010**, *46*, 6120-6122.
84. Chui, S. S.-Y.; Lo, S. M.-F.; Charmant, J. P. H.; Orpen, A. G.; Williams, I. D., A Chemically Functionalizable Nanoporous Material [Cu₃(TMA)₂(H₂O)₃]n. *Science* **1999**, *283* (5405), 1148-1150.
85. O'Neill, L. D.; Zhang, H.; Bradshaw, D., Macro-/microporous MOF composite beads. *J. Mater. Chem.* **2010**, *20* (27), 5720-5726.

References

86. Ethiraj, J.; Bonino, F.; Lamberti, C.; Bordiga, S., H₂S interaction with HKUST-1 and ZIF-8 MOFs: A multitechnique study. *Micropor. Mesopor. Mat.* **2015**, *207* (0), 90-94.
87. Chowdhury, P.; Bikkina, C.; Meister, D.; Dreisbach, F.; Gumma, S., Comparison of adsorption isotherms on Cu-BTC metal organic frameworks synthesized from different routes. *Micropor. Mesopor. Mat.* **2009**, *117* (1-2), 406-413.
88. Kim, J.; Kim, S.-H.; Yang, S.-T.; Ahn, W.-S., Bench-scale preparation of Cu₃(BTC)₂ by ethanol reflux: Synthesis optimization and adsorption/catalytic applications. *Micropor. Mesopor. Mat.* **2012**, *161*, 48-55.
89. Huo, J.; Brightwell, M.; El Hankari, S.; Garai, A.; Bradshaw, D., A versatile, industrially relevant, aqueous room temperature synthesis of HKUST-1 with high space-time yield. *J. Mater. Chem. A* **2013**, *1* (48), 15220-15223.
90. Lidstrom, P. T., J.; Wathey, B.; Westman, J., Microwave assisted organic synthesis - a review. *Tetrahedron* **2001**, *57*, 9228-9283.
91. Rao, K. J. V., B.; Ganguli, M.; Ramakrishnan, P. A., Synthesis of Inorganic Solids Using Microwaves. *Chem. Mater.* **1999**, *11*, 882-885.
92. Xu, H. Z., B. W.; Suslick, K. S., Sonochemical synthesis of nanomaterials. *Chem. Soc. Rev.* **2012**.
93. Pert, E. C., Y.; Birnboim, A.; Olorunyolemi, T.; Gershon, D.; Calame, J.; Lloyd, I. K.; Wilson, O. C., Temperature Measurements during Microwave Processing: The Significance of Thermocouple Effects. *Journal of the American Ceramic Society* **2001**, *84* (9), 1981-1986.
94. de la Hoz, A. D.-O., A.; Moreno, A., Microwaves in organic synthesis. Thermal and non-thermal microwave effects. *Chem. Soc. Rev.* **2005**, *34*, 164-178.
95. Schanche, J.-S., Microwave synthesis solutions from Personal Chemistry. *Molecular Diversity* **2003**, *7*, 292-300.
96. Pitchai, K. B., S. L.; Jones, D.; Subbiah, J., Assessment of heating rate and non-uniform heating in domestic microwave ovens. *The Journal of Microwave Power and Electromagnetic Energy* **2012**, *46* (4), 229-240.
97. Tareen, J.; Kuty, T., *A basic course in crystallography*. Universities Press: 2001.
98. Studyblue.com (accessed December 4th 2014).
99. Williams, D. H. F., I., *Spectroscopic Methods in Organic Chemistry*. 1995.
100. Atkins, P. W., *The Elements of Physical Chemistry*. 1992.
101. Preface. In *Adsorption by Powders and Porous Solids*, Rouquerol, F.; Rouquerol, J.; Sing, K., Eds. Academic Press: London, 1999; pp xiii-xiv.
102. Atkins, P.; De Paula, J., *Physical Chemistry*. Oxford University Press: 2006.
103. Foreword. In *Surface Area and Porosity Determinations by Physisorption*, Condon, J. B., Ed. Elsevier Science: Amsterdam, 2006; pp xi-xiii.
104. Brunauer, S.; Emmett, P. H.; Teller, E., Adsorption of gases in multimolecular layers. *J. Am. Chem. Soc.* **1938**, *60*, 309-319.
105. Lastoskie, C. G., K. E.; Quirke, N, Pore Size Distribution Analysis and Networking: Studies of Microporous Sorbents. *Studies in Surface Science and Catalysis* **1994**, *87* (51-60).
106. Barrett, E. P.; Joyner, L. G.; Halenda, P. P., The Determination of Pore Volume and Area Distributions in Porous Substances. I. Computations from Nitrogen Isotherms. *J. Am. Chem. Soc.* **1951**, *73* (1), 373-380.
107. Abbe, E., Beiträge zur Theorie des Mikroskops und der mikroskopischen Wahrnehmung. *Archiv f. mikrosk. Anatomie* **1873**, *9* (1), 413-418.
108. Beyond the diffraction limit. *Nat Photon* **2009**, *3* (7), 361-361.
109. Saha, D.; Deng, S. G., Synthesis, characterization and hydrogen adsorption in mixed crystals of MOF-5 and MOF-177. *Int. J. Hydrogen Energ.* **2009**, *34* (6), 2670-2678.
110. Threlfall, T., Structural and thermodynamic explanations of Ostwald's rule. *Org. Process Res. Dev.* **2003**, *7* (6), 1017-1027.
111. Chung, S. Y.; Kim, Y. M.; Kim, J. G.; Kim, Y. J., Multiphase transformation and Ostwald's rule of stages during crystallization of a metal phosphate. *Nature Phys.* **2009**, *5* (1), 68-73.
112. McKinstry, C.; Cussen, E. J.; Fletcher, A. J.; Patwardhan, S. V.; Sefcik, J., Effect of Synthesis Conditions on Formation Pathways of Metal Organic Framework (MOF-5) Crystals. *Cryst. Growth. Des.* **2013**, *13* (12), 5481-5486.

References

113. Kim, H.; Das, S.; Kim, M. G.; Dybtsev, D. N.; Kim, Y.; Kim, K., Synthesis of Phase-Pure Interpenetrated MOF-5 and Its Gas Sorption Properties. *Inorg. Chem.* **2011**, *50* (8), 3691-3696.
114. Sheldon, R. A., Why green chemistry and sustainability of resources are essential to our future. *J. Environ. Monit.* **2008**, *10* (4), 406-407.
115. Borfecchia, E. M., S.; Gianolio, D.; Groppo, E.; Chiesa, M.; Bonino, F.; Lamberti, C., Insights into Adsorption of NH₃ on HKUST-1 Metal–Organic Framework: A Multitechnique Approach. *J. Phys. Chem. C* **2012**, *116*, 19839-19850.
116. Yakovenko, A.; Reibenspies, J.; Bhuvanesh, N.; Zhou, H.-C., Generation and applications of structure envelopes for porous metal-organic frameworks. *Journal of Applied Crystallography* **2013**, *46* (2), 346-353.
117. Seo, Y.-K.; Hundal, G.; Jang, I. T.; Hwang, Y. K.; Jun, C.-H.; Chang, J.-S., Microwave synthesis of hybrid inorganic–organic materials including porous Cu₃(BTC)₂ from Cu(II)-trimesate mixture. *Micropor. Mesopor. Mat.* **2009**, *119* (1–3), 331-337.
118. Chen, J.; Yu, T.; Chen, Z.; Xiao, H.; Zhou, G.; Weng, L.; Tu, B.; Zhao, D., Synthesis and Structure of a New 3D Porous Cu(II)-Benzene-1,3,5-tricarboxylate Coordination Polymer, [Cu₂(OH)(BTC)(H₂O)]_n · 2_nH₂O. *Chemistry Letters* **2003**, *32* (7), 590-591.
119. Rubio-Martinez, M.; Batten, M. P.; Polyzos, A.; Carey, K.-C.; Mardel, J. I.; Lim, K.-S.; Hill, M. R., Versatile, High Quality and Scalable Continuous Flow Production of Metal-Organic Frameworks. *Sci. Rep.* **2014**, *4*.
120. Peterson, G. W.; DeCoste, J. B.; Glover, T. G.; Huang, Y.; Jasuja, H.; Walton, K. S., Effects of pelletization pressure on the physical and chemical properties of the metal–organic frameworks Cu₃(BTC)₂ and UiO-66. *Micropor. Mesopor. Mat.* **2013**, *179* (0), 48-53.